The internalization of α-synuclein and the formation of Lewy body-like inclusions

Armin Bayati

The Integrated Program in Neuroscience

Montreal Neurological Institute

McGill University

Montreal, November 2023

A thesis submitted to McGill University in

partial fulfillment of the requirements of the degree of

Doctor of Philosophy in Neurological Science

ABSTRACT

Parkinson's disease (PD) is a common neurodegenerative disorder characterized by motor symptoms resulting from the degeneration of dopaminergic neurons in the substantia nigra. α-synuclein (α-syn) is major constituent of Lewy bodies (LBs), proteinaceous inclusions prevalent in idiopathic and familial PD. This doctoral research initially aimed to investigate the mechanism underlying the internalization of α-syn oligomeric/fibril forms, which are involved in the seeding of α-syn aggregation. While previous studies implicated Clathrin-mediated endocytosis as the entry mechanism, our findings proposed a rapid form of macropinocytosis as the primary form of entry for pre-formed fibrils (PFFs) of α-syn. This conclusion was supported by the generation of nanogold-labelled PFFs, used to examine the endocytosis of PFFs via EM. Utilizing our established nanogold-labelled PFFs, we examined the trafficking of PFFs long-term and found that PFFs are incorporated into organellar, filamentous, LB-like inclusions when administered along with an immune challenge, such as interferon-gamma. Our data suggests that dopaminergic neurons are more adept at forming LB-like inclusions than other cell types. This doctoral thesis provides insights into the journey of α-syn PFFs from internalization to their incorporation into newly formed LB-like inclusions.

RÉSUMÉ

La maladie de Parkinson est une maladie neurodégénérative caractérisée par des symptômes moteurs résultant de la dégénération des neurones dopaminergiques dans la partie substantia nigra du cerveau. L'α-synucléine (α-syn) est le constituent majeur des corps de Lewy (Lewy bodies; LBs), des inclusions protéiques prédominants dans les patients de la maladie de Parkinson idiopathique et familiale. Ce projet doctoral investigue le mécanisme d'internalisation des fibrilles et oligomères d'α-syn impliqués dans la propagation des agrégats α-syn. Bien que des études précédentes démontrent l'endocytose dépendante de la clathrine comme mécanisme d'internalisation, nos données suggèrent qu'une macropinocytose permet l'entrée primaire et rapide des fibrilles précoces d'α-syn (preformed fibrils; PFFs). Cette conclusion est supportée par la génération des PFFs couplées au nanogold utilisées pour examiner cette endocytose par microscopie électronique (EM). À l'aide d'un protocole bien établie pour ces PFFs marquées au nanogold, nous avons suivi le trafic des PFFs pour de longues durées et trouvé qu'une fois soumises à un défi immunologique comme l'interféron-gamma, ces fibrilles s'incorporent dans des filaments ressemblant les inclusions LBs. Nos données proposent que les neurones dopaminergiques sont plus habiles à former ces inclusions LBs que les autres types cellulaires. Cette thèse doctorale aperçoit le parcours des PFFs α-syn du moment de leur internalisation jusqu'à leur incorporation dans les inclusions similaires aux LBs qui sont nouvellement formées.

ACKNOWLEDGEMENTS

I would like to thank my supervisor, Dr. Peter S. McPherson, and my committee members, Drs. Edward A. Fon, and Thomas M. Durcan, all our collaborators and lab members who helped me with my projects and helped take my findings to the next level. A special thanks to my co-authors and good friends, Adriana Aguila, Emily Banks, and Riham Ayoubi, for their help inside and outside the laboratory.

I would like to thank Dr. Patrick C. Nahirney for instilling in me the skills required to conduct electron microscopy imaging and yielding quality images. I would also like to thank Dr. Bruce Wright for supporting my academic career when it was most needed. Your help will not be forgotten.

DEDICATION

I would like to dedicate this thesis to my loving wife, Dr. Taryn Berman, who has supported me through all my struggles and has empowered me to achieve as much as I have during my Ph.D. Of course, this thesis is also dedicated to my parents. None of this would have been possible without my parents, Ali, and Leila; from immigration to your financial support for all these years, none could have been done without you. Lastly, I dedicate this to my father-in-law, Tim Berman, for his wise words, which he offered to me whether I wanted to hear it or not.

ABBREVIATIONS

α-syn	α-synuclein
BSA	Bovine Serum Albumin
CHC	Clathrin heavy chain
CME	Clathrin-mediated endocytosis
CPA	Chaperone-mediated autophagy
DA	Dopaminergic
ddH_2O	Double distilled water
DLS	Dynamic light scattering
EDTA	Ethylenediaminetetraacetic acid
EEA1	Early endosome antigen 1
EGF	Epidermal Growth Factor
EIPA	Ethylisopropylamiloride
EM	Electron microscopy
ER	Endoplasmic reticulum
FOXA2	Forkhead box protein A2
FS	FluoSpheres
GBA	Glucosidase, Beta, Acid 1
GCIs	Glial cytoplasmic inclusions
GFAP	Glial fibrillary acidic protein
GPe	Globus Pallidus external segment
GPi	Globus Pallidus internal segment
Hsc70	Heat shock cognate 70
HSP90	90 kDa heat-shock protein
IFN-γ	Interferon-gamma
IP	Immunopercipitated
iPSC	Induced pluripotent stem cells
IPTG	Isopropyl-β-D-thiogalactoside
KD	Knockdown
KO	Knockout
LAG3	Lymphocyte-activation gene 3

LAMP1/2	Lysosomal associated membrane protein 1/2
LatA/B	Latrunculin A/B
LBD	Lewy body dementia
LBs	Lewy bodies
LPS	Lipopolysaccharides
LRRK2	Leucine-rich repeat kinase 2
Lys	Autolysosome/Lysosome
M_1, M_2	Manders' coefficients
MA	Manumycin A
MAP2	microtubule-associated protein 2
Mito	Mitochondria
MSA	Multiple system atrophy
MVBs	Multivesicular bodies
MW	Molecular Weight
NAC	Non-amyloid component
NGN2	Neurogenin 2
NPC	Neuronal progenitor cells
NRF2	Nuclear factor erythroid 2-related factor 2
PAH	Perillaldehyde
PBS	Phosphate-buffered saline
PD	Parkinson's disease
PDB	Protein data bank
PFFs	Pre-formed fibrils
PINK1	PTEN Induced Kinase 1
PLL	Poly-L-Lysine
PO	Poly-L-Ornithine
PRKN	parkin RBR E3 ubiquitin protein ligase
Rac1	Ras-related C3 botulinum toxin substrate 1
RFP	Red fluorescent protein
SM	Starting material
SNc	Substantia nigra pars compacta
SNr	Substantia nigra pars reticulata

STED	Stimulated emission depletion microscopy
STN	Subthalamic nucleus
Tf	Transferrin
TFEB	Transcription factor EB
TH	Tyrosine hydroxylase
TMEM	Transmembrane
UB	Unbound material
VA	Ventral Anterior
VL	Ventral Lateral

Table of Contents

LIST OF FIGURES AND TABLES

Supplementary Figure 3.3	**PFFs are not trafficked through early/recycling endosomes**
Supplementary Figure 3.4	**PFF internalization does not depend on phagocytosis**
Supplementary Figure 3.5	**PFF internalization is mediated through a unique form of macropinocytosis**
Supplementary Figure 3.6	**PFFs induces membrane ruffling at the cell membrane and is localized to macropinosomes, MVBs, and lysosomes**
Supplementary Figure 3.7	**CD63 positive exosomes play a role in the intercellular transmission of PFFs from donor to acceptor cells**
Figure 4.1	**IFN-γ treated DA neurons form PFF-positive inclusions**
Figure 4.2	**LB-like inclusions form over 14 d**
Figure 4.3	**Highly dense, mature inclusions form in DA neurons with increased incubation time**
Figure 4.4	**Microglial co-culture led to inclusions in DA neurons while cortical neurons did not form inclusions with IFN-γ treatment**
Figure 4.5	**The dual hit treatment resulted in the downregulation of lysosomal proteins**
Figure 4.6	**PAH treatment reduces inclusion formation**
Figure 4.7	**PAH restores lysosomal protein expression**
Extended Data Figure 4.1	**Dual hit treatment, PFF characterization, and neuronal characterization**
Extended Data Figure 4.2	**IFN-γ receptor expression, IFN-γ dose-response curve, and inclusions in DA neurons from other iPSC cell lines**
Extended Data Figure 4.3	**IL-1β administration following PFF treatment also leads to the formation of PFF-positive inclusions**
Extended Data Figure 4.4	**Lysosomal leakage of PFFs occurs in PFF + IFN-γ treated samples**
Extended Data Figure 4.5	**Isolation of inclusions formed in DA neurons**
Extended Data Figure 4.6	**Microglia-neuron co-culture, characterization of forebrain and NGN2-induced neurons, and NGN2-induced neurons did not form inclusions**
Extended Data Figure 4.7	**Cell lines do not form LB-like inclusions but show signs of lysosomal dysfunction**
Extended Data Figure 4.8	**Phospho-α-syn is a marker for inclusions and is dependent on the endogenous pool of α-syn**
Extended Data Figure 4.9	**Inclusions forming in DA neurons are enveloped by LC3B, PFF and IFN-γ impair autophagic flux by altering lysosomal pH, and lysosomal proteins are also affected in cell lines undergoing the dual hit treatment**
Extended Data Figure 4.10	**Possible mechanism for the formation of membrane-bound, membranous, organelle filled, LB-like inclusions**

List of Tables

Statement of Original Contribution

In chapter 2 and 3, we establish a protocol to conjugate PFFs with nanogold beads, and then explore the sequence of events involved in the internalization of PFFs using EM. We showed, for the first time, the engulfment of PFFs by membrane ruffles, their internalization into the cells via macropinosomes, which are then rapidly transported to lysosomes and multivesicular bodies, circumventing the conventional endosomal pathway. We further disproved the role of CME in PFF internalization, by taking a genetic approach to knockdown Clathrin. We found that cells with a knockdown of Clathrin heavy chain showed similar PFF internalization ability as control cells. As CME was thought to be the way in which PFFs are internalized into cells, this marked a paradigm shift in the field.

Using our EM assay, we then went onto explore the trafficking of PFFs immediately following internalization. We found PFFs not only in lysosomes, but in newly forming MVBs, on the surface of intralumenal vesicles, and were able to capture PFFs attached to membrane invaginations in newly-forming MVBs. We also found PFFs in mature and acidic MVBs, again on the surface of intralumenal vesicles. We followed this further to find that PFFs are exocytosed and transported to other cells via exosomes, while remaining on the surface of exosomes. This data implies that PFFs that were initially internalized by cells, may still play a role in their internalization into other cells, as they are on the exosomal surface. We found that macropinocytic inhibitors that blocked the initial internalization of PFFs into the cell, also blocked the internalization of exosomal-PFFs into other cells. All these findings were novel contributions to the field.

At this point, we hypothesized that some external factor or cellular stress, such as an immune challenge, may push the neurons into a state in which α-syn inclusions could be formed

via the release of PFFs from lysosome into the cytoplasm. We believed an external stressor to the lysosomal system was required to allow the exit of PFFs from lysosomes and allow their seeding of endogenous α-syn. This was achieved by interferon gamma and allowed us to develop a treatment regime to consistently form homogenous Lewy body-like inclusions in DA neurons. We then used this treatment regime to further characterize the structure of the LB-like inclusions, their formation, and the potential molecular underpinnings. The strength of our observations regarding LB-like inclusion formation, lend further credibility to our molecular findings which can be summarized as follows: IFN-γ along with exogenous PFFs, work cooperatively in impairing lysosomal biogenesis and downregulating lysosomal proteins involved in degradation and autophagy, i.e., LAMP1 and LAMP2. Lastly, our findings further emphasize the importance of microglia and the immune system, in the formation of LB-like inclusions, and therefore, potentially PD.

Our last project represents our most unique contribution which combines neuroimmunology and lysosomal biology to help us understand the sequence of events that may be involved in the formation of Lewy bodies in Parkinson's disease. Not only do we use a dual hit approach to form inclusions reliably and repeatedly in dopaminergic neurons, but we also take the characterization of Lewy body-like inclusions to the next level, with some of the highest resolution images to ever capture Lewy body morphology.

AUTHOR CONTRIBUTIONS

Chapter 1:

The role of α-syn in PD: mutations, propagation, aggregation, and the formation of LBs

Armin Bayati [1] and Peter S. McPherson [1]
[1] Department of Neurology and Neurosurgery, Montreal Neurological Institute, McGill University, Montreal, Quebec, H3A 2B4, Canada
Modified from © Bayati & McPherson, 2024.
Planned to be submitted for peer review by 2024.

AB Wrote Manuscript and made the figures.
PSM Wrote Manuscript.

Chapter 2:

Visualization of α-synuclein trafficking via nanogold labeling and electron microscopy

Armin Bayati [1,3,4,5]*, Wen Luo [2], Esther Del Cid-Pellitero [1], Edward A. Fon [1], Thomas M. Durcan[2,3]**, Peter S. McPherson [1,4]***
[1] Department of Neurology and Neurosurgery, Montreal Neurological Institute, McGill University, Montreal, Quebec, Canada, H3A 2B4
[2] The Neuro's Early Drug Discovery Unit (EDDU), McGill University, Montreal, Quebec, H3A 2B4, Canada
[3] Technical Contacts
[4] Corresponding authors
[5] Lead contact

Originally published in STAR Protocols.
https://doi.org/10.1016/j.xpro.2023.102113

AB planned and conducted the experiments, wrote the manuscript.
WL generation of PFFs, provided input on experimental design.
EDCP aided in the characterization of the full length and sonicated fibrils.
EAF contributed to the manuscript, supervised the generation of unlabeled PFFs.
TMD contributed to the manuscript, supervised the generation of unlabeled PFFs.
PSM funded and supervised the project and contributed to the manuscript.

Chapter 3:

Rapid macropinocytic transfer of α-synuclein to lysosomes

Armin Bayati [1], Emily Banks [1], Chanshuai Han [1], Wen Luo [1], Wolfgang E. Reintsch [1], Cornelia E. Zorca [1], Irina Shlaifer [1], Esther Del Cid Pellitero [1], Benoit Vanderperre [2], Heidi M. McBride [1], Edward A. Fon [1], Thomas M. Durcan [1], and Peter S. McPherson [1,3]
[1] Department of Neurology and Neurosurgery, Montreal Neurological Institute, McGill University, Montreal, QC, Canada

[2] Department of Biological Sciences, Université du Québec à Montréal
[3] Lead Contact/Corresponding Author

Originally published in Cell Reports.
https://doi.org/10.1016/j.celrep.2022.111102

AB	planned and conducted the experiments and wrote the manuscript.
EB	performed lysosomal immunoprecipitation experiment along with analyzing protein expression through western blotting.
CH	provided NPCs and differentiated iPSCs into cortical and dopaminergic neurons
WL	produced and characterized PFFs.
WER	conducted 24 h PFF uptake experiment with dopaminergic NPCs using LatA
CZ	provided additional NPCs and differentiated iPSCs.
RS	measured and analyzed PFF length from multiple batches of PFF using dynamic light scattering.
EDCP	characterized and measured PFF size via EM.
BV	suggested experiments investigating macropinocytosis
HMM	edited the manuscript and helped provide overall direction of the project.
EAF	supervised the generation of iPSCs and PFFs.
TMD	supervised the generation of iPSCs and PFFs, edited the manuscript.
PSM	funded and supervised the project and wrote the manuscript.

Chapter 4:

A dual-hit assay of α-syn internalization and immune-challenge results in the formation and chronic maintenance of Lewy body-like inclusions in human dopaminergic neurons

Armin Bayati [1,4], Riham Ayoubi [1], Cornelia E. Zorca [1], Adriana Aguila [1], Emily Banks [1], Chanshuai Han [2], Emmanuelle Nguyen-Renou [2], Wen Luo [2], Irina Shlaifer [2], Moein Yaqubi [1], Esther Del Cid-Pellitero [1], Edward A. Fon [1], Jo Anne Stratton [1], Thomas M. Durcan [2], Patrick Nahirney [3], Peter S. McPherson [1,5]
[1] Department of Neurology and Neurosurgery, Montreal Neurological Institute, McGill

University, Montreal, QC, Canada
[2] The Neuro's Early Drug Discovery Unit (EDDU), McGill University, Montreal, Quebec, Canada, H3A 2B4
[3] Division of Medical Sciences, University of Victoria, Victoria, BC, Canada, V8P 5C2
[4] Technical Contact
[5] Lead Contact

Planned to be submitted for peer review by 2023.

AB planned and conducted the experiments, wrote the manuscript.
RA conducted inclusions isolation experiments, western blot experiments, analyzed microglial media for secreted proteins and aided with the writing of the manuscript.
CZ provided us with NPCs and differentiated iPSCs and helped with the designing of the experiments.
AA conducted western blots for protein expression related to knockdowns and overexpression experiments, aided with the writing of the manuscript.
EB performed lysosomal immunoprecipitation experiment along with analyzing protein expression through western blotting.
CH provided NPCs and differentiated iPSCs into cortical and dopaminergic neurons.
ENR helped generate all the dopaminergic NPCs and characterized the SNCA, AIW0020-02, and 3450 iPSC lines.
WL produced PFFs and conducted fluorescent conjugation experiments.
IS characterized PFFs through dynamic light scattering.
EDCP characterized and measured PFF size via electron microscopy.
MY provided overall direction of the project.
EAF supervised generation of iPSCs and PFFs.
JAS provided overall direction of the project.
TMD edited the manuscript and helped with the direction of the project.
PN processed electron microscopy samples, helped with the identification of neuronal ultrastructure, and aided in writing the manuscript.
PSM funded and supervised the project, wrote the manuscript.

Chapter 5:

Lewy bodies could be enlarged, dysfunctional, and failed autophagosomes

Armin Bayati [1] and Peter S. McPherson [1]
[1] Department of Neurology and Neurosurgery, Montreal Neurological Institute, McGill University, Montreal, Quebec, H3A 2B4, Canada

Planned to be submitted for peer review in 2024.

AB Wrote Manuscript and made the figures.
PSM Wrote Manuscript.

CHAPTER 1. INTRODUCTION TO PARKINSON'S DISEASE, ALPHA-SYNUCLEIN, ALPHA-SYNUCLEIN SPREAD, AND LEWY BODY INCLUSIONS

1.1 Parkinson's disease

Parkinson's disease (PD), is the second most common neurodegenerative disease, characterized by motor symptoms such as bradykinesia, dystonia, rigidity, postural instability, and resting tremors (Figure 1.1) (Thomas & Beal, 2007). PD is also accompanied by a whole host of nonmotor symptoms, such as depression, anxiety, cognitive impairment, and several gastrointestinal-related impairments (Magistrelli et al., 2021). Motor symptoms in PD are mainly associated with the death of the pigmented dopaminergic (DA) neurons in the substantia nigra pars compacta (SNc), along with the formation of proteinaceous inclusions known as Lewy bodies (LBs; Figure 1.2). The main recipient of the dopamine output of these neurons is the dorsal striatum, located in the basal ganglia, whose lack of dopaminergic innervation is detrimental to "smooth" and "fluid" movement (Diaz-Hernandez et al., 2018; Parker et al., 2016; Smith et al., 2004). The dorsal striatum, composed of the caudate and the putamen, is involved in assessing motor patterns and complex motor plans outputted by the cortex along with the selection of motor movements (Herrero et al., 2002). The dorsal striatum's inhibitory output is necessary for curtailing unnecessary movements and creating a smooth gait (Figure 1.3). With the lack of dopamine stimulation, the necessary inhibitory outputs of the striatum are abolished (Figure 1.4), leading to many of the motor symptoms seen in PD patients.

1.2 Ramifications for the Basal Ganglia

The dopaminergic input into the basal ganglia plays a role in two different pathways: the direct and the indirect pathway (Figure 1.3) (Calabresi et al., 2014). In the direct pathway,

dopamine stimulates neurons in the lateral striatum equipped with D1 receptors. Excitatory cortical projections outputted from the glutamatergic neurons of the cortex also feed into the striatum. The lateral striatum, which contains inhibitory GABAergic neurons, then inhibits the Globus Pallidus internal segment (GPi) and the substantia nigra pars reticulata (SNr). Outputs of the SNr and GPi are directed to the thalamus. The excitatory outputs of the ventral anterior (VA) and the ventral lateral (VL) regions of the thalamus are then directed to the frontal cortex, modulating the planning of movement. In the indirect pathway, inputs from the SNc stimulate the D2 receptors of the lateral striatum. Cortical glutamatergic projections also feed into this region. The lateral striatum then outputs an inhibitory signal to the external segment of the Globus Pallidus (GPe). Inhibitory projections from the GPe feed into the subthalamic nucleus (STN), whose excitatory outputs stimulate GPi. GPi goes on to inhibit the thalamus, as it does in the direct pathway. Excitatory signals are then outputted from the thalamus to the motor cortex, responsible for the selection of movement. Together, the direct and indirect pathways affect the planning and the selection of movements.

In the absence of the DA output from the SNc, due to degeneration observed in PD, the GABAergic neurons of the lateral striatum over-inhibit the GPe and do not sufficiently inhibit the GPi (Figure 1.4) (McGregor & Nelson, 2019). For the direct pathway, the lack of inhibition of the GPi leads to over-inhibition of the thalamus, resulting in less excitatory output to the cortex, impairing motor planning. For the indirect pathway, the lack of inhibition of the subthalamic nucleus, leads to overstimulation of the GPi, which in turn over-inhibits the thalamus, crippling its excitatory signal to the cortex, impairing the selection of movement. The impairments of these pathways explain the rigidity and bradykinesia symptoms of PD.

1.3 Beyond Motor Symptoms

Although the motor symptoms of PD drastically reduce patients' quality of life, these motor symptoms are not responsible for the widespread degeneration of neurons that occurs in PD. The degenerative mechanism that first initiates by the death of DA neurons in SNc, continues to spread and affect neurons through the central nervous system (Bayati & Berman, 2017). The hallmark of this degeneration are proteinaceous inclusions known as LBs (Figure 1.2) (Lewy, 1912), which are also present in Lewy body dementia (LBD) (McKeith et al., 2004). LBD, another neurodegenerative disease with no initial motor symptoms, is marked with an onset of cognitive and memory impairments. In sum, while treating the motor symptoms of PD is important to improve quality of life, it is more important to understand the mechanism involved in the degeneration of neurons. Due to it being a major constituent of LBs, and its aggregation being present in all synucleinopathies (Calabresi et al., 2023), α-synuclein (α-syn) will be the focus of this review.

1.4 α-syn

With the discovery that α-syn is a major component of LBs (M. G. Spillantini et al., 1997), coupled with its role in familial Parkinson's disease (Polymeropoulos et al., 1997), both in its mutated and overexpressing form (Chartier-Harlin et al., 2004; Ki et al., 2007; Li et al., 2002; Nishioka et al., 2006; Singleton et al., 2003), α-syn has become the central protein in PD research, and one of the most enigmatic proteins in biology. With its 14 kDa size, composed of 140 amino acids, it is hard to imagine how this protein has remained a mystery for so long. Part of this mystery stems from its intrinsically disordered nature (Kumari et al., 2021), with its native structure and form being hard to ascertain. Moreover, it has also been posited that physiologically,

α-syn may function as a multimeric protein (Bartels et al., 2011; Dettmer et al., 2015; Dettmer et al., 2017; Nuber et al., 2018). α-syn's cellular localization and function are somewhat diverse, as physiologically, it resides in the cytoplasm but has an affinity towards membranes (Fortin et al., 2004). Findings in recent years have found that α-syn interacts with anionic phospholipids, associate with membrane curvature, and is involved in the organization and tethering of synaptic vesicles (Davidson et al., 1998; Vargas et al., 2017), modulating synaptic vesicle release (Liu et al., 2004), vesicle recycling (Wang et al., 2014), and mediating SNARE-complex assembly (Burre et al., 2010). Its ability to interact with membranes is enabled through its seven imperfect KTKEGV repeats (Figure 1.5) (Zarbiv et al., 2014). Under disease conditions, α-syn accumulation has been shown in the cytosol, endolysosomal system, exosomes, and even the nucleus (Fortin et al., 2004; Guardia-Laguarta et al., 2015; Lee et al., 2005; Miraglia et al., 2018; Pan et al., 2022). Its ability to aggregate is largely due to its non-amyloid-component (NAC) which is hydrophobic (Ihse et al., 2017). A detailed structure accompanied by labeling of domains, regions, repeats, and mutations of the α-syn are illustrated in Figure 1.5.

Although α-syn's association with membranes is undeniable, few have suggested that these membrane-associated functions of α-syn are only secondary to its main function in the cell: stress, cellular homeostasis, and mRNA stability (Hallacli et al., 2022; Hashimoto et al., 2002; Lam et al., 2022; Ludtmann et al., 2016; Zhang et al., 2005). α-syn expression levels are indicators of cellular function when it comes to autophagy (Arotcarena et al., 2019; Fussi et al., 2018; Lee et al., 2013; Sarkar et al., 2021), specifically chaperone-mediated autophagy (CPA) (Cuervo et al., 2004; Malkus & Ischiropoulos, 2012; Sala et al., 2016). Stress signaling (such as immune activation) and exposure to toxic chemicals have also been shown to upregulate α-syn (Jiang et al., 2014; Kasen et

al., 2022; Sala et al., 2013). Increased α-syn expression has also been associated with mitochondrial stress, higher levels of oxidative species, and even endoplasmic reticulum (ER) stress (Mou et al., 2020; Pukass & Richter-Landsberg, 2014; Puspita et al., 2017; Shaltouki et al., 2018). Lastly, α-syn's clear ability to interact and modulate processing bodies, organelles that play a role in mRNA turnover and storage, adds yet another facet to our understanding of α-syn's function in the cell (Hallacli et al., 2022). For all these reasons, it is clear that α-syn homeostasis is paramount to maintaining healthy neuronal function (Dettmer et al., 2016). These functions suggest that although membrane association and synaptic vesicle trafficking might be some of α-syn's roles in the cell, they are certainly not the only functions this protein serves. Table 1.1 lists some of the more recent findings about the physiological functions of α-syn.

1.5 α-syn in Lewy bodies

Under disease conditions, especially in synucleinopathies, α-syn is known for its accumulation and aggregation (Calabresi et al., 2023). α-syn's accumulation in cytoplasmic inclusions, such as LBs and glial cytoplasmic inclusions (GCIs) (Araki et al., 2020), have earned α-syn its "toxic" and "pathological" labels. Perhaps the most crucial question to be addressed is whether α-syn is a symptom or the reason behind the cellular aggresomal/sequestration processes. Most would argue that α-syn is essential for the pathophysiology and the mechanisms driving inclusion formation and that its aggregation is linked to the formation of inclusions through tethering and pulling together of cellular organelles, stabilizing them in inclusionary bodies in the cytoplasm, which go on to mature into LBs (Fares et al., 2021; Lee & Lee, 2002; Mahul-Mellier et al., 2020), in a cell-autonomous manner. This fibrillization theory is contrary to what others have

suggested: α-syn fibrillization is not the underlying process (Conway, Lee, et al., 2000), or may not even be necessary (Shahmoradian et al., 2019), in driving the formation of LBs, but that its oligomerization and accumulation leads to downstream effects such as oxidative stress and impaired organelles (Hijaz & Volpicelli-Daley, 2020; Scudamore & Ciossek, 2018; Zhang et al., 2005). This, coupled with dysfunctional autophagy (Arotcarena et al., 2019), degradation (Cuervo et al., 2004; Rahmani et al., 2022; Vila et al., 2011), and exposure to external toxic chemicals (Scudamore & Ciossek, 2018), may lead to the onset and progression of PD.

1.6 α-syn in familial PD

Genetic data involving familial PD cases suggests that α-syn plays a more fundamental role in the formation of cellular inclusions, as individuals with mutations in *SNCA*, the gene encoding α-syn, exhibit an autosomal dominant inheritance of PD (Lesage et al., 2020). Two types of modifications of the *SNCA* locus have become central in PD research: missense point mutations and locus multiplication. The first type of mutation, missense mutations, have been shown to occur across different families (Xu & Pu, 2016), with the A53T mutation being the first to be discovered (Polymeropoulos et al., 1997), and garnering the most attention. Common amongst most of these missense mutations in the *SNCA* locus, is that they enhance the aggregation ability of α-syn (Ohgita et al., 2022). Additionally, most of these mutations occur near the end of the membrane-binding region of the protein (Figure 1.5), immediately preceding the aggregation-prone NAC region. These misfolded monomers are then believed to act as prions to enable the misfolding of other α-syn monomers, and, therefore, serve as a seed for the aggregation of α-syn (Karpowicz et al., 2019; Tyson et al., 2016).

The second type of modification of the *SNCA* locus is *SNCA* duplication and triplication (Chartier-Harlin et al., 2004; Nishioka et al., 2006; Singleton et al., 2003) (Figure 1.6). In these familial cases, patients present with extra copies of the *SNCA* locus in their genome, driving higher expression levels of α-syn in cells. These cases show another side of α-syn aggregation: higher concentrations of α-syn increase the likelihood of its aggregation (Pinto-Costa et al., 2023; Song et al., 2015). This relationship between α-syn concentration and aggregation has been well-established in *in vitro* and *in vivo* models (Delenclos et al., 2019; Lee & Lee, 2002; Parihar et al., 2009).

The missense mutations and multiplication of *SNCA* have cemented the role of α-syn aggregation in PD. One key question is why patients with *SNCA* mutations, with cells expressing misfolded and aggregate-prone α-syn variants, or those expressing higher concentrations of α-syn, present with PD-related symptoms in middle age or even later in life. Although patients with missense mutations usually exhibit early-onset PD (Magistrelli et al., 2021), (i.e., < 50 age of PD motor symptoms), it is still puzzling why it takes so many years for higher concentrations and misfolded forms of α-syn to form aggregates, disrupting neuronal function and initiating neurodegeneration. *In vitro*, α-syn variants have been shown to quickly form oligomers and initiate fibrilization (Conway et al., 1998; Fredenburg et al., 2007; Ghosh et al., 2013; Narhi et al., 1999; Rutherford et al., 2014), yet this aggregation alone seems to be not associated with the onset of the motor symptoms of PD but are associated with more prodromal PD (Cheng et al., 2023; Kulkarni et al., 2022; Mahlknecht et al., 2022). This has led some to explore a secondary hit, an additional insult, that must present for the manifestation and onset of PD motor symptoms (Tan et al., 2020; Tansey et al., 2022).

Finally, it is important to note that more prevalent and penetrant forms of PD-related mutations exist, such as GBA, LRRK2, PRKN, and PINK1 (Tomiyama et al., 2015), which provide another view to our understanding of PD pathophysiology. Many patients with LRRK2 mutations and all patients with PRKN and PINK1 mutations, do not present with Lewy pathology while exhibiting all the symptoms of PD. However, since idiopathic PD comprises more than 85% of cases in PD (Rajput et al., 1984), most of which present with LBs (Braak et al., 2003), the focus on α-syn-related aggregation has become one of the main avenues of inquiry into PD.

1.7 α-syn propagation

One reason why PD, whether idiopathic or familial, has an age of onset later in life, and a long prodromal period might be associated with α-syn propagation; disease progression and α-syn propagation may, therefore, be linked (Hansen & Li, 2012). Many have emphasized the role of α-syn propagation, allowing aggregated or misfolded forms of α-syn originating from one neuron, to propagate and seed the aggregation of endogenous α-syn in neighboring neurons. These are said to follow connectivity pathways in the brain (Yau et al., 2018). Although this process has been observed on a rapid time scale *in vitro*, partially facilitated by a smaller number of cells and higher concentrations exogenous α-syn, this process may take years to occur *in vivo*. While some have suggested their disbelief in the role of the prion-like transfer of α-syn in PD (Surmeier et al., 2017), others have maintained that it is a crucial and a central event in PD (Masuda-Suzukake et al., 2013; Visanji et al., 2013; Volpicelli-Daley & Brundin, 2018).

1.8 α-syn oligomers

If α-syn propagation plays a central role in PD, it is then important to find out exactly what form of α-syn is involved in propagation (Figure 1.7); a hotly debated topic in α-syn research (Cascella et al., 2022). For many years, the fibril form of α-syn was thought to be responsible for propagation due to its ability to seed α-syn aggregation in cells once internalized. More recently, protofibril and oligomeric forms of α-syn have gained prominence for their potential to act as the propagating form of α-syn due to their ability to be quickly internalized while still maintaining the ability to seed aggregates (Alam et al., 2019). Also, as point mutations in *SNCA* enhance oligomerization but not fibrillization (Conway, Lee, et al., 2000), it suggests that fibrillization is not a major factor in disease progression and that the fibril form of α-syn is not the most "toxic" form. Whether soluble or insoluble forms of α-syn are involved in seeding and aggregate formation in PD will need to be investigated further. These studies will need to ascertain which form of α-syn can be found early in PD and is, therefore, involved in its onset.

1.9 Strains of α-syn

Further complexities are associated with α-syn oligomers and fibrils, as different strains of α-syn aggregates have different branching characteristics, different thioflavin T fluorescence, and have different cell internalization and aggregation properties. In one study, the fibrillization of α-syn in presence and absence of NaCl, resulted in markedly different fibrillized products (Bousset et al., 2013). These different strains then targeted different brain regions *in vivo,* along with a propensity to target specific cell types (Lau et al., 2020). These strains went on to form conformationally different intracellular phospho-α-syn aggregates. The establishment of ribbons

and fibrils strains of α-syn led to the strain-dependent propagation in another *in vivo* study (Peelaerts et al., 2015). These findings further complicate research into α-syn propagation; however, research into this topic can potentially provide us with an explanation of the differential nigral and striatal pathologies, along with morphologically different aggregates/inclusions that form in various synucleinopathies (Malfertheiner et al., 2021; Peng et al., 2018).

1.10 α-syn endocytosis

The next important question in the propagation of α-syn is how it is internalized into the cell (Figure 1.8). For many years, researchers believed that Clathrin-mediated endocytosis (CME) was involved in the uptake of α-syn (Hoffmann et al., 2019; Liu et al., 2007; Oh et al., 2016; Samuel et al., 2016; Shearer et al., 2021), with some papers even proposing that the internalization mechanism is receptor-mediated, the most known and somewhat controversial receptor being Lymphocyte-activation gene 3 (Emmenegger et al., 2021; Mao et al., 2016). Although some papers are very careful to differentiate between dynamin-mediated internalization and CME (Masaracchia et al., 2018), most papers conflate dynamin-mediated inhibition of α-syn uptake to also suggest that α-syn internalization occurs through CME. As we discussed in our previous paper (Bayati et al., 2022), dynamin inhibition can affect multiple endocytic pathways (Henley et al., 1998; Krueger et al., 2003; Mulherkar et al., 2011; Oh et al., 1998; Schlunck et al., 2004). Additionally, inhibitors such as Dynasore and Pitstop have many off-target effects (Park et al., 2013; Willox et al., 2014), making them a suboptimal option for selective inhibition of cargo internalization. Multiple other pathways for α-syn internalization have been proposed such as the macrophage-specific phagocytosis (Du et al., 2018), lipid raft-mediated endocytosis (Park et al., 2009), and

caveolae-dependent internalization (Kawahata et al., 2021). The lack of specific inhibitors, the employment of silencing technology to inhibit CME directly, and the various pathways suggested in the internalization of α-syn, led us to study this process ourselves (Bayati et al., 2022).

1.11 α-syn macropinocytosis

Previously, very few papers discussed the macropinocytic entry of α-syn, with only one paper showing that macropinocytosis may play a role (Holmes et al., 2013), while another paper reported the ability of α-syn to induce membrane ruffling but its internalization was not inhibited by EIPA (Zeineddine et al., 2015), a macropinocytic inhibitor. Much of the confusion arises from the many different forms of α-syn used to study its internalization (i.e., monomeric, oligomeric, protofibril, and fibril), and the lack of specific cell biological assays to assess internalization. Using the genetic approach of Clathrin heavy chain knockdown, coupled with following α-syn internalization via electron microscopy (EM) we found no evidence for CME as it pertains to α-syn preformed fibrils (PFFs) uptake (Bayati et al., 2022). Actin-mediated membrane ruffling, the recruitment of Rac1, and the engulfment of α-syn PFFs by membrane ruffles captured via EM, provide convincing evidence for the macropinocytic uptake of PFFs. Since publishing our findings, others have corroborated our results in other studies (Hivare et al., 2022).

1.12 α-syn exocytosis

Another area of research regarding α-syn propagation focuses on its exocytosis. One hypothesis suggests that membrane leakage caused by cellular apoptosis or necrosis, results in the release of aggregate forms of α-syn, which are then available for uptake by neighboring cells

(Valdinocci et al., 2017). Others have suggested regulated pathways in which α-syn can be transported to other cells (Bieri et al., 2018). The apoptosis model of α-syn spread has remained less than convincing to us since *in vitro* α-syn overexpression and internalization models have rarely resulted in cellular apoptosis in our hands. Additionally, while degeneration is rampant in dopaminergic (DA) neurons of the SNc, this degeneration takes decades to occur, as does the onset of PD motor symptoms, while α-syn aggregates continue to spread during the prodromal period (Horsager et al., 2022; Klann et al., 2021).

Exosomal release of α-syn internalization has garnered the most support in the study of the intercellular transfer of α-syn aggregates (Danzer et al., 2012; Fussi et al., 2018; Guo et al., 2020; Kluge et al., 2022; Loov et al., 2016; Nakase et al., 2015). Still, a few have suggested that tunneling nanotubes may play a role in this process (Abounit et al., 2016; Dieriks et al., 2017; Grudina et al., 2019; Rostami et al., 2017). In our previous study of α-syn internalization and trafficking, we inquired into the exocytic transport of α-syn PFFs (Bayati et al., 2022). We observed that α-syn PFFs, previously internalized, are then transported to other cells via extracellular vesicles/exosomes, with α-syn PFFs residing on the surface of exosomes and not within their lumen. Furthermore, we found that internalization of α-syn exosomes was inhibited using the macropinocytic inhibitors, previously used to inhibit the initial internalization of PFFs into the cell, suggesting that α-syn aggregates may continue to play a role in their own propagation even after their internalization by cells, due to their position on the surface of exosomes. Table 1.2 contains a collection of previous publications that studied the internalization and/or intercellular transmission of α-syn.

1.13 Lysosomal membrane permeabilization

One aspect of α-syn propagation that has been difficult to ascertain is how do intercellularly propagating α-syn aggregates seed endogenous α-syn in their intercellular journey. A closer look into lysosomal membrane permeabilization and the recruitment of galectin-3, used as a marker for ruptured vesicles/vacuoles (Ray et al., 2010), has provided a potential answer (Jiang et al., 2017). Lysosomal membrane rupture can occur due to cellular stress (Gomez-Sintes et al., 2016). Although, we have not found PFFs alone to induce lysosomal leakage, others have (Dilsizoglu Senol et al., 2021; Freeman et al., 2013). This would allow the contents of lysosomes meeting cytosolic proteins, allowing α-syn aggregates to seed the aggregation of endogenous α-syn. Several papers have shown the mechanisms underlying lysosomal membrane permeabilization, and galectin-3 recruitment (Freeman et al., 2013). The only question left: how is this level of lysosomal dysfunction readily-induced, and how does it occur in the brains of PD patients. In our recent study (Bayati et al., 2023), we show direct evidence for the leakage of lysosomal contents, specifically PFFs, into the cytosol, caused by the combined exposure of α-syn PFFs and Interferon-gamma.

1.14 α-syn inclusions in synucleinopathies

The discussion regarding forms of α-syn, its endocytosis and propagation, are all important steps that lead to the eventual consequence of α-syn accumulation and aggregation in PD: formation of LBs. Whether α-syn, in its different forms, plays a mechanistic role in the initiation of LBs or are incorporated in LBs is debated; however, the presence of α-syn in LBs is not. α-syn has been found in LBs, repeatedly, since its original localization in LBs (M. G. Spillantini et al.,

1997). However, α-syn aggregation is not specific to PD and is present in other synucleinopathies, most notably Lewy body dementia (LBD), multiple system atrophy (MSA), and Krabbe disease (Jellinger, 2018; McKeith et al., 2004; Smith et al., 2014). In LBD, α-syn accumulates in LBs as in PD; however, LBD differs symptomatically from PD due to the initial neurodegeneration also occurring in the neocortex, rather than just the substantia nigra, as is the case in PD (Donaghy & McKeith, 2014; Jellinger & Korczyn, 2018; Lin & Truong, 2019). In MSA, α-syn accumulates in inclusions termed Papp-Lentos bodies (Jellinger & Lantos, 2010), which occur in mostly in glial cells. Krabbe disease, a rare case of infantile neurodegenerative disease, is a disease in which α-syn aggregation and inclusion formation occurs in infant brains (Hatton et al., 2022). Due to the prevalence of PD and LBD, LBs have garnered more attention than α-syn-positive inclusions occurring in other synucleinopathies; however, even in the case of LBs, the field is still lagging in understanding their structure, origin, and formation.

α-syn aggregates and inclusions look different across different synucleinopathies. This may be due to the different strains of α-syn aggregates that are formed. Environmental differences such as the presence of NaCl, have drastic effects on the aggregation of α-syn (Bousset et al., 2013). Cryo-EM and NMR structures of α-syn fibrils/filaments formed *in vitro* using patient aggregate seeds, have exemplified how different α-syn aggregates can be. Four examples of the different *in vitro* aggregates formed from different synucleinopathy seeds or using patient cerebrospinal fluid to feed α-syn aggregation, have been shown in Figure 1.9.

1.15 LB ultrastructure

For many years, the ultrastructural study of LBs yielded a unanimous observation: a proteinaceous inclusion, filled with filaments and aggregated proteins, most prominent of which was α-syn (M. Baba et al., 1998; Philip E. Duffy & Virginia M. Tennyson, 1965; Forno, 1996; Galloway et al., 1992; Kuzuhara et al., 1988). Although some evidence was presented for the incorporation of organelles in LBs (L. S. Forno & R. L. Norville, 1976; Gai et al., 2000; James H Soper et al., 2008), the paper by Shahmoradian et al. (2019) cemented the following findings and uncovered the true nature of LBs: LBs are composed of an organellar medley, filled with membranous and organelle fragments that also contains filamentous structures. This has dramatically changed our understanding regarding the structure of LBs and their origin. As opposed to LBs simply being aggregated proteins within the cytoplasm of neurons, they are now a collection of dysfunctional organelles, membrane fragments, filaments, and cytoskeletal structures. The scope of our understanding regarding then contents of LBs has changed, and with it, the understanding of the underlying mechanisms involved in the formation of LBs should also change.

1.16 Formation of LBs

Prior to James H Soper et al. (2008) and Shahmoradian et al. (2019), the process in which LBs were formed was simple: α-syn in the cytosol begins aggregation, due to mutation, increased expression, or some external factor, and the protein begins the process of LB formation; however, with the incorporation of membranes and organelles, the issue of LB formation is now more complex. Still, the majority opinion in the field is that LB formation occurs as a function α-syn fibrilization (Lashuel, 2020): through its fibrilization, α-syn associates with a multitude of membranes and organelles during its fibrillization, brings together a plethora cellular components,

and packages them into an inclusionary body (Figure 1.10). However, that hypothesis would entail that fibril forms of α-syn be readily found in LBs, during their formation and following their maturation, as they are the driving force behind the formation of LBs. However, Shahmoradian et al. (2019) pointed out the relative absence of fibrils in their isolated LBs.

In our recent study (Bayati et al., 2023), we characterize the formation of LB-like inclusions that are membrane-enclosed. In the formative stages of inclusion formation, there are no signs of fibrils, and the "mini-inclusions" consists mainly of dark, aberrant lysosomes. Fibrils and filaments are incorporated into these structures at later stages. This finding suggests that α-syn fibrillization is not the driving force behind LB formation. Our membrane-bound inclusions continued to mature through incorporation of more and more organelles including mitochondria, endoplasmic reticulum, lysosomes, and neurofilaments, resulting in similar structures as those shown by Shahmoradian et al. (2019). A model of the possible mechanism by which our LB-like inclusions formed is illustrated in Figure 1.11.

In recent years, a few papers have attempted to form LB-like inclusions *in vitro*, and each have been able to recapitulate different characteristics of LBs. Table 1.3 lists studies that included an ultrastructural study of their LB-like inclusions.

1.17 LBs: neurotoxic or neuroprotective

If LBs are the result of α-syn fibrillization, and α-syn's need to aggregate, then the formation of inclusions such as LBs occur in a cell-autonomous manner: α-syn aggregates bind and tether organelles as they continue aggregation, which lead to cytosolic LBs (Figure 1.10). This would most likely make LBs neurotoxic, as the sequestration of organelles, inhibiting the transport of enzymes, proteins, and RNAs to and from them, would result in impaired mitochondria

releasing cytochrome c and leaky lysosomes releasing hydrolases into the cytosol (Nagakannan et al., 2020; Ott et al., 2007; Rocha et al., 2018; Tait & Green, 2008; Van Opdenbosch & Lamkanfi, 2019; Zhu et al., 2020). The fibrillization of α-syn would therefore not only cause the formation of inclusions, but would lead to Caspase-mediated cell death, necrosis, and apoptosis.

If LBs are formed not by the fibrillization of α-syn, but through the cell's attempt to sequester aggregates and damaged organelles, clearing them from the cytosol, this would make LBs neuroprotective, protecting the host neuron from the deleterious releases of damaged organelles, protein misfolding, and aggregation. If LBs are formed through cell-mediated processes, this can only be accomplished through an aggresomal response (Olanow et al., 2004; Tanaka et al., 2004), or through autophagic uptake of damaged organelles and protein aggregates. The former would result in the formation of inclusions with a somewhat impermeable cytoskeletal cage (Johnston et al., 1998), while the latter would result in the formation of gigantic autophagosomes, that could not degrade the contents in their lumen due to lysosomal defect (Button & Luo, 2017), but could at least recognize and sequester protein aggregates and damaged organelles and clear them from the cytosol (Figure 1.11).

1.18 Contents of LBs

Consistent among previous research, LBs were described as collection of fibrillar and filamentous materials. With the new ultrastructural information that has been described by Shahmoradian et al. (2019), organelles such as lysosomes, autolysosomes (double membrane), mitochondria, cytoskeletal/filamentous materials, and vesicles are all present in LBs. Despite their unprecedented insights into LBs, Shahmoradian et al. (2019) were not the only ones to report the incorporation of cellular organelles in LBs (L. S. Forno & R. L. Norville, 1976; Gai et al., 2000;

James H Soper et al., 2008). In fact, James H Soper et al. (2008) published some of the most clear electron micrographs of LBs known to date. However, all of these previous studies were limited to the resolution afforded to them by post-mortem tissues; hence, much more information about the ultrastructural nature of LBs is yet to be unearthed, using *in vitro* 2D and 3D models or perhaps through culturing of post-mortem sections, allowing neurons to recover prior to fixation (Verwer et al., 2002).

1.19 LBs and lysosomal proteins

As mentioned previously, the main question in PD and DLB is whether LBs are part of the pathophysiology of these diseases, or a by-product/symptom of their pathophysiology. Some have suggested that LBs are the result of an aggresomal response, resulting from the accumulation of proteins (Olanow et al., 2004; Wakabayashi et al., 2013). This response is indicative of impaired autophagy and dysfunctional degradation by lysosomes. Supporting this hypothesis, others have posed the idea that PD is a type of lysosomal storage disorder (Klein & Mazzulli, 2018), and recent research have implicated multiple lysosomal proteins as playing a role in PD such as TMEM175 (Jinn et al., 2017; Krohn et al., 2020; Palomba et al., 2023; Wie et al., 2021), GBA (Alcalay et al., 2015; Gan-Or et al., 2019; Gan-Or et al., 2018; Kim et al., 2018; Lwin et al., 2004; Sidransky et al., 2009), LAMP1 (Cheng et al., 2018; Rahmani et al., 2022; Sjodin et al., 2019), and LAMP2 (Alvarez-Erviti et al., 2010; Malkus & Ischiropoulos, 2012; Murphy et al., 2015; Sala et al., 2016). LAMP2A, the lysosomal membrane protein responsible for CPA (Bandyopadhyay et al., 2010), is hypothesized to be involved in maintaining α-syn homeostasis (i.e., controlling α-syn concentration) under physiological conditions (Xilouri et al., 2016), since impaired CPA and downregulation of LAMP2 has not only been reported in PD (Alvarez-Erviti et al., 2010; Sala et

al., 2016) but has also been associated with higher α-syn levels in *in vivo* models (Malkus & Ischiropoulos, 2012). Moreover, LAMP2 is also responsible for autophagy-lysosomal fusion (Eskelinen, 2006; Eskelinen et al., 2002), and therefore critical for the degradation of contents accumulating in autophagosomes. Lastly, misfolded, and aggregated forms of α-syn that form in the cytosol lead to the disruption of the LAMP2A translocation pore, through altering its structure, inhibiting CPA (Xilouri et al., 2016). Thus, LAMP2 is responsible for controlling α-syn levels in the cell to prevent aggregation, its expression is associated with lower α-syn levels, but α-syn aggregates can disrupt its function, causing a buildup of cytosolic α-syn.

Other lysosomal-related proteins such as TMEM106B (Schweighauser et al., 2022), TFEB (Cortes & La Spada, 2019; Decressac et al., 2013; Gu et al., 2022; Martini-Stoica et al., 2016), and NRF2 (Abokyi et al., 2020; Gan & Johnson, 2014; Rojo et al., 2017; Saha et al., 2021; Suzen et al., 2022; Zoungrana et al., 2022) have also been implicated in neurodegenerative diseases. TFEB is a master transcription factor encoding much of the proteins associated with lysosomal activity and biogenesis (Bajaj et al., 2019). NRF2 is involved in the cellular inflammasome response and also serves as a transcription factor for LAMP2 (Ahmed et al., 2017; Pajares et al., 2018), making NRF2 expression vital in preserving CPA and autophagosome-lysosomal fusion (Abokyi et al., 2020; Zhu et al., 2022). Its upregulation is associated with cellular antioxidative response. In sum, researchers studying neurodegeneration have come to understand and further explore the role of lysosomes in neurodegenerative diseases, especially in PD and AD; making the inclusions that form a symptom of the disease and not the disease-causing factor.

1.20 LBs and an immune challenge

Finally, it is important to note the most recent trend in the field of neurodegeneration: neuroinflammation. The involvement of the immune system and microglia in neurodegeneration has been in the zeitgeist (Cao & Zheng, 2018; Cao et al., 2013; Doty et al., 2015; Smith et al., 2012; Thakur et al., 2017; Zhang et al., 2005), but has recently received more attention (Berriat et al., 2023; DeMaio et al., 2022; Guo et al., 2020; Hammond et al., 2019; Hobson & Sulzer, 2022; Kasen et al., 2022; Mason & McGavern, 2022; Panagiotakopoulou et al., 2020; Tan et al., 2020), with its most staunch support stemming from a paper by Matheoud et al. (2019) in which researchers show that PINK1$^{-/-}$mice, notorious for not recapitulating PD-like neurodegeneration (Gispert et al., 2009; Hernandez et al., 2019; Kitada et al., 2007; McWilliams et al., 2018; Moisoi et al., 2014; Zhi et al., 2019), experience Parkinsonism and neurodegeneration only after the introduction of gastrointestinal bacteria. Their research suggests, that although the PINK1$^{-/-}$ mutation (a PD insult) is present in the mice, it takes an external factor, a gastrointestinal infection and associated immune system activity, to initiate the onset of PD motor symptoms. Other papers have also come to similar conclusions in other neurodegenerative diseases, such as a recent work published by Burberry et al. (2020), focusing on the role of the immune system in amyotrophic lateral sclerosis mice models. The potential involvement of proinflammatory cytokines in neurodegeneration (Ahmadi Rastegar et al., 2022; Panagiotakopoulou et al., 2020), coupled with research further popularizing the possible infiltration of immune cells into the brain (Yang et al., 2020; Zhang et al., 2022), has resulted in another viewpoint in neurodegenerative research. This has culminated into researchers' increased awareness of microglia and the immune system's role in neurodegeneration.

Data collected in our most recent work on observing the formation of LB-like inclusions in vitro (Bayati et al., 2023), involves a treatment regime, resulting in the formation of LB-like inclusions in DA neurons exposed to IFN-gamma (IFN-γ). In the absence of this dual hit treatment regime, internalized exogenous α-syn PFFs remain within lysosomes and MVBs, maintaining their punctate fluorescence. Neurons that are exposed to IFN-γ, on the other hand, exhibited diffuse PFF fluorescence and underwent the process of forming large PFF-positive aggregates. By EM, these PFF-positive aggregates were full of organelles and filaments, resembling the organelle-filled LBs previously reported (Shahmoradian et al., 2019; James H Soper et al., 2008). A summary of our dual hit hypothesis is illustrated in Figure 1.12. Our findings cement the dual hit treatment as a possible pathway for the formation of LBs, the pathological hallmark of PD.

1.21 Figures

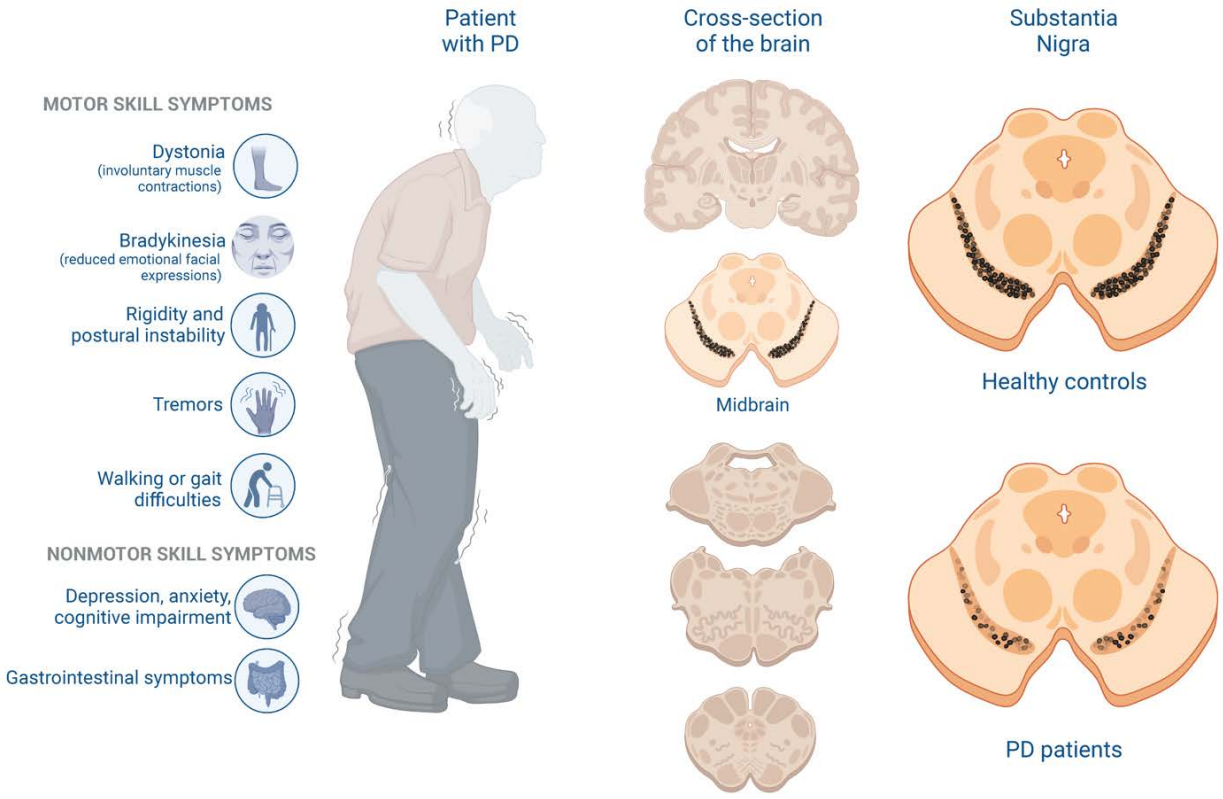
Patient with PD
Cross-section of the brain
Substantia Nigra
MOTOR SKILL SYMPTOMS
Dystonia
(involuntary muscle contractions)
Bradykinesia
(reduced emotional facial expressions)
Rigidity and postural instability
Tremors
Walking or gait difficulties
NONMOTOR SKILL SYMPTOMS
Depression, anxiety, cognitive impairment
Gastrointestinal symptoms
Midbrain
Healthy controls
PD patients

Figure 1.1 Symptoms and pathology of PD

The onset of PD in patients is marked by the appearance of the Parkinsonian motor symptoms which include dystonia, bradykinesia, rigidity, postural instability, resting tremors, and walking/gait difficulties. Accompanying these motor symptoms are a multiple nonmotor symptoms including depression, anxiety, cognitive impairment, gastrointestinal symptoms and more. The presence of the motor symptoms in PD are marked by the loss of dopaminergic neurons of the substantia nigra, located in the midbrain. While healthy patients show many pigmented cells in this region, PD patients show a loss of these cells.

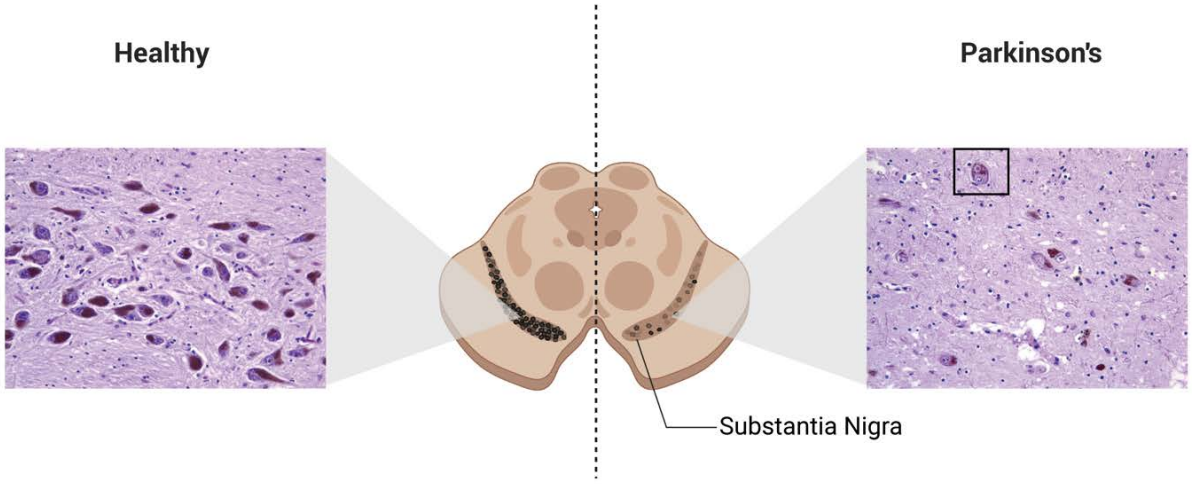
Healthy vs. Parkinson's
Healthy
Parkinson's
Substantia Nigra

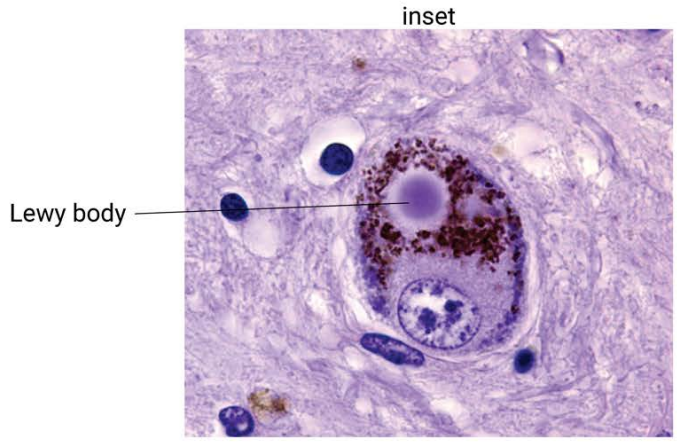
inset
Lewy body

Figure 1.2 Immunohistology samples show the loss of pigmented DA neurons in the SNc

Healthy patients show a high density of the melanin-filled DA neurons in the substantia nigra, while PD patients exhibit the loss of cells in this region. Upon a closer look, many of the remaining DA neurons in PD patients show a structure similar to what is shown in the inset: a larger than normal neuron containing a Lewy body. Histological images were retrieved from https://neuropathology-web.org/.

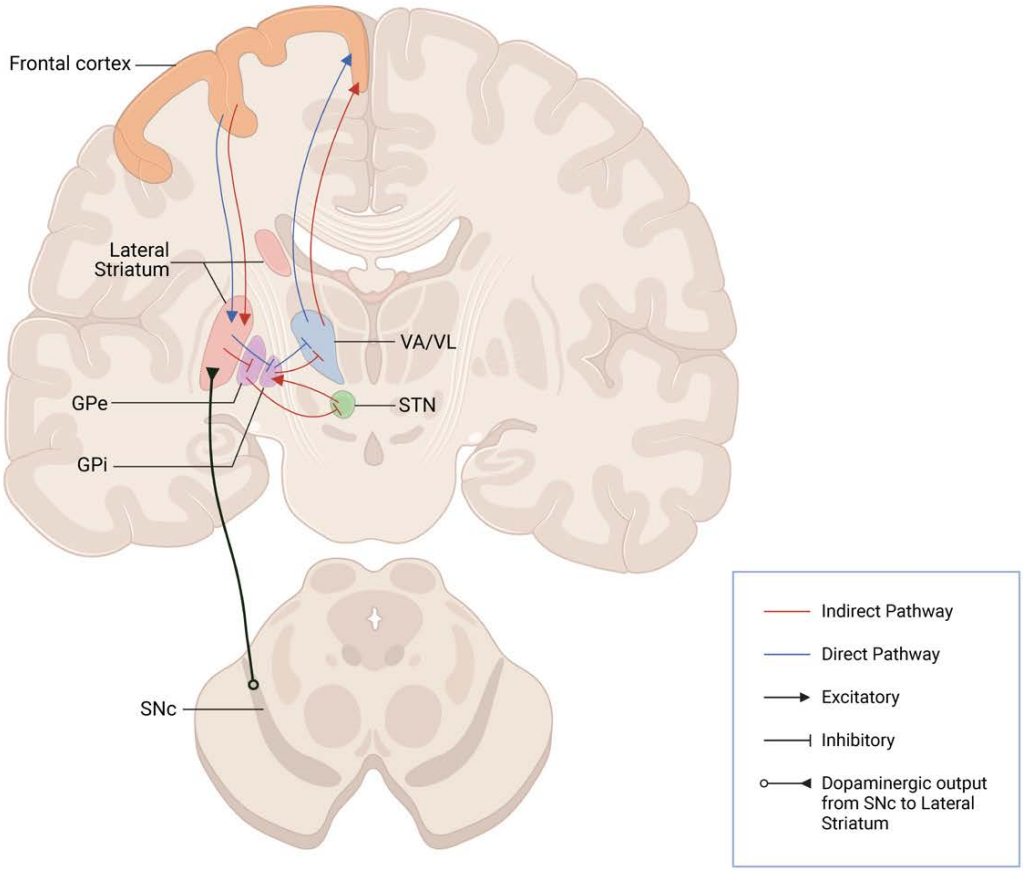
Frontal cortex
Lateral Striatum
VA/VL
GPe
STN
GPi
SNc
Indirect Pathway
Direct Pathway
Excitatory
Inhibitory
Dopaminergic output from SNc to Lateral Striatum

Figure 1.3 The downstream effects of the SNc's dopaminergic output into the basal ganglia

DA neurons of the substantia nigra release dopamine to stimulate and inhibit nuclei located in the lateral striatum, which include the caudate and the putamen. Both pathways require DA input from the SNc to appropriately modulate planning and selection of motor actions.

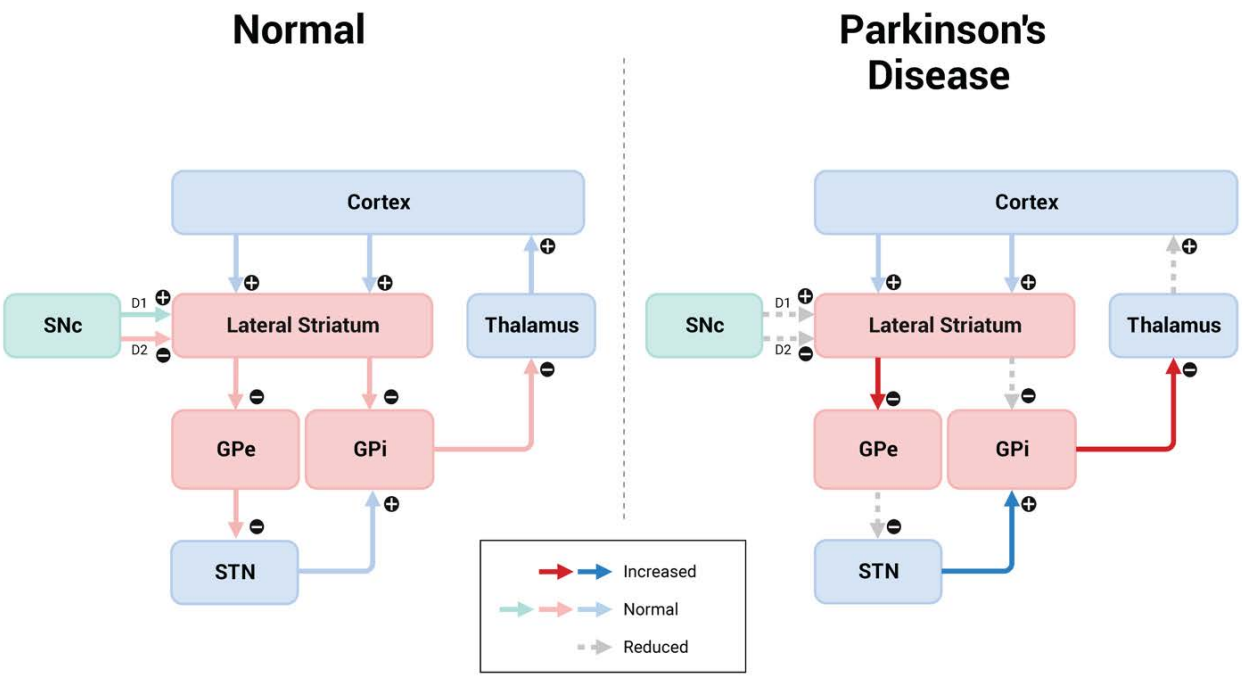
Normal
Parkinson's Disease
Cortex
SNc
D1
D2
Lateral Striatum
Thalamus
GPe
GPi
STN
Increased
Normal
Reduced

Figure 1.4 Consequences of Parkinson's disease on the basal ganglia pathways

With adequate DA stimulation of the lateral striatum, neurons with D1 and D2 receptors, both the direct and indirect pathways that modulate the planning and selection of movement, respectively, are carried out by the basal ganglia. In short, the loss of dopaminergic input results in decreased activity of the direct pathway, and the increased activity of the indirect pathway, which all culminates in the lack of thalamic input to the motor cortex.

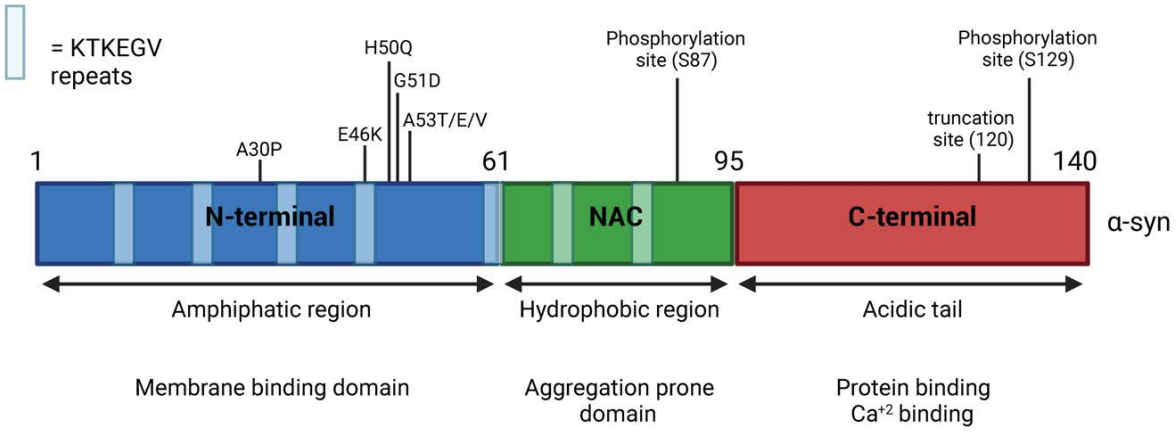
= KTKEGV repeats
H50Q
G51D
A53T/E/V
E46K
A30P
Phosphorylation site (S87)
Phosphorylation site (S129)
truncation site (120)
1
61
95
140
N-terminal
NAC
C-terminal
α-syn
Amphiphatic region
Hydrophobic region
Acidic tail
Membrane binding domain
Aggregation prone domain
Protein binding
Ca+2 binding

Figure 1.5 α-syn protein structures containing mutation sites, phosphorylation sites, and labelled domains

α-syn, 14 kDa protein with 140 amino acids, contains three domains: Membrane binding domain, the NAC region, and the protein binding domain. The membrane binding domain which is on the N-terminal side of the protein contains most of the KTKEGV (imperfect) repeats that aid in membrane binding. The NAC domain is the hydrophobic region that is critical for the aggregation of α-syn monomers. The C-terminal contains the protein-binding domain, that also includes the most widely known phosphorylation site: serine 129. Familial PD caused by mutations in *SNCA,* translate to the variants detailed in the membrane binding region of the protein. These mutations include: A53T, A53E, A53V, A30P, H50Q, G51D and E46K. H50Q and A53T are best known for their rapid aggregation ability.

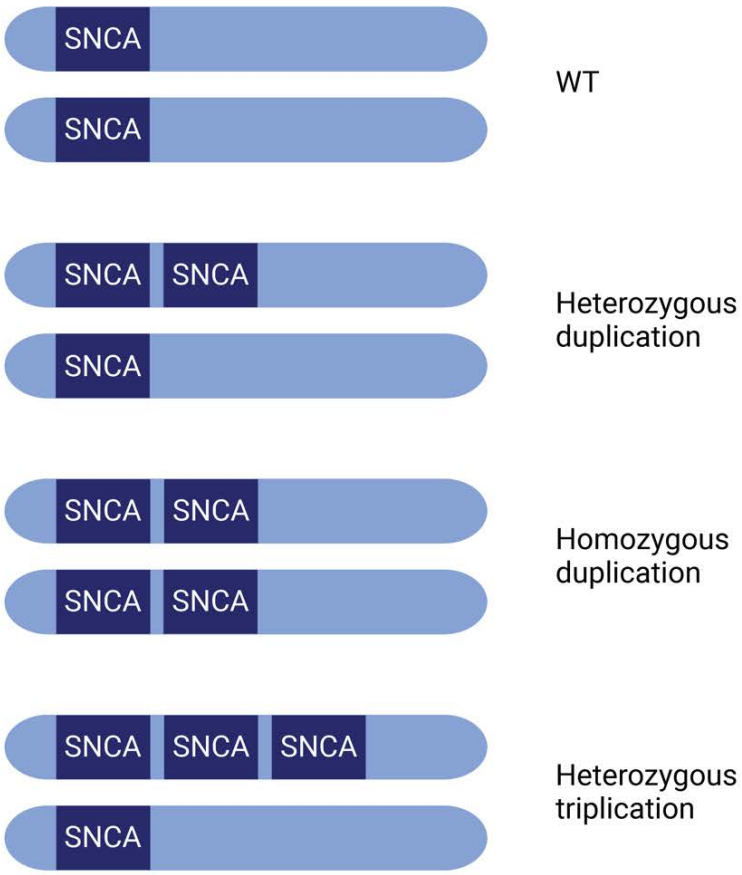
SNCA
SNCA
WT
SNCA
SNCA
SNCA
Heterozygous duplication
SNCA
SNCA
SNCA
SNCA
Homozygous duplication
SNCA
SNCA
SNCA
SNCA
Heterozygous triplication

Figure 1.6 *SNCA* multiplication schematic

Patients with familial cases of PD, due to multiplication of the *SNCA* locus, have one additional copy of the *SNCA* gene compared to WT, when an extra copy is inherited from one parent (i.e., heterozygous duplication). In cases where additional copies of the gene are inherited from both parents, patients have two additional copies of the *SNCA* gene. Such cases are referred to as homozygous duplication. Finally, patients that are known to have a heterozygous triplication of the *SNCA* gene, inherited three copies of the *SNCA* gene from one parent, and inherited only one copy of the *SNCA* gene from another parent. Theoretically, homozygous duplication and heterozygous triplication should express similar amounts of α-syn, but epigenetic factors and allele preferences creates a lot of variety in protein expression. Both homozygous duplication and heterozygous triplication are associated with earlier onset of PD.

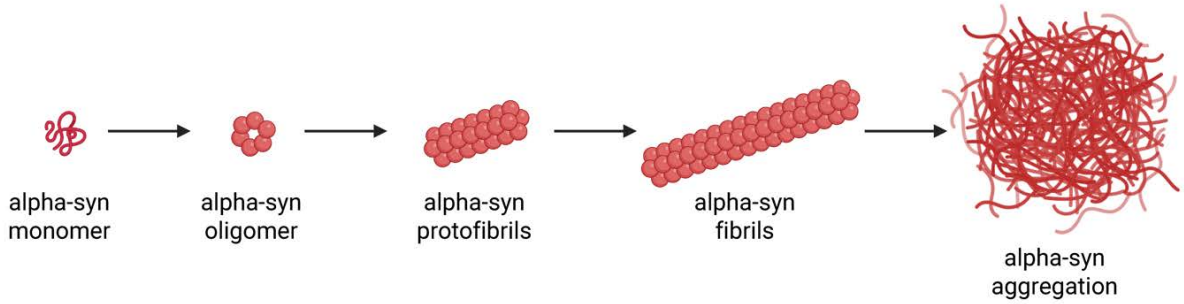
alpha-syn
monomer
alpha-syn
oligomer
alpha-syn
protofibrils
alpha-syn
fibrils
alpha-syn
aggregation

Figure 1.7 The forms of α-syn through its aggregation journey

α-syn monomers have been shown to aggregate into oligomers and protofibrils prior to their fibrillization. Protocols have been established for the generation of oligomeric and protofibril α-syn, along with protocols to produce full-length fibrils (larger than 100 μm) or preformed fibrils (smaller than 100 μm), usually made from the sonication of full-length fibrils into smaller chunks. With enough time, α-syn fibrils have been shown to form aggregates *in vitro*.

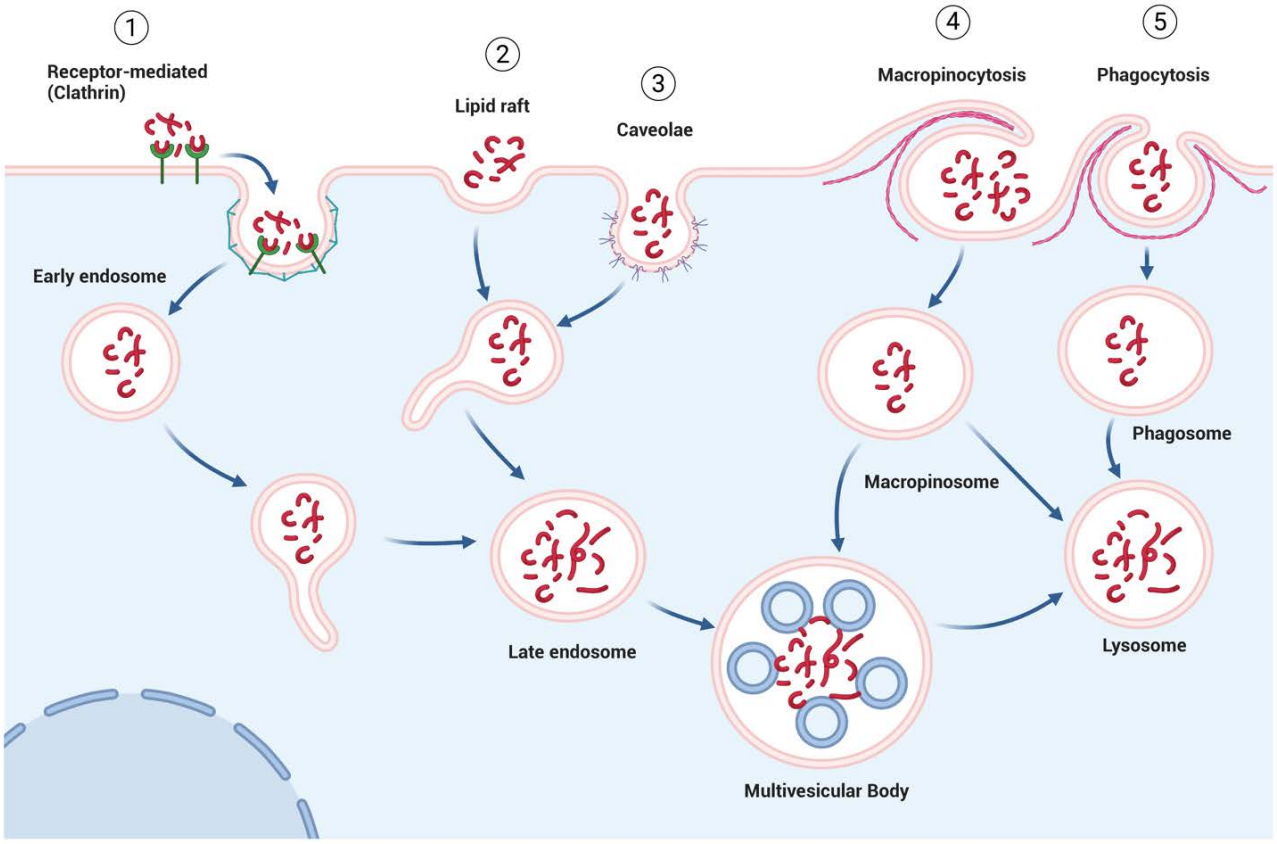
1
Receptor-mediated
(Clathrin)
2
Lipid raft
3
Caveolae
4
Macropinocytosis
5
Phagocytosis
Early endosome
Late endosome
Macropinosome
Phagosome
Lysosome
Multivesicular Body

Figure 1.8 α-syn internalization pathways

Multiple pathways have been proposed for the internalization of α-syn monomers, oligomers, and fibrils. Here we illustrate five of the most reported pathways: receptor-mediated (CME), lipid raft, caveolae, macropinocytic, and phagocytic internalization pathways. Cargo internalized through CME, lipid raft, and caveolae, all go through the endosomal system, undergo endosomal maturation, and are then transported to lysosomes. Although traditional macropinocytosis also colocalizes with markers of early endosomes and late endosomes, the type of macropinocytic pathway discovered by us did not undertake this maturation, therefore, cargo within macropinosomes is quickly transported to lysosomes. Finally, phagocytosis, an internalization mechanism specific to macrophages, has been shown to take up α-syn, be transported into phagosomes, and eventually be transported to lysosomes. Conventional phagocytic internalization also colocalizes with markers of early endosomes and undergoes maturation prior to reaching lysosomes.

PDB	Top View	Side View
7NCA	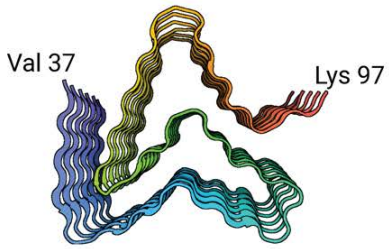	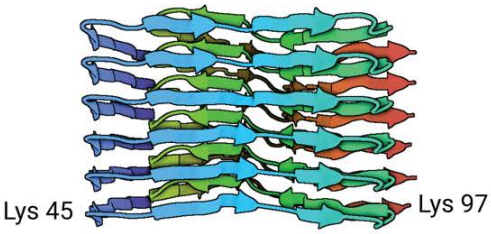
8CYV	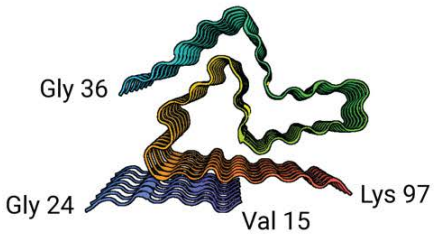	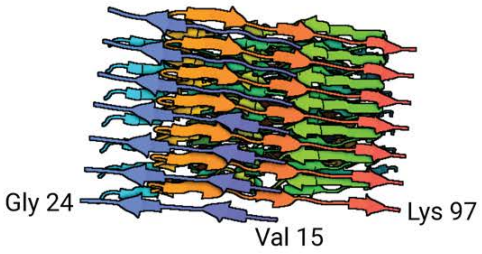
7V49	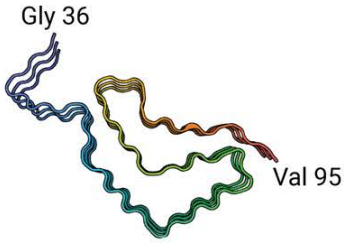	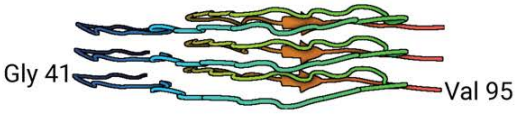
8BQV	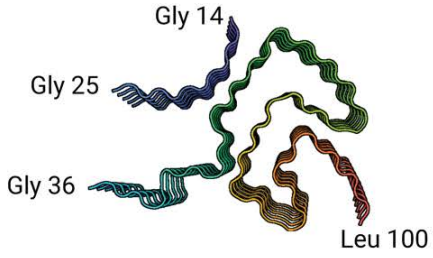	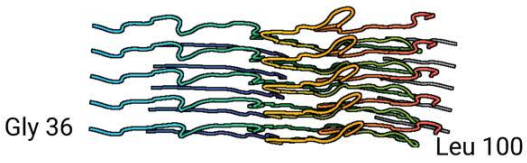

Figure 1.9 α-syn aggregates in different synucleinopathies

Structures of α-syn fibrils and filaments, seeded *in vitro* or isolated from brains, were resolved using Cryo-EM. The protein data bank (PDB) number for each structure is listed. The structure in 7NCA, was assembled using an MSA seed, incubated with recombinant α-syn. This structure was resolved by Lovestam et al. (2021). 8CYV, shows the resolved structure of α-syn fibrils amplified using CSF from a DLB case, resolved by Sokratian et al. (2022). 7V49, shows an α-syn fibril seeded by CSF of a PD patient (Fan et al., 2023). 8BQV, shows the structure of α-syn filament from Juvenile-onset synucleinopathy (Yang et al., 2023). Although α-syn is the building block of all these aggregates, the distinct fibril/filamentous structures of these indicates some of the, yet unknown, factors that lead to distinct strains of α-syn aggregates, with distinctly different folds, twists, and stabilization.

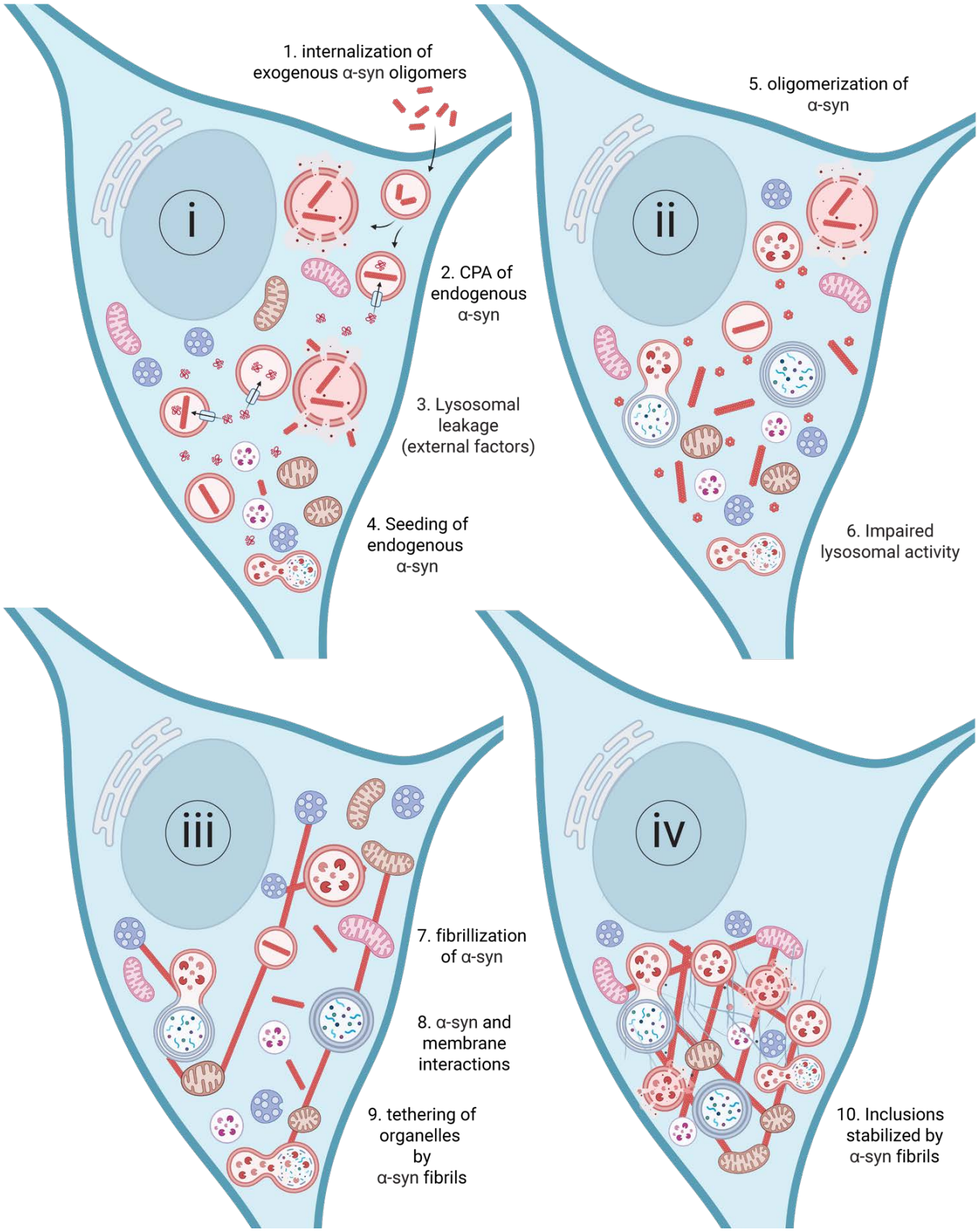
1. internalization of exogenous α-syn oligomers
i
2. CPA of endogenous α-syn
3. Lysosomal leakage (external factors)
4. Seeding of endogenous α-syn
5. oligomerization of α-syn
ii
6. Impaired lysosomal activity
iii
7. fibrillization of α-syn
8. α-syn and membrane interactions
9. tethering of organelles by α-syn fibrils
iv
10. Inclusions stabilized by α-syn fibrils

Figure 1.10 Model for the formation of LBs through fibrillization of α-syn

Internalization of PFFs and their accumulation in lysosomes (1), is followed by the introduction of cytosolic α-syn into lysosomes through CPA (2), initiating the first steps of endogenous α-syn aggregation. Lysosomal stress caused by α-syn accumulation and aggregation, both from the cytosol and PFFs, and potentially external factors, lead to lysosomal membrane permeabilization which leads to lysosomal leakage (3). Aggregated α-syn then gain access to the cytosol and seed the aggregation of endogenous α-syn (4 and 5). Impaired lysosomal activity is then exacerbated by aggregated forms of α-syn blocking the CPA pore, composed mostly of LAMP2A, leading to further accumulation of monomeric α-syn (6). Fibrillization of α-syn continues and α-syn aggregates begin to associate with different organelles through membrane and protein interactions (7-9). α-syn fibrils then act as tethers and form a cytoplasmic inclusion, eventually maturing into LBs (10).

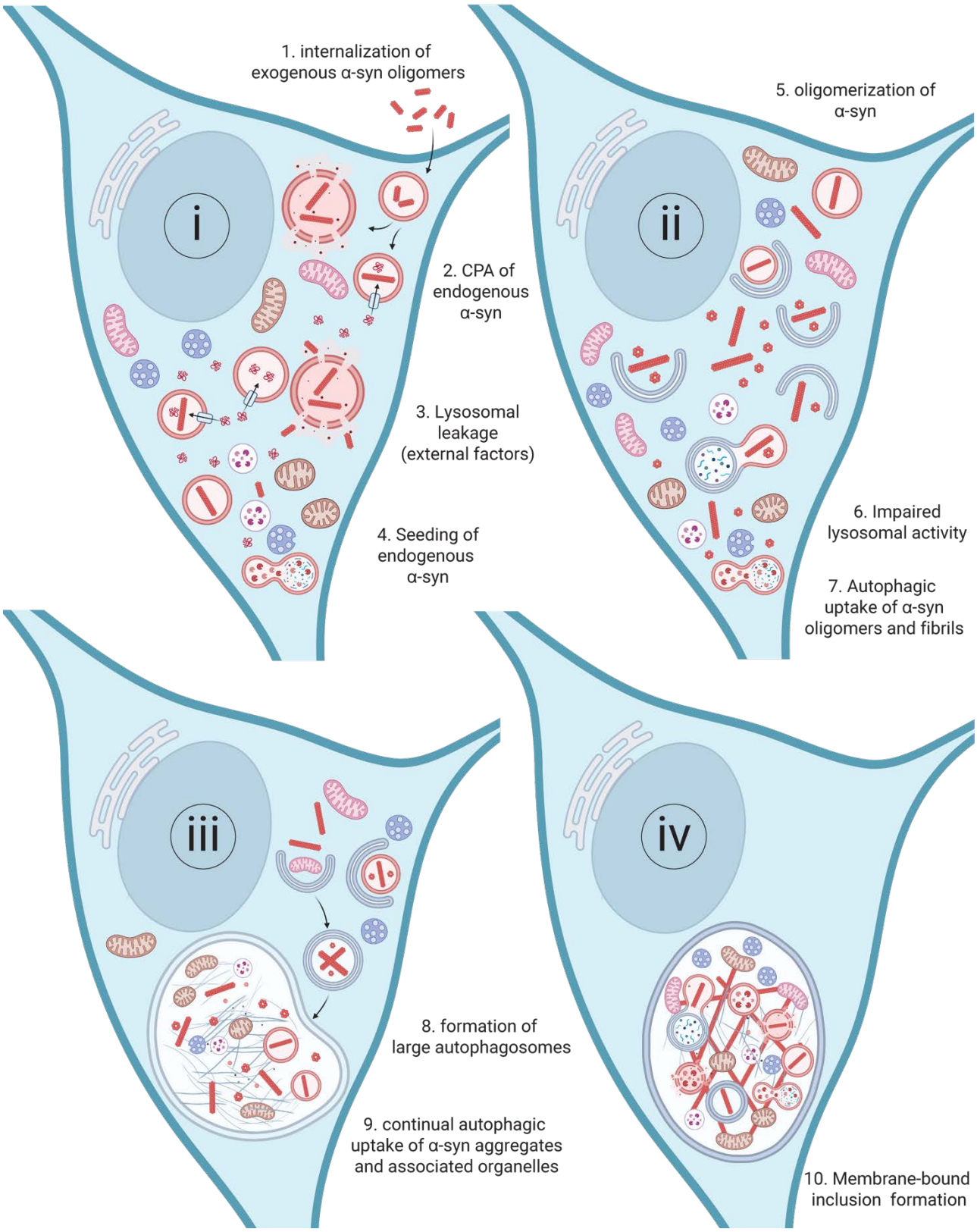
1. internalization of exogenous α-syn oligomers
i
2. CPA of endogenous α-syn
3. Lysosomal leakage (external factors)
4. Seeding of endogenous α-syn
5. oligomerization of α-syn
ii
6. Impaired lysosomal activity
7. Autophagic uptake of α-syn oligomers and fibrils
iii
8. formation of large autophagosomes
9. continual autophagic uptake of α-syn aggregates and associated organelles
iv
10. Membrane-bound inclusion formation

Figure 1.11 Potential model for the formation of membrane-bound LBs

Formation of membrane-bound LBs can occur through the internalization of aggregate forms of α-syn, potentially coupled with an external factor (1). Endogenous α-syn, whose concentration is controlled by CPA then meets internalized PFFs in lysosomes, leading to α-syn aggregation occurring within lysosomes (2). Eventually, mounting lysosomal stress caused by PFFs (and potentially an external factor) leads to lysosomal membrane permeabilization (lysosomal leakage), leading to the leaking of PFFs into the cytosol (3). PFFs then seed the aggregation of endogenous α-syn (4 and 5). CPA is then impaired as aggregated and misfolded α-syn block the pores required in CPA (6). Autophagosomes attempt to clear aggregation and damaged/dysfunctional organelles through autophagic uptake (7). Due to impaired lysosomal activity, contents within autophagosomes are not degraded, and autophagosomes begin expanding in size as the sequestration of aggregates and organelles continues (8 and 9). Eventually, this leads to the formation of membrane-bound LB inclusions (10). This model was adapted from Bayati et al., (2023).

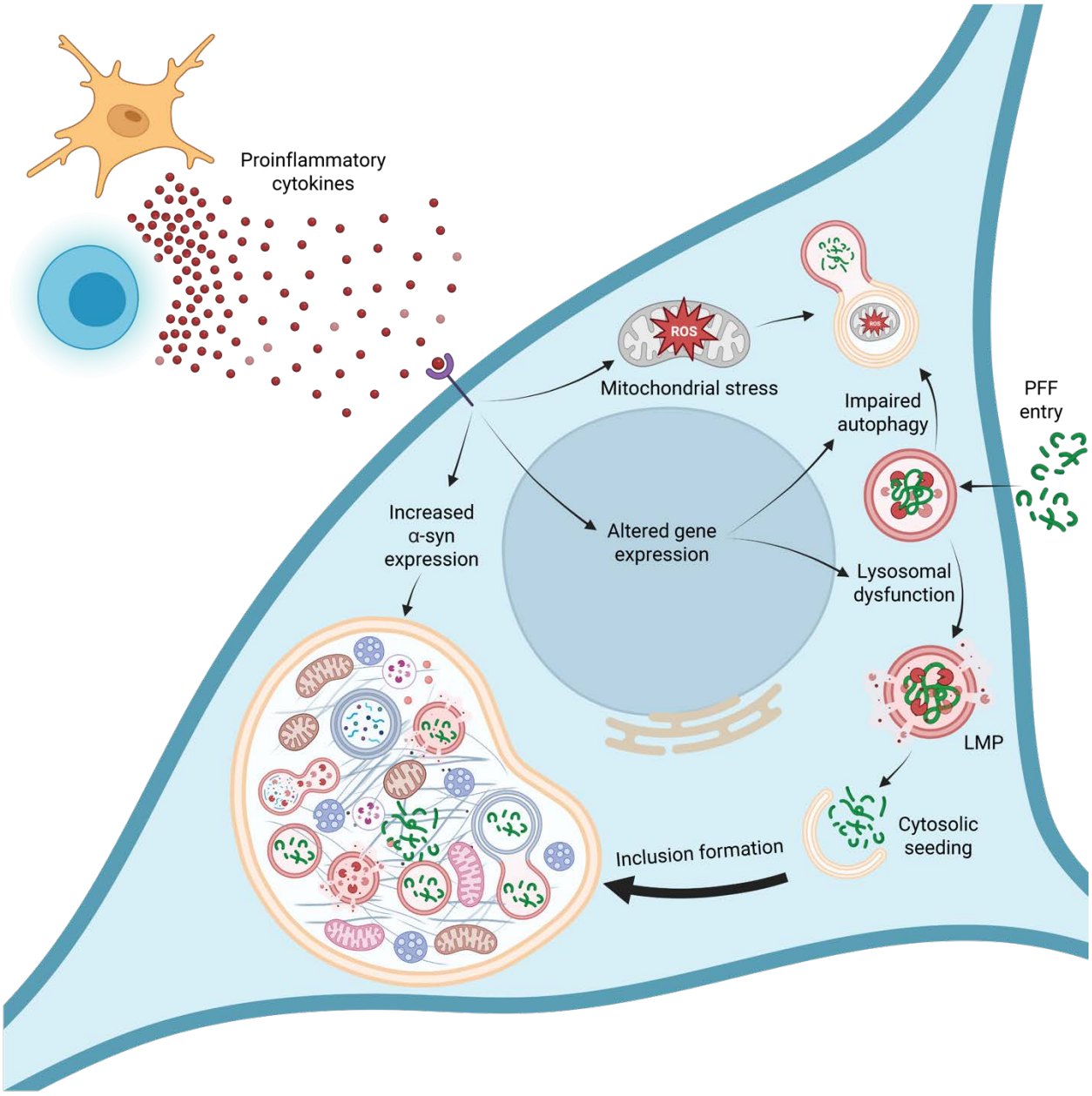
Proinflammatory cytokines
ROS
Mitochondrial stress
Impaired autophagy
PFF entry
Increased α-syn expression
Altered gene expression
Lysosomal dysfunction
LMP
Cytosolic seeding
Inclusion formation

Figure 1.12 Model of LB-like inclusion formation through a dual hit treatment regime

Internalization of an aggregate form of α-syn, coupled by exposure to proinflammatory cytokines (released by microglia or T-cells), results in two different pathways that work to stress the cell. PFF internalization (a PD insult), results in lysosomal stress, and their occupation of lysosomes results in impaired degradative activity in the cell. The introduction of proinflammatory cytokines result in the activation of immune-related pathways in the cell that lead to the alteration of gene expression. Downregulation of lysosomal proteins result in exacerbating lysosomal dysfunction. Proinflammatory cytokines also lead to the rise of oxidative stress and elevated expression of endogenous α-syn in the cell. The combination of PFF accumulation in lysosomes, altered gene expression, and oxidative stress, leads to lysosomal membrane permeabilization and the leaking of PFFs into the cytosol. PFFs gain access to the cytosol and seed the aggregation of endogenous α-syn. Autophagosomes attempt to clear aggregation and dysfunctional organelles, but they cannot be due to impaired lysosomal activity. This leads to the formation of membrane-bound LB-like inclusions. This model was adapted from Armin Bayati et al. (2023).

1.22 Tables

Table 1.1 Physiological functions of α-syn

Function of α-syn	Reference
Involved in synaptic vesicle exocytosis, through modulating the assembly of the SNARE-complex	(Burre et al., 2010)
Detection and formation of membrane curvature	(Westphal & Chandra, 2013)
Highly abundant and localized to the synaptic bouton	(Wilhelm et al., 2014)

Attenuates neurotransmitter release and synaptic vesicle clustering	(Wang et al., 2014)
Regulation of synaptic vesicle endocytosis	(Vargas et al., 2014)
Tethering of synaptic vesicles, determinant of synaptic size, and involved in synaptic vesicle clustering	(Vargas et al., 2017)
Interaction with endocytic trafficking, retromer complex, and mRNA binding proteins	(Chung et al., 2017)
Association with calcium allow for synaptic vesicle binding at the C-terminal	(Lautenschlager et al., 2018)
Modulation of exocytosis, binding to membranes, association with mitochondria	(Ramezani et al., 2019)
Enables endocytosis through upregulation of phosphatidylinositol 4,5-bisphosphate, mutations alter Clathrin-mediated endocytosis	(Schechter et al., 2020)
Modulation of dopamine release in substantia nigra neurons – in an action potential related manner	(Somayaji et al., 2020)
Regulation of cellular iron homeostasis	(Bi et al., 2020)
Docking of synaptic vesicles to the presynaptic membrane through lipid links	(Man et al., 2021)
Involved in Clathrin assembly	(Vargas et al., 2021)
Regulation of Iron metabolism	(Shekoohi et al., 2021)
Modulates processing bodies along with mRNA stability	(Hallacli et al., 2022)

Table 1.2 Internalization and intercellular transfer of α-syn.

Findings	Reference
Rab5A-mediated uptake of monomeric α-syn was observed.	(Sung et al., 2001)
Cytochalasin D treatment led to decreased fibril α-syn uptake in microglia.	(Zhang et al., 2005)
Co-immunoprecipitation of Clathrin and α-syn aggregates; colocalization of aggregated α-syn with Clathrin in microglia.	(Liu et al., 2007)
Microglia can internalize and degrade α-syn aggregates; accumulation occurred upon activation of microglia.	(H.-J. Lee et al., 2008)
Internalization of α-syn fibrils was inhibited by low temperature and dynamin dominant-negative. Monomeric α-syn entered cells through diffusion and colocalized with EEA1 and LAMP2.	(H. J. Lee et al., 2008)
Internalization of α-syn monomers not inhibited with dynamin dominant-negative nor with Dynasore, but lipid-raft mediated.	(Park et al., 2009)

α-syn transmission was inhibited with the use of dynamin dominant-negative; using an endogenous expression model.	(P. Desplats et al., 2009)
α-syn endocytosis was inhibited in cells expressing dynamin dominant-negative; using an endogenous expression model.	(Lee et al., 2010)
α-syn endocytosis and transfer occur in a dynamin-dependent manner.	(Hansen et al., 2011)
Monomeric α-syn endocytosis was decreased by inhibiting dynamin GTPases.	(Konno et al., 2012)
Intercellular transfer of α-syn from rat brain to graft DA neurons. The transferred α-syn colocalize with EEA1. Non-aggregated forms of α-syn can transfer from host to graft.	(Angot et al., 2012)
Administered together, tau, TAT, and α-syn colocalize, indicating α-syn fibrils are internalized using macropinocytosis.	(Holmes et al., 2013)
Dynasore inhibited monomeric, oligomeric, and fibril α-syn uptake in a concentration-dependent manner.	(Reyes et al., 2014)
Monoclonal antibodies targeting α-syn inhibit its internalization and intercellular transfer.	(Tran et al., 2014)
α-syn fibrils induced membrane ruffling, but EIPA, a macropinocytic inhibitor, did not inhibit its internalization.	(Zeineddine et al., 2015)
Clathrin-mediated internalization of α-syn, using an endogenous expression model and intercellular transfer of α-syn. Colocalization of α-syn with EEA1, NR1, and NR2A.	(Oh et al., 2016)
Oligomeric α-syn's intercellular trafficking is elevated following knockdown of Rab8b and Rab13. Endocytic recycling of α-syn relies on Rab11a and Rab13; overexpression leads to increased secretion.	(Goncalves et al., 2016)
Dynamin is partially required for the uptake, but not the intercellular transfer of α-syn fibrils. Colocalization of the fibrils with LAMP1. Intercellular spread of α-syn relies on tunneling nanotubes.	(Abounit et al., 2016)
Inhibition of Clathrin-mediated endocytosis using Dynasore resulted in decreased uptake of α-syn fibrils and phospho-fibrils.	(Samuel et al., 2016)
LAG3 mediated endocytosis of α-syn PFF: receptor-mediated endocytosis. Colocalization with Rab5, Rab7, and LAMP1.	(Mao et al., 2016)
PFFs are transported through the endolysosomal pathway and colocalizes with LAMP1.	(Karpowicz et al., 2017)
DJ-1 knockdown reduces phagocytic uptake of soluble α-syn by microglia.	(Nash et al., 2017)
GGA3 contributes to endosomal oligomerization of α-syn and drives its secretion.	(von Einem et al., 2017)
Serine protease KLK6, along with proMMP2, can cleaves extracellular fibril α-syn, inhibiting its propagation. KLK6 deficient showed increased α-syn uptake.	(Pampalakis et al., 2017)
α-syn aggregates depend on heparan sulfate for internalization.	(Ihse et al., 2017)
In vivo injection of phosphorylated fibrils resulted in more toxicity and neuronal loss compared non-phosphorylated fibrils. S129 phosphorylation enhanced α-syn fibril uptake by neurons.	(Karampetsou et al., 2017)
Exosome associated-oligomeric α-syn does not rely on Heparan sulfate proteoglycans for internalization, and its internalization is much higher than naked α-syn oligomers.	(Delenclos et al., 2017)
α-syn monomers use dynamin-mediated endocytosis, colocalize with Rab4, 5, and 7. α-syn fibrils undertake a different pathway.	(Masaracchia et al., 2018)
Ubiquitin C-terminal hydrolase L1 is involved in the intercellular transmission of α-syn.	(Kang et al., 2018)
LAG3 and RAB5A found to be genetic predictors for regional brain atrophy. Highly expressing LAG3 regions of brain correlated with greater atrophy.	(Freeze et al., 2018)
FcγRIIB binds α-syn fibrils and mediated intercellular transmission through its signaling.	(Choi et al., 2018)
Oligomeric α-syn binding and colocalization with connexin-32, during its uptake. Expression of connexin-32 was linked to the intercellular transfer of α-syn. Inhibitors of connexin-32 reduce α-syn uptake.	(Reyes et al., 2019)
TRPML1 activation, resulted in the upregulation of lysosomal exocytosis, reducing the burden of α-syn accumulation.	(Tsunemi et al., 2019)

CME of aggregated α-syn: colocalization of α-syn with transferrin, EEA1, LAMP1, LAMP2, and Rab11. Aggregated α-syn shows higher cellular accumulation than monomeric α-syn.	(Hoffmann et al., 2019)
Rab27b is involved in the release and clearing of α-syn, using a doxycycline-inducible α-syn expression.	(Underwood et al., 2020)
Cellular entry of α-syn fibrils is facilitated through a myosin-7B-dependent pathway.	(Zhang et al., 2020)
Caveolae-dependent uptake of α-syn in dopaminergic neurons was observed.	(Kawahata et al., 2021)
Synaptic transmission of α-syn is bidirectional, mainly occurring in retrograde. Retrograde trans-synaptic uptake of α-syn occurred through an endophilin-independent manner.	(X. Wang et al., 2021)
α-syn fibrils are intercellularly transferred through tunneling nanotubes.	(Dilsizoglu Senol et al., 2021)
Large oligomers are dependent on Clathrin-mediated endocytosis and colocalize with early endosomes and lysosomes.	(Shearer et al., 2021)
LAG3 D1 and APLP1 E1 domains bind to α-syn's c-terminal. Phosphorylation of α-syn at S129, enhances its internalization.	(Zhang et al., 2021)
Sequestration of LC3 by mutated endogenously expressed α-syn, stresses the degradative/autophagy pathway, facilitating exocytosis of α-syn.	(Stykel et al., 2021)
α-syn PFFs were found to colocalize with Lysotracker.	(Jarvela et al., 2021)
Endogenously expressed α-syn undergoes caveolin-dependent endocytosis and colocalizes with EEA1 and Rab7.	(Fakhree et al., 2021)
Lysosomes release non-membrane-bound α-syn aggregates from neurons.	(Xie et al., 2022)
Heparan sulfate proteoglycans mediate α-syn PFFs toxicity. Knockdown of proteins responsible for heparan sulfate proteoglycan synthesis was protective against degeneration.	(Chen et al., 2022)
α-syn fibrils utilize actin-mediated macropinocytosis to be internalized into cells. No significant involvement of caveolae-mediated endocytosis and Clathrin-mediated endocytosis was found.	(Hivare et al., 2022)
α-syn PFFs use a rapid form of macropinocytosis to be internalized into cells and be transferred to lysosomes. PFFs are transported on the surface of exosomes to neighboring cells.	(Bayati et al., 2022)
Antibodies targeting the c-terminal of α-syn, block PFF uptake; decreased phospho-synuclein accumulation.	(Brendza et al., 2023)

Table 1.3 In vitro models of LB-like inclusions

Publication	Recapitulated characteristic of LBs	Structure of LB-like inclusions formed	Reference
Yamagishi et al., 2007	Ubiquitin-positive inclusions	Fibril containing, dense, proteinaceous inclusions	(Yamagishi et al., 2007)
Bedford et al., 2008	Ubiquitin, p62, and α-syn positive inclusions.	Inclusions include mitochondria, membrane-bound vesicles, autophagosome like structures, filamentous contents	(Bedford et al., 2008)

Luk et al., 2009	Ubiquitin, phospho-α-syn and thioflavin S positive inclusions	Proteinaceous aggregate with fibrillar α-syn	(Luk et al., 2009)
Mahul-Mellier et al., 2019	Phospho-α-syn positive inclusions	Cytoplasmic organellar medley	(Mahul-Mellier et al., 2020)
Trinkaus et al., 2021	α-syn-positive inclusions	α-syn fibrils crisscrossing organelles such as lysosomes, mitochondria, and MVBs.	(Trinkaus et al., 2021)
Jo et al., 2021	Halo-like α-syn staining in TH-positive neurons	LB-like core with fibrillar α-syn in the periphery	(Jo et al., 2021)
Lam et al., 2022	Ubiquitin, p62, α-syn positive inclusions	An organellar medley, containing vesicles, lysosomes, and filamentous materials.	(Lam et al., 2022)
Bayati et al., 2023	Phospho-α-syn positive inclusions with mitochondria, lysosomal contents within	Membrane-bound filamentous structures containing an organellar medley. Organelles within inclusions look dysfunctional.	(Armin Bayati et al., 2023)

1.23 Acknowledgement

Graphical figures in this chapter were made with Biorender.com.

1.24 References

Abokyi, S., Shan, S. W., To, C. H., Chan, H. H., & Tse, D. Y. (2020). Autophagy Upregulation by the TFEB Inducer Trehalose Protects against Oxidative Damage and Cell Death Associated with NRF2 Inhibition in Human RPE Cells. *Oxid Med Cell Longev*, *2020*, 5296341. https://doi.org/10.1155/2020/5296341

Abounit, S., Bousset, L., Loria, F., Zhu, S., de Chaumont, F., Pieri, L., Olivo-Marin, J. C., Melki, R., & Zurzolo, C. (2016). Tunneling nanotubes spread fibrillar alpha-synuclein by intercellular trafficking of lysosomes. *EMBO J*, *35*(19), 2120-2138. https://doi.org/10.15252/embj.201593411

Ahmadi Rastegar, D., Hughes, L. P., Perera, G., Keshiya, S., Zhong, S., Gao, J., Halliday, G. M., Schule, B., & Dzamko, N. (2022). Effect of LRRK2 protein and activity on stimulated cytokines in human monocytes and macrophages. *NPJ Parkinsons Dis*, *8*(1), 34. https://doi.org/10.1038/s41531-022-00297-9

Ahmed, S. M., Luo, L., Namani, A., Wang, X. J., & Tang, X. (2017). Nrf2 signaling pathway: Pivotal roles in inflammation. *Biochim Biophys Acta Mol Basis Dis*, *1863*(2), 585-597. https://doi.org/10.1016/j.bbadis.2016.11.005

Alam, P., Bousset, L., Melki, R., & Otzen, D. E. (2019). alpha-synuclein oligomers and fibrils: a spectrum of species, a spectrum of toxicities. *J Neurochem*, *150*(5), 522-534. https://doi.org/10.1111/jnc.14808

Alcalay, R. N., Levy, O. A., Waters, C. C., Fahn, S., Ford, B., Kuo, S. H., Mazzoni, P., Pauciulo, M. W., Nichols, W. C., Gan-Or, Z., Rouleau, G. A., Chung, W. K., Wolf, P., Oliva, P., Keutzer, J., Marder, K., & Zhang, X. (2015). Glucocerebrosidase activity in Parkinson's disease with and without GBA mutations. *Brain*, *138*(Pt 9), 2648-2658. https://doi.org/10.1093/brain/awv179

Alvarez-Erviti, L., Rodriguez-Oroz, M. C., Cooper, J. M., Caballero, C., Ferrer, I., Obeso, J. A., & Schapira, A. H. (2010). Chaperone-mediated autophagy markers in Parkinson disease brains. *Arch Neurol*, *67*(12), 1464-1472. https://doi.org/10.1001/archneurol.2010.198

Angot, E., Steiner, J. A., Lema Tome, C. M., Ekstrom, P., Mattsson, B., Bjorklund, A., & Brundin, P. (2012). Alpha-synuclein cell-to-cell transfer and seeding in grafted dopaminergic neurons in vivo. *PLoS One*, *7*(6), e39465. https://doi.org/10.1371/journal.pone.0039465

Araki, K., Yagi, N., Ikemoto, Y., Hayakawa, H., Fujimura, H., Moriwaki, T., Nagai, Y., Murayama, S., & Mochizuki, H. (2020). The secondary structural difference between Lewy body and glial cytoplasmic inclusion in autopsy brain with synchrotron FTIR micro-spectroscopy. *Sci Rep*, *10*(1), 19423. https://doi.org/10.1038/s41598-020-76565-6

Arotcarena, M. L., Teil, M., & Dehay, B. (2019). Autophagy in Synucleinopathy: The Overwhelmed and Defective Machinery. *Cells*, *8*(6). https://doi.org/10.3390/cells8060565

Baba, M., Nakajo, S., Tu, P. H., Tomita, T., Nakaya, K., Lee, V. M., Trojanowski, J. Q., & Iwatsubo, T. (1998). Aggregation of alpha-synuclein in Lewy bodies of sporadic Parkinson's disease and dementia with Lewy bodies. *The American Journal of Pathology*, *152*(4), 879-884. https://pubmed.ncbi.nlm.nih.gov/9546347
https://www.ncbi.nlm.nih.gov/pmc/articles/PMC1858234/

Bajaj, L., Lotfi, P., Pal, R., Ronza, A. D., Sharma, J., & Sardiello, M. (2019). Lysosome biogenesis in health and disease. *J Neurochem*, *148*(5), 573-589. https://doi.org/10.1111/jnc.14564

Bandyopadhyay, U., Sridhar, S., Kaushik, S., Kiffin, R., & Cuervo, A. M. (2010). Identification of regulators of chaperone-mediated autophagy. *Mol Cell*, *39*(4), 535-547. https://doi.org/10.1016/j.molcel.2010.08.004

Bartels, T., Choi, J. G., & Selkoe, D. J. (2011). alpha-Synuclein occurs physiologically as a helically folded tetramer that resists aggregation. *Nature*, *477*(7362), 107-110. https://doi.org/10.1038/nature10324

Bayati, A., Ayoubi, R., Zorca, C. E., Aguila, A., Han, C., Banks, E., Nguyen-Renou, E., Luo, W., Shlaifer, I., Cid-Pellitero, E. D., Yaqubi, M., Fon, E. A., Stratton, J. A., Durcan, T. M., Nahirney, P., & McPherson, P. S. (2023). *A dual hit of α-synuclein internalization and immune challenge leads to formation and maintenance of Lewy body-like inclusions in human dopaminergic neurons* (542776).

Bayati, A., Banks, E., Han, C., Luo, W., Reintsch, W. E., Zorca, C. E., Shlaifer, I., Del Cid Pellitero, E., Vanderperre, B., McBride, H. M., Fon, E. A., Durcan, T. M., & McPherson, P. S. (2022). Rapid macropinocytic transfer of alpha-synuclein to lysosomes. *Cell Rep*, *40*(3), 111102. https://doi.org/10.1016/j.celrep.2022.111102

Bayati, A., & Berman, T. (2017). Localized vs. Systematic Neurodegeneration: A Paradigm Shift in Understanding Neurodegenerative Diseases. *Front Syst Neurosci*, *11*, 62. https://doi.org/10.3389/fnsys.2017.00062

Bedford, L., Hay, D., Devoy, A., Paine, S., Powe, D. G., Seth, R., Gray, T., Topham, I., Fone, K., Rezvani, N., Mee, M., Soane, T., Layfield, R., Sheppard, P. W., Ebendal, T., Usoskin, D., Lowe, J., & Mayer, R. J. (2008). Depletion of 26S proteasomes in mouse brain neurons causes neurodegeneration and Lewy-like inclusions resembling human pale bodies. *J Neurosci*, *28*(33), 8189-8198. https://doi.org/10.1523/JNEUROSCI.2218-08.2008

Berriat, F., Lobsiger, C. S., & Boillée, S. (2023). The contribution of the peripheral immune system to neurodegeneration. *Nature Neuroscience*. https://doi.org/10.1038/s41593-023-01323-6

Bi, M., Du, X., Jiao, Q., Liu, Z., & Jiang, H. (2020). alpha-Synuclein Regulates Iron Homeostasis via Preventing Parkin-Mediated DMT1 Ubiquitylation in Parkinson's Disease Models. *ACS Chem Neurosci*, *11*(11), 1682-1691. https://doi.org/10.1021/acschemneuro.0c00196

Bieri, G., Gitler, A. D., & Brahic, M. (2018). Internalization, axonal transport and release of fibrillar forms of alpha-synuclein. *Neurobiol Dis*, *109*(Pt B), 219-225. https://doi.org/10.1016/j.nbd.2017.03.007

Bousset, L., Pieri, L., Ruiz-Arlandis, G., Gath, J., Jensen, P. H., Habenstein, B., Madiona, K., Olieric, V., Bockmann, A., Meier, B. H., & Melki, R. (2013). Structural and functional characterization of two alpha-synuclein strains. *Nat Commun*, *4*, 2575. https://doi.org/10.1038/ncomms3575

Braak, H., Tredici, K. D., Rüb, U., de Vos, R. A. I., Jansen Steur, E. N. H., & Braak, E. (2003). Staging of brain pathology related to sporadic Parkinson's disease. *Neurobiology of Aging*, *24*(2), 197-211. https://doi.org/10.1016/s0197-4580(02)00065-9

Brendza, R., Gao, X., Stark, K. L., Lin, H., Lee, S. H., Hu, C., Cai, H., DiCara, D., Hsiao, Y. C., Ngu, H., Foreman, O., Baca, M., Dohse, M., Fortin, J. P., Corpuz, R., Seshasayee, D., Easton, A., Ayalon, G., Hotzel, I., & Chih, B. (2023). Anti-alpha-synuclein c-terminal antibodies block PFF uptake and accumulation of phospho-synuclein in preclinical models of Parkinson's disease. *Neurobiol Dis*, *177*, 105969. https://doi.org/10.1016/j.nbd.2022.105969

Burberry, A., Wells, M. F., Limone, F., Couto, A., Smith, K. S., Keaney, J., Gillet, G., van Gastel, N., Wang, J. Y., Pietilainen, O., Qian, M., Eggan, P., Cantrell, C., Mok, J., Kadiu, I., Scadden, D. T., & Eggan, K. (2020). C9orf72 suppresses systemic and neural inflammation induced by gut bacteria. *Nature*, *582*(7810), 89-94. https://doi.org/10.1038/s41586-020-2288-7

Burre, J., Sharma, M., Tsetsenis, T., Buchman, V., Etherton, M. R., & Sudhof, T. C. (2010). Alpha-synuclein promotes SNARE-complex assembly in vivo and in vitro. *Science*, *329*(5999), 1663-1667. https://doi.org/10.1126/science.1195227

Button, R. W., & Luo, S. (2017). The formation of autophagosomes during lysosomal defect: A new source of cytotoxicity. *Autophagy*, *13*(10), 1797-1798. https://doi.org/10.1080/15548627.2017.1358850

Calabresi, P., Mechelli, A., Natale, G., Volpicelli-Daley, L., Di Lazzaro, G., & Ghiglieri, V. (2023). Alpha-synuclein in Parkinson's disease and other synucleinopathies: from overt neurodegeneration back to early synaptic dysfunction. *Cell Death Dis*, *14*(3), 176. https://doi.org/10.1038/s41419-023-05672-9

Calabresi, P., Picconi, B., Tozzi, A., Ghiglieri, V., & Di Filippo, M. (2014). Direct and indirect pathways of basal ganglia: a critical reappraisal. *Nat Neurosci*, *17*(8), 1022-1030. https://doi.org/10.1038/nn.3743

Cao, W., & Zheng, H. (2018). Peripheral immune system in aging and Alzheimer's disease. *Mol Neurodegener*, *13*(1), 51. https://doi.org/10.1186/s13024-018-0284-2

Cao, Y., Chtarbanova, S., Petersen, A. J., & Ganetzky, B. (2013). Dnr1 mutations cause neurodegeneration in Drosophila by activating the innate immune response in the brain. *Proc Natl Acad Sci U S A*, *110*(19), E1752-1760. https://doi.org/10.1073/pnas.1306220110

Cascella, R., Bigi, A., Cremades, N., & Cecchi, C. (2022). Effects of oligomer toxicity, fibril toxicity and fibril spreading in synucleinopathies. *Cell Mol Life Sci*, *79*(3), 174. https://doi.org/10.1007/s00018-022-04166-9

Chartier-Harlin, M. C., Kachergus, J., Roumier, C., Mouroux, V., Douay, X., Lincoln, S., Levecque, C., Larvor, L., Andrieux, J., Hulihan, M., Waucquier, N., Defebvre, L., Amouyel, P., Farrer, M., & Destée, A. (2004). Alpha-synuclein locus duplication as a cause of familial Parkinson's disease. *Lancet*, *364*(9440), 1167-1169. https://doi.org/10.1016/s0140-6736(04)17103-1

Chen, M., Vincent, J., Ezeanii, A., Wakade, S., Yerigenahally, S., & Mor, D. E. (2022). Heparan sulfate proteoglycans mediate prion-like alpha-synuclein toxicity in Parkinson's in vivo models. *Life Sci Alliance*, *5*(11). https://doi.org/10.26508/lsa.202201366

Cheng, X. T., Xie, Y. X., Zhou, B., Huang, N., Farfel-Becker, T., & Sheng, Z. H. (2018). Characterization of LAMP1-labeled nondegradative lysosomal and endocytic compartments in neurons. *J Cell Biol*, *217*(9), 3127-3139. https://doi.org/10.1083/jcb.201711083

Cheng, Y., Tong, Q., Yuan, Y., Song, X., Jiang, W., Wang, Y., Li, W., Li, Y., & Zhang, K. (2023). alpha-Synuclein induces prodromal symptoms of Parkinson's disease via activating TLR2/MyD88/NF-kappaB pathway in Schwann cells of vagus nerve in a rat model. *J Neuroinflammation*, *20*(1), 36. https://doi.org/10.1186/s12974-023-02720-1

Choi, Y. R., Cha, S. H., Kang, S. J., Kim, J. B., Jou, I., & Park, S. M. (2018). Prion-like Propagation of alpha-Synuclein Is Regulated by the FcgammaRIIB-SHP-1/2 Signaling Pathway in Neurons. *Cell Rep*, *22*(1), 136-148. https://doi.org/10.1016/j.celrep.2017.12.009

Chung, C. Y., Khurana, V., Yi, S., Sahni, N., Loh, K. H., Auluck, P. K., Baru, V., Udeshi, N. D., Freyzon, Y., Carr, S. A., Hill, D. E., Vidal, M., Ting, A. Y., & Lindquist, S. (2017). In Situ Peroxidase Labeling and Mass-Spectrometry Connects Alpha-Synuclein Directly to Endocytic Trafficking and mRNA Metabolism in Neurons. *Cell Syst*, *4*(2), 242-250 e244. https://doi.org/10.1016/j.cels.2017.01.002

Conway, K. A., Harper, J. D., & Lansbury, P. T. (1998). Accelerated in vitro fibril formation by a mutant alpha-synuclein linked to early-onset Parkinson disease. *Nat Med*, *4*(11), 1318-1320. https://doi.org/10.1038/3311

Conway, K. A., Lee, S. J., Rochet, J. C., Ding, T. T., Williamson, R. E., & Lansbury, P. T., Jr. (2000). Acceleration of oligomerization, not fibrillization, is a shared property of both alpha-synuclein mutations linked to early-onset Parkinson's disease: implications for pathogenesis and therapy. *Proc Natl Acad Sci U S A*, *97*(2), 571-576. https://doi.org/10.1073/pnas.97.2.571

Cortes, C. J., & La Spada, A. R. (2019). TFEB dysregulation as a driver of autophagy dysfunction in neurodegenerative disease: Molecular mechanisms, cellular processes, and emerging therapeutic opportunities. *Neurobiol Dis*, *122*, 83-93. https://doi.org/10.1016/j.nbd.2018.05.012

Cuervo, A. M., Stefanis, L., Fredenburg, R., Lansbury, P. T., & Sulzer, D. (2004). Impaired degradation of mutant alpha-synuclein by chaperone-mediated autophagy. *Science*, *305*(5688), 1292-1295. https://doi.org/10.1126/science.1101738

Danzer, K. M., Kranich, L. R., Ruf, W. P., Cagsal-Getkin, O., Winslow, A. R., Zhu, L., Vanderburg, C. R., & McLean, P. J. (2012). Exosomal cell-to-cell transmission of alpha synuclein oligomers. *Mol Neurodegener*, *7*, 42. https://doi.org/10.1186/1750-1326-7-42

Davidson, W. S., Jonas, A., Clayton, D. F., & George, J. M. (1998). Stabilization of alpha-synuclein secondary structure upon binding to synthetic membranes. *J Biol Chem*, *273*(16), 9443-9449. https://doi.org/10.1074/jbc.273.16.9443

Decressac, M., Mattsson, B., Weikop, P., Lundblad, M., Jakobsson, J., & Bjorklund, A. (2013). TFEB-mediated autophagy rescues midbrain dopamine neurons from alpha-synuclein toxicity. *Proc Natl Acad Sci U S A*, *110*(19), E1817-1826. https://doi.org/10.1073/pnas.1305623110

Delenclos, M., Burgess, J. D., Lamprokostopoulou, A., Outeiro, T. F., Vekrellis, K., & McLean, P. J. (2019). Cellular models of alpha-synuclein toxicity and aggregation. *J Neurochem*, *150*(5), 566-576. https://doi.org/10.1111/jnc.14806

Delenclos, M., Trendafilova, T., Mahesh, D., Baine, A. M., Moussaud, S., Yan, I. K., Patel, T., & McLean, P. J. (2017). Investigation of Endocytic Pathways for the Internalization of Exosome-Associated Oligomeric Alpha-Synuclein [Original Research]. *11*(172). https://doi.org/10.3389/fnins.2017.00172

DeMaio, A., Mehrotra, S., Sambamurti, K., & Husain, S. (2022). The role of the adaptive immune system and T cell dysfunction in neurodegenerative diseases. *J Neuroinflammation*, *19*(1), 251. https://doi.org/10.1186/s12974-022-02605-9

Desplats, P., Lee, H. J., Bae, E. J., Patrick, C., Rockenstein, E., Crews, L., Spencer, B., Masliah, E., & Lee, S. J. (2009). Inclusion formation and neuronal cell death through neuron-to-neuron transmission of alpha-synuclein. *Proc Natl Acad Sci U S A*, *106*(31), 13010-13015. https://doi.org/10.1073/pnas.0903691106

Dettmer, U., Newman, A. J., Soldner, F., Luth, E. S., Kim, N. C., von Saucken, V. E., Sanderson, J. B., Jaenisch, R., Bartels, T., & Selkoe, D. (2015). Parkinson-causing alpha-synuclein missense mutations shift native tetramers to monomers as a mechanism for disease initiation. *Nat Commun*, *6*, 7314. https://doi.org/10.1038/ncomms8314

Dettmer, U., Ramalingam, N., von Saucken, V. E., Kim, T. E., Newman, A. J., Terry-Kantor, E., Nuber, S., Ericsson, M., Fanning, S., Bartels, T., Lindquist, S., Levy, O. A., & Selkoe, D. (2017). Loss of native alpha-synuclein multimerization by strategically mutating its amphipathic helix causes abnormal vesicle interactions in neuronal cells. *Hum Mol Genet*, *26*(18), 3466-3481. https://doi.org/10.1093/hmg/ddx227

Dettmer, U., Selkoe, D., & Bartels, T. (2016). New insights into cellular alpha-synuclein homeostasis in health and disease. *Curr Opin Neurobiol*, *36*, 15-22. https://doi.org/10.1016/j.conb.2015.07.007

Diaz-Hernandez, E., Contreras-Lopez, R., Sanchez-Fuentes, A., Rodriguez-Sibrian, L., Ramirez-Jarquin, J. O., & Tecuapetla, F. (2018). The Thalamostriatal Projections Contribute to the Initiation and Execution of a Sequence of Movements. *Neuron*, *100*(3), 739-752 e735. https://doi.org/10.1016/j.neuron.2018.09.052

Dieriks, B. V., Park, T. I., Fourie, C., Faull, R. L., Dragunow, M., & Curtis, M. A. (2017). alpha-synuclein transfer through tunneling nanotubes occurs in SH-SY5Y cells and primary brain pericytes from Parkinson's disease patients. *Sci Rep*, *7*, 42984. https://doi.org/10.1038/srep42984

Dilsizoglu Senol, A., Samarani, M., Syan, S., Guardia, C. M., Nonaka, T., Liv, N., Latour-Lambert, P., Hasegawa, M., Klumperman, J., Bonifacino, J. S., & Zurzolo, C. (2021). alpha-Synuclein fibrils subvert lysosome structure and function for the propagation of protein misfolding between cells through tunneling nanotubes. *PLoS Biol*, *19*(7), e3001287. https://doi.org/10.1371/journal.pbio.3001287

Donaghy, P. C., & McKeith, I. G. (2014). The clinical characteristics of dementia with Lewy bodies and a consideration of prodromal diagnosis. *Alzheimers Res Ther*, *6*(4), 46. https://doi.org/10.1186/alzrt274

Doty, K. R., Guillot-Sestier, M. V., & Town, T. (2015). The role of the immune system in neurodegenerative disorders: Adaptive or maladaptive? *Brain Res*, *1617*, 155-173. https://doi.org/10.1016/j.brainres.2014.09.008

Du, C., Zhang, F., & Zhang, C. X. (2018). Phagocytosis Assay for alpha-Synuclein Fibril Uptake by Mouse Primary Microglia. *Bio Protoc*, *8*(17), e2986. https://doi.org/10.21769/BioProtoc.2986

Duffy, P. E., & Tennyson, V. M. (1965). Phase and Electron Microscopic Observations of Lewy Bodies and Melanin Granules in the Substantia Nigra and Locus Caeruleus in Parkinson's Disease. *Journal of Neuropathology and Experimental Neurology*, *24*(3), 398-414. https://doi.org/10.1097/00005072-196507000-00003

Emmenegger, M., De Cecco, E., Hruska-Plochan, M., Eninger, T., Schneider, M. M., Barth, M., Tantardini, E., de Rossi, P., Bacioglu, M., Langston, R. G., Kaganovich, A., Bengoa-Vergniory, N., Gonzalez-Guerra, A., Avar, M., Heinzer, D., Reimann, R., Hasler, L. M., Herling, T. W., Matharu, N. S., . . . Aguzzi, A. (2021). LAG3 is not expressed in human and murine neurons and does not modulate alpha-synucleinopathies. *EMBO Mol Med*, *13*(9), e14745. https://doi.org/10.15252/emmm.202114745

Eskelinen, E. L. (2006). Roles of LAMP-1 and LAMP-2 in lysosome biogenesis and autophagy. *Mol Aspects Med*, *27*(5-6), 495-502. https://doi.org/10.1016/j.mam.2006.08.005

Eskelinen, E. L., Illert, A. L., Tanaka, Y., Schwarzmann, G., Blanz, J., Von Figura, K., & Saftig, P. (2002). Role of LAMP-2 in lysosome biogenesis and autophagy. *Mol Biol Cell*, *13*(9), 3355-3368. https://doi.org/10.1091/mbc.e02-02-0114

Fakhree, M. A. A., Konings, I. B. M., Kole, J., Cambi, A., Blum, C., & Claessens, M. (2021). The Localization of Alpha-synuclein in the Endocytic Pathway. *Neuroscience*, *457*, 186-195. https://doi.org/10.1016/j.neuroscience.2021.01.017

Fan, Y., Sun, Y., Yu, W., Tao, Y., Xia, W., Liu, Y., Zhao, Q., Tang, Y., Sun, Y., Liu, F., Cao, Q., Wu, J., Liu, C., Wang, J., & Li, D. (2023). Conformational change of alpha-synuclein fibrils in cerebrospinal fluid from different clinical phases of Parkinson's disease. *Structure*, *31*(1), 78-87 e75. https://doi.org/10.1016/j.str.2022.11.013

Fares, M. B., Jagannath, S., & Lashuel, H. A. (2021). Reverse engineering Lewy bodies: how far have we come and how far can we go? *Nat Rev Neurosci*, *22*(2), 111-131. https://doi.org/10.1038/s41583-020-00416-6

Forno, L. S. (1996). Neuropathology of Parkinson's disease. *J Neuropathol Exp Neurol*, *55*(3), 259-272. https://doi.org/10.1097/00005072-199603000-00001

Forno, L. S., & Norville, R. L. (1976). Ultrastructure of Lewy bodies in the stellate ganglion. *Acta Neuropathol*, *34*(3), 183-197. https://doi.org/10.1007/BF00688674

Fortin, D. L., Troyer, M. D., Nakamura, K., Kubo, S., Anthony, M. D., & Edwards, R. H. (2004). Lipid rafts mediate the synaptic localization of alpha-synuclein. *J Neurosci*, *24*(30), 6715-6723. https://doi.org/10.1523/JNEUROSCI.1594-04.2004

Fredenburg, R. A., Rospigliosi, C., Meray, R. K., Kessler, J. C., Lashuel, H. A., Eliezer, D., & Lansbury, P. T., Jr. (2007). The impact of the E46K mutation on the properties of alpha-synuclein in its monomeric and oligomeric states. *Biochemistry*, *46*(24), 7107-7118. https://doi.org/10.1021/bi7000246

Freeman, D., Cedillos, R., Choyke, S., Lukic, Z., McGuire, K., Marvin, S., Burrage, A. M., Sudholt, S., Rana, A., O'Connor, C., Wiethoff, C. M., & Campbell, E. M. (2013). Alpha-synuclein induces lysosomal rupture and cathepsin dependent reactive oxygen species following endocytosis. *PLoS One*, *8*(4), e62143. https://doi.org/10.1371/journal.pone.0062143

Freeze, B., Acosta, D., Pandya, S., Zhao, Y., & Raj, A. (2018). Regional expression of genes mediating trans-synaptic alpha-synuclein transfer predicts regional atrophy in Parkinson disease. *Neuroimage Clin*, *18*, 456-466. https://doi.org/10.1016/j.nicl.2018.01.009

Fussi, N., Hollerhage, M., Chakroun, T., Nykanen, N. P., Rosler, T. W., Koeglsperger, T., Wurst, W., Behrends, C., & Hoglinger, G. U. (2018). Exosomal secretion of alpha-synuclein as protective mechanism after upstream blockage of macroautophagy. *Cell Death Dis*, *9*(7), 757. https://doi.org/10.1038/s41419-018-0816-2

Gai, W., Yuan, H., Li, X., Power, J., Blumbergs, P., & Jensen, P. (2000). In situ and in vitro study of colocalization and segregation of α-synuclein, ubiquitin, and lipids in Lewy bodies. *Experimental neurology*, *166*(2), 324-333.

Galloway, P., Mulvihill, P., & Perry, G. (1992). Filaments of Lewy bodies contain insoluble cytoskeletal elements. *The American Journal of Pathology*, *140*(4), 809.

Gan, L., & Johnson, J. A. (2014). Oxidative damage and the Nrf2-ARE pathway in neurodegenerative diseases. *Biochim Biophys Acta*, *1842*(8), 1208-1218. https://doi.org/10.1016/j.bbadis.2013.12.011

Gan-Or, Z., Alcalay, R. N., Makarious, M. B., Scholz, S. W., Blauwendraat, C., & International Parkinson's Disease Genomics, C. (2019). Classification of GBA Variants and Their Effects in Synucleinopathies. *Mov Disord*, *34*(10), 1581-1582. https://doi.org/10.1002/mds.27803

Gan-Or, Z., Liong, C., & Alcalay, R. N. (2018). GBA-Associated Parkinson's Disease and Other Synucleinopathies. *Curr Neurol Neurosci Rep*, *18*(8), 44. https://doi.org/10.1007/s11910-018-0860-4

Ghosh, D., Mondal, M., Mohite, G. M., Singh, P. K., Ranjan, P., Anoop, A., Ghosh, S., Jha, N. N., Kumar, A., & Maji, S. K. (2013). The Parkinson's disease-associated H50Q mutation accelerates alpha-Synuclein aggregation in vitro. *Biochemistry*, *52*(40), 6925-6927. https://doi.org/10.1021/bi400999d

Gispert, S., Ricciardi, F., Kurz, A., Azizov, M., Hoepken, H. H., Becker, D., Voos, W., Leuner, K., Muller, W. E., Kudin, A. P., Kunz, W. S., Zimmermann, A., Roeper, J., Wenzel, D., Jendrach, M., Garcia-Arencibia, M., Fernandez-Ruiz, J., Huber, L., Rohrer, H., . . . Auburger, G. (2009). Parkinson phenotype in aged PINK1-deficient mice is accompanied by progressive mitochondrial dysfunction in absence of neurodegeneration. *PLoS One*, *4*(6), e5777. https://doi.org/10.1371/journal.pone.0005777

Gomez-Sintes, R., Ledesma, M. D., & Boya, P. (2016). Lysosomal cell death mechanisms in aging. *Ageing Res Rev*, *32*, 150-168. https://doi.org/10.1016/j.arr.2016.02.009

Goncalves, S. A., Macedo, D., Raquel, H., Simoes, P. D., Giorgini, F., Ramalho, J. S., Barral, D. C., Ferreira Moita, L., & Outeiro, T. F. (2016). shRNA-Based Screen Identifies Endocytic Recycling Pathway Components That Act as Genetic Modifiers of Alpha-Synuclein Aggregation, Secretion and Toxicity. *PLoS Genet*, *12*(4), e1005995. https://doi.org/10.1371/journal.pgen.1005995

Grudina, C., Kouroupi, G., Nonaka, T., Hasegawa, M., Matsas, R., & Zurzolo, C. (2019). Human NPCs can degrade alpha-syn fibrils and transfer them preferentially in a cell contact-

dependent manner possibly through TNT-like structures. *Neurobiol Dis*, *132*, 104609. https://doi.org/10.1016/j.nbd.2019.104609

Gu, Z., Cao, H., Zuo, C., Huang, Y., Miao, J., Song, Y., Yang, Y., Zhu, L., & Wang, F. (2022). TFEB in Alzheimer's disease: From molecular mechanisms to therapeutic implications. *Neurobiol Dis*, *173*, 105855. https://doi.org/10.1016/j.nbd.2022.105855

Guardia-Laguarta, C., Area-Gomez, E., Schon, E. A., & Przedborski, S. (2015). Novel subcellular localization for alpha-synuclein: possible functional consequences. *Front Neuroanat*, *9*, 17. https://doi.org/10.3389/fnana.2015.00017

Guo, M., Wang, J., Zhao, Y., Feng, Y., Han, S., Dong, Q., Cui, M., & Tieu, K. (2020). Microglial exosomes facilitate alpha-synuclein transmission in Parkinson's disease. *Brain*, *143*(5), 1476-1497. https://doi.org/10.1093/brain/awaa090

Hallacli, E., Kayatekin, C., Nazeen, S., Wang, X. H., Sheinkopf, Z., Sathyakumar, S., Sarkar, S., Jiang, X., Dong, X., Di Maio, R., Wang, W., Keeney, M. T., Felsky, D., Sandoe, J., Vahdatshoar, A., Udeshi, N. D., Mani, D. R., Carr, S. A., Lindquist, S., . . . Khurana, V. (2022). The Parkinson's disease protein alpha-synuclein is a modulator of processing bodies and mRNA stability. *Cell*, *185*(12), 2035-2056 e2033. https://doi.org/10.1016/j.cell.2022.05.008

Hammond, T. R., Marsh, S. E., & Stevens, B. (2019). Immune Signaling in Neurodegeneration. *Immunity*, *50*(4), 955-974. https://doi.org/10.1016/j.immuni.2019.03.016

Hansen, C., Angot, E., Bergstrom, A. L., Steiner, J. A., Pieri, L., Paul, G., Outeiro, T. F., Melki, R., Kallunki, P., Fog, K., Li, J. Y., & Brundin, P. (2011). alpha-Synuclein propagates from mouse brain to grafted dopaminergic neurons and seeds aggregation in cultured human cells. *J Clin Invest*, *121*(2), 715-725. https://doi.org/10.1172/JCI43366

Hansen, C., & Li, J. Y. (2012). Beyond alpha-synuclein transfer: pathology propagation in Parkinson's disease. *Trends Mol Med*, *18*(5), 248-255. https://doi.org/10.1016/j.molmed.2012.03.002

Hashimoto, M., Hsu, L. J., Rockenstein, E., Takenouchi, T., Mallory, M., & Masliah, E. (2002). alpha-Synuclein protects against oxidative stress via inactivation of the c-Jun N-terminal kinase stress-signaling pathway in neuronal cells. *J Biol Chem*, *277*(13), 11465-11472. https://doi.org/10.1074/jbc.M111428200

Hatton, C., Ghanem, S. S., Koss, D. J., Abdi, I. Y., Gibbons, E., Guerreiro, R., Bras, J., International, D. L. B. G. C., Walker, L., Gelpi, E., Heywood, W., Outeiro, T. F., Attems, J., McFarland, R., Forsyth, R., El-Agnaf, O. M., & Erskine, D. (2022). Prion-like alpha-synuclein pathology in the brain of infants with Krabbe disease. *Brain*, *145*(4), 1257-1263. https://doi.org/10.1093/brain/awac002

Henley, J. R., Krueger, E. W., Oswald, B. J., & McNiven, M. A. (1998). Dynamin-mediated internalization of caveolae. *J Cell Biol*, *141*(1), 85-99. https://doi.org/10.1083/jcb.141.1.85

Hernandez, C. J., Baez-Becerra, C., Contreras-Zarate, M. J., Arboleda, H., & Arboleda, G. (2019). PINK1 Silencing Modifies Dendritic Spine Dynamics of Mouse Hippocampal Neurons. *J Mol Neurosci*, *69*(4), 570-579. https://doi.org/10.1007/s12031-019-01385-x

Herrero, M. T., Barcia, C., & Navarro, J. M. (2002). Functional anatomy of thalamus and basal ganglia. *Childs Nerv Syst*, *18*(8), 386-404. https://doi.org/10.1007/s00381-002-0604-1

Hijaz, B. A., & Volpicelli-Daley, L. A. (2020). Initiation and propagation of alpha-synuclein aggregation in the nervous system. *Mol Neurodegener*, *15*(1), 19. https://doi.org/10.1186/s13024-020-00368-6

Hivare, P., Gadhavi, J., Bhatia, D., & Gupta, S. (2022). alpha-Synuclein fibrils explore actin-mediated macropinocytosis for cellular entry into model neuroblastoma neurons. *Traffic*, *23*(7), 391-410. https://doi.org/10.1111/tra.12859

Hobson, B. D., & Sulzer, D. (2022). Neuronal Presentation of Antigen and Its Possible Role in Parkinson's Disease. *J Parkinsons Dis*, *12*(s1), S137-S147. https://doi.org/10.3233/JPD-223153

Hoffmann, A. C., Minakaki, G., Menges, S., Salvi, R., Savitskiy, S., Kazman, A., Vicente Miranda, H., Mielenz, D., Klucken, J., Winkler, J., & Xiang, W. (2019). Extracellular aggregated alpha synuclein primarily triggers lysosomal dysfunction in neural cells prevented by trehalose. *Sci Rep*, *9*(1), 544. https://doi.org/10.1038/s41598-018-35811-8

Holmes, B. B., DeVos, S. L., Kfoury, N., Li, M., Jacks, R., Yanamandra, K., Ouidja, M. O., Brodsky, F. M., Marasa, J., Bagchi, D. P., Kotzbauer, P. T., Miller, T. M., Papy-Garcia, D., & Diamond, M. I. (2013). Heparan sulfate proteoglycans mediate internalization and propagation of specific proteopathic seeds. *Proc Natl Acad Sci U S A*, *110*(33), E3138-3147. https://doi.org/10.1073/pnas.1301440110

Horsager, J., Knudsen, K., & Sommerauer, M. (2022). Clinical and imaging evidence of brain-first and body-first Parkinson's disease. *Neurobiol Dis*, *164*, 105626. https://doi.org/10.1016/j.nbd.2022.105626

Ihse, E., Yamakado, H., van Wijk, X. M., Lawrence, R., Esko, J. D., & Masliah, E. (2017). Cellular internalization of alpha-synuclein aggregates by cell surface heparan sulfate depends on aggregate conformation and cell type. *Sci Rep*, *7*(1), 9008. https://doi.org/10.1038/s41598-017-08720-5

Jarvela, T. S., Chaplot, K., & Lindberg, I. (2021). A protease protection assay for the detection of internalized alpha-synuclein pre-formed fibrils. *PLoS One*, *16*(1), e0241161. https://doi.org/10.1371/journal.pone.0241161

Jellinger, K. A. (2018). Multiple System Atrophy: An Oligodendroglioneural Synucleinopathy. *J Alzheimers Dis*, *62*(3), 1141-1179. https://doi.org/10.3233/JAD-170397

Jellinger, K. A., & Korczyn, A. D. (2018). Are dementia with Lewy bodies and Parkinson's disease dementia the same disease? *BMC Med*, *16*(1), 34. https://doi.org/10.1186/s12916-018-1016-8

Jellinger, K. A., & Lantos, P. L. (2010). Papp-Lantos inclusions and the pathogenesis of multiple system atrophy: an update. *Acta Neuropathol*, *119*(6), 657-667. https://doi.org/10.1007/s00401-010-0672-3

Jiang, P., Gan, M., Yen, S. H., McLean, P. J., & Dickson, D. W. (2017). Impaired endo-lysosomal membrane integrity accelerates the seeding progression of alpha-synuclein aggregates. *Sci Rep*, *7*(1), 7690. https://doi.org/10.1038/s41598-017-08149-w

Jiang, W., Li, J., Zhang, Z., Wang, H., & Wang, Z. (2014). Epigenetic upregulation of alpha-synuclein in the rats exposed to methamphetamine. *Eur J Pharmacol*, *745*, 243-248. https://doi.org/10.1016/j.ejphar.2014.10.043

Jinn, S., Drolet, R. E., Cramer, P. E., Wong, A. H., Toolan, D. M., Gretzula, C. A., Voleti, B., Vassileva, G., Disa, J., Tadin-Strapps, M., & Stone, D. J. (2017). TMEM175 deficiency impairs lysosomal and mitochondrial function and increases alpha-synuclein aggregation. *Proc Natl Acad Sci U S A*, *114*(9), 2389-2394. https://doi.org/10.1073/pnas.1616332114

Jo, J., Yang, L., Tran, H. D., Yu, W., Sun, A. X., Chang, Y. Y., Jung, B. C., Lee, S. J., Saw, T. Y., Xiao, B., Khoo, A. T. T., Yaw, L. P., Xie, J. J., Lokman, H., Ong, W. Y., Lim, G. G. Y., Lim,

K. L., Tan, E. K., Ng, H. H., & Je, H. S. (2021). Lewy Body-like Inclusions in Human Midbrain Organoids Carrying Glucocerebrosidase and alpha-Synuclein Mutations. *Ann Neurol*, *90*(3), 490-505. https://doi.org/10.1002/ana.26166

Johnston, J. A., Ward, C. L., & Kopito, R. R. (1998). Aggresomes: a cellular response to misfolded proteins. *J Cell Biol*, *143*(7), 1883-1898. https://doi.org/10.1083/jcb.143.7.1883

Kang, S. J., Kim, J. S., & Park, S. M. (2018). Ubiquitin C-terminal Hydrolase L1 Regulates Lipid Raft-dependent Endocytosis. *Exp Neurobiol*, *27*(5), 377-386. https://doi.org/10.5607/en.2018.27.5.377

Karampetsou, M., Ardah, M. T., Semitekolou, M., Polissidis, A., Samiotaki, M., Kalomoiri, M., Majbour, N., Xanthou, G., El-Agnaf, O. M. A., & Vekrellis, K. (2017). Phosphorylated exogenous alpha-synuclein fibrils exacerbate pathology and induce neuronal dysfunction in mice. *Sci Rep*, *7*(1), 16533. https://doi.org/10.1038/s41598-017-15813-8

Karpowicz, R. J., Jr., Haney, C. M., Mihaila, T. S., Sandler, R. M., Petersson, E. J., & Lee, V. M. (2017). Selective imaging of internalized proteopathic alpha-synuclein seeds in primary neurons reveals mechanistic insight into transmission of synucleinopathies. *J Biol Chem*, *292*(32), 13482-13497. https://doi.org/10.1074/jbc.M117.780296

Karpowicz, R. J., Jr., Trojanowski, J. Q., & Lee, V. M. (2019). Transmission of alpha-synuclein seeds in neurodegenerative disease: recent developments. *Lab Invest*, *99*(7), 971-981. https://doi.org/10.1038/s41374-019-0195-z

Kasen, A., Houck, C., Burmeister, A. R., Sha, Q., Brundin, L., & Brundin, P. (2022). Upregulation of alpha-synuclein following immune activation: Possible trigger of Parkinson's disease. *Neurobiol Dis*, *166*, 105654. https://doi.org/10.1016/j.nbd.2022.105654

Kawahata, I., Sekimori, T., Wang, H., Wang, Y., Sasaoka, T., Bousset, L., Melki, R., Mizobata, T., Kawata, Y., & Fukunaga, K. (2021). Dopamine D2 Long Receptors Are Critical for Caveolae-Mediated alpha-Synuclein Uptake in Cultured Dopaminergic Neurons. *Biomedicines*, *9*(1). https://doi.org/10.3390/biomedicines9010049

Ki, C. S., Stavrou, E. F., Davanos, N., Lee, W. Y., Chung, E. J., Kim, J. Y., & Athanassiadou, A. (2007). The Ala53Thr mutation in the alpha-synuclein gene in a Korean family with Parkinson disease. *Clin Genet*, *71*(5), 471-473. https://doi.org/10.1111/j.1399-0004.2007.00781.x

Kim, S., Yun, S. P., Lee, S., Umanah, G. E., Bandaru, V. V. R., Yin, X., Rhee, P., Karuppagounder, S. S., Kwon, S. H., Lee, H., Mao, X., Kim, D., Pandey, A., Lee, G., Dawson, V. L., Dawson, T. M., & Ko, H. S. (2018). GBA1 deficiency negatively affects physiological alpha-synuclein tetramers and related multimers. *Proc Natl Acad Sci U S A*, *115*(4), 798-803. https://doi.org/10.1073/pnas.1700465115

Kitada, T., Pisani, A., Porter, D. R., Yamaguchi, H., Tscherter, A., Martella, G., Bonsi, P., Zhang, C., Pothos, E. N., & Shen, J. (2007). Impaired dopamine release and synaptic plasticity in the striatum of PINK1-deficient mice. *Proc Natl Acad Sci U S A*, *104*(27), 11441-11446. https://doi.org/10.1073/pnas.0702717104

Klann, E. M., Dissanayake, U., Gurrala, A., Farrer, M., Shukla, A. W., Ramirez-Zamora, A., Mai, V., & Vedam-Mai, V. (2021). The Gut-Brain Axis and Its Relation to Parkinson's Disease: A Review. *Front Aging Neurosci*, *13*, 782082. https://doi.org/10.3389/fnagi.2021.782082

Klein, A. D., & Mazzulli, J. R. (2018). Is Parkinson's disease a lysosomal disorder? *Brain*, *141*(8), 2255-2262. https://doi.org/10.1093/brain/awy147

Kluge, A., Bunk, J., Schaeffer, E., Drobny, A., Xiang, W., Knacke, H., Bub, S., Luckstadt, W., Arnold, P., Lucius, R., Berg, D., & Zunke, F. (2022). Detection of neuron-derived pathological alpha-synuclein in blood. *Brain*, *145*(9), 3058-3071. https://doi.org/10.1093/brain/awac115

Konno, M., Hasegawa, T., Baba, T., Miura, E., Sugeno, N., Kikuchi, A., Fiesel, F. C., Sasaki, T., Aoki, M., Itoyama, Y., & Takeda, A. (2012). Suppression of dynamin GTPase decreases alpha-synuclein uptake by neuronal and oligodendroglial cells: a potent therapeutic target for synucleinopathy. *Mol Neurodegener*, *7*, 38. https://doi.org/10.1186/1750-1326-7-38

Krohn, L., Ozturk, T. N., Vanderperre, B., Ouled Amar Bencheikh, B., Ruskey, J. A., Laurent, S. B., Spiegelman, D., Postuma, R. B., Arnulf, I., Hu, M. T. M., Dauvilliers, Y., Hogl, B., Stefani, A., Monaca, C. C., Plazzi, G., Antelmi, E., Ferini-Strambi, L., Heidbreder, A., Rudakou, U., . . . Gan-Or, Z. (2020). Genetic, Structural, and Functional Evidence Link TMEM175 to Synucleinopathies. *Ann Neurol*, *87*(1), 139-153. https://doi.org/10.1002/ana.25629

Krueger, E. W., Orth, J. D., Cao, H., & McNiven, M. A. (2003). A dynamin-cortactin-Arp2/3 complex mediates actin reorganization in growth factor-stimulated cells. *Mol Biol Cell*, *14*(3), 1085-1096. https://doi.org/10.1091/mbc.e02-08-0466

Kulkarni, A. S., Burns, M. R., Brundin, P., & Wesson, D. W. (2022). Linking alpha-synuclein-induced synaptopathy and neural network dysfunction in early Parkinson's disease. *Brain Commun*, *4*(4), fcac165. https://doi.org/10.1093/braincomms/fcac165

Kumari, P., Ghosh, D., Vanas, A., Fleischmann, Y., Wiegand, T., Jeschke, G., Riek, R., & Eichmann, C. (2021). Structural insights into alpha-synuclein monomer-fibril interactions. *Proc Natl Acad Sci U S A*, *118*(10). https://doi.org/10.1073/pnas.2012171118

Kuzuhara, S., Mori, H., Izumiyama, N., Yoshimura, M., & Ihara, Y. (1988). Lewy bodies are ubiquitinated. A light and electron microscopic immunocytochemical study. *Acta Neuropathol*, *75*(4), 345-353. https://doi.org/10.1007/BF00687787

Lam, I., Ndayisaba, A., Lewis, A. J., Fu, Y., Sagredo, G. T., Zaccagnini, L., Sandoe, J., Sanz, R. L., Vahdatshoar, A., Martin, T. D., Morshed, N., Ichihashi, T., Tripathi, A., Ramalingam, N., Oettgen-Suazo, C., Bartels, T., Schäbinger, M., Hallacli, E., Jiang, X., . . . Khurana, V. (2022). Rapid iPSC inclusionopathy models shed light on formation, consequence and molecular subtype of α-synuclein inclusions. In: BioRxiv.

Lashuel, H. A. (2020). Do Lewy bodies contain alpha-synuclein fibrils? and Does it matter? A brief history and critical analysis of recent reports. *Neurobiol Dis*, *141*, 104876. https://doi.org/10.1016/j.nbd.2020.104876

Lau, A., So, R. W. L., Lau, H. H. C., Sang, J. C., Ruiz-Riquelme, A., Fleck, S. C., Stuart, E., Menon, S., Visanji, N. P., Meisl, G., Faidi, R., Marano, M. M., Schmitt-Ulms, C., Wang, Z., Fraser, P. E., Tandon, A., Hyman, B. T., Wille, H., Ingelsson, M., . . . Watts, J. C. (2020). alpha-Synuclein strains target distinct brain regions and cell types. *Nat Neurosci*, *23*(1), 21-31. https://doi.org/10.1038/s41593-019-0541-x

Lautenschlager, J., Stephens, A. D., Fusco, G., Strohl, F., Curry, N., Zacharopoulou, M., Michel, C. H., Laine, R., Nespovitaya, N., Fantham, M., Pinotsi, D., Zago, W., Fraser, P., Tandon, A., St George-Hyslop, P., Rees, E., Phillips, J. J., De Simone, A., Kaminski, C. F., & Schierle, G. S. K. (2018). C-terminal calcium binding of alpha-synuclein modulates synaptic vesicle interaction. *Nat Commun*, *9*(1), 712. https://doi.org/10.1038/s41467-018-03111-4

Lee, H.-J., Suk, J.-E., Bae, E.-J., & Lee, S.-J. (2008). Clearance and deposition of extracellular α-synuclein aggregates in microglia. *Biochemical and Biophysical Research Communications*, *372*(3), 423-428. https://doi.org/https://doi.org/10.1016/j.bbrc.2008.05.045

Lee, H. J., Cho, E. D., Lee, K. W., Kim, J. H., Cho, S. G., & Lee, S. J. (2013). Autophagic failure promotes the exocytosis and intercellular transfer of alpha-synuclein. *Exp Mol Med*, *45*, e22. https://doi.org/10.1038/emm.2013.45

Lee, H. J., & Lee, S. J. (2002). Characterization of cytoplasmic alpha-synuclein aggregates. *J Biol Chem*, *277*(50), 48976-48983. https://doi.org/10.1074/jbc.M208192200

Lee, H. J., Patel, S., & Lee, S. J. (2005). Intravesicular localization and exocytosis of alpha-synuclein and its aggregates. *J Neurosci*, *25*(25), 6016-6024. https://doi.org/10.1523/JNEUROSCI.0692-05.2005

Lee, H. J., Suk, J. E., Bae, E. J., Lee, J. H., Paik, S. R., & Lee, S. J. (2008). Assembly-dependent endocytosis and clearance of extracellular alpha-synuclein. *Int J Biochem Cell Biol*, *40*(9), 1835-1849. https://doi.org/10.1016/j.biocel.2008.01.017

Lee, H. J., Suk, J. E., Patrick, C., Bae, E. J., Cho, J. H., Rho, S., Hwang, D., Masliah, E., & Lee, S. J. (2010). Direct transfer of alpha-synuclein from neuron to astroglia causes inflammatory responses in synucleinopathies. *J Biol Chem*, *285*(12), 9262-9272. https://doi.org/10.1074/jbc.M109.081125

Lesage, S., Houot, M., Mangone, G., Tesson, C., Bertrand, H., Forlani, S., Anheim, M., Brefel-Courbon, C., Broussolle, E., Thobois, S., Damier, P., Durif, F., Roze, E., Tison, F., Grabli, D., Ory-Magne, F., Degos, B., Viallet, F., Cormier-Dequaire, F., . . . French Parkinson disease Genetics Study, G. (2020). Genetic and Phenotypic Basis of Autosomal Dominant Parkinson's Disease in a Large Multi-Center Cohort. *Front Neurol*, *11*, 682. https://doi.org/10.3389/fneur.2020.00682

Lewy, F. (1912). *Handbuch der Neurologie*. Julius Springer.

Li, J., Uversky, V. N., & Fink, A. L. (2002). Conformational Behavior of Human α-Synuclein is Modulated by Familial Parkinson's Disease Point Mutations A30P and A53T. *NeuroToxicology*, *23*(4-5), 553-567. https://doi.org/10.1016/s0161-813x(02)00066-9

Lin, Y. W., & Truong, D. (2019). Diffuse Lewy body disease. *J Neurol Sci*, *399*, 144-150. https://doi.org/10.1016/j.jns.2019.02.021

Liu, J., Zhou, Y., Wang, Y., Fong, H., Murray, T. M., & Zhang, J. (2007). Identification of proteins involved in microglial endocytosis of alpha-synuclein. *J Proteome Res*, *6*(9), 3614-3627. https://doi.org/10.1021/pr0701512

Liu, S., Ninan, I., Antonova, I., Battaglia, F., Trinchese, F., Narasanna, A., Kolodilov, N., Dauer, W., Hawkins, R. D., & Arancio, O. (2004). alpha-Synuclein produces a long-lasting increase in neurotransmitter release. *EMBO J*, *23*(22), 4506-4516. https://doi.org/10.1038/sj.emboj.7600451

Loov, C., Scherzer, C. R., Hyman, B. T., Breakefield, X. O., & Ingelsson, M. (2016). alpha-Synuclein in Extracellular Vesicles: Functional Implications and Diagnostic Opportunities. *Cell Mol Neurobiol*, *36*(3), 437-448. https://doi.org/10.1007/s10571-015-0317-0

Lovestam, S., Schweighauser, M., Matsubara, T., Murayama, S., Tomita, T., Ando, T., Hasegawa, K., Yoshida, M., Tarutani, A., Hasegawa, M., Goedert, M., & Scheres, S. H. W. (2021). Seeded assembly in vitro does not replicate the structures of alpha-synuclein filaments

from multiple system atrophy. *FEBS Open Bio*, *11*(4), 999-1013. https://doi.org/10.1002/2211-5463.13110

Ludtmann, M. H., Angelova, P. R., Ninkina, N. N., Gandhi, S., Buchman, V. L., & Abramov, A. Y. (2016). Monomeric Alpha-Synuclein Exerts a Physiological Role on Brain ATP Synthase. *J Neurosci*, *36*(41), 10510-10521. https://doi.org/10.1523/JNEUROSCI.1659-16.2016

Luk, K. C., Song, C., O'Brien, P., Stieber, A., Branch, J. R., Brunden, K. R., Trojanowski, J. Q., & Lee, V. M. (2009). Exogenous alpha-synuclein fibrils seed the formation of Lewy body-like intracellular inclusions in cultured cells. *Proc Natl Acad Sci U S A*, *106*(47), 20051-20056. https://doi.org/10.1073/pnas.0908005106

Lwin, A., Orvisky, E., Goker-Alpan, O., LaMarca, M. E., & Sidransky, E. (2004). Glucocerebrosidase mutations in subjects with parkinsonism. *Mol Genet Metab*, *81*(1), 70-73. https://doi.org/10.1016/j.ymgme.2003.11.004

Magistrelli, L., Contaldi, E., & Comi, C. (2021). The Impact of SNCA Variations and Its Product Alpha-Synuclein on Non-Motor Features of Parkinson's Disease. *Life (Basel)*, *11*(8). https://doi.org/10.3390/life11080804

Mahlknecht, P., Marini, K., Werkmann, M., Poewe, W., & Seppi, K. (2022). Prodromal Parkinson's disease: hype or hope for disease-modification trials? *Transl Neurodegener*, *11*(1), 11. https://doi.org/10.1186/s40035-022-00286-1

Mahul-Mellier, A. L., Burtscher, J., Maharjan, N., Weerens, L., Croisier, M., Kuttler, F., Leleu, M., Knott, G. W., & Lashuel, H. A. (2020). The process of Lewy body formation, rather than simply alpha-synuclein fibrillization, is one of the major drivers of neurodegeneration. *Proc Natl Acad Sci U S A*, *117*(9), 4971-4982. https://doi.org/10.1073/pnas.1913904117

Malfertheiner, K., Stefanova, N., & Heras-Garvin, A. (2021). The Concept of alpha-Synuclein Strains and How Different Conformations May Explain Distinct Neurodegenerative Disorders. *Front Neurol*, *12*, 737195. https://doi.org/10.3389/fneur.2021.737195

Malkus, K. A., & Ischiropoulos, H. (2012). Regional deficiencies in chaperone-mediated autophagy underlie alpha-synuclein aggregation and neurodegeneration. *Neurobiol Dis*, *46*(3), 732-744. https://doi.org/10.1016/j.nbd.2012.03.017

Man, W. K., Tahirbegi, B., Vrettas, M. D., Preet, S., Ying, L., Vendruscolo, M., De Simone, A., & Fusco, G. (2021). The docking of synaptic vesicles on the presynaptic membrane induced by alpha-synuclein is modulated by lipid composition. *Nat Commun*, *12*(1), 927. https://doi.org/10.1038/s41467-021-21027-4

Mao, X., Ou, M. T., Karuppagounder, S. S., Kam, T. I., Yin, X., Xiong, Y., Ge, P., Umanah, G. E., Brahmachari, S., Shin, J. H., Kang, H. C., Zhang, J., Xu, J., Chen, R., Park, H., Andrabi, S. A., Kang, S. U., Goncalves, R. A., Liang, Y., . . . Dawson, T. M. (2016). Pathological alpha-synuclein transmission initiated by binding lymphocyte-activation gene 3. *Science*, *353*(6307). https://doi.org/10.1126/science.aah3374

Martini-Stoica, H., Xu, Y., Ballabio, A., & Zheng, H. (2016). The Autophagy-Lysosomal Pathway in Neurodegeneration: A TFEB Perspective. *Trends Neurosci*, *39*(4), 221-234. https://doi.org/10.1016/j.tins.2016.02.002

Masaracchia, C., Hnida, M., Gerhardt, E., Lopes da Fonseca, T., Villar-Pique, A., Branco, T., Stahlberg, M. A., Dean, C., Fernandez, C. O., Milosevic, I., & Outeiro, T. F. (2018). Membrane binding, internalization, and sorting of alpha-synuclein in the cell. *Acta Neuropathol Commun*, *6*(1), 79. https://doi.org/10.1186/s40478-018-0578-1

Mason, H. D., & McGavern, D. B. (2022). How the immune system shapes neurodegenerative diseases. *Trends Neurosci*, *45*(10), 733-748. https://doi.org/10.1016/j.tins.2022.08.001

Masuda-Suzukake, M., Nonaka, T., Hosokawa, M., Oikawa, T., Arai, T., Akiyama, H., Mann, D. M., & Hasegawa, M. (2013). Prion-like spreading of pathological alpha-synuclein in brain. *Brain*, *136*(Pt 4), 1128-1138. https://doi.org/10.1093/brain/awt037

Matheoud, D., Cannon, T., Voisin, A., Penttinen, A. M., Ramet, L., Fahmy, A. M., Ducrot, C., Laplante, A., Bourque, M. J., Zhu, L., Cayrol, R., Le Campion, A., McBride, H. M., Gruenheid, S., Trudeau, L. E., & Desjardins, M. (2019). Intestinal infection triggers Parkinson's disease-like symptoms in Pink1(-/-) mice. *Nature*, *571*(7766), 565-569. https://doi.org/10.1038/s41586-019-1405-y

McGregor, M. M., & Nelson, A. B. (2019). Circuit Mechanisms of Parkinson's Disease. *Neuron*, *101*(6), 1042-1056. https://doi.org/10.1016/j.neuron.2019.03.004

McKeith, I., Mintzer, J., Aarsland, D., Burn, D., Chiu, H., Cohen-Mansfield, J., Dickson, D., Dubois, B., Duda, J. E., Feldman, H., Gauthier, S., Halliday, G., Lawlor, B., Lippa, C., Lopez, O. L., Carlos Machado, J., O'Brien, J., Playfer, J., Reid, W., & International Psychogeriatric Association Expert Meeting on, D. L. B. (2004). Dementia with Lewy bodies. *Lancet Neurol*, *3*(1), 19-28. https://doi.org/10.1016/s1474-4422(03)00619-7

McWilliams, T. G., Prescott, A. R., Montava-Garriga, L., Ball, G., Singh, F., Barini, E., Muqit, M. M. K., Brooks, S. P., & Ganley, I. G. (2018). Basal Mitophagy Occurs Independently of PINK1 in Mouse Tissues of High Metabolic Demand. *Cell Metab*, *27*(2), 439-449 e435. https://doi.org/10.1016/j.cmet.2017.12.008

Miraglia, F., Ricci, A., Rota, L., & Colla, E. (2018). Subcellular localization of alpha-synuclein aggregates and their interaction with membranes. *Neural Regen Res*, *13*(7), 1136-1144. https://doi.org/10.4103/1673-5374.235013

Moisoi, N., Fedele, V., Edwards, J., & Martins, L. M. (2014). Loss of PINK1 enhances neurodegeneration in a mouse model of Parkinson's disease triggered by mitochondrial stress. *Neuropharmacology*, *77*, 350-357. https://doi.org/10.1016/j.neuropharm.2013.10.009

Mou, Z., Yuan, Y. H., Zhang, Z., Song, L. K., & Chen, N. H. (2020). Endoplasmic reticulum stress, an important factor in the development of Parkinson's disease. *Toxicol Lett*, *324*, 20-29. https://doi.org/10.1016/j.toxlet.2020.01.019

Mulherkar, N., Raaben, M., de la Torre, J. C., Whelan, S. P., & Chandran, K. (2011). The Ebola virus glycoprotein mediates entry via a non-classical dynamin-dependent macropinocytic pathway. *Virology*, *419*(2), 72-83. https://doi.org/10.1016/j.virol.2011.08.009

Murphy, K. E., Gysbers, A. M., Abbott, S. K., Spiro, A. S., Furuta, A., Cooper, A., Garner, B., Kabuta, T., & Halliday, G. M. (2015). Lysosomal-associated membrane protein 2 isoforms are differentially affected in early Parkinson's disease. *Mov Disord*, *30*(12), 1639-1647. https://doi.org/10.1002/mds.26141

Nagakannan, P., Tabeshmehr, P., & Eftekharpour, E. (2020). Oxidative damage of lysosomes in regulated cell death systems: Pathophysiology and pharmacologic interventions. *Free Radic Biol Med*, *157*, 94-127. https://doi.org/10.1016/j.freeradbiomed.2020.04.001

Nakase, I., Kobayashi, N. B., Takatani-Nakase, T., & Yoshida, T. (2015). Active macropinocytosis induction by stimulation of epidermal growth factor receptor and oncogenic Ras expression potentiates cellular uptake efficacy of exosomes. *Sci Rep*, *5*, 10300. https://doi.org/10.1038/srep10300

Narhi, L., Wood, S. J., Steavenson, S., Jiang, Y., Wu, G. M., Anafi, D., Kaufman, S. A., Martin, F., Sitney, K., Denis, P., Louis, J. C., Wypych, J., Biere, A. L., & Citron, M. (1999). Both familial Parkinson's disease mutations accelerate alpha-synuclein aggregation. *J Biol Chem*, *274*(14), 9843-9846. https://doi.org/10.1074/jbc.274.14.9843

Nash, Y., Schmukler, E., Trudler, D., Pinkas-Kramarski, R., & Frenkel, D. (2017). DJ-1 deficiency impairs autophagy and reduces alpha-synuclein phagocytosis by microglia. *J Neurochem*, *143*(5), 584-594. https://doi.org/10.1111/jnc.14222

Nishioka, K., Hayashi, S., Farrer, M. J., Singleton, A. B., Yoshino, H., Imai, H., Kitami, T., Sato, K., Kuroda, R., Tomiyama, H., Mizoguchi, K., Murata, M., Toda, T., Imoto, I., Inazawa, J., Mizuno, Y., & Hattori, N. (2006). Clinical heterogeneity of alpha-synuclein gene duplication in Parkinson's disease. *Ann Neurol*, *59*(2), 298-309. https://doi.org/10.1002/ana.20753

Nuber, S., Rajsombath, M., Minakaki, G., Winkler, J., Muller, C. P., Ericsson, M., Caldarone, B., Dettmer, U., & Selkoe, D. J. (2018). Abrogating Native alpha-Synuclein Tetramers in Mice Causes a L-DOPA-Responsive Motor Syndrome Closely Resembling Parkinson's Disease. *Neuron*, *100*(1), 75-90 e75. https://doi.org/10.1016/j.neuron.2018.09.014

Oh, P., McIntosh, D. P., & Schnitzer, J. E. (1998). Dynamin at the neck of caveolae mediates their budding to form transport vesicles by GTP-driven fission from the plasma membrane of endothelium. *J Cell Biol*, *141*(1), 101-114. https://doi.org/10.1083/jcb.141.1.101

Oh, S. H., Kim, H. N., Park, H. J., Shin, J. Y., Bae, E. J., Sunwoo, M. K., Lee, S. J., & Lee, P. H. (2016). Mesenchymal Stem Cells Inhibit Transmission of alpha-Synuclein by Modulating Clathrin-Mediated Endocytosis in a Parkinsonian Model. *Cell Rep*, *14*(4), 835-849. https://doi.org/10.1016/j.celrep.2015.12.075

Ohgita, T., Namba, N., Kono, H., Shimanouchi, T., & Saito, H. (2022). Mechanisms of enhanced aggregation and fibril formation of Parkinson's disease-related variants of alpha-synuclein. *Sci Rep*, *12*(1), 6770. https://doi.org/10.1038/s41598-022-10789-6

Olanow, C. W., Perl, D. P., DeMartino, G. N., & McNaught, K. S. P. (2004). Lewy-body formation is an aggresome-related process: a hypothesis. *The Lancet Neurology*, *3*(8), 496-503. https://doi.org/10.1016/s1474-4422(04)00827-0

Ott, M., Gogvadze, V., Orrenius, S., & Zhivotovsky, B. (2007). Mitochondria, oxidative stress and cell death. *Apoptosis*, *12*(5), 913-922. https://doi.org/10.1007/s10495-007-0756-2

Pajares, M., Rojo, A. I., Arias, E., Diaz-Carretero, A., Cuervo, A. M., & Cuadrado, A. (2018). Transcription factor NFE2L2/NRF2 modulates chaperone-mediated autophagy through the regulation of LAMP2A. *Autophagy*, *14*(8), 1310-1322. https://doi.org/10.1080/15548627.2018.1474992

Palomba, N. P., Fortunato, G., Pepe, G., Modugno, N., Pietracupa, S., Damiano, I., Mascio, G., Carrillo, F., Di Giovannantonio, L. G., Ianiro, L., Martinello, K., Volpato, V., Desiato, V., Acri, R., Storto, M., Nicoletti, F., Webber, C., Simeone, A., Fucile, S., . . . Esposito, T. (2023). Common and Rare Variants in TMEM175 Gene Concur to the Pathogenesis of Parkinson's Disease in Italian Patients. *Mol Neurobiol*, *60*(4), 2150-2173. https://doi.org/10.1007/s12035-022-03203-9

Pampalakis, G., Sykioti, V. S., Ximerakis, M., Stefanakou-Kalakou, I., Melki, R., Vekrellis, K., & Sotiropoulou, G. (2017). KLK6 proteolysis is implicated in the turnover and uptake of extracellular alpha-synuclein species. *Oncotarget*, *8*(9), 14502-14515. https://doi.org/10.18632/oncotarget.13264

Pan, Y., Zong, Q., Li, G., Wu, Z., Du, T., Huang, Z., Zhang, Y., & Ma, K. (2022). Nuclear localization of alpha-synuclein affects the cognitive and motor behavior of mice by inducing DNA damage and abnormal cell cycle of hippocampal neurons. *Front Mol Neurosci*, *15*, 1015881. https://doi.org/10.3389/fnmol.2022.1015881

Panagiotakopoulou, V., Ivanyuk, D., De Cicco, S., Haq, W., Arsic, A., Yu, C., Messelodi, D., Oldrati, M., Schondorf, D. C., Perez, M. J., Cassatella, R. P., Jakobi, M., Schneiderhan-Marra, N., Gasser, T., Nikic-Spiegel, I., & Deleidi, M. (2020). Interferon-gamma signaling synergizes with LRRK2 in neurons and microglia derived from human induced pluripotent stem cells. *Nat Commun*, *11*(1), 5163. https://doi.org/10.1038/s41467-020-18755-4

Parihar, M. S., Parihar, A., Fujita, M., Hashimoto, M., & Ghafourifar, P. (2009). Alpha-synuclein overexpression and aggregation exacerbates impairment of mitochondrial functions by augmenting oxidative stress in human neuroblastoma cells. *Int J Biochem Cell Biol*, *41*(10), 2015-2024. https://doi.org/10.1016/j.biocel.2009.05.008

Park, J. Y., Kim, K. S., Lee, S. B., Ryu, J. S., Chung, K. C., Choo, Y. K., Jou, I., Kim, J., & Park, S. M. (2009). On the mechanism of internalization of alpha-synuclein into microglia: roles of ganglioside GM1 and lipid raft. *J Neurochem*, *110*(1), 400-411. https://doi.org/10.1111/j.1471-4159.2009.06150.x

Park, R. J., Shen, H., Liu, L., Liu, X., Ferguson, S. M., & De Camilli, P. (2013). Dynamin triple knockout cells reveal off target effects of commonly used dynamin inhibitors. *J Cell Sci*, *126*(Pt 22), 5305-5312. https://doi.org/10.1242/jcs.138578

Parker, P. R., Lalive, A. L., & Kreitzer, A. C. (2016). Pathway-Specific Remodeling of Thalamostriatal Synapses in Parkinsonian Mice. *Neuron*, *89*(4), 734-740. https://doi.org/10.1016/j.neuron.2015.12.038

Peelaerts, W., Bousset, L., Van der Perren, A., Moskalyuk, A., Pulizzi, R., Giugliano, M., Van den Haute, C., Melki, R., & Baekelandt, V. (2015). alpha-Synuclein strains cause distinct synucleinopathies after local and systemic administration. *Nature*, *522*(7556), 340-344. https://doi.org/10.1038/nature14547

Peng, C., Gathagan, R. J., & Lee, V. M. (2018). Distinct alpha-Synuclein strains and implications for heterogeneity among alpha-Synucleinopathies. *Neurobiol Dis*, *109*(Pt B), 209-218. https://doi.org/10.1016/j.nbd.2017.07.018

Pinto-Costa, R., Harbachova, E., La Vitola, P., & Di Monte, D. A. (2023). Overexpression-Induced alpha-Synuclein Brain Spreading. *Neurotherapeutics*, *20*(1), 83-96. https://doi.org/10.1007/s13311-022-01332-6

Polymeropoulos, M. H., Lavedan, C., Leroy, E., Ide, S. E., Dehejia, A., Dutra, A., Pike, B., Root, H., Rubenstein, J., Boyer, R., Stenroos, E. S., Chandrasekharappa, S., Athanassiadou, A., Papapetropoulos, T., Johnson, W. G., Lazzarini, A. M., Duvoisin, R. C., Di Iorio, G., Golbe, L. I., & Nussbaum, R. L. (1997). Mutation in the alpha-synuclein gene identified in families with Parkinson's disease. *Science*, *276*(5321), 2045-2047. https://doi.org/10.1126/science.276.5321.2045

Pukass, K., & Richter-Landsberg, C. (2014). Oxidative stress promotes uptake, accumulation, and oligomerization of extracellular alpha-synuclein in oligodendrocytes. *J Mol Neurosci*, *52*(3), 339-352. https://doi.org/10.1007/s12031-013-0154-x

Puspita, L., Chung, S. Y., & Shim, J. W. (2017). Oxidative stress and cellular pathologies in Parkinson's disease. *Mol Brain*, *10*(1), 53. https://doi.org/10.1186/s13041-017-0340-9

Rahmani, Z., Surabhi, S., Rojo-Cortes, F., Dulac, A., Jenny, A., & Birman, S. (2022). Lamp1 Deficiency Enhances Sensitivity to alpha-Synuclein and Oxidative Stress in Drosophila Models of Parkinson Disease. *Int J Mol Sci*, *23*(21). https://doi.org/10.3390/ijms232113078

Rajput, A. H., Offord, K. P., Beard, C. M., & Kurland, L. T. (1984). Epidemiology of parkinsonism: incidence, classification, and mortality. *Ann Neurol*, *16*(3), 278-282. https://doi.org/10.1002/ana.410160303

Ramezani, M., Wilkes, M. M., Das, T., Holowka, D., Eliezer, D., & Baird, B. (2019). Regulation of exocytosis and mitochondrial relocalization by Alpha-synuclein in a mammalian cell model. *NPJ Parkinsons Dis*, *5*, 12. https://doi.org/10.1038/s41531-019-0084-6

Ray, K., Bobard, A., Danckaert, A., Paz-Haftel, I., Clair, C., Ehsani, S., Tang, C., Sansonetti, P., Tran, G. V., & Enninga, J. (2010). Tracking the dynamic interplay between bacterial and host factors during pathogen-induced vacuole rupture in real time. *Cell Microbiol*, *12*(4), 545-556. https://doi.org/10.1111/j.1462-5822.2010.01428.x

Reyes, J. F., Rey, N. L., Bousset, L., Melki, R., Brundin, P., & Angot, E. (2014). Alpha-synuclein transfers from neurons to oligodendrocytes. *Glia*, *62*(3), 387-398. https://doi.org/10.1002/glia.22611

Reyes, J. F., Sackmann, C., Hoffmann, A., Svenningsson, P., Winkler, J., Ingelsson, M., & Hallbeck, M. (2019). Binding of alpha-synuclein oligomers to Cx32 facilitates protein uptake and transfer in neurons and oligodendrocytes. *Acta Neuropathol*, *138*(1), 23-47. https://doi.org/10.1007/s00401-019-02007-x

Rocha, E. M., De Miranda, B., & Sanders, L. H. (2018). Alpha-synuclein: Pathology, mitochondrial dysfunction and neuroinflammation in Parkinson's disease. *Neurobiol Dis*, *109*(Pt B), 249-257. https://doi.org/10.1016/j.nbd.2017.04.004

Rojo, A. I., Pajares, M., Rada, P., Nunez, A., Nevado-Holgado, A. J., Killik, R., Van Leuven, F., Ribe, E., Lovestone, S., Yamamoto, M., & Cuadrado, A. (2017). NRF2 deficiency replicates transcriptomic changes in Alzheimer's patients and worsens APP and TAU pathology. *Redox Biol*, *13*, 444-451. https://doi.org/10.1016/j.redox.2017.07.006

Rostami, J., Holmqvist, S., Lindstrom, V., Sigvardson, J., Westermark, G. T., Ingelsson, M., Bergstrom, J., Roybon, L., & Erlandsson, A. (2017). Human Astrocytes Transfer Aggregated Alpha-Synuclein via Tunneling Nanotubes. *J Neurosci*, *37*(49), 11835-11853. https://doi.org/10.1523/JNEUROSCI.0983-17.2017

Rutherford, N. J., Moore, B. D., Golde, T. E., & Giasson, B. I. (2014). Divergent effects of the H50Q and G51D SNCA mutations on the aggregation of alpha-synuclein. *J Neurochem*, *131*(6), 859-867. https://doi.org/10.1111/jnc.12806

Saha, S., Buttari, B., Profumo, E., Tucci, P., & Saso, L. (2021). A Perspective on Nrf2 Signaling Pathway for Neuroinflammation: A Potential Therapeutic Target in Alzheimer's and Parkinson's Diseases. *Front Cell Neurosci*, *15*, 787258. https://doi.org/10.3389/fncel.2021.787258

Sala, G., Arosio, A., Stefanoni, G., Melchionda, L., Riva, C., Marinig, D., Brighina, L., & Ferrarese, C. (2013). Rotenone upregulates alpha-synuclein and myocyte enhancer factor 2D independently from lysosomal degradation inhibition. *Biomed Res Int*, *2013*, 846725. https://doi.org/10.1155/2013/846725

Sala, G., Marinig, D., Arosio, A., & Ferrarese, C. (2016). Role of Chaperone-Mediated Autophagy Dysfunctions in the Pathogenesis of Parkinson's Disease. *Front Mol Neurosci*, *9*, 157. https://doi.org/10.3389/fnmol.2016.00157

Samuel, F., Flavin, W. P., Iqbal, S., Pacelli, C., Sri Renganathan, S. D., Trudeau, L. E., Campbell, E. M., Fraser, P. E., & Tandon, A. (2016). Effects of Serine 129 Phosphorylation on alpha-Synuclein Aggregation, Membrane Association, and Internalization. *J Biol Chem*, *291*(9), 4374-4385. https://doi.org/10.1074/jbc.M115.705095

Sarkar, S., Olsen, A. L., Sygnecka, K., Lohr, K. M., & Feany, M. B. (2021). alpha-synuclein impairs autophagosome maturation through abnormal actin stabilization. *PLoS Genet*, *17*(2), e1009359. https://doi.org/10.1371/journal.pgen.1009359

Schechter, M., Atias, M., Abd Elhadi, S., Davidi, D., Gitler, D., & Sharon, R. (2020). alpha-Synuclein facilitates endocytosis by elevating the steady-state levels of phosphatidylinositol 4,5-bisphosphate. *J Biol Chem*, *295*(52), 18076-18090. https://doi.org/10.1074/jbc.RA120.015319

Schlunck, G., Damke, H., Kiosses, W. B., Rusk, N., Symons, M. H., Waterman-Storer, C. M., Schmid, S. L., & Schwartz, M. A. (2004). Modulation of Rac localization and function by dynamin. *Mol Biol Cell*, *15*(1), 256-267. https://doi.org/10.1091/mbc.e03-01-0019

Schweighauser, M., Arseni, D., Bacioglu, M., Huang, M., Lovestam, S., Shi, Y., Yang, Y., Zhang, W., Kotecha, A., Garringer, H. J., Vidal, R., Hallinan, G. I., Newell, K. L., Tarutani, A., Murayama, S., Miyazaki, M., Saito, Y., Yoshida, M., Hasegawa, K., . . . Scheres, S. H. W. (2022). Age-dependent formation of TMEM106B amyloid filaments in human brains. *Nature*, *605*(7909), 310-314. https://doi.org/10.1038/s41586-022-04650-z

Scudamore, O., & Ciossek, T. (2018). Increased Oxidative Stress Exacerbates alpha-Synuclein Aggregation In Vivo. *J Neuropathol Exp Neurol*, *77*(6), 443-453. https://doi.org/10.1093/jnen/nly024

Shahmoradian, S. H., Lewis, A. J., Genoud, C., Hench, J., Moors, T. E., Navarro, P. P., Castano-Diez, D., Schweighauser, G., Graff-Meyer, A., Goldie, K. N., Sutterlin, R., Huisman, E., Ingrassia, A., Gier, Y., Rozemuller, A. J. M., Wang, J., Paepe, A., Erny, J., Staempfli, A., . . . Lauer, M. E. (2019). Lewy pathology in Parkinson's disease consists of crowded organelles and lipid membranes. *Nat Neurosci*, *22*(7), 1099-1109. https://doi.org/10.1038/s41593-019-0423-2

Shaltouki, A., Hsieh, C. H., Kim, M. J., & Wang, X. (2018). Alpha-synuclein delays mitophagy and targeting Miro rescues neuron loss in Parkinson's models. *Acta Neuropathol*, *136*(4), 607-620. https://doi.org/10.1007/s00401-018-1873-4

Shearer, L. J., Petersen, N. O., & Woodside, M. T. (2021). Internalization of alpha-synuclein oligomers into SH-SY5Y cells. *Biophys J*. https://doi.org/10.1016/j.bpj.2020.12.031

Shekoohi, S., Rajasekaran, S., Patel, D., Yang, S., Liu, W., Huang, S., Yu, X., & Witt, S. N. (2021). Knocking out alpha-synuclein in melanoma cells dysregulates cellular iron metabolism and suppresses tumor growth. *Sci Rep*, *11*(1), 5267. https://doi.org/10.1038/s41598-021-84443-y

Sidransky, E., Nalls, M. A., Aasly, J. O., Aharon-Peretz, J., Annesi, G., Barbosa, E. R., Bar-Shira, A., Berg, D., Bras, J., Brice, A., Chen, C. M., Clark, L. N., Condroyer, C., De Marco, E. V., Durr, A., Eblan, M. J., Fahn, S., Farrer, M. J., Fung, H. C., . . . Ziegler, S. G. (2009). Multicenter analysis of glucocerebrosidase mutations in Parkinson's disease. *N Engl J Med*, *361*(17), 1651-1661. https://doi.org/10.1056/NEJMoa0901281

Singleton, A. B., Farrer, M., Johnson, J., Singleton, A., Hague, S., Kachergus, J., Hulihan, M., Peuralinna, T., Dutra, A., Nussbaum, R., Lincoln, S., Crawley, A., Hanson, M., Maraganore, D., Adler, C., Cookson, M. R., Muenter, M., Baptista, M., Miller, D., . . .

Gwinn-Hardy, K. (2003). alpha-Synuclein locus triplication causes Parkinson's disease. *Science*, *302*(5646), 841. https://doi.org/10.1126/science.1090278

Sjodin, S., Brinkmalm, G., Ohrfelt, A., Parnetti, L., Paciotti, S., Hansson, O., Hardy, J., Blennow, K., Zetterberg, H., & Brinkmalm, A. (2019). Endo-lysosomal proteins and ubiquitin CSF concentrations in Alzheimer's and Parkinson's disease. *Alzheimers Res Ther*, *11*(1), 82. https://doi.org/10.1186/s13195-019-0533-9

Smith, B. R., Santos, M. B., Marshall, M. S., Cantuti-Castelvetri, L., Lopez-Rosas, A., Li, G., van Breemen, R., Claycomb, K. I., Gallea, J. I., Celej, M. S., Crocker, S. J., Givogri, M. I., & Bongarzone, E. R. (2014). Neuronal inclusions of alpha-synuclein contribute to the pathogenesis of Krabbe disease. *J Pathol*, *232*(5), 509-521. https://doi.org/10.1002/path.4328

Smith, J. A., Das, A., Ray, S. K., & Banik, N. L. (2012). Role of pro-inflammatory cytokines released from microglia in neurodegenerative diseases. *Brain Res Bull*, *87*(1), 10-20. https://doi.org/10.1016/j.brainresbull.2011.10.004

Smith, Y., Raju, D. V., Pare, J. F., & Sidibe, M. (2004). The thalamostriatal system: a highly specific network of the basal ganglia circuitry. *Trends Neurosci*, *27*(9), 520-527. https://doi.org/10.1016/j.tins.2004.07.004

Sokratian, A., Zhou, Y., Xu, E., Viverette, E., Dillard, L., Yuan, Y., Li, J. Y., Matarangas, A., Bouvette, J., Borgnia, M., Bartesaghi, A., & West, A. (2022). *Structural and functional landscape of α-synuclein fibril conformations amplified from cerebrospinal fluid*.

Somayaji, M., Cataldi, S., Choi, S. J., Edwards, R. H., Mosharov, E. V., & Sulzer, D. (2020). A dual role for alpha-synuclein in facilitation and depression of dopamine release from substantia nigra neurons in vivo. *Proc Natl Acad Sci U S A*, *117*(51), 32701-32710. https://doi.org/10.1073/pnas.2013652117

Song, L. K., Ma, K. L., Yuan, Y. H., Mu, Z., Song, X. Y., Niu, F., Han, N., & Chen, N. H. (2015). Targeted Overexpression of alpha-Synuclein by rAAV2/1 Vectors Induces Progressive Nigrostriatal Degeneration and Increases Vulnerability to MPTP in Mouse. *PLoS One*, *10*(6), e0131281. https://doi.org/10.1371/journal.pone.0131281

Soper, J. H., Roy, S., Stieber, A., Lee, E., Wilson, R. B., Trojanowski, J. Q., Burd, C. G., & Lee, V. M.-Y. (2008). α-Synuclein–induced Aggregation of Cytoplasmic Vesicles in Saccharomyces cerevisiae. *Molecular biology of the cell*, *19*(3), 1093-1103.

Spillantini, M. G., Schmidt, M. L., Lee, V. M., Trojanowski, J. Q., Jakes, R., & Goedert, M. (1997). Alpha-synuclein in Lewy bodies. *Nature*, *388*(6645), 839-840. https://doi.org/https://doi.org/10.1038/42166

Stykel, M. G., Humphries, K. M., Kamski-Hennekam, E., Buchner-Duby, B., Porte-Trachsel, N., Ryan, T., Coackley, C. L., Bamm, V. V., Harauz, G., & Ryan, S. D. (2021). alpha-Synuclein mutation impairs processing of endomembrane compartments and promotes exocytosis and seeding of alpha-synuclein pathology. *Cell Rep*, *35*(6), 109099. https://doi.org/10.1016/j.celrep.2021.109099

Sung, J. Y., Kim, J., Paik, S. R., Park, J. H., Ahn, Y. S., & Chung, K. C. (2001). Induction of neuronal cell death by Rab5A-dependent endocytosis of alpha-synuclein. *J Biol Chem*, *276*(29), 27441-27448. https://doi.org/10.1074/jbc.M101318200

Surmeier, D. J., Obeso, J. A., & Halliday, G. M. (2017). Parkinson's Disease Is Not Simply a Prion Disorder. *J Neurosci*, *37*(41), 9799-9807. https://doi.org/10.1523/JNEUROSCI.1787-16.2017

Suzen, S., Tucci, P., Profumo, E., Buttari, B., & Saso, L. (2022). A Pivotal Role of Nrf2 in Neurodegenerative Disorders: A New Way for Therapeutic Strategies. *Pharmaceuticals (Basel)*, *15*(6). https://doi.org/10.3390/ph15060692

Tait, S. W., & Green, D. R. (2008). Caspase-independent cell death: leaving the set without the final cut. *Oncogene*, *27*(50), 6452-6461. https://doi.org/10.1038/onc.2008.311

Tan, E. K., Chao, Y. X., West, A., Chan, L. L., Poewe, W., & Jankovic, J. (2020). Parkinson disease and the immune system - associations, mechanisms and therapeutics. *Nat Rev Neurol*, *16*(6), 303-318. https://doi.org/10.1038/s41582-020-0344-4

Tanaka, M., Kim, Y. M., Lee, G., Junn, E., Iwatsubo, T., & Mouradian, M. M. (2004). Aggresomes formed by alpha-synuclein and synphilin-1 are cytoprotective. *J Biol Chem*, *279*(6), 4625-4631. https://doi.org/10.1074/jbc.M310994200

Tansey, M. G., Wallings, R. L., Houser, M. C., Herrick, M. K., Keating, C. E., & Joers, V. (2022). Inflammation and immune dysfunction in Parkinson disease. *Nat Rev Immunol*, *22*(11), 657-673. https://doi.org/10.1038/s41577-022-00684-6

Thakur, P., Breger, L. S., Lundblad, M., Wan, O. W., Mattsson, B., Luk, K. C., Lee, V. M. Y., Trojanowski, J. Q., & Bjorklund, A. (2017). Modeling Parkinson's disease pathology by combination of fibril seeds and alpha-synuclein overexpression in the rat brain. *Proc Natl Acad Sci U S A*, *114*(39), E8284-E8293. https://doi.org/10.1073/pnas.1710442114

Thomas, B., & Beal, M. F. (2007). Parkinson's disease. *Hum Mol Genet*, *16 Spec No. 2*, R183-194. https://doi.org/10.1093/hmg/ddm159

Tomiyama, H., Lesage, S., Tan, E. K., & Jeon, B. S. (2015). Familial Parkinson's disease/parkinsonism. *Biomed Res Int*, *2015*, 736915. https://doi.org/10.1155/2015/736915

Tran, H. T., Chung, C. H., Iba, M., Zhang, B., Trojanowski, J. Q., Luk, K. C., & Lee, V. M. (2014). Alpha-synuclein immunotherapy blocks uptake and templated propagation of misfolded alpha-synuclein and neurodegeneration. *Cell Rep*, *7*(6), 2054-2065. https://doi.org/10.1016/j.celrep.2014.05.033

Trinkaus, V. A., Riera-Tur, I., Martinez-Sanchez, A., Bauerlein, F. J. B., Guo, Q., Arzberger, T., Baumeister, W., Dudanova, I., Hipp, M. S., Hartl, F. U., & Fernandez-Busnadiego, R. (2021). In situ architecture of neuronal alpha-Synuclein inclusions. *Nat Commun*, *12*(1), 2110. https://doi.org/10.1038/s41467-021-22108-0

Tsunemi, T., Perez-Rosello, T., Ishiguro, Y., Yoroisaka, A., Jeon, S., Hamada, K., Rammonhan, M., Wong, Y. C., Xie, Z., Akamatsu, W., Mazzulli, J. R., Surmeier, D. J., Hattori, N., & Krainc, D. (2019). Increased Lysosomal Exocytosis Induced by Lysosomal Ca(2+) Channel Agonists Protects Human Dopaminergic Neurons from alpha-Synuclein Toxicity. *J Neurosci*, *39*(29), 5760-5772. https://doi.org/10.1523/JNEUROSCI.3085-18.2019

Tyson, T., Steiner, J. A., & Brundin, P. (2016). Sorting out release, uptake and processing of alpha-synuclein during prion-like spread of pathology. *J Neurochem*, *139 Suppl 1*, 275-289. https://doi.org/10.1111/jnc.13449

Underwood, R., Wang, B., Pathak, A., Volpicelli-Daley, L., & Yacoubian, T. A. (2020). Rab27 GTPases regulate alpha-synuclein uptake, cell-to-cell transmission, and toxicity [Preprint]. *bioRxiv*. https://doi.org/10.1101/2020.11.17.387449

Valdinocci, D., Radford, R. A., Siow, S. M., Chung, R. S., & Pountney, D. L. (2017). Potential Modes of Intercellular alpha-Synuclein Transmission. *Int J Mol Sci*, *18*(2). https://doi.org/10.3390/ijms18020469

Van Opdenbosch, N., & Lamkanfi, M. (2019). Caspases in Cell Death, Inflammation, and Disease. *Immunity*, *50*(6), 1352-1364. https://doi.org/10.1016/j.immuni.2019.05.020

Vargas, K. J., Colosi, P. L., Girardi, E., Park, J.-M., & Chandra, S. S. (2021). *α-Synuclein facilitates clathrin assembly in synaptic vesicle endocytosis*.

Vargas, K. J., Makani, S., Davis, T., Westphal, C. H., Castillo, P. E., & Chandra, S. S. (2014). Synucleins regulate the kinetics of synaptic vesicle endocytosis. *J Neurosci*, *34*(28), 9364-9376. https://doi.org/10.1523/JNEUROSCI.4787-13.2014

Vargas, K. J., Schrod, N., Davis, T., Fernandez-Busnadiego, R., Taguchi, Y. V., Laugks, U., Lucic, V., & Chandra, S. S. (2017). Synucleins Have Multiple Effects on Presynaptic Architecture. *Cell Rep*, *18*(1), 161-173. https://doi.org/10.1016/j.celrep.2016.12.023

Verwer, R. W., Hermens, W. T., Dijkhuizen, P., ter Brake, O., Baker, R. E., Salehi, A., Sluiter, A. A., Kok, M. J., Muller, L. J., Verhaagen, J., & Swaab, D. F. (2002). Cells in human postmortem brain tissue slices remain alive for several weeks in culture. *FASEB J*, *16*(1), 54-60. https://doi.org/10.1096/fj.01-0504com

Vila, M., Bove, J., Dehay, B., Rodriguez-Muela, N., & Boya, P. (2011). Lysosomal membrane permeabilization in Parkinson disease. *Autophagy*, *7*(1), 98-100. https://doi.org/10.4161/auto.7.1.13933

Visanji, N. P., Brooks, P. L., Hazrati, L.-N., & Lang, A. E. (2013). The prion hypothesis in Parkinson's disease: Braak to the future. *Acta Neuropathologica Communications*, *1*(1), 2. https://doi.org/10.1186/2051-5960-1-2

Volpicelli-Daley, L., & Brundin, P. (2018). Prion-like propagation of pathology in Parkinson disease. *Handb Clin Neurol*, *153*, 321-335. https://doi.org/10.1016/B978-0-444-63945-5.00017-9

von Einem, B., Eschbach, J., Kiechle, M., Wahler, A., Thal, D. R., McLean, P. J., Weishaupt, J. H., Ludolph, A. C., von Arnim, C. A. F., & Danzer, K. M. (2017). The Golgi-localized, gamma ear-containing, ARF-binding (GGA) protein family alters alpha synuclein (alpha-syn) oligomerization and secretion. *Aging (Albany NY)*, *9*(7), 1677-1697. https://doi.org/10.18632/aging.101261

Wakabayashi, K., Tanji, K., Odagiri, S., Miki, Y., Mori, F., & Takahashi, H. (2013). The Lewy body in Parkinson's disease and related neurodegenerative disorders. *Mol Neurobiol*, *47*(2), 495-508. https://doi.org/10.1007/s12035-012-8280-y

Wang, L., Das, U., Scott, D. A., Tang, Y., McLean, P. J., & Roy, S. (2014). alpha-synuclein multimers cluster synaptic vesicles and attenuate recycling. *Curr Biol*, *24*(19), 2319-2326. https://doi.org/10.1016/j.cub.2014.08.027

Wang, X., Shinkai, Y., & Doi, M. (2021). Retrogradely transmitted α-synuclein is taken up by the endophilin-independent endocytosis in the C. elegans neural circuit. *Biochemical and Biophysical Research Communications*, *552*, 176-182. https://doi.org/https://doi.org/10.1016/j.bbrc.2021.03.029

Westphal, C. H., & Chandra, S. S. (2013). Monomeric synucleins generate membrane curvature. *J Biol Chem*, *288*(3), 1829-1840. https://doi.org/10.1074/jbc.M112.418871

Wie, J., Liu, Z., Song, H., Tropea, T. F., Yang, L., Wang, H., Liang, Y., Cang, C., Aranda, K., Lohmann, J., Yang, J., Lu, B., Chen-Plotkin, A. S., Luk, K. C., & Ren, D. (2021). A growth-factor-activated lysosomal K+ channel regulates Parkinson's pathology. *Nature*. https://doi.org/10.1038/s41586-021-03185-z

Wilhelm, B. G., Mandad, S., Truckenbrodt, S., Krohnert, K., Schafer, C., Rammner, B., Koo, S. J., Classen, G. A., Krauss, M., Haucke, V., Urlaub, H., & Rizzoli, S. O. (2014). Composition of isolated synaptic boutons reveals the amounts of vesicle trafficking proteins. *Science*, *344*(6187), 1023-1028. https://doi.org/10.1126/science.1252884

Willox, A. K., Sahraoui, Y. M., & Royle, S. J. (2014). Non-specificity of Pitstop 2 in clathrin-mediated endocytosis. *Biol Open*, *3*(5), 326-331. https://doi.org/10.1242/bio.20147955

Xie, Y. X., Naseri, N. N., Fels, J., Kharel, P., Na, Y., Lane, D., Burre, J., & Sharma, M. (2022). Lysosomal exocytosis releases pathogenic alpha-synuclein species from neurons in synucleinopathy models. *Nat Commun*, *13*(1), 4918. https://doi.org/10.1038/s41467-022-32625-1

Xilouri, M., Brekk, O. R., & Stefanis, L. (2016). Autophagy and Alpha-Synuclein: Relevance to Parkinson's Disease and Related Synucleopathies. *Mov Disord*, *31*(2), 178-192. https://doi.org/10.1002/mds.26477

Xu, L., & Pu, J. (2016). Alpha-Synuclein in Parkinson's Disease: From Pathogenetic Dysfunction to Potential Clinical Application. *Parkinsons Dis*, *2016*, 1720621. https://doi.org/10.1155/2016/1720621

Yamagishi, S., Koyama, Y., Katayama, T., Taniguchi, M., Hitomi, J., Kato, M., Aoki, M., Itoyama, Y., Kato, S., & Tohyama, M. (2007). An in vitro model for Lewy body-like hyaline inclusion/astrocytic hyaline inclusion: induction by ER stress with an ALS-linked SOD1 mutation. *PLoS One*, *2*(10), e1030. https://doi.org/10.1371/journal.pone.0001030

Yang, Q., Wang, G., & Zhang, F. (2020). Role of Peripheral Immune Cells-Mediated Inflammation on the Process of Neurodegenerative Diseases. *Front Immunol*, *11*, 582825. https://doi.org/10.3389/fimmu.2020.582825

Yang, Y., Garringer, H. J., Shi, Y., Lovestam, S., Peak-Chew, S., Zhang, X., Kotecha, A., Bacioglu, M., Koto, A., Takao, M., Spillantini, M. G., Ghetti, B., Vidal, R., Murzin, A. G., Scheres, S. H. W., & Goedert, M. (2023). New SNCA mutation and structures of alpha-synuclein filaments from juvenile-onset synucleinopathy. *Acta Neuropathol*, *145*(5), 561-572. https://doi.org/10.1007/s00401-023-02550-8

Yau, Y., Zeighami, Y., Baker, T. E., Larcher, K., Vainik, U., Dadar, M., Fonov, V. S., Hagmann, P., Griffa, A., Misic, B., Collins, D. L., & Dagher, A. (2018). Network connectivity determines cortical thinning in early Parkinson's disease progression. *Nat Commun*, *9*(1), 12. https://doi.org/10.1038/s41467-017-02416-0

Zarbiv, Y., Simhi-Haham, D., Israeli, E., Elhadi, S. A., Grigoletto, J., & Sharon, R. (2014). Lysine residues at the first and second KTKEGV repeats mediate alpha-Synuclein binding to membrane phospholipids. *Neurobiol Dis*, *70*, 90-98. https://doi.org/10.1016/j.nbd.2014.05.031

Zeineddine, R., Pundavela, J. F., Corcoran, L., Stewart, E. M., Do-Ha, D., Bax, M., Guillemin, G., Vine, K. L., Hatters, D. M., Ecroyd, H., Dobson, C. M., Turner, B. J., Ooi, L., Wilson, M. R., Cashman, N. R., & Yerbury, J. J. (2015). SOD1 protein aggregates stimulate macropinocytosis in neurons to facilitate their propagation. *Mol Neurodegener*, *10*, 57. https://doi.org/10.1186/s13024-015-0053-4

Zhang, Q., Xu, Y., Lee, J., Jarnik, M., Wu, X., Bonifacino, J. S., Shen, J., & Ye, Y. (2020). A myosin-7B-dependent endocytosis pathway mediates cellular entry of alpha-synuclein fibrils and polycation-bearing cargos. *Proc Natl Acad Sci U S A*, *117*(20), 10865-10875. https://doi.org/10.1073/pnas.1918617117

Zhang, S., Liu, Y. Q., Jia, C., Lim, Y. J., Feng, G., Xu, E., Long, H., Kimura, Y., Tao, Y., Zhao, C., Wang, C., Liu, Z., Hu, J. J., Ma, M. R., Liu, Z., Jiang, L., Li, D., Wang, R., Dawson, V. L., . . . Liu, C. (2021). Mechanistic basis for receptor-mediated pathological alpha-synuclein fibril cell-to-cell transmission in Parkinson's disease. *Proc Natl Acad Sci U S A*, *118*(26). https://doi.org/10.1073/pnas.2011196118

Zhang, W., Wang, T., Pei, Z., Miller, D. S., Wu, X., Block, M. L., Wilson, B., Zhang, W., Zhou, Y., Hong, J. S., & Zhang, J. (2005). Aggregated alpha-synuclein activates microglia: a process leading to disease progression in Parkinson's disease. *FASEB J*, *19*(6), 533-542. https://doi.org/10.1096/fj.04-2751com

Zhang, X., Wang, R., Chen, H., Jin, C., Jin, Z., Lu, J., Xu, L., Lu, Y., Zhang, J., & Shi, L. (2022). Aged microglia promote peripheral T cell infiltration by reprogramming the microenvironment of neurogenic niches. *Immun Ageing*, *19*(1), 34. https://doi.org/10.1186/s12979-022-00289-6

Zhi, L., Qin, Q., Muqeem, T., Seifert, E. L., Liu, W., Zheng, S., Li, C., & Zhang, H. (2019). Loss of PINK1 causes age-dependent decrease of dopamine release and mitochondrial dysfunction. *Neurobiol Aging*, *75*, 1-10. https://doi.org/10.1016/j.neurobiolaging.2018.10.025

Zhu, L., He, S., Huang, L., Ren, D., Nie, T., Tao, K., Xia, L., Lu, F., Mao, Z., & Yang, Q. (2022). Chaperone-mediated autophagy degrades Keap1 and promotes Nrf2-mediated antioxidative response. *Aging Cell*, *21*(6), e13616. https://doi.org/10.1111/acel.13616

Zhu, S. Y., Yao, R. Q., Li, Y. X., Zhao, P. Y., Ren, C., Du, X. H., & Yao, Y. M. (2020). Lysosomal quality control of cell fate: a novel therapeutic target for human diseases. *Cell Death Dis*, *11*(9), 817. https://doi.org/10.1038/s41419-020-03032-5

Zoungrana, L. I., Krause-Hauch, M., Wang, H., Fatmi, M. K., Bates, L., Li, Z., Kulkarni, P., Ren, D., & Li, J. (2022). The Interaction of mTOR and Nrf2 in Neurogenesis and Its Implication in Neurodegenerative Diseases. *Cells*, *11*(13). https://doi.org/10.3390/cells11132048

Preface for Chapter 2

Although the paper describing the conjugation process α-synuclein PFFs to nanogold beads was published following our initial paper on PFF endocytosis, the protocol involved in the conjugation process is integral to our findings in our initial paper, hence why that methodology is presented here first, prior to our initial paper on PFF endocytosis. By following PFF internalization using nanogold-labeled PFFs, we were able to follow the step-by-step internalization of PFFs in a way that had never been visualized before. Apart from our genetic and chemical approaches to show that CME does not play a role in PFF internalization, we definitively show that PFFs do not use CME through our EM data, showing no signs of Clathrin-coated pits internalizing PFFs, but the presence of membrane ruffles engulfing PFFs. This is what set our paper apart from the many others that explored the internalization of α-syn fibrils. Additionally, the nanogold-labeled PFFs allowed us to make unprecedented observations about PFF trafficking including their association with the formation of intraluminal vesicles, the presence on the surface of intraluminal vesicles in MVBs, which led us to discovering the transport of PFFs on the surface of exosomes. All these discoveries would not have been possible without the methodology detailed in our protocol paper in Chapter 2.

CHAPTER 2. VISUALIZATION OF ALPHA-SYNUCLEIN TRAFFICKING VIA NANOGOLD LABELING AND ELECTRON MICROSCOPY

2.1 Summary

There is conflicting evidence regarding the mechanisms of α-synuclein internalization, and its trafficking itinerary following cellular entry remains largely unknown. To examine these issues, we describe steps for coupling α-synuclein preformed fibrils (PFFs) to nanogold beads and their subsequent characterization by electron microscopy (EM). Then we describe the uptake of conjugated PFFs by U2OS cells plated on permanox 8-well chamber slides. This process eliminates the reliance on antibody specificity and the need to employ complex immunoEM staining protocols.

2.2 Before you begin

The protocol below outlines the conjugation of PFFs with nanogold beads, to observe PFFs internalization using EM. Before beginning this conjugation process, please plan to have the necessary protocol and reagents in place to produce α-synuclein PFFs. We recommend following the production protocol established by Maneca et al. (2019). Below we outline a summary of the production process.

2.3 Production of alpha-syn preformed fibrils

Timing: ~12 d

1. Produce recombinant human α-synuclein monomers
    a. Transform the pGEX6 plasmid construct into BL21 (DE3) *E. coli* for expression. The GST tag is incorporated on the N terminus of α-synuclein along with a 3C protease cleavage site providing a straightforward route to enrich and cleave GST-

α-synuclein using glutathione beads. Through this route, high levels of monomeric synuclein can be enriched and purified from GST-α-synuclein

b. Separately, express GST-α-synuclein and GST-HRV 3C protease in cultures using Isopropyl-β-D-thiogalactoside (IPTG) induction and purify them with a Glutathione Sepharose 4B affinity column
c. Cleave off the GST tag from GST-α-synuclein with GST-HRV 3C protease
d. Remove GST and GST-HRV 3C protease with the Glutathione Sepharose 4B column and purify untagged α-synuclein to homogeneity as demonstrated by SDS-PAGE gel (with purity at least >95%)
e. Exchange the purified α-synuclein into PBS buffer, pH 7.4, and adjust the final protein concentration to 5 mg/ml as determined by Bradford assay with Bovine Serum Albumin (BSA) as a reference
f. Filter-sterilize α-synuclein solution through a 0.22-µm filter. Make 0.5 ml aliquots in each 1.5-ml low protein binding microtube and store at -80ºC

2. Generate α-synuclein PFFs
    a. Place monomeric α-synuclein tube(s) in a thermomixer with constant shaking at 1000 rpm at 37ºC for 5 d. The contents in the tube(s) will become turbid/opaque, indicating the formation of aggregates
    b. Sonicate the resulting PFFs in the Bioruptor Pico sonicator using at least 40 cycles of 30s ON-30s OFF program ensuring the particle size after sonication is ~50 - 80nm in hydrodynamic diameters as assessed using dynamic light scattering (DLS) Zetasizer Nano S (using the Malvern Zetasizer software)

c. The sonicated PFFs will be stored in aliquots (5-50 µl depending on experimental needs) at -80°C

Note: The ideal concentration of PFFs required for conjugation can vary based on the size of the nanogold particles used (see the nanogold manufacturer's instructions). For instance, for 5 nm nanogold beads, the manufacturer recommends a protein concentration of 5 mg/mL; conversely, with 10 nm nanogold beads, they recommend a 2.5 mg/mL concentration for the protein.

Timing: 2 days

The following steps should be carried out on parafilm. This protocol is adapted from Del Cid Pellitero et al. (2019).

1) Prepare a diluted sample of PFFs at 1 mg/mL
   a) Dilute using ddH_2O
2) Place 5 µL of diluted PFFs on a carbon/formvar covered copper grid and allow the sample to sit for 10 min at room temperature
   a) Using a Whatman filter paper, remove the liquid drop from the grid
3) Fix PFFs on the grid using 2% PFA
   a) Place one drop of 2% PFA onto the grid and let the sample sit for 10 min at 4°C
   b) Remove the PFA drop with Whatman filter paper
4) Wash the grid with ddH_2O
   a) Add one drop of ddH_2O onto the grid for 1 min at room temperature
   b) Remove the drop with Whatman filter paper
   c) Repeat steps a-b once more

5) Stain the grid with uranyl acetate
    a) Centrifuge 1 mL of uranyl acetate at 14,000 x g for 1 min
    b) Add one drop of the supernatant to the grid and wait for 5 min at room temperature
6) Wash the grid with ddH_2O
    a) Repeat step 4
7) Let the grid sit overnight on parafilm
8) Visualize by EM to assess and measure the length of fibrils
    a) See Figure 2.1

Characteristics of optimal PFFs:

- A mean length of less than 100 nm
- Sonicated PFFs must retain the same thickness as full length PFFs

Note: for PFFs visualization (unlabeled, use a magnification between x10,000 and x30,000).

Note: The characterization of α-synuclein PFFs was adapted from Del Cid Pellitero et al. (2019).

2.4 Methods and equipment

REAGENT or RESOURCE	SOURCE	IDENTIFIER
Chemicals, peptides, and recombinant proteins		
DMEM high-glucose	GE Healthcare	Cat# SH30081.01
Bovine calf serum	GE Healthcare	Cat# SH30072.03
L-Glutamine	Wisent	Cat# 609065EL
Penicillin-Streptomycin solution	Wisent	Cat# 450201
Nunc 8-well slide (Permanox)	Lab-Tek	Cat# 177445
Phosphate-buffered saline	Wisent	Cat# 311-010-CL
Paraformaldehyde	Thermo Fisher Scientific	Cat# A1131322
Poly-L-Lysine	Sigma Aldrich	Cat# A-005-M
Glutaraldehyde 2.5% in Sodium Cacodylate Buffer	Electron Microscopy Sciences	Cat# 15960

Diamond Knife (Ultra 35°)	Electron Microscopy Sciences	Cat# 30-SL
Epon-812 or EMbed-812	Electron Microscopy Sciences	Cat# 14900
Whatman qualitative filter paper	GE Life Sciences	Cat# 1001-0155
Sodium Cacodylate Buffer, 0.2M, pH 7.4	Electron Microscopy Sciences	Cat# 11650
Calcium Chloride Solution, Fisher Chemical	Fisher Scientific	Cat# SC101
Osmium Tetroxide Aqueous Solution	Electron Microscopy Sciences	Cat#19100
Uranyl Acetate, Reagent, A.C.S.	Electron Microscopy Sciences	Cat# 22400
UranyLess	Electron Microscopy Sciences	Cat# 22409
Potassium Ferrocyanide Aqueous Solution	Electron Microscopy Sciences	Cat# 25154-2
Carbon/formvar covered copper grid	Electron Microscopy Sciences	Cat# FCF400CU50
1.5 ml low protein-binding microtube	SARSTEDT	Cat# 72.703.600
5 nm gold beads	Cytodiagnostics	Cat# CGN5K-5-2
0.05% Trypsin/0.53 mM EDTA	Wisent	Cat# 325-042-CL
Ethanol/Ethyl alcohol, Pure	Sigma	Cat# 459836
Glutathione beads	Sigma Aldrich	G4251
Glutathione Sepharose bead slurry	GE Healthcare Life Sciences	17075605
Isopropyl-β-D-thiogalactoside (IPTG)	Biobasic	IB0168
Syringe filter 0.22-µm	Mandel Scientific	WYV-SFNY013022NC
Equipment		
Tecnai 12 BioTwin 120 kV transmission electron microscope (TEM) or Tecnai G2 Spirit Twin 120 kV Cryo-TEM	FEI	N/A
The Perfect Loop	Science Services	Cat# E70944
Zetasizer Nano S	Malvern Panalytical	https://www.malvernpanalytical.com/en/support/product-support/zetasizer-range/zetasizer-nano-range/zetasizer-nano-s
Digital heating shaking thermomixer	Thermo Fisher Scientific	Cat# 88880027
Bioruptor® Plus sonication device with metallic soundproof box (B01200001) and water cooler (B02010003)	Diagenode	Cat# B01020001
Bacterial strain		
BL21(DE3) Competent *E. coli* cells	New England Biolabs	Cat # C2527H
Recombinant DNA/Vector		
GST-α-synuclein plasmid, human	(Maneca et al., 2019)	N/A
GST-HRV 3C plasmid	(Maneca et al., 2019)	N/A

pGEX6P1	University of Dundee MRC Protein Phosphorylation and Ubiquitination Unit	Cat# DU30005
Critical commercial assays		
Mycoplasma detection kit	Biotool	Cat# B39038
Bradford Assay Kit	Thermo Fisher Scientific	Cat# 23236
Experimental models: Cell lines		
U-2 OS	ATCC	Cat# HTB-96
Software and algorithms		
ImageJ	(Schneider et al., 2012)	https://imagej.nih.gov/ij/
Malvern Zetasizer Software	Malvern Panalytical	https://www.malvernpanalytical.com/en/support/product-support/software/Zetasizer-family-software-update-v8-02
GMS 3	Gatan	https://www.gatan.com/products/tem-analysis/gatan-microscopy-suite-software

U2OS complete growth medium (store at 4°C when not in use)

REAGENT	Final Concentration	Amount
DMEM high-glucose	N/A	500 mL
Bovine calf serum	10%	56 mL
L-Glutamine	200uM	5 mL
Penicillin-Streptomycin 10,000 U/mL (100×)	1x	5 mL

This protocol explains the conjugation of PFFs to nanogold beads while preventing PFFs from aggregating into longer or more aggregated fibrils. Once the nanogold PFFs are generated, the protocol describes the use of EM to visualize their internalization into cells and their subsequent cellular trafficking. This protocol can be used to visualize the cellular trafficking itineraries of numerous proteins. Furthermore, this protocol can be used to examine the internalization of PFFs and trafficking in various cell types, provided that the appropriate changes

are made to facilitate cell attachment to the plate (e.g., poly-L-ornithine and Laminin would be used instead of poly-L-lysine for neuronal cultures).

PFFs are conjugated with 5 nm nanogold beads, and a small portion of the conjugated sample is prepared and characterized using EM (Steps 1-3: PFFs conjugation and characterization). Provided that the nanogold-labeled PFFs match the ideal criteria (see below for details), cells are plated onto poly-L-lysine treated Nunc 8-well Permanox plates, and nanogold-PFFs are added to the cells (Steps 4-8: Cell attachment, culturing, and PFFs administration, fixation). Finally, a brief description of the processing of the cell monolayers for EM is provided (Steps 9-10: Processing samples and imaging with EM).

The main advantage of an EM approach to protein internalization is that the specific details involved in internalization (e.g., membrane ruffling and the attachment of proteins to cell membrane) can be visualized directly, rather than using fluorescent microscopy and antibodies or more indirect approaches. We hope that this protocol can be used to elucidate other trafficking pathways for other proteins, specifically those involved in neurodegenerative diseases.

2.5 Main body

In this section, we explain the protocol used to conjugate PFFs to 5 nm nanogold beads (Cytodiagnostics). We altered and optimized the standard conjugation protocol provided by the manufacturer (see product sheet on the manufacturer's website: https://www.cytodiagnostics.com/collections/NHS-Activated-Gold-Nanoparticles).

Note: Since PFFs are very susceptible to aggregation, the nanogold-PFFs need to be administered to cells immediately after conjugation. Prepare the cells such that they are ready to coincide with

the conjugation of PFFs to nanogold. Following the administration of PFFs to cells, proceed to prepare grids to characterize the nanogold-PFFs.

Timing: 1 day

Note: all of step 1 should be performed in a tissue culture hood.

1) The conjugation of PFFs with 5 nm nanogold
    a) Add 48 µL of 5 mg/mL PFFs to 60 µL of the reaction buffer provided with the nanogold conjugation kit.
        i) Thaw reaction buffer for 1 h on ice
        ii) Retrieve 48 µL of 5 mg/mL PFFs (stored at -80°C) and immediately add 60 µL of ice-cold reaction buffer to the aliquot
        iii) Incubate for 2 min at room temperature
        iv) Slowly pipette the mixture up and down
    b) Add the reaction buffer-PFFs mixture to 1 vial of 5 nm nanogold
    c) Incubate for 1 h at 18°C
    d) Add 10 µL of quencher buffer (provided by the manufacturer) to the mixture
        i) Slowly pipette up and down using a p10 pipette set at 10 µL
        ii) Avoid creating bubbles in the solution
    e) Incubate at room temperature for 5 min

Note: the amount of reaction buffer and quencher buffer used, the amount and concentration of protein used, are all specified by the manufacturer (Cytodiagnostics). The steps above are an adaptation of their protocol for our specific conjugation assay.

Note: for PFFs visualization (labeled with nanogold beads, use a magnification between x30,000 and x68,000).

Critical: Avoid rapid pipetting of the samples or sudden movements of the experimental microtube as they will aid in protein aggregation.

2) Characterization of conjugated PFFs
    a) Prepare a diluted sample of PFFs with a 1 mg/mL concentration
        i) Dilute using ddH_2O
    b) Place one drop of diluted PFFs on a carbon/formvar covered copper grid and allow the sample to sit for 10 min at room temperature
        i) Using a Whatman filter paper, remove the drop from the grid
    c) Fix the PFFs sample on the grid using 2% PFA (retrieved immediately from storage at 4°C)
        i) Place one drop onto the grid and let the sample sit for 10 min at room temperature
        ii) Remove PFA drop using filter paper
    d) Add one drop of ddH_2O onto the grid for 1 min at room temperature.
        i) Remove with filter paper
        ii) Repeat once more
    e) Stain the grid with Uranyless
        i) Centrifuge 1 mL of UranyLess at 14,000 x g
        ii) add one drop of the supernatant to the grid and wait for 5 min at room temperature
    f) Wash grid with ddH_2O as detailed in **d**
    g) Remove the drop using a Whatman filter paper
    h) Let the grid sit overnight on parafilm at room temperature

Critical step: place grids in a box/chamber for their storage overnight to avoid the addition of contaminants (such as bacteria, dust, etc.) to the EM grid.

3) Visualize using EM to assess and measure the length of fibrils
    a) See Figure 2.2 for an example

Criteria for successful/ideal PFFs conjugation

a. The majority of PFFs should have a length of less than 100 nm
b. Most PFFs should be conjugated with at least one nanogold bead
c. Only 1 in 20 nanogold beads should be unconjugated (free-floating).

Cell attachment, culturing, and PFFs administration

Here, we will be culturing and plating cells onto Nunc 8-well permanox plates previously treated with poly-L-lysine. The protocol described below uses U2OS cells, however, this protocol can be adapted for use with other cell types. We have used the same protocol to examine the internalization of PFFs in primary human astrocytes and glioblastoma cell lines (i.e., U87 and U251).

Timing: ~3 days

4) Treat 8-well permanox plates with poly-L-lysine
    a) Wash wells with 100% ethanol
        i) Repeat 3 times
    b) Wash wells with ddH_2O
        i) Repeat 3 times

c) Add 200 µL of 0.01% poly-L-lysine (stock concentration and working concentration) to each well.
    i) Incubate wells for 1 h at 37°C
d) Wash wells with ddH_2O
    i) Repeat 3 times

Critical: For better attachment, allow cells to grow in wells for over 48 h. Allowing cells 48 h between passaging and experimentation will result in healthier cells, which will improve experimental results (i.e., PFFs uptake) and a lower incidence of cells lifting due to fixation.

5) Subculture U2OS cells
    a) Trypsinize U2OS cells currently in culture, pellet, remove supernatant, resuspend with growth media
    b) Plate ~50,000 cells per well
    c) A total of 150-200 µL of media per well is optimal
    d) Incubate for 48 – 72 h.

Note: Before the experiment, use the mycoplasma kit to test samples for mycoplasma infection. The presence of mycoplasma could have effects on cellular processes, altering your experimental results.

6) Add 5 µL of conjugated PFFs to each well (assuming a final concentration of 2 mg/mL of conjugated PFFs).
    a) Following the addition of conjugated PFFs to each well, incubate cells for 30 min at 37°C

b) Remove cell media

7) The following step is optional as it details our exclusion assay involving the use of trypsin to wash off extracellular PFFs.
   a) Place cells on ice and administer 200 µL of ice-cold trypsin (0.05% Trypsin/EDTA 0.53 mM) to each well
   b) Incubate for 60-90 s on ice
      i) exposure time may need to be adjusted to prevent the lifting of cells
   c) remove trypsin and wash cells with 200 µL of ice-cold trypsin
   d) wash cells gently with PBS

8) Sample fixation
   a) fix cells with 2.5% glutaraldehyde (in sodium cacodylate buffer) supplemented with 2 mM Calcium chloride ($CaCl_2$)
      i) $CaCl_2$ is used to aid in membrane preservation during fixation. The concentration might need to be optimized for specific cell types.
      ii) Fix cells at 4°C overnight (a minimum of 2 h of fixation is recommended at 4°C)
   b) Wash cells with 0.1 mM sodium cacodylate buffer (dilute stock solution using ddH_2O)
      i) Remove fixative solution
      ii) Add 200 µL of sodium cacodylate buffer to each well
      iii) Aspirate the buffer
      iv) Replace with 200 µl of sodium cacodylate buffer

Note: a more detailed description of handling the samples will be provided in Step 9.

Processing samples and imaging with EM

Timing: 2-3 days

Here, we discuss the steps to process the monolayer samples for EM imaging. This should be conducted following overnight fixation of samples in 2.5% glutaraldehyde.

9) Processing samples for EM
    a) Wash out glutaraldehyde fixative
        i) Remove fixative
        ii) Add 300 μL of 0.1M sodium cacodylate buffer
        iii) Incubate for 10 min at room temperature
        iv) Repeat i-iii twice
    b) Post-fix samples
        i) Add the following post-fixation solution to each well: 1% osmium tetroxide and 1.5% potassium ferrocyanide (diluted in ddH_2O)
            (1) This step should be done in a fume hood
            (2) Add potassium ferrocyanide powder in ddH_2O
            (3) Add the appropriate amount of osmium tetroxide to the mixture (based on the concentration used)
        ii) Incubate at 4°C for 1-2 h
    c) Wash out the post-fixative solution
        i) Wash cells with ddH_2O
        ii) Incubate for 10 min at room temperature

iii) Repeat i and ii twice

d) Gradual dehydration of samples

i) Aspirate ddH_2O

ii) Add 30% ethanol/ddH_2O (dilute using pure ethanol)

iii) Incubate at room temperature for 10 min

iv) Repeat i-iii using 50%, 60%, and 70% ethanol solutions

e) Block staining with uranyl acetate

i) Prepare a solution of 2% uranyl acetate in 70% ethanol.

ii) Add 200 µL of staining solution to each well (200 µL volume should be used for all the following steps).

iii) Incubate at 4°C for 2 hours

f) Wash out the staining solution

i) Aspirate samples

ii) Wash samples twice with 70% ethanol

g) Continue sample dehydration

i) Aspirate wells

ii) Add 80% ethanol solution to each well

iii) Incubate for 10 min at room temperature

iv) Repeat i-iii once more, and remove the solution

v) Add 90% ethanol solution to each well

vi) Incubate for 15 min at room temperature

vii) Repeat v-vi once more, and remove the solution

h) Add 100% ethanol solution to each well

i) Incubate for 15 min at room temperature

ii) Remove solution

iii) Repeat viii-x twice more

i) Infiltration with Epon-812

i) Add a 50% solution of Epon-812 (diluted in 100% ethanol) to each well

ii) Incubate at room temperature for 1 h

iii) Aspirate wells

iv) Add a 75% solution of Epon-812/ethanol to each well

v) Incubate at room temperature for 1 h

vi) Aspirate wells

vii) Add a 100% solution of Epon-812 to each well

viii) Incubate at room temperature for 1 h

ix) Aspirate wells

x) Add a 100% solution of Epon-812 to each well

j) Incubate samples with Epon-812 at 60°C for 48 h

i) Allow samples to cool at room temperature overnight before sectioning

k) Trim and section prepared blocks

i) Trim the block to a small area of interest (use a light microscope to find regions of interest).

ii) Use a diamond knife to section samples (Ultra 35°) – samples will end up floating in the ddH_2O-filled boat of the diamond knife where they can be collected.

iii) Place one section onto a grid using the Perfect Loop tool.

iv) Place the grid onto a Whatman filter paper and allow it to dry

Note: ideally, each section should be 70-100 nm thick.

l) Stain grids with uranyl acetate and lead citrate (concentration is based on tissue and staining preferences).

Note: our grid staining protocol is based on a previously published paper by Santhana Raj et al. (2021).

Note: EMbed 812 is a suitable alternative to Epon-812

Critical: Do not let samples dry out. Ensure that they do not go without a covering of liquid for more than 10 sec.

10) Image grids using a transmission EM at x9300 to x18500 magnification (allowing imaging of the fibrils along with cellular structures).

Note: Electron micrographs can be viewed and analyzed with ImageJ or GMS software, both freely available at the links mentioned in the Key Resource Table.

2.6 Expected outcomes

One would expect to observe conjugated PFFs with mostly small, preformed fibrils (<100 nm) and not large, aggregated fibril structures. We expect that the internalization and the trafficking of nanogold-PFFs can be easily spotted in cells when viewing sections using EM. In Figure 2.2, one can see an example of what a typical fibril sample should look like: mostly small, preformed fibrils, conjugated by 2-8 nanogold particles per PFFs. See internalization of nanogold labeled PFFs in Figure 2.3.

Note: as mentioned above, the objective is to have a very small number of free nanogold beads that have not been conjugated with PFFs.

2.7 Limitations and troubleshooting

One major limitation of this protocol is that there is no specific ratio between PFFs and the number of conjugated nanogold particles. This makes quantification of the results difficult as the number of nanogold particles does not directly imply the size of the fibrils or the number of fibrils when imaging intracellular PFFs trafficking.

The other limitation is the inability to control the size of the resulting conjugated fibrils. Although our protocol yields many PFFs with a length that is less than 100 nm, the appearance of larger fibrils cannot be avoided. We believe that this issue is largely moot in quick endocytic experiments, where administered nanogold-PFFs are in contact with cells for 30 min or less. It remains that our protocol does not allow for PFFs size-related experiments to occur (i.e., 50 nm PFFs internalization vs 75 nm PFFs internalization).

Troubleshooting

While certain outcomes are unavoidable using our protocol, such as the presence of a small number of free-floating nanogold particles, and the formation of large fibrils conjugated with nanogold, experimental conditions can be optimized to reduce the likelihood of such events occurring. Here we address some of the common issues that can be addressed. As a guiding principle, it is okay to have unconjugated PFFs if almost all nanogold beads are attached to PFFs (i.e., unconjugated PFFs are acceptable but unconjugated nanogold beads are not).

Problem 1: Presence of unconjugated nanogold particles

Our guideline for using a sample is that only 1 out of 20 nanogold particles can be unconjugated when characterizing a conjugated sample. Should free gold particles be more frequent (Figure 2.4 A), the sample should be discarded, and the conjugation process should be optimized. Below, we outline some ways in which this problem can be alleviated.

Potential solution: Manipulate the temperature or duration of the conjugation experiment

Instead of incubating the mixture of reaction buffer, nanogold, and PFFs at 18°C as suggested by our protocol, try incubating the mixture at a higher temperature (e.g., 21°C/room temperature). This will ensure that more covalent bonds occur between the PFFs and nanogold beads.

Increased conjugation of nanogold beads with PFFs can also be achieved by increasing the incubation time from 1 h to 1.5 or 2 h. This enables the ability to keep the incubation temperature at 18°C which results in a less aggregated product.

Problem 2: Over-conjugation of PFFs

While successful conjugation of PFFs with multiple nanogold beads is the desired outcome, over-conjugation of fibrils with nanogold beads can also occur (Figure 2.4 B). This is not optimal, as the increased size and weight of the resulting conjugated protein might affect its internalization and delay or even prevent its uptake by cells. Below we describe a solution that effectively eliminates this issue.

Potential solution: Increase PFFs concentration

As the conjugation experiment is a chemical reaction that results in the formation of covalent bonds between PFFs and nanogold, stoichiometry, or more simply, the amount of each reactant is important. By increasing the number of PFFs added, through the increase of concentration and not volume, you can decrease the likelihood of over-conjugation of nanogold particles onto PFFs. A concentration range of 1-5 mg/mL is desirable when conducting the conjugation experiment. Refer to the manufacturer's protocol regarding the desirable concentration for different sizes of nanogold beads.

Problem 3: Presence of large fibril aggregates: Most common

The most common, and least favorable outcome is the presence of conjugated PFFs with lengths over 100 nm. Although a low number of such fibrils will occur, samples that mostly contain these large structures must be discarded (Figure 2.4 C), since the conjugated proteins can no longer be referred to as PFFs, and hence, may utilize a different pathway for entry and trafficking into cells.

Potential solutions: Manipulate experimental conditions and utilize proper handling of PFFs

Prior to conjugation, characterize the PFFs batch by aliquoting and visualizing the unconjugated sample using EM. If the presence of large fibrils is frequent, do not conjugate the batch as the issue with PFFs length will only be exacerbated during conjugation.

In addition, avoid the following behaviors when conjugating nanogold beads onto PFFs:

- rapid movement of the sample
- holding the tube with PFFs between one’s fingers

- the transfer of body temperature to the tube can result in accelerating the aggregation process.

- rapid pipetting up and down
- repeated freeze and thaw

Another solution to reduce the aggregation of conjugated PFFs is to allow the experiment to occur at a lower temperature. The correct temperature (e.g., room temperature, 4ºC, 37ºC, etc.) for your experiment will therefore be a balance between decreased aggregation and decreasing the likelihood of nanogold conjugation onto PFFs.

Problem 4: Spotting of nanogold-PFFs in lysosomes

Lysosomes are electron-lucent organelles when observed using EM, which makes it difficult to spot nanogold-conjugated proteins in their lumen. Although this issue can often be resolved by adjusting image contrast, sometimes a change in protocol is necessary for clear viewing of lysosomal contents.

Potential solution: No grid staining

In our protocol, the samples are stained with uranyl acetate both prior to embedding (*en bloc*) and after embedding (grid staining). To lower the overall staining of the samples, and have a better view of the lysosomal lumen, avoid grid staining with uranyl acetate and lead citrate. This will result in samples with much less staining, and hence, a better look into the lysosomal lumen.

Problem 5: Uranyl acetate-related artifacts

Uranyl acetate staining can have potential drawbacks since its exposure to light results in its precipitation. Stock solutions of uranyl acetate are also prone to precipitation with age. The result will be large, dark artifacts in EM samples, which will result in suboptimal images.

Potential solution: Regular filtration and centrifugation of uranyl acetate before use

To avoid uranyl acetate-related artifacts, first centrifuge an aliquot of uranyl acetate to pellet aggregate chunks. Collect the supernatant and run it through a 0.22-µm filter. Uranyl acetate can now be used for sample staining

2.8 Acknowledgements

We acknowledge the Facility for Electron Microscopy Research at McGill University, specifically Dr. S Kelly Sears, for his help with the EM. The graphical abstract was made using biorender.com. A.B. is supported by the Fonds de recherche du Québec doctoral award and a studentship from the Parkinson Society of Canada. This work was supported by a grant from the Canada First Research Excellence Fund, Healthy Brain, Healthy Lives, awarded to P.S.M. P.S.M. is a Distinguished James McGill Professor and Fellow of the Royal Society of Canada.

2.9 Figures

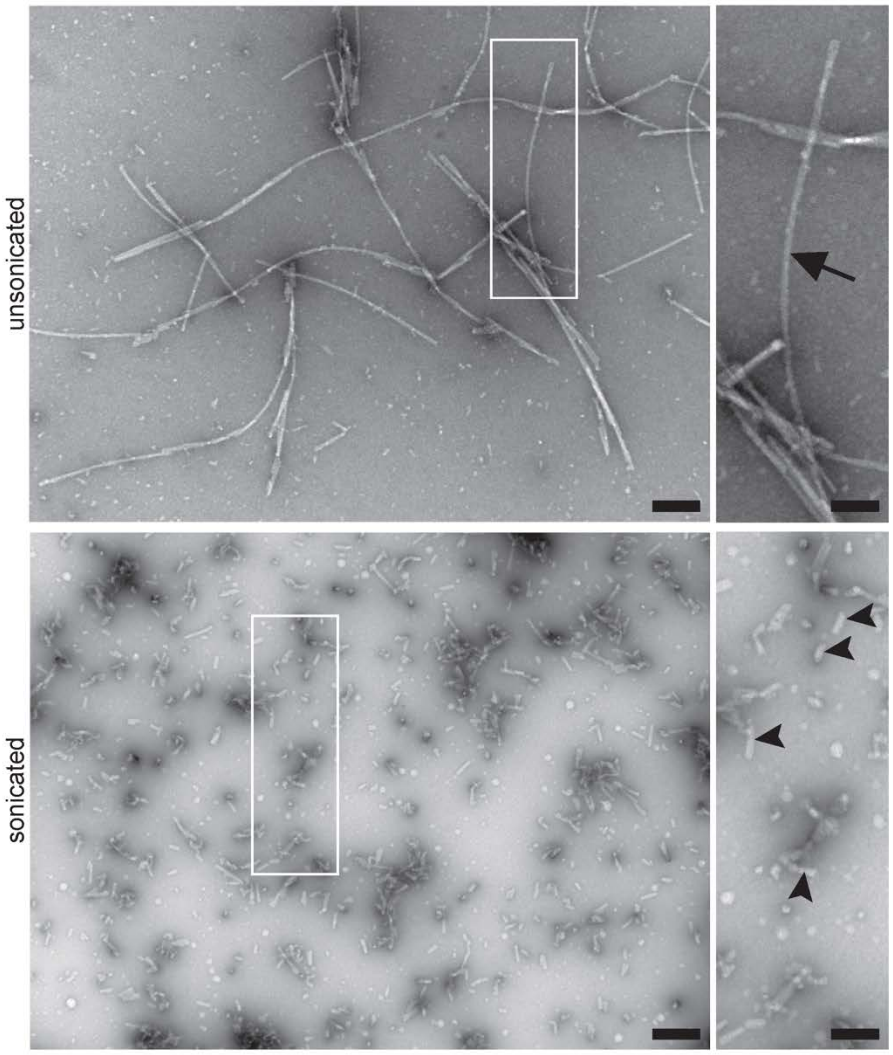

Figure 2.1

PFFs visualized using negative staining before and after sonication

Samples are stained with uranyl acetate. The arrow points to an example of a long fibril. Arrowheads point to multiple examples of preformed fibrils with a length of less than 100 nm, Scale bar = 200 nm and 100nm for insets.

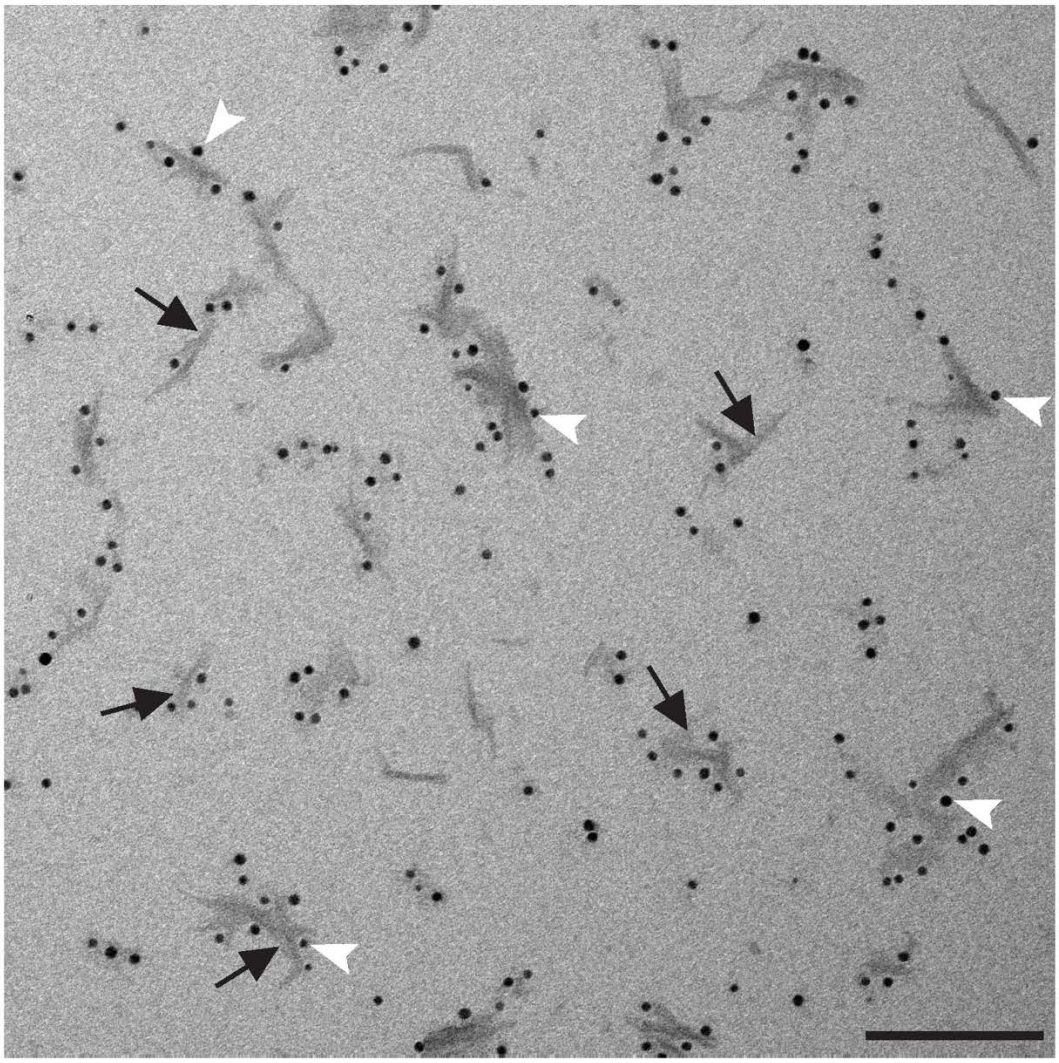

Figure 2.2

Electron micrograph of nanogold conjugated PFFs

Uranyless was used for staining. Arrowheads point to a few examples of conjugated nanogold beads. Arrows indicate optimal examples of nanogold-labeled PFFs: small size and the appropriate amount of conjugation (>1 and <20 beads per PFFs). Scale bar = 100 nm.

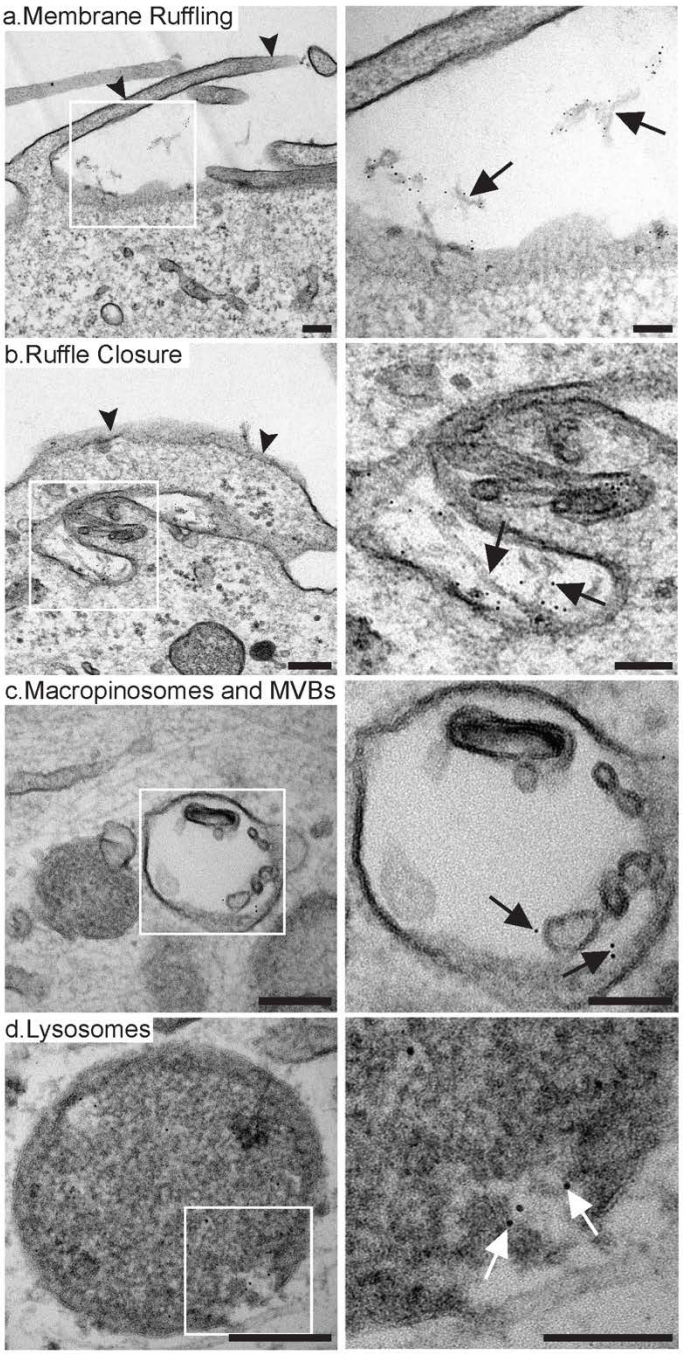
a.Membrane Ruffling
b.Ruffle Closure
c.Macropinosomes and MVBs
d.Lysosomes

Figure 2.3

Internalization of nanogold-PFFs visualized using EM

Images show the internalization of PFFs in U2OS cells in 4 stages (a-d). Nanogold PFFs (arrows) are seen at the cell surface, being engulfed by membrane ruffles (arrowhead). They are then trafficked to macropinosomes, early multivesicular bodies (MVBs), and lysosomes. Scale bar = 200 nm, and 100 nm for insets.

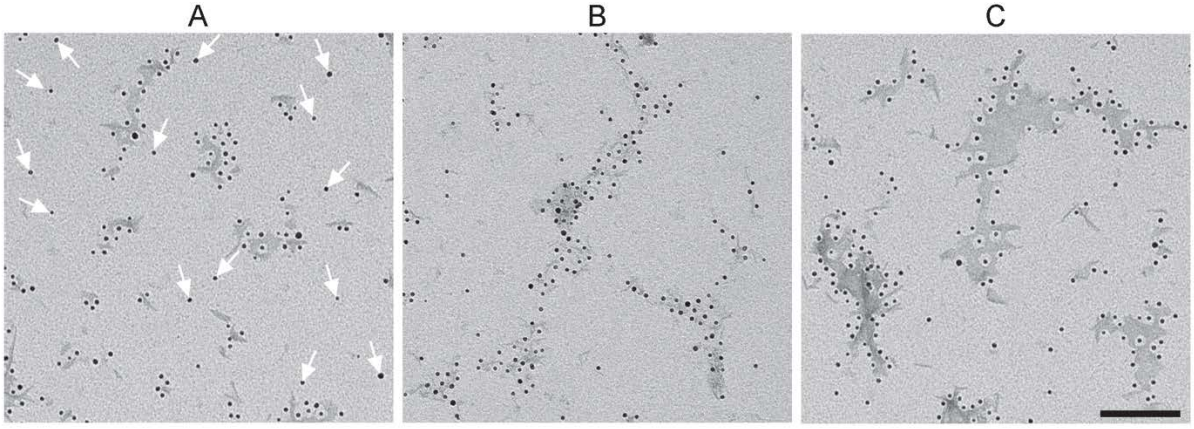
A
B
C

Figure 2.4

Problematic outcomes of PFFs conjugation

(A) an example of many free-floating unconjugated nanogold beads (arrows). (B) an example of PFFs over-conjugation with nanogold particles. (C) an example of PFFs conjugation that results in large PFFs aggregates spanning several hundred microns. Scale bar = 100 nm.

2.10 References

Del Cid Pellitero, E., Shlaifer, R., Luo, W., Krahn, A., Nguyen-Renou, E., Manecka, D.-L., Rao, T., Beitel, L., & Durcan, T. M. (2019). Quality Control Characterization of α-Synuclein Preformed Fibrils (PFFs) [Technical Note]. *Zenodo*. https://doi.org/https://doi.org/10.5281/zenodo.3738340

Maneca, D.-L., Luo, W., Krahn, A., Del Cid Pellitero, E., Shlaifer, I., Beitel, L. K., Rao, T., & Durcan, T. M. (2019). Production of Recombinant α Synuclein Monomers and Preformed Fibrils (PFFs). *Zenodo*. https://doi.org/http://doi.org/10.5281/zenodo.3738335

Santhana Raj, L., Nur Dayana, M. A., Norzarila, S. N., Tan, C. V., & Nur Afrina, M. H. (2021). New Preparation Method of Reynolds' Stain for Transmission Electron Microscope for Liver Samples. *International Journal of Medical Nano Research*, *8*(1). https://doi.org/10.23937/2378-3664.1410033

Schneider, C. A., Rasband, W. S., & Eliceiri, K. W. (2012). NIH Image to ImageJ: 25 years of image analysis. *Nat Methods*, *9*(7), 671-675. https://doi.org/10.1038/nmeth.2089

Preface to Chapter 3

This chapter provides evidence for the internalization of PFFs through a rapid macropinocytic pathway. Using the nanogold-labelled PFFs, described in the previous chapter, we were able to follow the internalization process via electron microscopy. Furthermore, due to the increased resolution and the ability to view ultrastructural details, we found that PFFs are trafficked in multivesicular bodies as well lysosomes. Additionally, within these multivesicular bodies, PFFs sat on the surface of the intralumenal vesicles. Through collection and purification of exosomes from cells given PFFs, we found that exosomes were released with PFFs on their surface, that could be easily cleaved off using trypsin. This, along with additional electron microscopy data, allowed us to provide proof that PFFs resided on the surface of exosomes, a trafficking pathway for PFFs not explored previously. Lastly, we discovered that the intercellular transfer of exosomal-PFFs was halted with the use of macropinocytic inhibitors.

CHAPTER 3. RAPID MACROPINOCYTIC TRANSFER OF ALPHA-SYNUCLEIN TO LYSOSOMES

3.1 Abstract

The nervous system spread of alpha-synuclein fibrils is thought to cause Parkinson's disease (PD) and other synucleinopathies; however, the mechanisms underlying internalization and cellular spread are enigmatic. Here, we use confocal and superresolution microscopy, subcellular fractionation, and electron microscopy (EM) of immunogold-labeled α-synuclein preformed fibrils (PFFs) to demonstrate that this form of the protein undergoes rapid internalization and is targeted directly to lysosomes in as little as 2 min. Uptake of PFFs is disrupted by macropinocytic inhibitors and circumvents classical endosomal pathways. Immunogold-labeled PFFs are seen at the highly curved inward edge of membrane ruffles, in newly formed macropinosomes, in multivesicular bodies and in lysosomes. While most fibrils remain in lysosomes, a portion is transferred to neighboring naive cells along with markers of exosomes. These data indicate that PFFs use a unique internalization mechanism as a component of cell-to-cell propagation.

3.2 Introduction

A classic hallmark of Parkinson's disease (PD) is the formation of Lewy Bodies (LBs). First discovered in 1912 (Lewy, 1912), LBs are cytoplasmic inclusions composed of fragments of membranous organelles and filamentous proteins (Shahmoradian et al., 2019; Tanaka et al., 2004). LBs are also observed in PD-related disorders such as Lewy body dementia. Alpha-synuclein (α-syn), encoded by the *SNCA* gene, is a major component of LBs and is implicated in their formation (Conway et al., 1998; Maria Grazia Spillantini et al., 1997). α-syn appears to function in membrane trafficking and membrane curvature (Fortin et al., 2004; Jao et al., 2004; Nakamura et

al., 2008; Vargas et al., 2017), and increased knowledge of its protein structure and the conformation of altered variants has led to enhanced understanding of α-syn misfolding and aggregation in disease (Lee et al., 2002; Li et al., 2002; Sandal et al., 2008).

Since the early 2000s, the Braak hypothesis has stated that PD develops with the spread of α-syn through the brain (Braak et al., 2003). This model gained traction with the observation that proteinaceous inclusions spread from brain tissue into implanted embryonic stem cells (Li et al., 2008), a result subsequently confirmed in animal models (P. Desplats et al., 2009; Li et al., 2010; Recasens & Dehay, 2014; Recasens et al., 2018). Propagating pathology is also observed following injection of the fibril form of α-syn into localized brain regions of mice (Betemps et al., 2014; Luk et al., 2012; Masuda-Suzukake et al., 2014). This tendency to spread, along with the ability of α-syn fibrils to disrupt the conformation of endogenous α-syn, has earned the protein a label as a prion-like (Masuda-Suzukake et al., 2013; Mougenot et al., 2012). However, questions remain regarding the cell biological itinerary of α-syn propagation, notably the mode of cellular entry (Fenyi et al., 2019; Gelpi et al., 2014; Nakamura et al., 2015; Uemura et al., 2018; Yan et al., 2018).

Different mutations in the *SNCA* locus have varying penetrance that may correlate to the propensity of α-syn to aggregate (Lazaro et al., 2016; Rutherford et al., 2014). α-syn concentration is also a factor in aggregation as increased protein levels enhance aggregation, be it mutant or wild-type protein (Anthony L. Fink, 2006; Manning-Bog et al., 2002; Uversky, 2007). Further, α-syn preformed fibrils (PFFs) and other fibril assemblies of α-syn have the ability to seed, propagate and amplify in size via the recruitment of α-syn monomers (Alam et al., 2019). PFFs comprise a heterogeneous number of α-syn monomers with various structural conformations (Pieri et al., 2016). Early studies using PFFs revealed their ability to seed and induce PD pathology in cultured

cells (Luk et al., 2009); hence, developing a protocol for consistent production of PFFs was a significant contribution (Volpicelli-Daley et al., 2014; Volpicelli-Daley et al., 2011).

A key question in PD research relates to how α-syn fibrils enter cells (Bieri et al., 2018). Several studies have concluded that α-syn endocytosis is Clathrin-dependent, based on the use of dynamin and Clathrin inhibitors, Dynasore and Pitstop, respectively, and Clathrin heavy chain (CHC) colocalization (Konno et al., 2012; Liu et al., 2007; Rodriguez et al., 2018). It is generally thought that PFFs are then trafficked to lysosomes via the endosomal system over the course of tens of minutes to multiple hours. We found approximately 40 studies examining α-syn endocytosis with variable conclusions (Supplementary Table 3.8). Some of the variability may arise from examining α-syn internalization at longer time courses and not immediately after its addition to cells. Moreover, dynamin inhibition is not synonymous with inhibition of Clathrin-mediated uptake and the specificity of Dynasore and Pitstop as inhibitors of Clathrin-mediated endocytosis (CME) has come under scrutiny as both have off-target effects (Gu et al., 2010; Oh et al., 1998; Park et al., 2013; Pelkmans et al., 2002; Preta et al., 2015). Apart from CME, it is suggested that α-syn enter cells via direct permeation of the plasma membrane (Danzer et al., 2007), via the formation of tunneling nanotubes that allow direct connections between cells (Dieriks et al., 2017), or through caveolae-dependent endocytosis (Madeira et al., 2011). Thus, there appears to be no consensus nor definitive evidence regarding the nature of α-syn endocytosis.

We thus sought to examine endocytosis of PFFs immediately after their addition to cells. Surprisingly, PFFs are internalized rapidly and appear in lysosomes within 2 min, bypassing conventional endosomal trafficking pathways. We confirmed this result in multiple cell lines, primary human cells, and neurons derived from induced pluripotent stem cells (iPSC). The internalization is not dependent on Clathrin but instead uses macropinocytosis. We used gold-

labelled PFFs and EM and discovered PFFs in membrane ruffles that form macropinosomes and in lysosomes. We also detected gold-labelled PFF on the outer edges of inward invaginating vesicles and on the outside of vesicles within multivesicular bodies (MVBs). While a portion of PFFs remain in lysosomes for a long period, a smaller portion are transferred to naïve cells along with markers of MVBs. Thus, our data unveils a unique form of macropinocytosis that mediates internalization of PFFs and allows for endocytosis to be coupled to release.

3.3 Results

PFFs are rapidly endocytosed to lysosomes

We used fluorescently-labeled PFFs (Del Cid Pellitero et al., 2019; Maneca et al., 2019) (Supplementary Figure 3.1 A/B) with live-cell imaging and a trypan blue exclusion assay (Karpowicz et al., 2017) that quenches extracellular PFF fluorescence (Supplementary Figure 3.1 D) to examine PFF internalization at the earliest possible time points. PFFs are rapidly internalized in U2OS cells and are targeted to lysosomes where they colocalize with Lysosomal Cytopainter within as little as 2 min (Figure 3.1 A). Similar results are seen when incubating cells with PFFs at 4°C for 30 min and then transferring the cells to 37°C (Supplementary Figure 3.1 E). We confirmed the live imaging findings in fixed samples of U2OS cells. PFFs are significantly internalized within 2 min and continue to accumulate within cells for up to 60 min (Figure 3.1 B & Supplementary Figure 3.1 H). Nearly all labeled PFFs that enter cells are colocalized with LAMP1-TurboRFP by 2 min, and this colocalization remains stable with all PFFs trafficking to lysosomes for up to 60 min in these experiments (Figure 3.1 C). As fixation makes cells permeable to trypan blue, for fixed cell experiments, we used trypsin to proteolyze off extracellular PFFs

(Supplementary Figure 3.1 F/G). The rapid uptake of PFFs and transport to lysosomes within 2 min was also observed in U87 (Supplementary Figure 3.2 A/D/E) and U251 (Supplementary Figure 3.2 B/F/G) glioblastoma cells.

To confirm the rapid transport of PFFs to lysosomes, we incubated U2OS cells expressing HA-TMEM192-RFP, a lysosomal protein, with PFFs for various time periods, then lysed the cells and purified lysosomes using HA-magnetic beads (Abu-Remaileh et al., 2017). The enrichment of lysosomes was confirmed in the immunoprecipitated fractions with antibodies recognizing LAMP1 and 2 (Figure 3.1 D). Rab7 was also enriched in the lysosome fractions, whereas Rab5 and LRRK2 were not detected. CD63/LAMP3, a marker of lysosomes and MVBs, was the most highly enriched marker. PFFs were enriched in the lysosome fractions as early as 2 min, confirming their rapid transport to lysosomes (Figure 3.1 D). The enriched lysosomes were placed on coverslips and visualized through the fluorescently labeled PFFs (Alexa Fluor 488) and TMEM192-RFP (Figure 3.1 E). PFFs were detected in the lumen of the lysosomes, which was most readily seen using STED super-resolution microscopy (Figure 3.1 F). Fluorescently conjugated PFFs of various sizes (Figure 3.1 G) were administered to U2OS cells revealing no significant difference in uptake in samples ranging from 50-100 nm (Figure 3.1 H). Thus, PFFs are rapidly endocytosed and transported to lysosomes in as little as 2 min, an unprecedented time frame for lysosomal targeting.

Rapid transfer of PFFs to lysosomes in nervous system cells including human dopaminergic neurons

Human cortical neurons derived from iPSCs (Supplementary Figure 3.1 I) were incubated with fluorescently labeled PFFs and colocalization with lysosomes was examined using a fixable

form of Lysotracker. PFFs were endocytosed in neurons with lysosomal colocalization observed as early as 2 min (Supplementary Figure 3.2 C/H/I), although lysosomes continued to accumulate in PFFs for up to 30 min. In both human dopaminergic neural progenitor cells (NPC) derived from iPSCs and in dopaminergic neurons derived from the NPC, PFFs were rapidly internalized and are detected at lysosomes within 2 min (Supplementary Figure 3.1 I; Figure 3.2 A, B, D, E). Similar results are seen in human astrocytes (Supplementary Figure 3.1 I; Figure 3.2 C and F). Thus, in multiple cell types, including those from the human nervous system, PFFs are rapidly transported to lysosomes.

To assess the localization of PFF over longer time periods, U343 glioblastoma cells were incubated with PFFs for 24 h followed by a change to fresh media. PFFs are seen to traffic to lysosomes and remain predominantly in the organelle, with fluorescent signal detected for up to 10 days (Supplementary Figure 3.2 J). In contrast, internalized fluorescently tagged epidermal growth factor (EGF) is detected at only very low levels in lysosomes at both 1 and 10 days after addition (Supplementary Figure 3.2 J). Similar to U343 glioblastoma cells, fluorescent PFFs are readily detected in the lysosomes of human astrocytes at 1 and 7 days (Figure 3.3 A) with the total fluorescent signal slowly decreasing over time (Figure 3.3 B). In human dopaminergic neurons, PFFs are detectable in lysosomes for up to 7 days (Figure 3.3 C).

PFFs are trafficked to lysosomes avoiding early/recycling endosomes

Considering the speed at which PFFs reach lysosomes it seems unlikely that PFFs follow endosomal pathways to lysosomes (Lee et al., 2005; Lee et al., 2008; Lee et al., 2016) as endosomal maturation generally takes 10-15 min (Huotari & Helenius, 2011). Transferrin (Tf), a well-studied marker of early and recycling endosomes (Trischler et al., 1999) was added to cells

along with PFFs and there was no co-localization at 2 min nor 30 min (Supplementary Figure 3.3 A and D). While a significant co-occurrence of Tf with PFFs was detected at 30 min (approximately 20%; $M_1 < 0.2$), the co-occurrence of PFFs with Tf was not significant. Moreover, internalized PFFs do not colocalize with EEA1, a marker of early endosomes (Mills et al., 1998), even at time points as early as 2 min (Figure 3.3 B and E). PFFs colocalize with the late endosome/lysosome markers Rab9 and LAMP1 but show little co-localization with early and recycling Rabs 4, 5 and 8 (Supplementary Figure 3.3 C, F, and G). Thus, PFFs appear to reach lysosomes independently of the early and recycling endosomal systems.

Endocytosis of PFFs is Clathrin-independent

The current consensus is that PFFs enter cells via CME (Uemura et al., 2020). However, we are aware of no mechanism by which cargo that enters cells via CME can gain access to lysosomes in 2 min while bypassing early endosomes. To test if CME is involved in the endocytosis of PFFs, we used an established genetic approach involving the knockdown of CHC with previously validated siRNA (Galvez et al., 2007; Kim et al., 2011). Immunoblot reveals effective CHC knockdown in U2OS cells (Figure 3.4 A). We then plated cells treated with control siRNA or CHC-targeting siRNA as a mosaic in the same well and incubated them with PFFs. Unlike previous studies showing the Clathrin-dependence of PFF entry (Supplementary table 3.8), we observed no difference in internalization of PFFs when comparing knockdown and control cells (Figure 3.4 B and C). Thus, it does not appear that CME plays a major role in PFF endocytosis.

Lysosomal transfer of PFFs does not depend on phagocytosis

Due to the rapid transport of PFF to lysosomes, we tested if internalization of PFFs utilizes phagocytosis. RAW 264.7 macrophage cells were activated with LPS (1 μg/ml) and after 24 h, cells were given fluorescent latex beads FluoSpheres (FS), along with PFFs. Little colocalization was observed between FS and PFFs (Supplementary Figure 3.4 A/B), indicating phagocytosis is not involved in the uptake of PFF.

Internalization of PFFs occurs through a unique form of macropinocytosis

Holmes et al. (2013) demonstrated that tau fibrils utilize macropinocytosis for cellular entry and that fibril α-syn colocalizes with tau during uptake, suggesting a potential role for macropinocytosis in the internalization of fibril α-syn. Similarly, Zeineddine et al. (2015) found that α-syn fibrils induce membrane ruffling, an early step in forming macropinosomes. Although macropinocytic cargo generally follow the endosomal pathway (Mayor & Pagano, 2007), we sought to test if macropinocytosis is involved in the internalization of PFFs. We first examined if EIPA, an established inhibitor of macropinocytosis (Commisso et al., 2014; Koivusalo et al., 2010; Nakase et al., 2015) influences the internalization of PFFs. EIPA disrupts the Na^+/H^+ exchanger, decreasing cytosolic pH and inhibiting the activation of Cdc42 and Rac1, required for macropinocytosis (Koivusalo et al., 2010). At a concentration of 20 μM, EIPA inhibits uptake of PFFs in human astrocytes (Figure 3.4 D and E). Latrunculin B (LatB), which inhibits macropinocytosis by disrupting actin polymerization (Williams & Kay, 2018), had a similar block on uptake of PFFs when used at 5 μM (Figure 3.4 D and E). In contrast, neither drug influenced the uptake of EGF (Figure 3.4 D and F), which at the concentration used, enters cells via CME (Sigismund et al., 2005). In addition to astrocytes, we confirmed our findings in dopaminergic NPCs. Latrunculin A (LatA), which like LatB is a potent actin polymerization inhibitor (Fujiwara

et al., 2018), demonstrated a dose-dependent inhibition in the uptake of PFFs in dopaminergic NPCs with uptake reduced by 81% compared to control at 2 μM (Figure 3.4 G).

Consistent with a role for macropinocytosis in endocytosis of PFFs, PFFs induce the formation of actin-rich membrane ruffles, precursors of macropinosomes (Condon et al., 2018) (Supplementary Figure 3.5 A and B). More specifically, PFFs induce recruitment of Rac1 to actin-rich membranes on the cell surface, a characteristic of macropinocytosis (Grimmer et al., 2002) (Supplementary Figure 3.5 A). The ability of PFFs to induce membrane ruffling is also observed by EM (Supplementary Figure 3.5 C). As a control, we examined the influence of EGF, a documented inducer of membrane ruffles, even though it does not use macropinocytosis itself for internalization (Bryant et al., 2007). We also examined Tf, which is not known to induce membrane ruffling or macropinocytosis. As expected, EGF causes the recruitment of Rac1 to the surface, where it colocalizes with F-actin, whereas no Rac1 recruitment is seen upon the addition of Tf (Supplementary Figure 3.5 D). Thus, PFFs appear to stimulate membrane ruffles and use macropinocytosis to gain direct access to lysosomes.

Dextrans are fluid phase endocytic markers that can utilize macropinocytosis (Li et al., 2015). Dextrans of different molecular weights were added to cells alongside PFFs. Colocalization of dextrans with PFFs (M_1) was ~25% while PFF colocalization with dextran (M_2) was less than 20% (Supplementary Figure 3.5 E and F). Thus, PFFs appear to use a unique form of macropinocytosis that only partially overlaps with conventional bulk entry.

Trafficking itinerary of PFFs revealed by immunogold EM

To observe the trafficking itinerary of PFF directly, we labeled the fibrils with gold (Supplementary Figure 3.1 C) and followed their trafficking by EM. At 2-3 min following addition

of PFFs, astrocytes were fixed and processed for EM. Gold-labeled PFFs appear under membrane ruffles and within intracellular macropinosomes formed by ruffle closures (Figure 3.5 Ai/ii). The immunogold-labeled PFFs remain in the lumen of the macropinosomes/endosomes that begin to demonstrate inward invagination of vesicles (Figure 3.5 Aiii/iv). At 3-5 min the PFFs can be found in the lumen of intracellular membranes that gradually acquire electron density, indicating that they are likely lysosomes (Figure 3.5 B and C; Supplementary Figure 3.6 A and B).

Remarkably, gold-labeled PFFs are often found in close association with regions of membrane curvature as they begin to bud inward into electron-lucent organelles approximately 300-500 nm in diameter (Figure 3.6 A). Thus, PFFs may contribute to the formation of MVB. In fact, PFFs are readily detected on the surface of vesicles in MVBs (Figure 3.6 B). Fluorescently labeled PFFs were also detected in LAMP1-positive MVBs using STED microscopy (Figure 3.6 C). Live-cell studies were performed to examine the dynamics of these structures, which appear to undergo multiple rounds of fusion and membrane budding (Figure 3.6 D and E). Thus, PFFs enter cells via macropinocytosis and appear rapidly in lysosomes and MVBs.

PFFs are transferred to naïve cells using exosomes

The spread of PFFs throughout the nervous system requires that the fibrils escape cells and be transferred to neighboring naïve cells. Exosomes provide a mechanism for cell-to-cell transfer of protein, lipids, and other cellular molecules, and the presence of PFFs in MVBs suggests a potential mechanism for cellular release. To test this hypothesis, U2OS cells with stable expression of CD63-GFP were incubated with fluorescently labeled PFFs for 24 h and then washed with trypsin and buffer before re-plating with PFF-naïve cells with stable expression of LAMP1-RFP. From 12-24 h following the start of co-culture, PFFs were observed to transfer from the CD63-

positive cells to the LAMP1-positive cells (Figure 3.7 A and C). Moreover, we observed transfer of CD63 (Figure 3.7 A and B), suggesting that transfer of PFFs involves exosomes. Similar results are seen with transfer to naïve cells expressing CD9-RFP (Supplementary Figure 3.7 A). Notably, the transfer of both CD63 and PFFs is blocked by the addition of manumycin A, a compound that disrupts exosome release (Supplementary Figure 3.7 A-C).

We next took CD63 expressing donor cells and incubated them with fluorescently labeled PFFs for 24 h before extensive trypsin/buffer wash. The cells were then re-plated in serum-free media and incubated for 36 h before the media was collected, spun at low speeds to remove any cells or cellular debris. The supernatant, containing exosomes was transferred to naïve cells. Extracellular vesicles (with CD63-GFP and PFF-Alexa633) were detected in PFF naïve cells using confocal microscopy (Figure 3.7 D). The appearance of these fluorescent signals in the naïve cells was blocked by using EIPA (Figure 3.7 D and E). We then followed a similar procedure but using gold-labelled PFFs. We detected exosomes decorated with PFFs in contact with naïve cells, sometimes seemingly near sites of membrane ruffles and forming macropinosomes (Figure 3.7 F).

We next used a series of centrifugation steps to isolate exosomes (Chhoy et al., 2021) from the culture media of U2OS cells that were exposed to unlabeled PFF for 24 h. EM analysis revealed fibril-like structures on their surface while exosomes isolated from the media of cells not exposed to PFFs did not (Supplementary Figure 3.7 B). A portion of the isolated exosomes from the PFF-treated samples were trypsinized to determine whether PFFs remains exclusively on the exosomal surface. Immunoblotting of the exosomal samples not only confirmed the identity of the exosomes (CD63-positive, GM130-negative) but additionally showed that the trypsinized exosomes did not contain any α-syn, hence PFF resides on their surface (Supplementary Figure 3.7

C). In summary, PFFs that have entered cells by macropinocytosis, are trafficked to MVBs and appear to be transported on the outer surface of exosomes to neighbouring cells.

3.4 Discussion

The mechanisms underlying PFF uptake remain incomplete (Bieri et al., 2018; Grozdanov & Danzer, 2018). Most studies investigating internalization of α-syn or PFFs evaluate uptake hours following addition to cells (Paula Desplats et al., 2009; Hansen et al., 2011; Konno et al., 2012; H. J. Lee et al., 2008; Liu et al., 2007; Luk et al., 2016; Luk et al., 2009; Madeira et al., 2011; Rodriguez et al., 2018; Sung et al., 2001; Volpicelli-Daley et al., 2014; Volpicelli-Daley et al., 2011). While such uptake assays are valuable for genetic screening, they lack the temporal resolution to identify the pathways involved in endocytosis, an early event. We performed a detailed analysis of early events in endocytosis of PFFs and were surprised to discover a unique uptake mechanism that allows the protein to reach lysosomes within 2 minutes, bypassing the early endosomal system.

Endocytosis of PFFs has been thought to follow canonical CME pathways, entering cells via Clathrin-coated pits and vesicles followed by trafficking through endosomes to lysosomes (Konno et al., 2012; H. J. Lee et al., 2008). However, we found no evidence for trafficking of PFFs through early or recycling endosomes, inconsistent with a CME pathway. Moreover, using a previously established pool of CHC siRNA (Bayati et al., 2021; Galvez et al., 2007; Kim et al., 2011), we attained ~95% knockdown efficiency, yet PFF endocytosis remained unperturbed. Thus, our data does not support a role for CME in uptake of PFFs.

PFFs induce the formation of actin- and Rac1-rich membrane ruffles, precursors of macropinocytic vesicles (Cox et al., 1997; Grimmer et al., 2002). Further, inhibitors of

macropinocytosis (Commisso et al., 2014; Koivusalo et al., 2010; Zwartkruis & Burgering, 2013) including EIPA, LatA and LatB (Erami et al., 2017; Furstner et al., 2007; Morton et al., 2000; Wakatsuki et al., 2001) significantly inhibited uptake of PFFs, while not affecting EGF uptake. Our findings point to endocytosis of PFF through a form of macropinocytosis, where macropinosomes either mature into MVBs and lysosomes or fuse with pre-existing LAMP1-positive compartments, i.e., late endosomes and lysosomes. Recent papers show promising results regarding the role of actin in PFF internalization (Underwood et al., 2020; Zhang et al., 2020).

Aspects of our findings corroborate previous studies. First, although slower, previous research demonstrates the direct fusion of macropinosomes with lysosomes (Yoshida et al., 2018). Second, the findings of previous studies on dynamin inhibition and reduction in uptake of PFFs can be due to dynamin's role in some forms of macropinocytosis and its involvement in actin remodeling (Gu et al., 2010; Krueger et al., 2003; Mulherkar et al., 2011). In fact, at high concentrations, we observed that Dynasore does block PFF internalization (data not shown). Finally, amilorides, such as EIPA, which block uptake of PFFs have been shown to have neuroprotective effects in PD (Arias et al., 2008).

Although previous studies attempted to examine the localization of exogenous α-syn using immuno-EM (Volpicelli-Daley et al., 2011), we conjugated PFFs directly with gold. Many antibodies to α-syn cannot distinguish between different conformations of the protein (Kumar et al., 2020), making the direct conjugation of gold to PFFs a more specific method. Consistent with previous literature (Vargas et al., 2017), we found that PFFs were almost always in close association with membranes, whether at the cell surface, during internalization, or while in MVBs and lysosomes.

At early time points after addition to cells, we observed gold-PFFs on inward invaginating vesicles within MVBs. At longer time points, gold-PFFs were seen to be transported on exosomes, which confocal microscopy, demonstrated were CD63-positive. Two important discoveries were made as a result of this: (1) PFF transmission is at least partly due to the exosomal transport of PFF; (2) PFFs reside on the surface of exosomes, rather than being contained within their lumen. Further, exosomes isolated from cells exposed to PFFs contained PFFs on their outer surface. Biochemically, we were able to show that PFFs can be removed from exosomes through trypsinization; this would only be possible if PFF resided on the surface of exosomes. We then used Manumycin A, a drug that blocks the release of CD63-positive exosomes (Datta et al., 2017), and found that Manumycin A disrupts PFF transmission from cell-to-cell. We suspect that since PFFs reside on the outside of exosomes, drugs like EIPA, LatA, and LatB that blocked their initial uptake can be used to block the spread of PFFs. Our hypothesis was confirmed with our experiment using EIPA, showing the inhibition in the uptake of PFF-transporting exosomes by PFF-naïve cells.

Although all evidence presented indicates that PFFs use macropinocytosis to gain access into cells, we are also cognizant that the properties of α-syn itself could drive membrane curvature and protrusions. As previously observed, PFFs associate and may even drive membrane curvature (Vargas et al., 2017; Westphal & Chandra, 2013). This could mean that PFFs drives its own internalization into the cell by causing membrane curvature, and then, once trafficked to MVB/lysosomes, it drives membrane invaginations, resulting in intralumenal vesicle formation, leading to its eventual release via exosomes. Once released, PFFs then go on to disrupt other cells, all the while remaining on the outer surface exosomes, allowing it to drive membrane curvature, enabling its internalization into neighbouring cells. Although PFFs are just oligomers, they

certainly have many prion-like characteristics. Above all else, PFFs may be taking advantage of α-syn's interaction with membranes to drive their own endocytosis, exocytosis, and drive the production of more aggregated α-syn. It is this evolutionary drive for PFFs to create more fibrillated forms of α-syn, that truly makes it more than just an oligomer and more like a prion.

In conclusion, our data demonstrate that PFFs enter cells via macropinocytosis, with seemingly direct transfer to MVBs and lysosomes, bypassing early endosomal pathways. It remains unclear if this represents fusion of macropinosomes with MVBs and lysosomes or maturation of macropinosomes into these structures. A portion of the PFFs that enter the cells are subsequently secreted on exosomes, providing a mechanism for cell-to-cell transport; yet our data does not explain how fibrillar α-syn interacts with α-syn in the cytosol to allow prion-like propagation. Regardless, inhibition of macropinocytic pathways may prove useful in limiting the progression of PD and other synucleinopathies.

Limitations of this study

While our experiments demonstrate the rapid transport of α-syn PFFs to lysosomes through a unique form of macropinocytosis in a Clathrin-independent manner, we acknowledge that our study has several limitations. First, amilorides and their inhibitive activity is not limited exclusively to macropinocytosis and their addition to cells can have other non-specific effects (Arias et al., 2008; Levenson et al., 1980; Mine et al., 2015; Vila-Carriles et al., 2006). Second, it is important to note that while we attempt to examine the internalization of α-syn preformed fibrils, PFFs may not be the true pathogenic component seen in synucleinopathies, as there are several forms of pathogenic α-syn that may be responsible (Alam et al., 2019; Emadi et al., 2009). In addition, we acknowledge that there are multiple strains of α-syn fibrils (Bousset et al., 2013; Peng

et al., 2018), which may utilize different endocytic pathways. Third, although we see gold-labeled PFFs in both MVBs and lysosomes, we have not established the relationship between these two pools of internalized α-syn; furthermore, our knowledge regarding the amount of PFFs in these two compartments is limited. Lastly, while our data suggests the role macropinocytosis could play in the spread of α-syn PFFs, further work needs to be done to address the relationship between internalized PFFs and its influence on endogenous α-syn, a key component in understanding the pathophysiology of PD.

3.5 Acknowledgements

We acknowledge the Facility for Electron Microscopy Research at McGill University, specifically Dr. S Kelly Sears, for his help with the EM. We acknowledge the Neuro Microscopy Imaging Center and the Advanced BioImaging Facility. We thank Dr. Michael Davidson and Dr. Paul Luzio for the LAMP1 and CD63 plasmids, respectively. We also thank Drs. Sabatini and Zoncu for the HA-TMEM192 plasmids. A.B. is supported by Fonds de recherche du Québec doctoral award and a studentship from the Parkinson Society of Canada. This work was supported by a grant from the Canada First Research Excellence Fund, Healthy Brain, Healthy Lives, McGill University, awarded to P.S.M. P.S.M. is a Distinguished James McGill Professor and Fellow of the Royal Society of Canada.

3.6 Figures

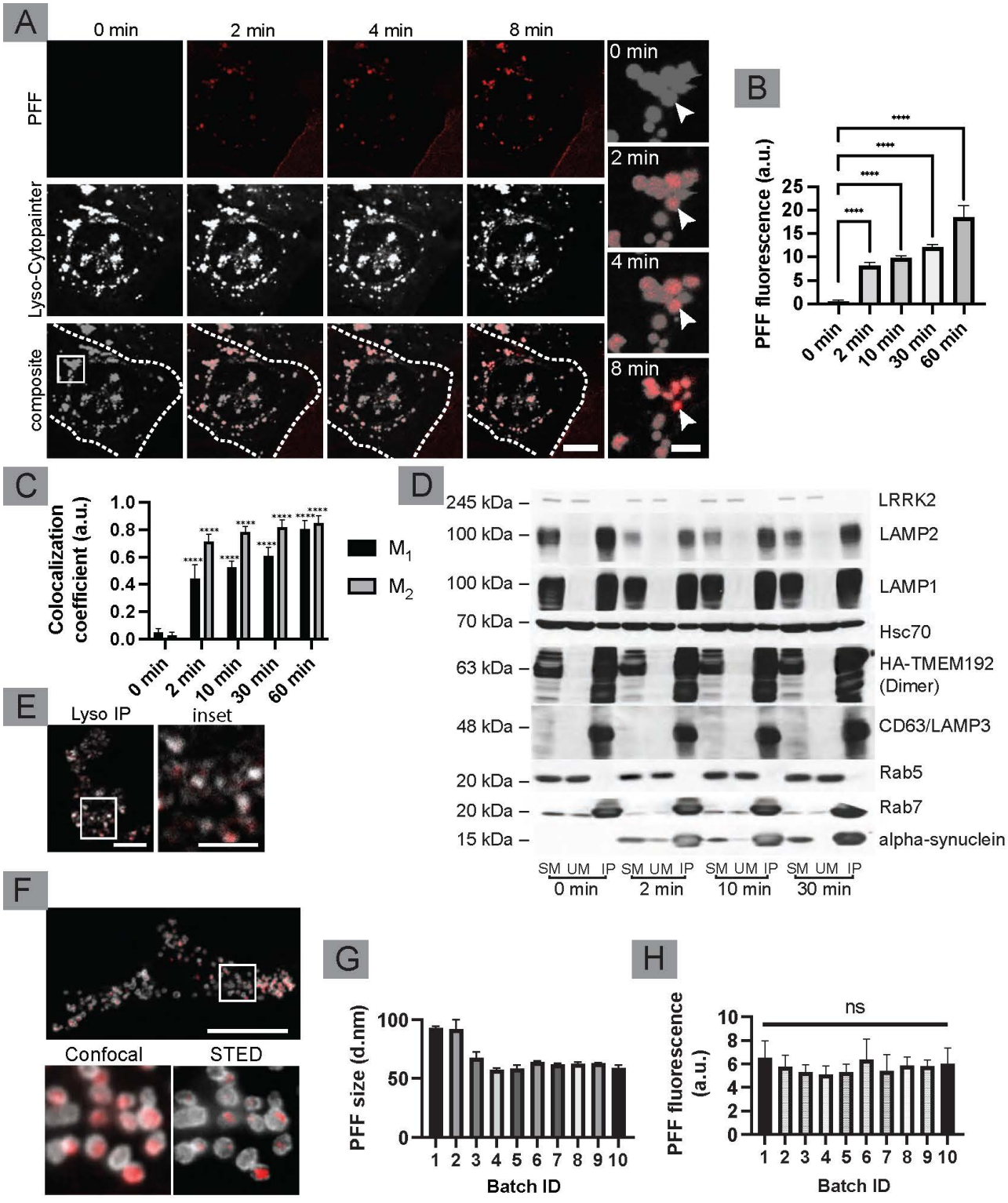
A
0 min
2 min
4 min
8 min
PFF
Lyso-Cytopainter
composite
B
PFF fluorescence (a.u.)
0 min
2 min
10 min
30 min
60 min
C
Colocalization coefficient (a.u.)
M1
M2
D
245 kDa
100 kDa
100 kDa
70 kDa
63 kDa
48 kDa
20 kDa
20 kDa
15 kDa
LRRK2
LAMP2
LAMP1
Hsc70
HA-TMEM192 (Dimer)
CD63/LAMP3
Rab5
Rab7
alpha-synuclein
SM UM IP
E
Lyso IP
inset
F
Confocal
STED
G
PFF size (d.nm)
Batch ID
H
PFF fluorescence (a.u.)
ns
Batch ID

Figure 3.1 Rapid internalization and transport of PFFs to lysosomes

(A) U2OS cells were stained with Lyso-Cytopainter and placed in a live-cell imaging chamber at 37°C. Imaging was performed at 1 frame/sec. PFFs tagged with Alexa488 at 2 μg/mL were added to cells while imaging. PFF (red) colocalization with lysosomes (gray) can be seen in as early as 2 min in both low mag and inset. Arrowheads point to lysosomes accumulating PFF. Scale bars = 10 μm for low mag images, and 5 μm for insets. Inset location shown at 0 min. (B) Quantification of PFF uptake in U2OS. Cells were plated on coverslips and transfected with LAMP1-TurboRFP. PFFs were added to each coverslip at 2 μg/ml. Cells were incubated for 0, 2, 10, 30 min at 37°C following addition of PFF. Cells were washed with trypsin and fixed. n = 12 for each condition (i.e., n = 48 total). (C) Manders' coefficients for LAMP1 and PFF were calculated using JACoP plugin. n = 12 for each condition (i.e., n = 48 total), from three independent experiments. M_1 describes the colocalization of LAMP1 with PFFs while M_2 describes the colocalization of PFFs with LAMP1. For both B and C, mean ± SD and data was statistically analyzed using one-way ANOVA followed by multiple comparisons Tukey's test to assess significance from control (0 min). $p < 0.0001$ denoted as ****. (D) Lysosomes were immunoprecipitated from U2OS cells expressing HA-TMEM192-RFP using HA-magnetic beads. Starting material (SM), unbound material (UB), and Immunoprecipitated (IP) sample for each time point were collected and processed for Western blot with the indicated antibodies. (E) IP samples from the experiments in D were fixed and placed on coverslips and imaged using confocal microscopes. HA-TMEM192-RFP construct allowed us to visualize the lysosomes (white), many of which contained PFF tagged with Alexa Fluor 488 (red). Scale bars = 5 μm for low mag and 2.5 μm for inset. (F) Confocal samples of U2OS cells described in A imaged using STED microscopy. Scale bar= 10 μm for low magnification, and 0.5 μm for insets. (G) Dynamic light scattering measurement of 10 different

batches (3 different measurements using DLS for each batch) of conjugated PFFs, were administered to U2OS cells and their uptake was measured in H. No significant difference was observed in the uptake of the different sizes of PFFs. n = 9 for images analyzed corresponding to each batch (i.e., n = 90 total) from three independent experiments. $p > 0.05$ is denoted as ns for not significant.

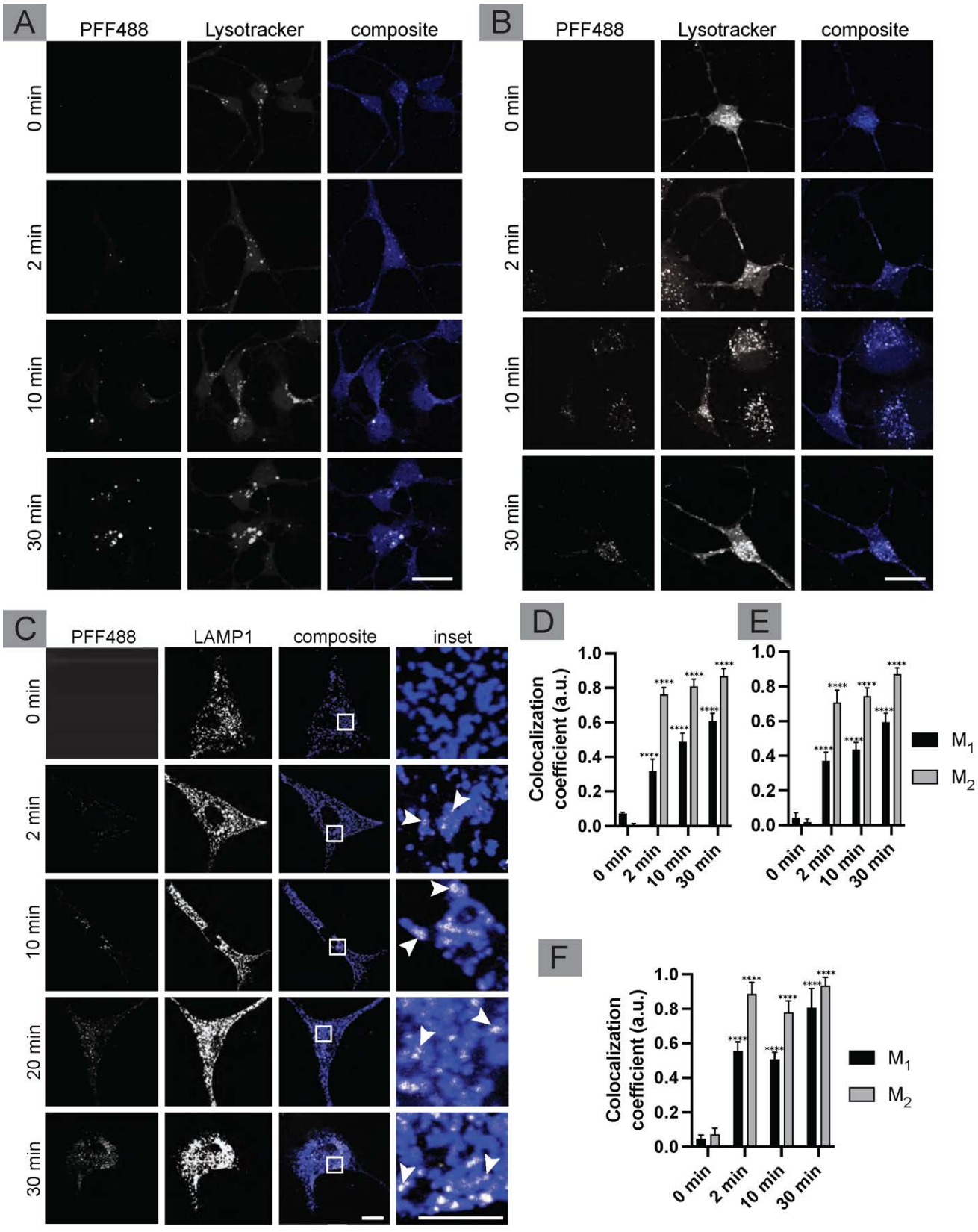
A
PFF488
Lysotracker
composite
0 min
2 min
10 min
30 min
B
PFF488
Lysotracker
composite
0 min
2 min
10 min
30 min
C
PFF488
LAMP1
composite
inset
0 min
2 min
10 min
20 min
30 min
D
Colocalization coefficient (a.u.)
1.0
0.8
0.6
0.4
0.2
0.0
0 min
2 min
10 min
30 min
E
M1
M2
F
Colocalization coefficient (a.u.)
M1
M2

Figure 3.2 Rapid PFF colocalization with lysosomes in human dopaminergic NPCs, dopaminergic neurons, and astrocytes

(A) Dopaminergic NPCs, stained with Lysotracker, were incubated for 0, 2, 10, 30 min at 37°C following addition of Alex488 labeled PFF (white) at 2 μg/mL. The cells were then washed lightly and briefly with trypsin and fixed. Scale bar = 20 μm. (B) NPCs differentiated into dopaminergic neurons were used in experiments described in A. Scale bar = 20 μm. (C) Human astrocytes, grown and mounted on coverslips, were given fluorescently labeled PFFs at 1 μg/ml concentration. Cells were then incubated for 0, 2, 10, 30 min at 37°C. Cells were washed with trypsin, fixed, permeabilized, and stained with LAMP1 antibody. Scale bar = 20 μm and 2.5 μm insets. (D/E) Manders' coefficients were calculated using the JACoP plugin to ascertain the colocalization of Lysotracker with PFFs from experiments described in A and B. n = 6 for NPCs and n = 6 for neurons in each condition (i.e., n = 48 total for NPCs and n = 48 total for neurons), from three independent experiments. (F) Manders' coefficients for LAMP1 with PFFs were calculated for experiments described in C. n = 10 for each condition (i.e., n = 40 total), from three independent experiments. For histograms depicting colocalization of lysosomes and PFFs as in D, E and F, M_1 represents the co-occurrence of Lysotracker/LAMP1 with PFFs, and M_2 represents the co-occurrence of PFFs with Lysotracker/LAMP1. In addition, for all histograms: mean ± SD and one-way ANOVA and multiple comparisons Tukey's test was conducted to assess significance from control (0 min). $p < 0.0001$ denoted as ****.

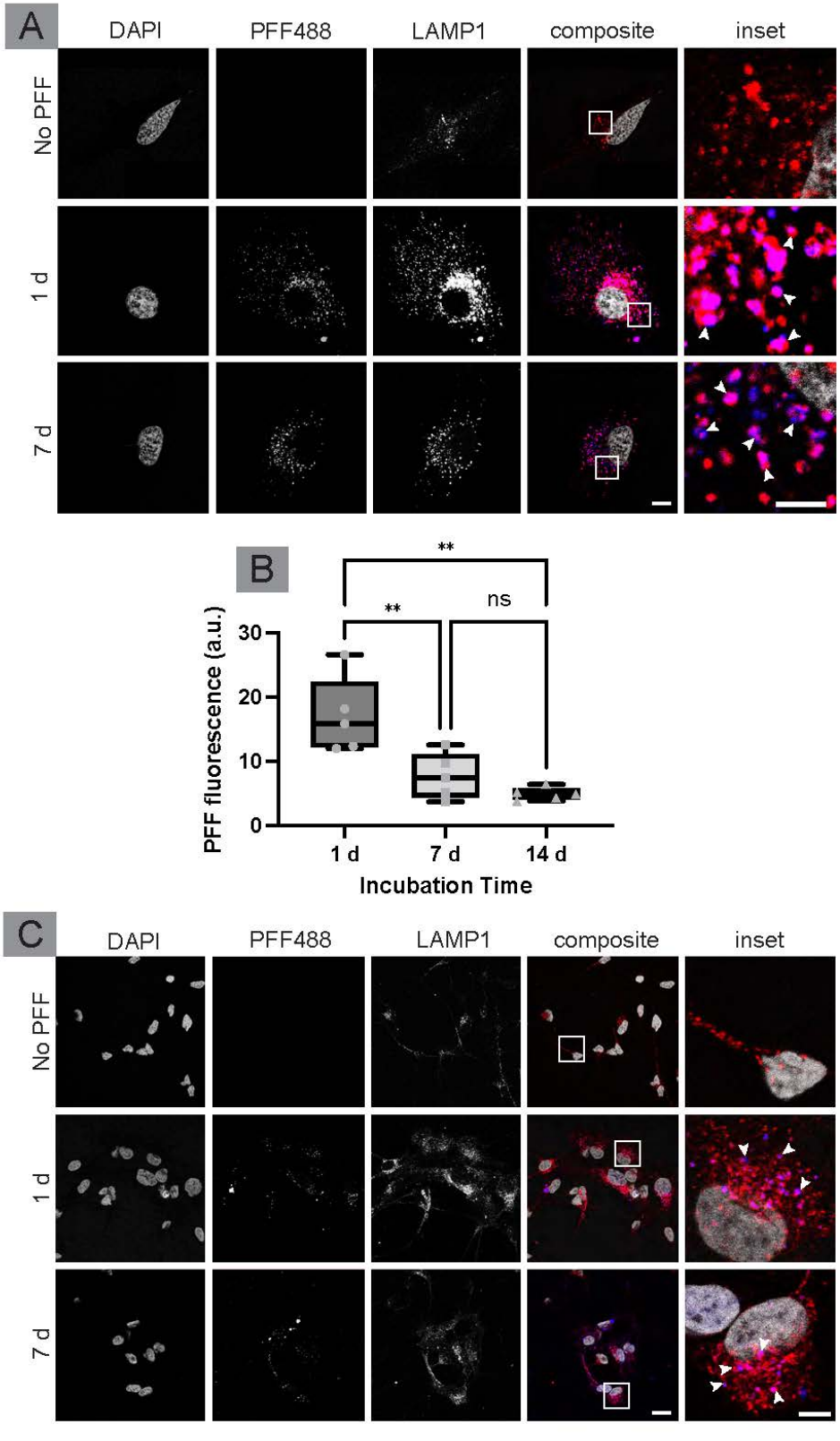
A
DAPI
PFF488
LAMP1
composite
inset
No PFF
1 d
7 d
B
**
**
ns
PFF fluorescence (a.u.)
30
20
10
0
1 d
7 d
14 d
Incubation Time
C
DAPI
PFF488
LAMP1
composite
inset
No PFF
1 d
7 d

Figure 3.3 PFFs remains in lysosomes days after exposure in dopaminergic neurons and astrocytes

(A) Human astrocytes were mounted on coverslips and were given PFF488 at 2 μg/ml on ice for 1 h. Cells were removed from ice, given fresh media, and were then incubated for 0 h, 1 day or 7 days at 37°C. Media was changed 24 h following the addition of PFFs. Following incubation, cells were lightly trypsin washed and fixed. Arrowheads point to LAMP1 and PFF colocalization. Scale bar = 20 μm for low magnification and 5 μm for insets. (B) Adult human astrocytes at passage 7, were plated on coverslips at 50% confluency and incubated with PFFs for 24 h. The cells were then trypsin washed and given fresh media. Some cells were fixed 1d while others were incubated for an additional 6 d or 13 d before fixation. Scale bar = 20 μm. PFF fluorescence intensity was then quantified. n = 5 for each condition (n = 15 total) collected from five independent experiments. Data was then analyzed using one-way ANOVA, and Tukey was conducted post-hoc to compare difference between means. $p < 0.001$ depicted as **, $p > 0.05$ was set to be not significant, denoted as ns. (C) Dopaminergic neurons derived from human iPSCs mounted onto coverslips and treated as in A. Lysosomes were stained using LAMP1 (red) antibody. PFF (blue) remains localized to lysosomes 7 days following its addition to the cell. Scale bar = 20 μm for low magnification and 5 μm for insets.

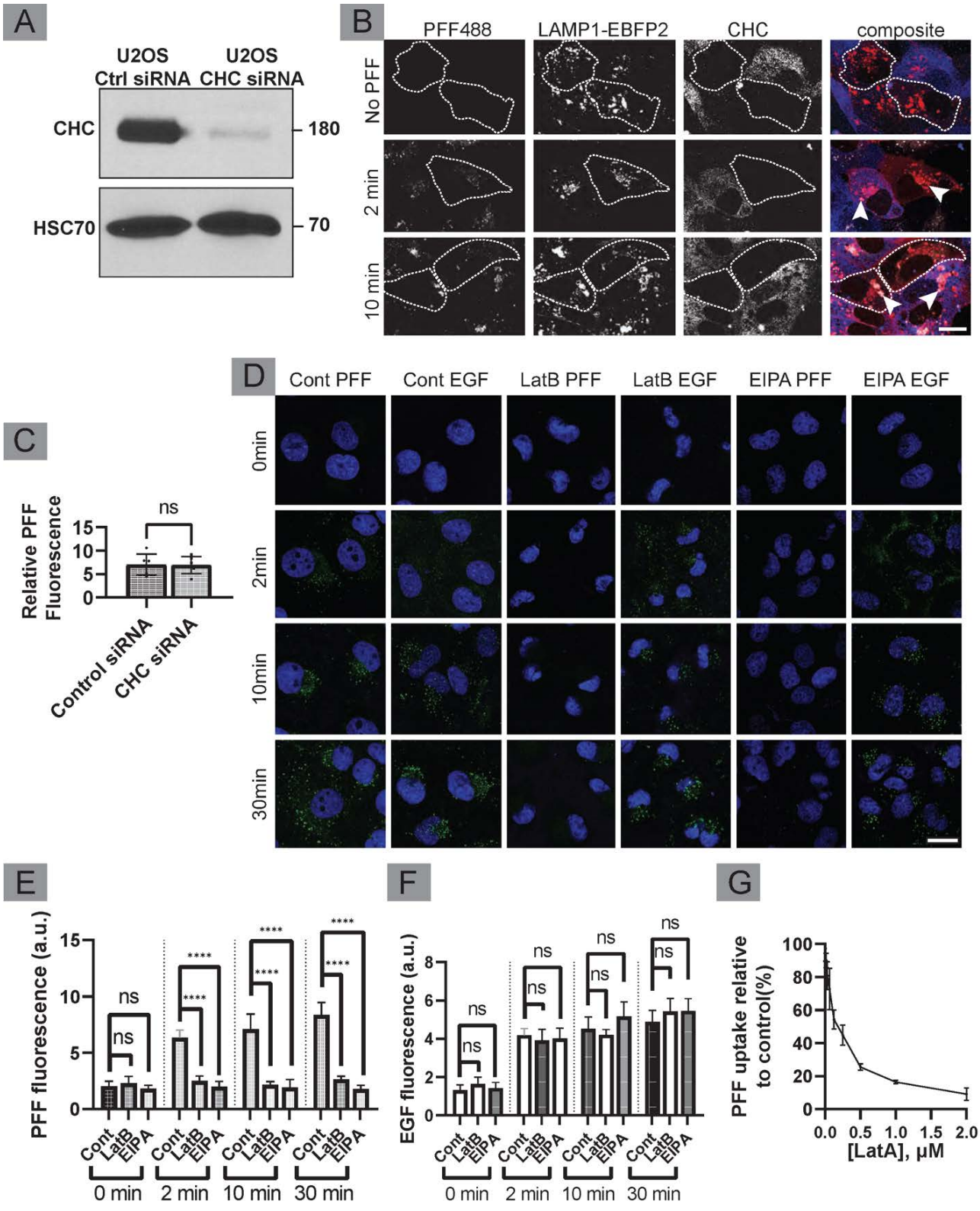
A
U2OS Ctrl siRNA
U2OS CHC siRNA
CHC
180
HSC70
70
B
PFF488
LAMP1-EBFP2
CHC
composite
No PFF
2 min
10 min
C
Relative PFF Fluorescence
ns
15
10
5
0
Control siRNA
CHC siRNA
D
Cont PFF
Cont EGF
LatB PFF
LatB EGF
EIPA PFF
EIPA EGF
0min
2min
10min
30min
E
PFF fluorescence (a.u.)
ns
****
Cont
LatB
EIPA
0 min
2 min
10 min
30 min
F
EGF fluorescence (a.u.)
ns
G
PFF uptake relative to control(%)
100
80
60
40
20
0
0.0
0.5
1.0
1.5
2.0
[LatA], μM

Figure 3.4 PFF internalization is unaffected by CHC KD but decreased using macropinocytic inhibitors

(A) U2OS cells previously transfected with EBFP2-LAMP1 were transfected with CHC siRNA or control siRNA. Cell lysates were immunoblotted with antibodies recognizing the indicated proteins (B) At 24 h, control and CHC siRNA-treated cells were re-plated as a mosaic onto coverslips. PFFs were added to each coverslip at 2 μg/ml. Cells were incubated for 0, 2, 10 at 37°C following addition of PFFs. Cells were washed with trypsin and fixed. Arrowheads show large LAMP1(red)- and PFF (white)-positive vesicles in both CHC (blue) positive and CHC negative cells, outlined by the CHC antibody. KD cells are outlined with dashed lines. Scale bar = 20 μm. (C) Internalization of PFF in CHC KD vs control cells at 2 min were quantified from experiments as in B, except that for quantification, KD and control cells were mounted on separate coverslips. n = 6 for each condition (i.e., n = 12 total), from three independent experiments. Individual data points shown and mean ± SD. Data was analyzed using two-sample *t*-test; $p > 0.05$ denoted as ns for not significant. (D) Astrocytes were grown and mounted on coverslips. Cell media was replaced with serum-free media containing 20 μM EIPA, 5 μM LatB or DMSO (vehicle control) for 30 min. Fluorescently labeled PFF or EGF (green) were added to each coverslip (at 2 μg/ml and 0.2 μg/ml, respectively) for 0, 2, 10, 30 min at 37°C. Cells were trypsin washed and fixed. Cell nuclei were stained with DRAQ7 (blue). Scale bar = 20 μm. (E) Quantification of PFF uptake from experiments as in D. n=6 for each condition (i.e., n = 96 total). (F) Quantification of EGF uptake from experiments shown in D. n=6 for each condition (i.e., n = 96 total), from three independent experiments. For both D and E, control was compared to LatB and EIPA treated samples at each time point; mean ± SD. Data was statistically analyzed by two-sample *t*-test; $p < 0.001$ denoted as *** and $p < 0.0001$ denoted as ****, ns = not significant. (G) Human dopaminergic NPCs were

treated with LatA and PFF for 24 h before fixation. y-axis: % intracellular PFF-Alexa fluorescence relative to DMSO (vehicle) only control (DMSO=100%). X-axis: Latrunculin A treatment concentration in μM.

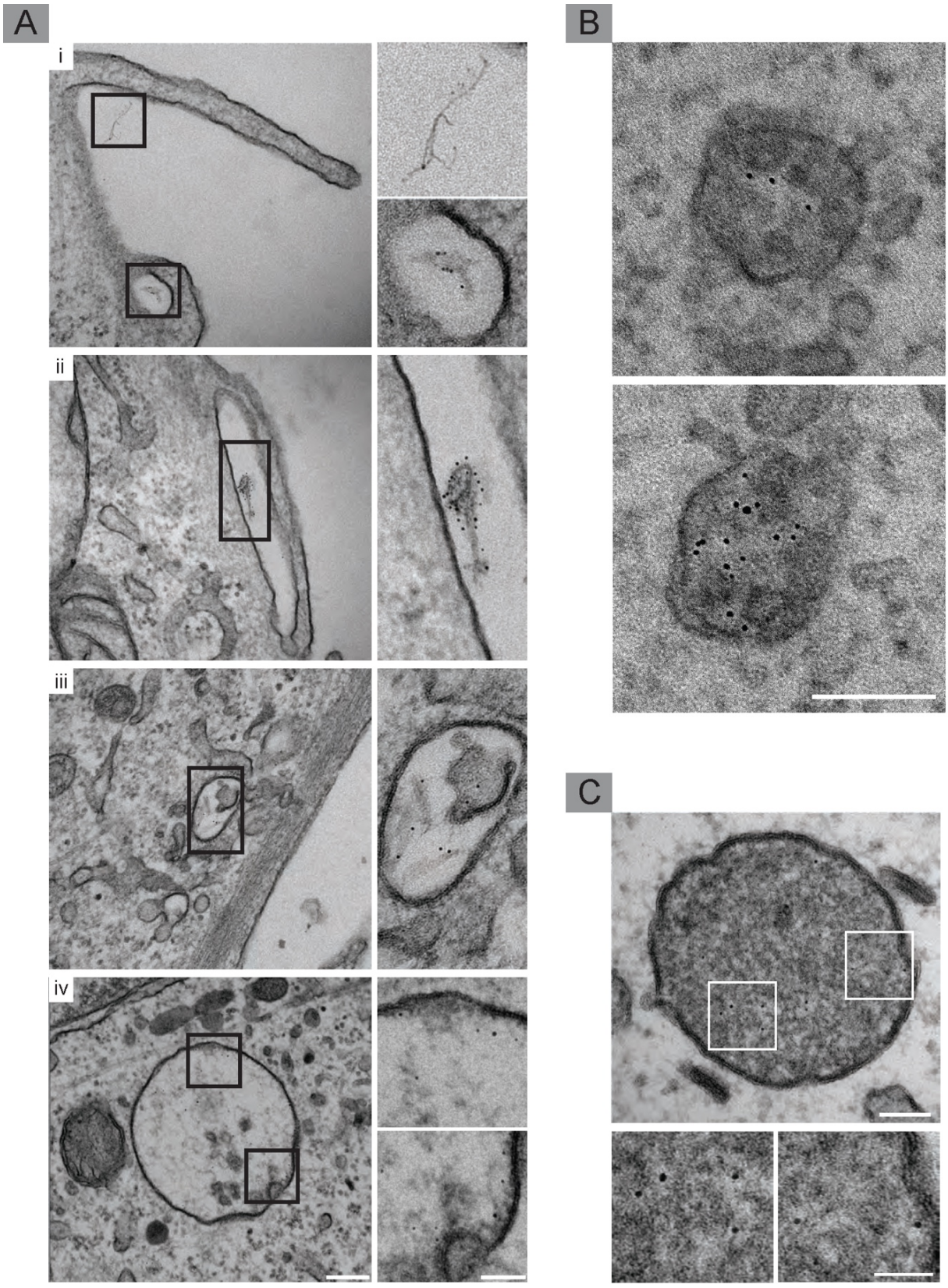
A
i
ii
iii
iv
B
C

Figure 3.5 Trafficking itinerary of PFFs revealed by nanogold-labeled PFFs and EM

(A) Early events involved in the internalization of PFFs were captured with EM. To allow direct detection, PFFs were conjugated with 5 nm gold. Astrocytes were plated on permanox 8 well plates, administered PFF-gold for 2-3 min, fixed, and processed for EM. Uranyl acetate staining was conducted both pre- and post-embedding. (i) shows the membrane protrusion/ruffle forming around PFF-gold and the subsequent closure of the ruffle, leading to the internalization of PFF. (ii) shows PFF inside a closed membrane ruffle, leading to a macropinosome containing PFF-gold. (iii) shows the internalized PFFs in a macropinosome. (iv) shows PFFs in large newly formed MVBs in proximity to the membrane, suggesting PFF and membrane interaction. Scale bar= 200 nm for low magnification images, and 50 nm for insets. (B) In order to visualize the contents of lysosomes, which appear as highly electron dense compartments using EM, astrocytes exposed to PFFs for 3-5 min were fixed and processed for EM; however, only *en bloc* uranyl acetate staining was conducted. Without staining of grids using uranyl acetate, PFF was easily visualized in multiple electron dense, lysosomal structures. Scale bar= 100 nm. (C) Uranyl-stained grids highly show electron dense lysosomes with PFF contents. Scale bar = 100 nm and 50 nm for insets.

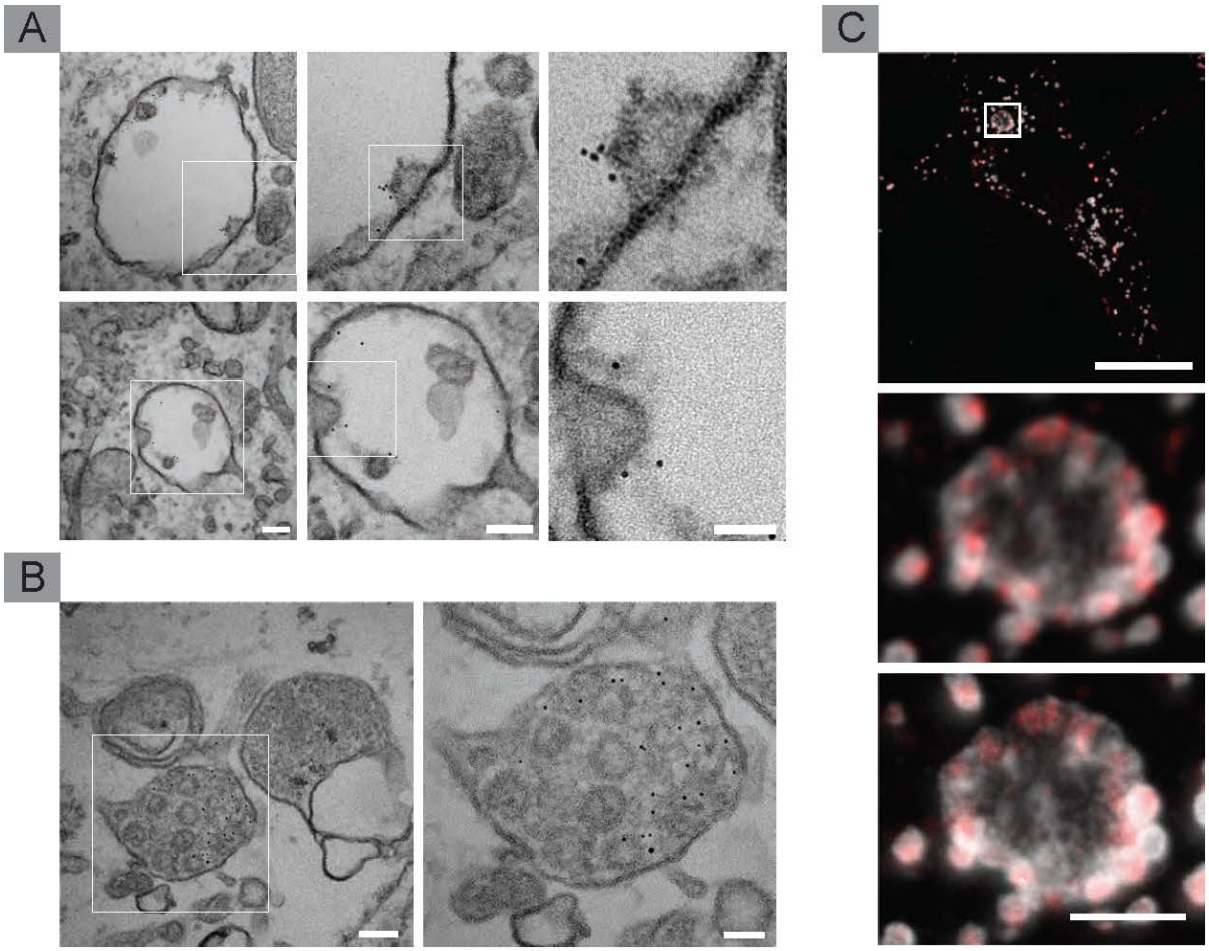
A
B
C
D
0 min
25 min
E
E
25m26s
25m58s
28m34s
29m44s
30m01s
31m32s
34m20s
35m09s
41m34s
46m43s
64m13s
65m09s

Figure 3.6 PFF trafficking to lysosomes and MVB

(A) Astrocytes administered PFFs for 10 min localize PFFs in larger newly forming MVB, always in proximity to the vesicular membrane, sometimes at invaginations, potentially signifying the early stages of exosome formation. Scale bar = 100 nm for low magnification, 80 nm for moderate magnification, 50 nm for highest magnification inset. (B) Localization of PFFs outside of vesicles in electron dense MVBs signifies the progression of MVB maturation. Scale bar= 100 nm and 50 nm for inset. (C) Similar findings regarding the formation of MVBs (LAMP1 positive; white) containing PFF (red) was confirmed using STED microscopy. Scale bar = 20 μm for low magnification, and 2.5 μm for high magnification images. (D) Large-field image showing colocalization of PFFs (red) with lysosomes(white): enhancement of lysosomal structures and their contents was carried out using "Find Edges" function in ImageJ, showing hollow lysosomal structures and the appearance of large acidic MVB at ~25 min following the addition of fluorescently labeled PFFs. Scale bar = 10 μm. (E) Higher magnification of images in D showing multiple budding events (arrowheads). Scale bar = 5 μm.

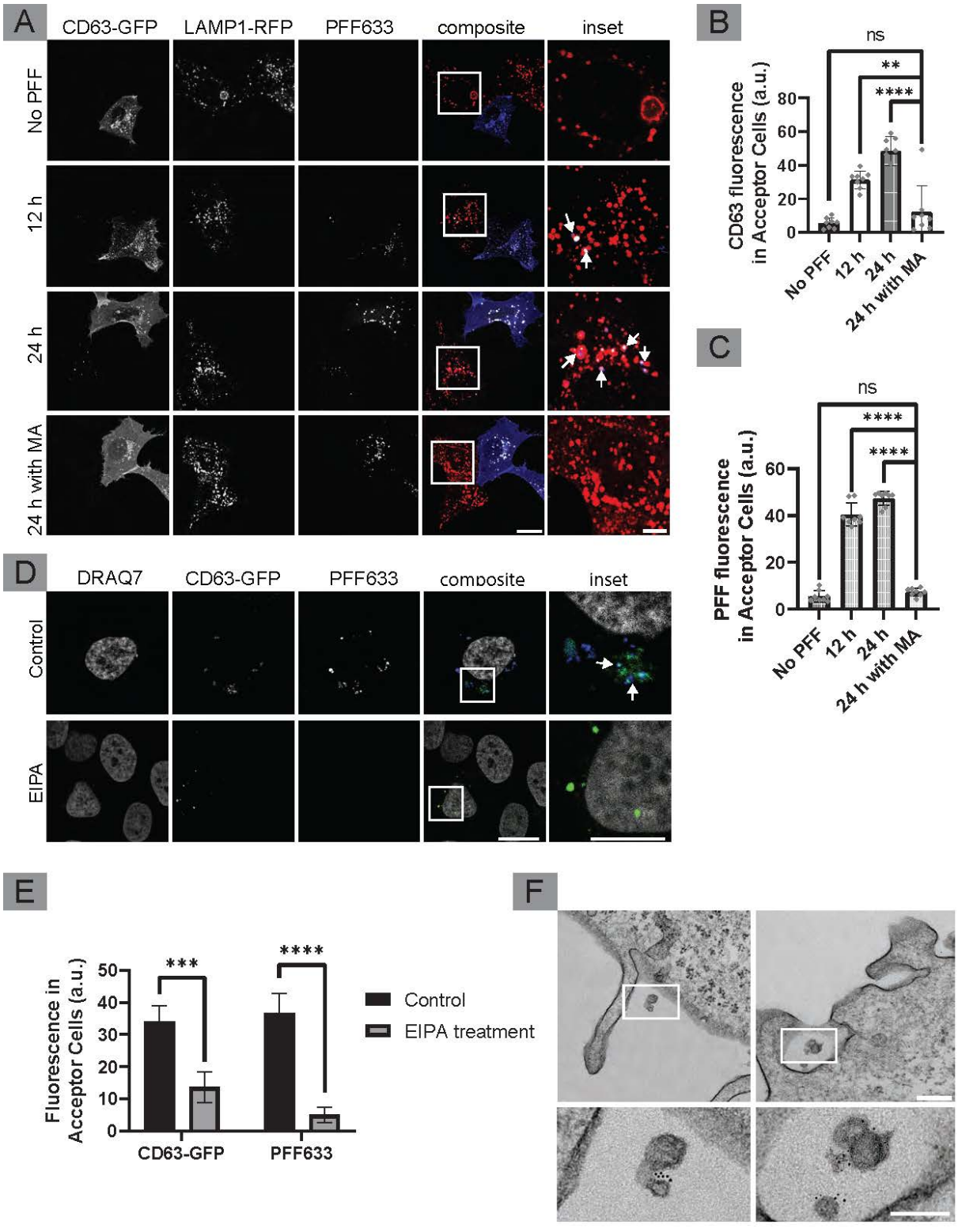
A
CD63-GFP
LAMP1-RFP
PFF633
composite
inset
No PFF
12 h
24 h
24 h with MA
B
ns
**
****
CD63 fluorescence in Acceptor Cells (a.u.)
80
60
40
20
0
No PFF
12 h
24 h
24 h with MA
C
ns
****
****
PFF fluorescence in Acceptor Cells (a.u.)
60
40
20
0
No PFF
12 h
24 h
24 h with MA
D
DRAQ7
CD63-GFP
PFF633
composite
inset
Control
EIPA
E
***
****
Fluorescence in Acceptor Cells (a.u.)
50
40
30
20
10
0
CD63-GFP
PFF633
Control
EIPA treatment
F

Figure 3.7 PFFs containing exosomes play a role in the transmission of PFFs from donor to acceptor cells

(A) U2OS cells stably expressing CD63-GFP were exposed to PFFs or PBS (vehicle control) for 24 h. CD63-GFP (donor cells; blue) were then trypsin washed three times, pelleted, trypsinized again, pelleted and PBS washed, prior to being co-plated with acceptor cells (PFF naïve cells stably expressing LAMP1-RFP; red). Donor and Acceptor cells were then incubated for 12 or 24 h. Half of the 24 h sample were given Manumycin A (MA) at 1.2 μM while the other half was given DMSO (vehicle control) at the time of plating. Both 12 h and 24 h samples show PFF (white) and CD63 (blue) fluorescence in acceptor cells, while the acceptor cells in the PBS and the MA treated condition show very little PFF and CD63 fluorescence. Arrows point to LAMP1 positive compartments in acceptor cells that contain both CD63 and PFF fluorescence within them. Scale bar = 10 μm for low magnification and 5 μm for insets. (B/C) Quantification of CD63 and PFF fluorescence in acceptor cells. n = 8 for each condition (i.e., n = 32 total), from three independent experiments, mean ± SD. No PFF, 12 h and 24 h conditions were statistically compared (two-sample *t*-test) to the 24 h samples with MA; $p < 0.0001$ denoted as ****, $p < 0.01$ denoted as **, and $p > 0.05$ denoted as ns for not significant. There was a significant reduction in CD63 and PFF in acceptor cells with MA. (D) At 24 h following the exposure of donor cells (CD63 positive) to PFF, cells were thoroughly trypsin washed and passaged onto plates and incubated with serum-free media for 36 h. The media was then collected, centrifuged for 5 min at 1000 RPM to pellet any floating cells, and given to acceptor cells (wildtype U2OS) some treated with DMSO (control) and other treated with EIPA. The cells were fixed following 6 h of incubation. Donor cells in control showed both PFF (blue) and CD63 (green) fluorescence, while EIPA treated cells did not. (E) Quantification of PFF and CD63 fluorescence in D. Multiple paired *t*-test was used to statistically

compare CD63 and PFF fluorescence in acceptor cells (control vs EIPA); n = 6 per condition (i.e., n = 12 total) from three independent experiments. $p < 0.001$ denoted as ***. (F) U2OS cells were given media (from donor cells treated with PFF-gold) isolated using the same protocol as D and incubated for 12 h. Cells were then processed for EM. Insets show extracellular vesicles with PFF-gold on their surface. Scale bar = 100 nm for low magnification images and 100 nm for inset.

3.7 Supplemental figures and tables

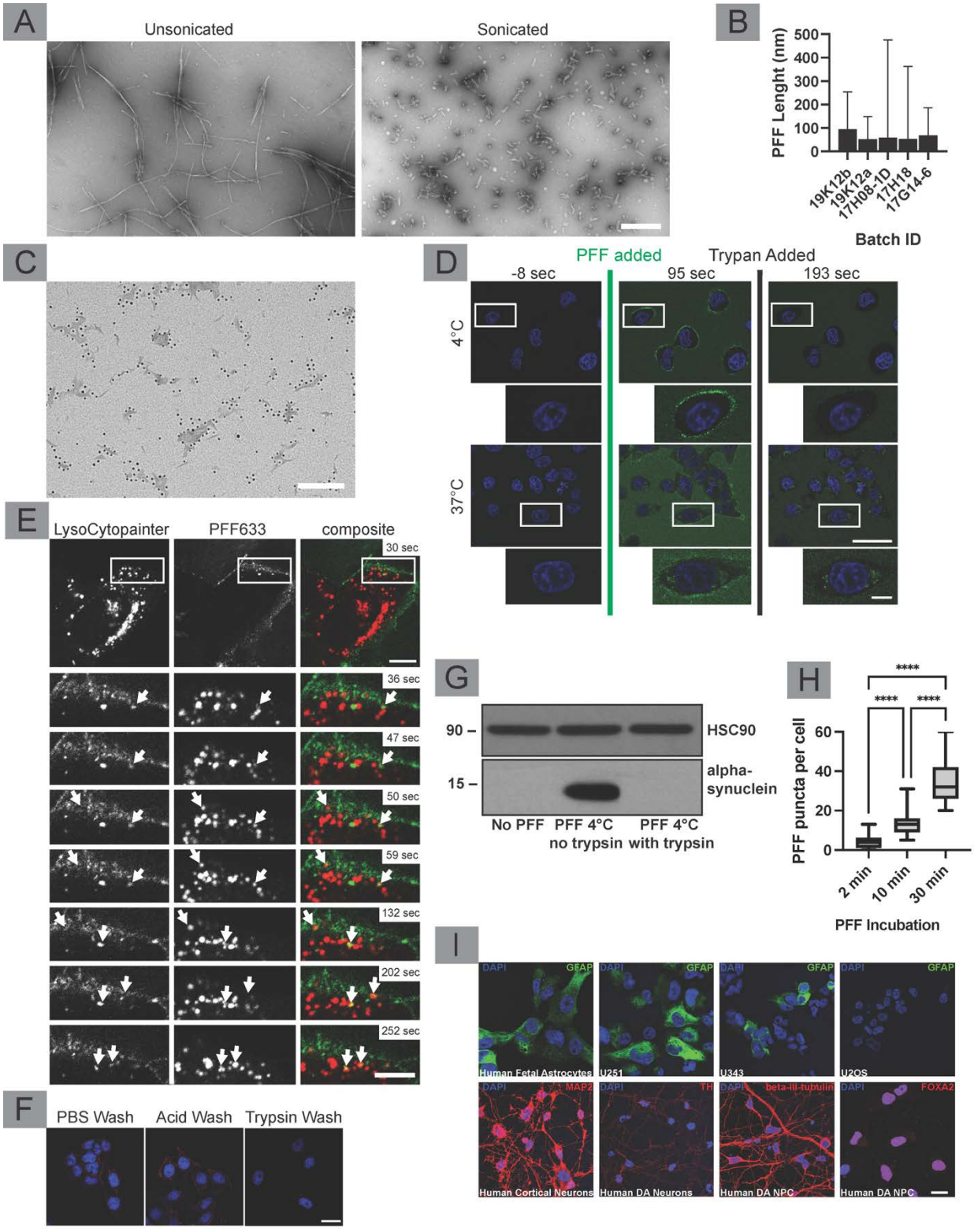

Supplementary Figure 3.1

Characterization of PFFs, trypan blue exclusion assay, live PFF uptake, trypsin wash and characterization of cell types

(A) Sonication of α-syn fibrils results in significantly smaller fibril length, allowing the α-syn oligomers to be characterized as PFF with a length of below 100 nm. (B) The mean length of unconjugated PFFs samples used were 51.72, 52.89, 58.28, 67.95, 95.04 nm; mean ± min and max. Once size was confirmed with electron microscopy, the corresponding batches were tagged with Alexa Fluor 488, Alexa Fluor 633, or 5 nm gold (C). Scale Bar = 100 nm. (D) Trypan blue exclusion assay was used to discriminate against intra- and extracellular PFFs. HeLa cells were grown on glass-bottomed plates and placed on ice for 30 min. They were then transferred to an imaging chamber for live imaging. In the first experiment, PFFs were administered to cells on ice (4^{o}C) and the live imaging chamber was not heated, allowing cells to remain at a low temperature (retrieved from ice immediately before imaging). Images were taken from before and after PFF addition. Trypan blue was added to cells 2 min following PFF. Next, the chamber was heated to 37^{o}C, and samples were placed within the imaging chamber, prior to the addition of PFFs. PFFs were then added, and 2 min following PFFs, trypan blue was added. PFF fluorescence that was not quenched by trypan blue is internalized. Scale bar = 20 μm for low magnification and 5 μm for insets. (E) PFF was added to cells at 4°C for 30 min to allow the binding of PFFs to the cell surface without internalization. Cells were then transferred to a pre-heated live imaging chamber and live imaging was started immediately after. Arrows point to specific PFF (green) punctae that eventually colocalize with lysosomes (red) over time. Scale bar = 10 μm for the low magnification image and 5 μm for the insets. (F) Unlike cargo proteins like Tf and EGF, trypsinization for 90 sec on ice is needed to remove extracellular PFF. In this experiment, Cells were incubated with PFFs

for 30 min at 4°C. Since PFF internalization is temperature dependent, we expected no PFF internalization. We then assessed the efficacy of PBS, Acid, and Trypsin wash on their ability to remove extracellular PFF. We found that trypsinization was the only method that removes extracellular PFFs. Scale bar = 20 μm. (G) To further confirm the efficacy of trypsin wash for the removal of extracellular PFFs, PBS (control) or PFFs were added to cells. Cells were incubated at 4°C for 30 min. Cells exposed to PFFs were then washed with either PBS or with trypsin. Cell lysates were then immunoblotted for α-syn, to assess the presence of PFFs. Samples washed with trypsin showed no α-syn signal, while the cells washed with PBS did, confirming the efficacy of trypsin in removing extracellular PFFs. (H) To better visualize the buildup of PFFs in cells, we also counted the number of PFF puncta appearing in cells at different time points; n = 50 (individual cells) for each time point (i.e., n = 150 total), from 9 images per time point collected from three independent experiments. One-way ANOVA and Tukey's test was conducted to assess the significance across means; mean ± min and max. $p < 0.0001$ denoted as ****. (I) To confirm the identity of astrocytes, glioblastoma cell lines, and the iPSC derived neural progenitor cells along with differentiated neurons, marker antibodies were used. Astrocytic and glial identity was confirmed using the glial fibrillary associated protein (GFAP) antibody. As expected, fetal astrocytes, and U251 had high levels of GFAP fluorescence while U343 had less, and U87 did not show any GFAP fluorescence. For neurons, the neuronal marker microtubule-associated protein 2 (MAP2) was used. To confirm the identity of dopaminergic neurons, tyrosine hydroxylase antibody (TH) was used. The confirm the identity of neural progenitor cells beta-III tubulin was used. Finally, to confirm the identity of dopaminergic neural progenitor cells, Forkhead box protein A2 (FOXA2) was used. Scale bar = 20 μm.

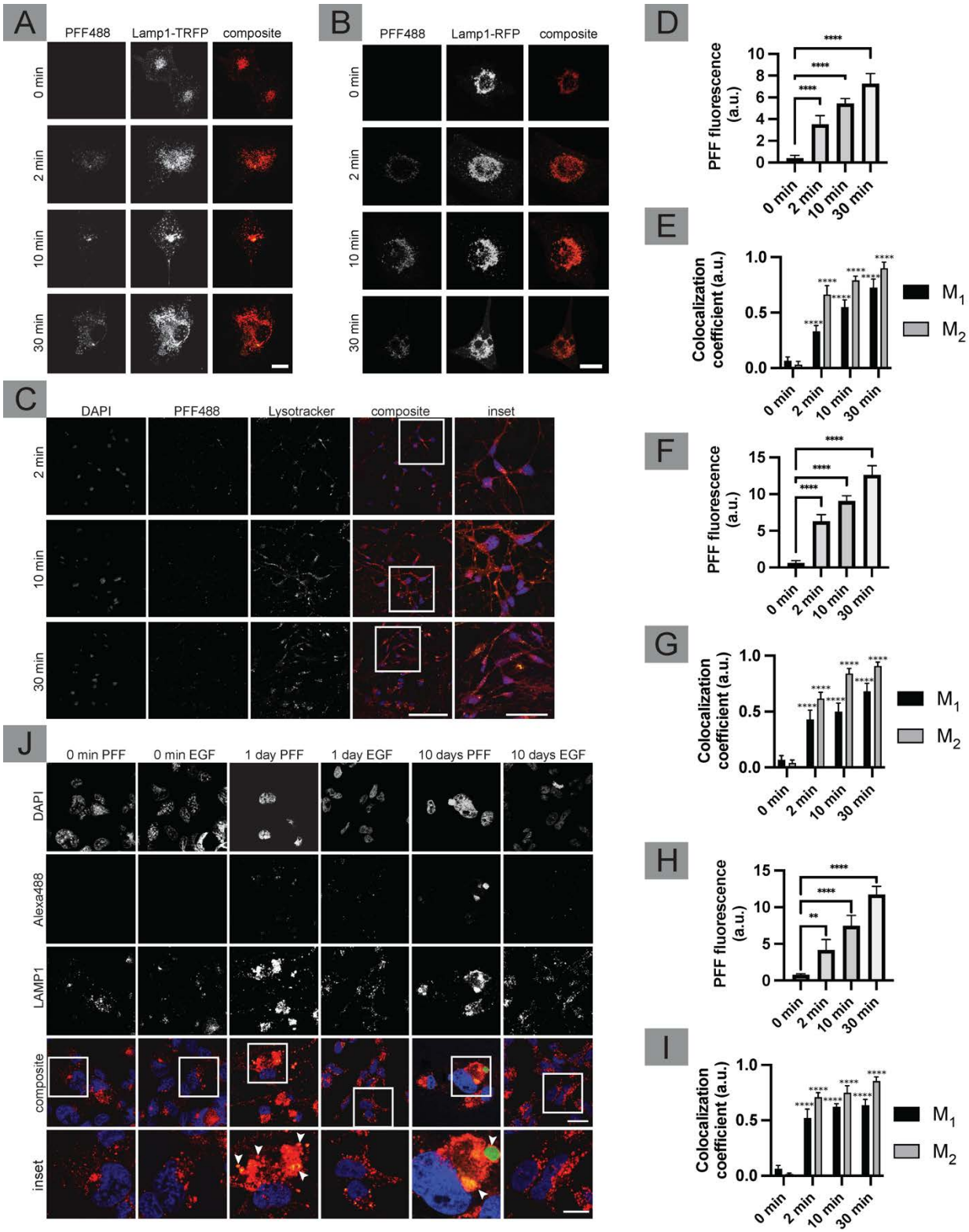
A
PFF488
Lamp1-TRFP
composite
0 min
2 min
10 min
30 min
B
PFF488
Lamp1-RFP
composite
C
DAPI
PFF488
Lysotracker
composite
inset
J
0 min PFF
0 min EGF
1 day PFF
1 day EGF
10 days PFF
10 days EGF
DAPI
Alexa488
LAMP1
composite
inset
D
PFF fluorescence (a.u.)
E
Colocalization coefficient (a.u.)
M1
M2
F
PFF fluorescence (a.u.)
G
Colocalization coefficient (a.u.)
M1
M2
H
PFF fluorescence (a.u.)
I
Colocalization coefficient (a.u.)
M1
M2

Supplementary Figure 3.2

PFF colocalization with lysosomes in glioblastomas and cortical neurons

(A) U87 cells were plated on coverslips and transfected with LAMP1-TurboRFP. PFFs were added to each coverslip at 2 μg/ml. Cells were incubated for 0, 2, 10, 30 min at 37°C following addition of PFFs. Cells were washed with trypsin and fixed. PFF (green) colocalization with LAMP1 (red) can be seen in as early as 2 min. Scale bar = 20 μm and 5 μm for insets. (B) U251 cells transduced with LAMP1-RFP lentivirus, were mounted onto coverslips, and were incubated with PFFs as in A. Cells were then trypsin washed and fixed. PFF colocalization with LAMP1 was once again observed at 2 min. (C) Cortical NPCs were mounted on coverslips and stained with lysotracker. PFF was added to each coverslip at 2 μg/ml. Cells were incubated for 0, 2, 10, 30 min at 37°C following addition of PFFs. PFF colocalization with lysotracker can be seen in as early as 2 min. Scale bar = 20 μm. (D/E) Uptake of PFFs and colocalization of LAMP1 and PFFs from experiment in A. n = 9 for each condition (i.e., n = 36 total for uptake and n = 36 for colocalization) from three independent experiments. (F/G) Uptake of PFFs and colocalization of LAMP1 with PFFs from experiment in B. n = 10 for each condition (i.e., n = 40 total for uptake and n = 40 for colocalization) from three independent experiments. (H/I) Uptake of PFFs and colocalization of Lysotracker with PFFs from experiments in C. n = 6 for each condition (i.e., n = 18 total for uptake and n = 18 for colocalization), from three independent experiments. All data reported as mean ± SD. For statistical analysis one-way ANOVA followed by Tukey's test was conducted to assess significance from control. For all colocalization experiments, Manders' coefficients, M_1 (lysosomal co-occurrence with PFFs) and M_2 (PFF co-occurrence with lysosomes) were compared across different time points. $p < 0.0001$ denoted as ****, $p < 0.001$ denoted as ***, $p < 0.05$ denoted as *. (J) U343 human glioblastoma cells were mounted on coverslips given

PFF488 or EGF488 at 2 μg/ml and 0.2 ug/ml concentration respectively on ice for 1 h. Cells were removed from ice, replaced with fresh media, and were then incubated for 0 h, 1 day or 10 days at 37°C. Following incubation, cells were trypsin washed and fixed. Samples were then permeabilized, blocked and stained with LAMP1 antibody. PFF fluorescence is readily detected over 10 days while EGF fluorescence is very weak even at 1 day. Arrowheads point to large PFF and LAMP1 structures which are only present in cells that were exposed to PFFs. Scale bar = 20 μm for low magnification and 5 μm for insets.

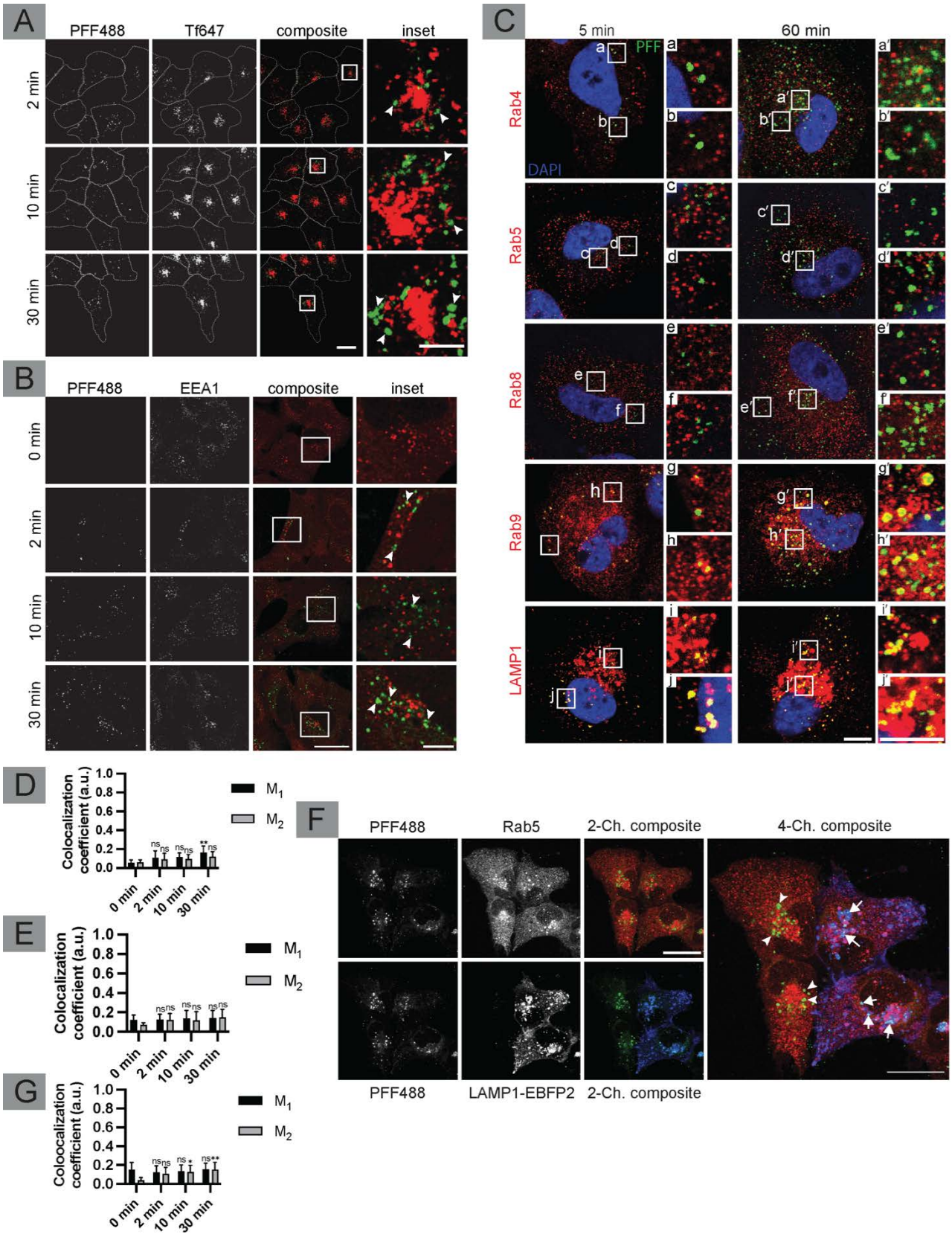
A
PFF488
Tf647
composite
inset
2 min
10 min
30 min
B
PFF488
EEA1
composite
inset
0 min
2 min
10 min
30 min
C
5 min
60 min
PFF
DAPI
Rab4
Rab5
Rab8
Rab9
LAMP1
D
Colocalization coefficient (a.u.)
M1
M2
0 min
2 min
10 min
30 min
E
Colocalization coefficient (a.u.)
M1
M2
F
PFF488
Rab5
2-Ch. composite
4-Ch. composite
PFF488
LAMP1-EBFP2
2-Ch. composite
G
Colocalization coefficient (a.u.)
M1
M2

Supplementary Figure 3.3

PFFs are not trafficked through early/recycling endosomes

(A) Fluorescently-labelled PFFs (green) and Tf (red) were added to U2OS cells at 2 μg/ml and 0.2 μg/ml concentration, respectively. Cells were incubated for 2, 10, 30 min at 37°C, washed with trypsin and fixed. Arrowheads point to PFF punctae. Scale bar = 20 μm and 10 μm for insets. (B) U2OS cells were mounted on coverslips, PFFs (green) were added to each coverslip at 2 μg/ml and the cells were incubated for 0, 2, 10, 30 min at 37°C. Cells were washed with trypsin, fixed, permeabilized, and stained with EEA1 antibody (red). Arrowheads point to PFF punctae. Scale bar = 20 μm and 5 μm. (C) PFF (green) colocalization with early endosome markers: Rab4 and Rab5; Rab8; and late endosome and lysosomal markers: Rab9 and LAMP1 was examined using antibodies (red). PFFs colocalized only with Rab9 and LAMP1 at 5 and 60 min. Scale bar for low magnification images is 10 μm and 5 μm for insets. (D) Colocalization of Tf with PFFs from experiments as in A. n = 9 for each condition (i.e., n = 36 total), from three independent experiments. (E) Colocalization of EEA1 with PFFs from experiments in B. n = 9 for each condition (i.e., n = 36 total), from three independent experiments. (F) U2OS cells were incubated with PFFs at 2 μg/ml for 5 minutes. Cells were washed with trypsin, fixed, permeabilized, and stained with Rab5 antibody. Scale bar = 20 μm. (G) Colocalization of Rab5 with PFF from experiments as in F. n = 9 for each condition (i.e., n = 36 total), from three independent experiments. For all colocalization quantifications, data is presented as mean ± SD. Manders' coefficients M_1 and M_2 were calculated using JACoP plugin in ImageJ. Statistical analysis of the data was done with one-way ANOVA followed by Tukey's test for mean comparisons; $p < 0.01$ is depicted as **, and $p < 0.05$ is depicted as *; lastly, $p > 0.05$ denoted as ns for not significant.

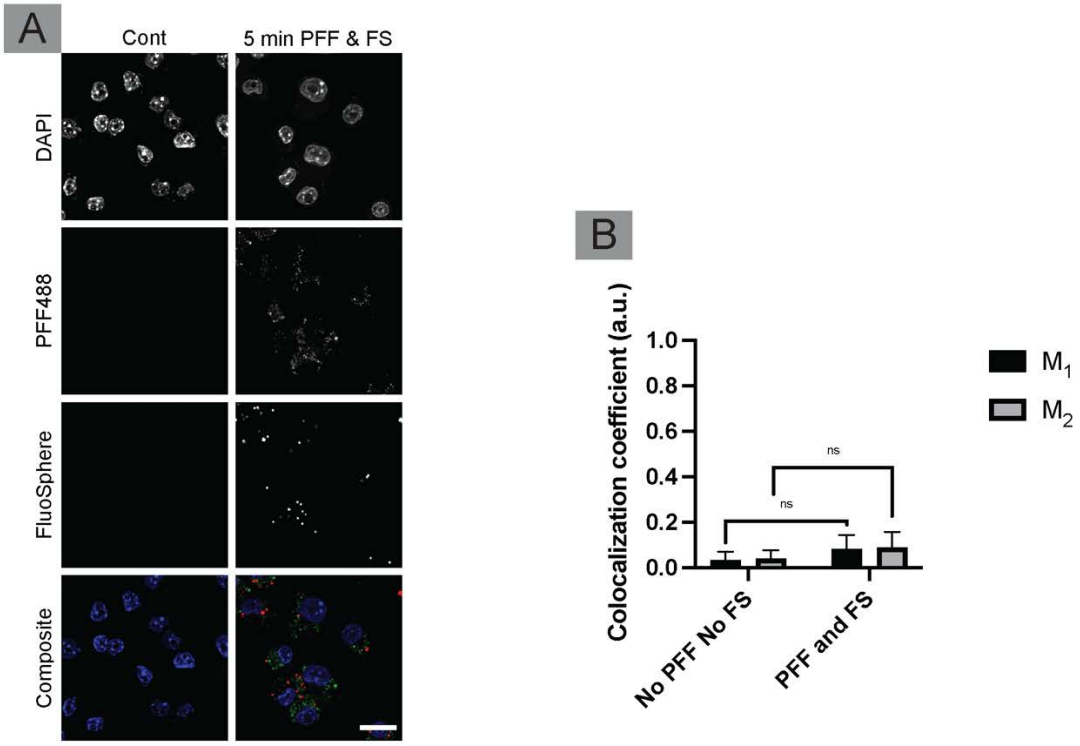
A
Cont
5 min PFF & FS
DAPI
PFF488
FluoSphere
Composite
B
Colocalization coefficient (a.u.)
1.0
0.8
0.6
0.4
0.2
0.0
ns
ns
No PFF No FS
PFF and FS
M1
M2

Supplementary Figure 3.4

PFF internalization does not depend on phagocytosis

(A) RAW 264.7 cells were plated on coverslips and administered FluoSpheres (FS) alongside PFFs. Scale bar = 20 μm. (B) Quantification of the colocalization (Manders' coefficients) of FS and PFFs showed no significant difference when compared to control using. M_1 (co-occurrence of FS with PFFs) and M_2 (co-occurrence of PFFs with FS) were calculated using JACoP plugin in ImageJ. Statistical analysis of the data was done with two-sample *t*-test; $p > 0.05$ denoted as ns for not significant. n = 6 for each condition (n = 12 total) collected from three independent experiments. Data represented as mean ± SD.

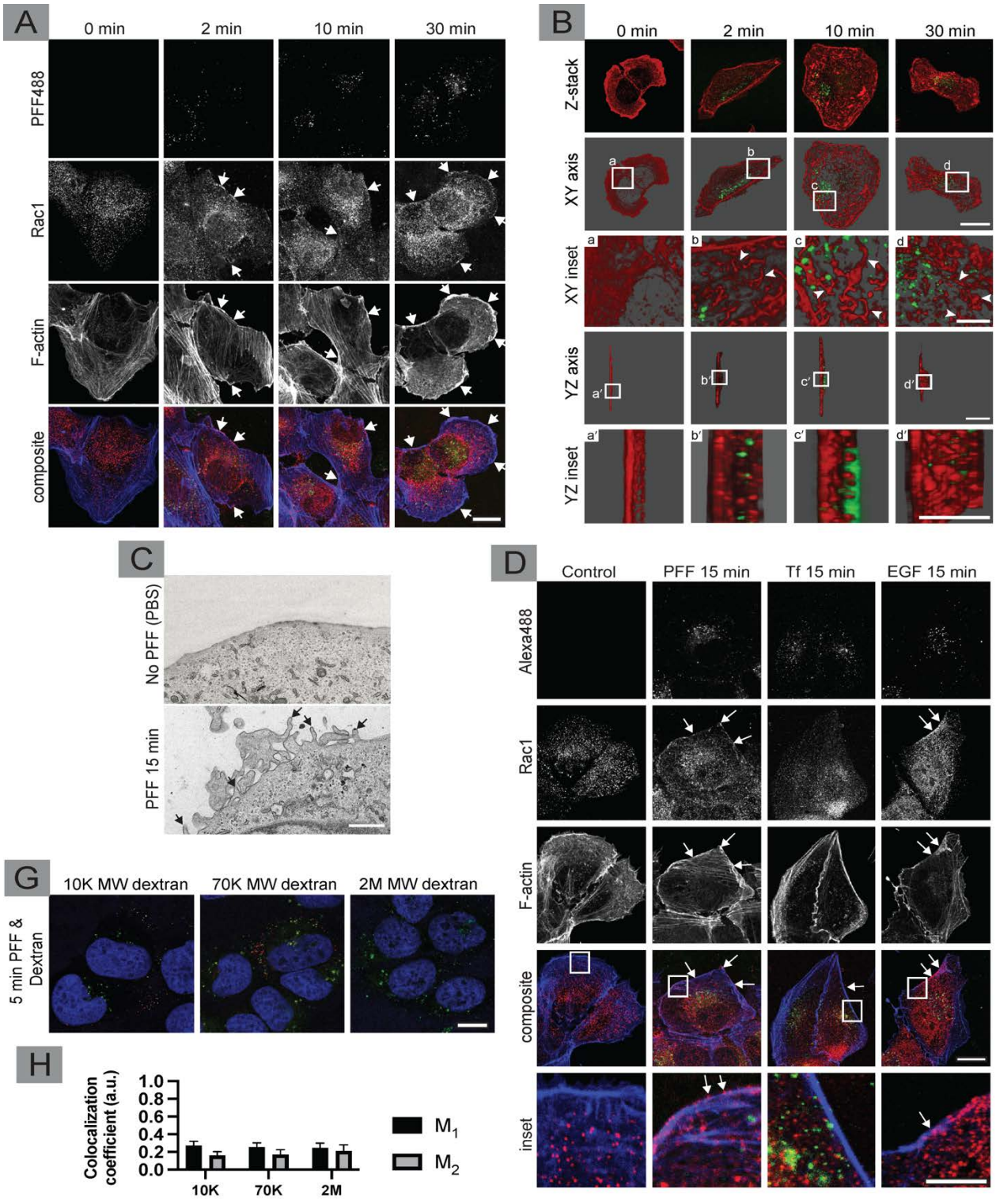
A
0 min
2 min
10 min
30 min
PFF488
Rac1
F-actin
composite
B
0 min
2 min
10 min
30 min
Z-stack
XY axis
XY inset
YZ axis
YZ inset
C
No PFF (PBS)
PFF 15 min
D
Control
PFF 15 min
Tf 15 min
EGF 15 min
Alexa488
Rac1
F-actin
composite
inset
G
10K MW dextran
70K MW dextran
2M MW dextran
5 min PFF & Dextran
H
Colocalization coefficient (a.u.)
1.0
0.8
0.6
0.4
0.2
0.0
10K
70K
2M
M1
M2

Supplementary Figure 3.5

PFF internalization is mediated through a unique form of macropinocytosis

(A) Astrocytes were grown and mounted on coverslips. Fluorescently labelled PFFs (green) were added to each coverslip at 2 μg/ml and cells were incubated for 0, 2, 10, 30 min at 37°C. Cells were washed with trypsin, fixed, permeabilized, and stained with Rac1(red) and F-actin (blue) antibodies. Arrows point to colocalization of F-actin and Rac1 at the cell surface, an indicator of membrane ruffling. Scale bar = 20 μm. (B) Phalloidin (red) was used to stain F-actin in astrocytes with varying PFF (green) incubation times. The Z-stacks were then combined to produce 3D images. Arrowheads point to actin ruffles. Scale bar = 20 μm and 5 μm for XY and YZ insets. (C) EM of astrocytes exposed to PBS or PFFs for 5 min. Arrows point to membrane protrusions and ruffling. Scale bar = 1 μm. (D) Astrocytes were grown and mounted on coverslips. PFFs, EGF, or Tf (all tagged with Alexa 488; green) were added to each coverslip at 2 μg/ml. Cells were then incubated for 0 or 15 min at 37°C. Cells were washed with trypsin, fixed, permeabilized, and stained with Rac1 (red) and F-actin (blue) antibodies. Arrowheads point to colocalization of F-actin and Rac1 at the cell surface, a marker for membrane ruffling. Scale bar = 20 μm. (G) U2OS cells were plated on coverslips and administered dextrans with different molecular weights (10,000; 70,000; 2,000,000) alongside PFFs. Scale bar = 20 μm. (H) Quantification of dextran colocalization with PFFs during uptake indicates a slight overlap in the endocytic pathway. Manders' coefficients were used to calculate colocalization. M_1 and M_2 were tabulated using the JACoP plugin in ImageJ; n = 6 for each condition (n = 18 total) collected from three independent experiments; mean ± SD.

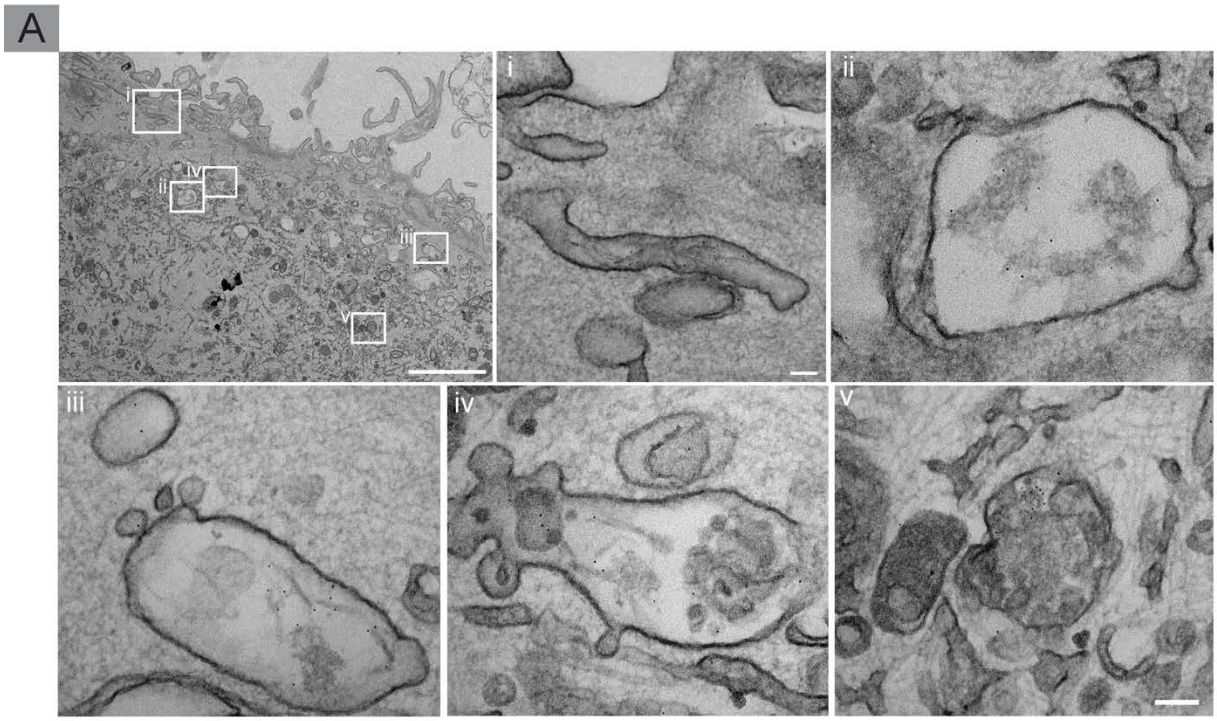
A
i
ii
iii
iv
v
i
ii
iii
iv
v

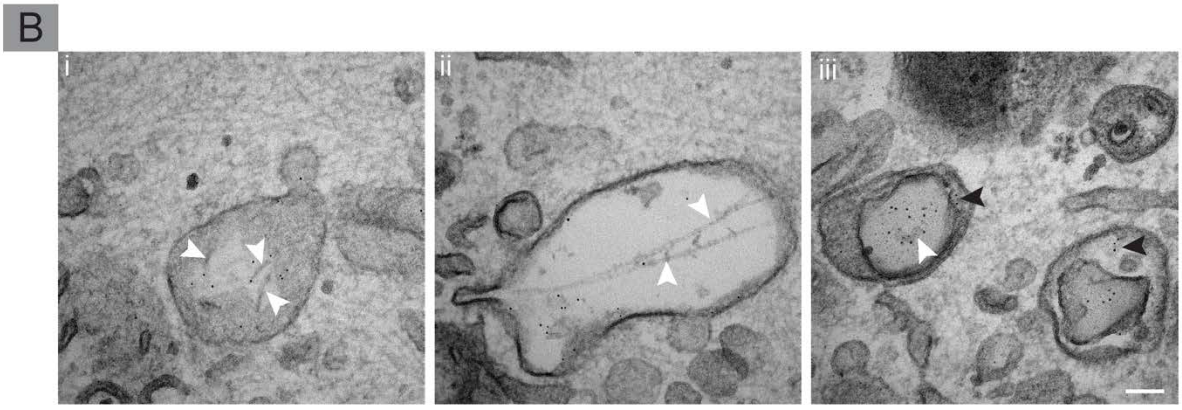
B
i
ii
iii

Supplementary Figure 3.6

PFFs induce membrane ruffling at the cell membrane and is localized to macropinosomes, MVBs, and lysosomes

(A) Astrocytes exposed to 10 min PFF-gold, showed PFF-gold localized to macropinosomes (i-iii). (iv) PFFs were also found in MVBs. (v) PFFs can also be found in electron dense lysosomes. Scale bar = 2 μm for low magnification, and 100 nm for all insets. (B) PFF located in various compartments within astrocytes exposed to PFF-gold for 30 min. (i) Visible PFFs in lumen of large electron-lucent vesicles (arrowhead). (ii) Long fibrils of α-syn (arrowhead) found in macropinosomes at 30 min, suggesting that it takes longer for lengthy fibrils to enter the cell. (iii) PFFs found both within (white arrowhead) and outside (black arrowhead) the lumen of large intralumenal vesicles. Scale bar = 100 nm.

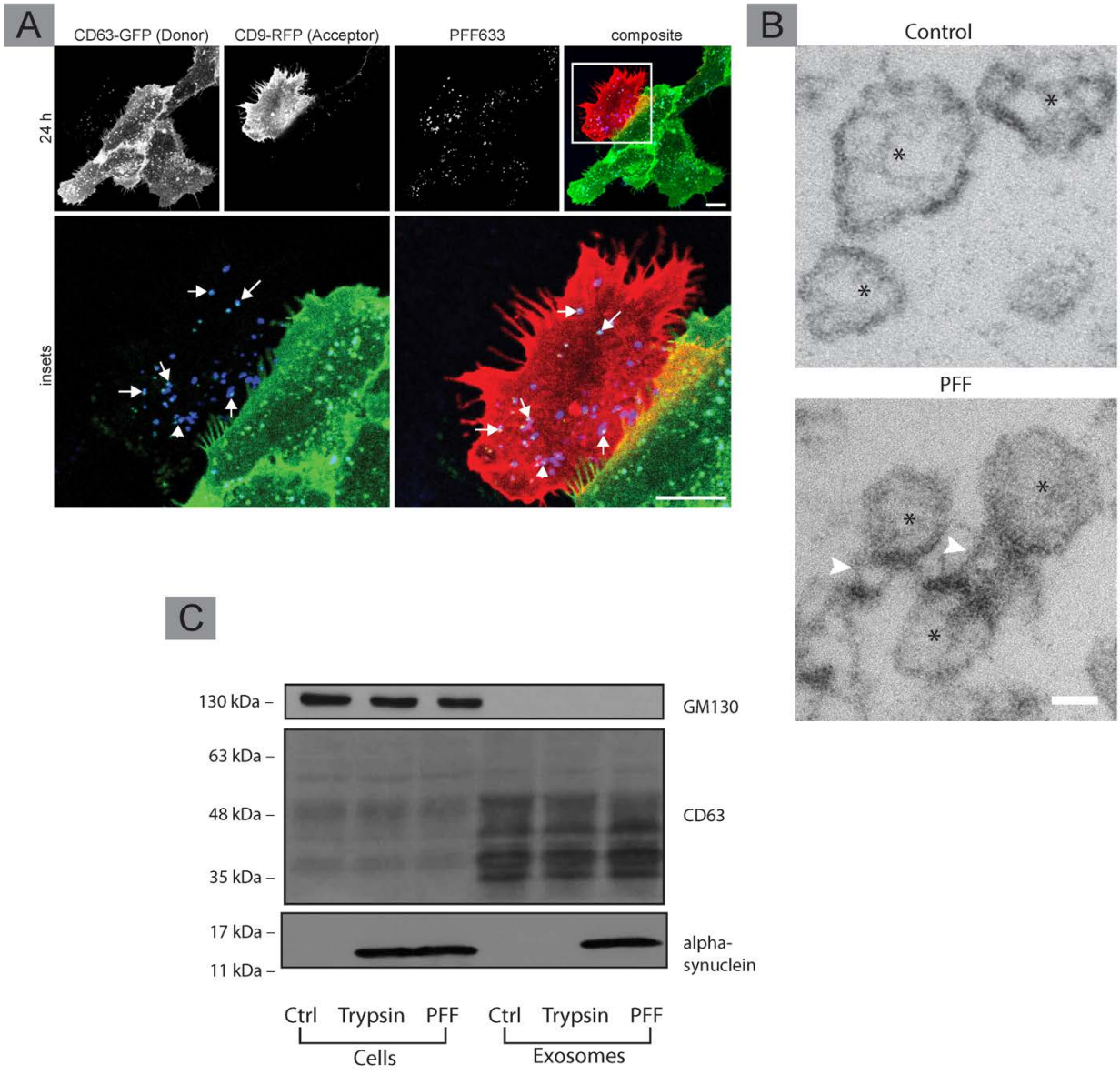
A
CD63-GFP (Donor)
CD9-RFP (Acceptor)
PFF633
composite
24 h
insets
B
Control
PFF
C
130 kDa –
63 kDa –
48 kDa –
35 kDa –
17 kDa –
11 kDa –
GM130
CD63
alpha-
synuclein
Ctrl
Trypsin
PFF
Ctrl
Trypsin
PFF
Cells
Exosomes

Supplementary Figure 3.7

CD63 positive exosomes play a role in the intercellular transmission of PFFs from donor to acceptor cells

(A) U2OS cells stably expressing CD63-GFP were exposed to PFFs or PBS (vehicle control) for 24 h. CD63-GFP (donor cells) were then trypsin washed three times, pelleted, trypsinized again, pelleted and PBS washed, prior to being co-cultured with acceptor cells (PFF naïve cells stably expressing CD9-mCherry). 24 h samples show PFF (blue) and CD63 (green) fluorescence in CD9-positive (red) acceptor cells. Arrows point to compartments in acceptor cells that contain both CD63 and PFFs. Scale bar = 20 μm for low magnification images and, and 10 μm for inset. (B) U2OS cells exposed to PFFs were trypsin washed three times and replated with media. Following incubation, cell media was collected and underwent multiple centrifugation steps to isolate exosomes. A small portion of the exosome samples were then processed for EM. Exosomes (indicated by *) collected from cells exposed to PFFs showed fibril-like structures on their surface. Scale bar = 20 nm. (C) The remaining portion of the exosome samples were immunoblotted along with their cells of origin. The exosome samples were enriched in CD63 and were negative for GM130. A portion of the exosomes isolated from PFF-treated cells were exposed to trypsin before being processed for immunoblotting. Like the control, trypsin exposed exosomes were not positive for α-syn.

Supplemental table 3.1

Previous studies on α-syn endocytosis

Type of α-syn	Inhibition/Inhibitors used	Incubation time following α-syn addition	Reported Intracellular trafficking	Findings	Publication
Monomer		1 h	Rab5A	Rab5A-mediated uptake of α-syn	(Sung et al., 2001)
Fibril	Cytochalasin D	2 and 12 h		Cytochalasin D treatment resulted in decreased α-syn uptake in microglia	(Zhang et al., 2005)
Fibril		3 h		Co-immunoprecipitation of Clathrin and α-syn; colocalization of α-syn and Clathrin	(Liu et al., 2007)
Fibril	dynamin-1 K44A	1 h	Partial colocalization of α-syn with EEA1 and LAMP2.	Internalization of α-syn fibrils was inhibited by low temperature and dynamin dominant-negative, while monomeric α-syn entered cells through diffusion. It was concluded that the endolysosomal pathway is involved.	(H. J. Lee et al., 2008)
Monomer	Dynamin dominant negative and Dynasore	1 h		Internalization of α-syn was not inhibited with dynamin dominant-negative or Dynasore but lipid-raft mediated.	(Park et al., 2009)
Cellular synuclein expression	Dynamin-1 K44A (dominant negative)	24 and 48 h		Synuclein transmission was inhibited with the use of dynamin dominant-negative	(P. Desplats et al., 2009)
Vector expression of α-syn	Dynamin dominant-negative	Coculture – 3 days	Endolysosomal system	α-syn endocytosis is inhibited in cells expressing dynamin dominant-negative	(Lee et al., 2010)
Transfected and exogenous α-syn monomer	Dynasore, monodansylcadaverine	Coculture, injection in rat cortex		α-syn endocytosis and transfer occur in a dynamin-dependent manner	(Hansen et al., 2011)
Monomeric α-syn	siRNA knockdown of dynamin, inhibition of dynamin GTPase activity by sertraline	24 h	Rab5A and LAMP1	Synuclein endocytosis was decreased by inhibiting dynamin GTPases	(Konno et al., 2012)
Tau and α-syn fibrils, TAT	Inhibition of tau uptake via Cytochalasin, Latrunculin, Rottlerin, Amiloride. Tau uptake was not inhibited by Dynasore. α-syn uptake was inhibited by heparin and chlorate	3 and 5 h		When administered together, tau, TAT, and α-syn colocalize, suggesting α-syn fibrils are endocytosed via macropinocytosis. Tau fibrils did not colocalize with the Clathrin antibody.	(Holmes et al., 2013)
Monomer, oligomer, fibril	Dynasore	0,3,6,12,24 h		Dynasore inhibited synuclein uptake in a concentration-dependent manner	(Reyes et al., 2014)
Transfection: α-syn expression	Dynasore, Pitstop 2,		EEA1, NR1, NR2A	Clathrin-mediated internalization of α-syn	(Oh et al., 2016)

Fibril	EIPA			α-syn induced membrane ruffling, but EIPA, a macropinocytic inhibitor, did not inhibit its internalization	(Zeineddine et al., 2015)
Fibrils	Dynamin 1 dominant negative	1 h	LAMP1	Dynamin is partially required for the uptake, but not the intercellular transfer of α-syn fibrils.	(Abounit et al., 2016)
Fibrils and phospho-fibrils	Dynasore	20 min		Inhibition of Clathrin-mediated endocytosis through Dynasore; decreased uptake of fibrils	(Samuel et al., 2016)
Fibrils	LAG3 KO, LAG3 antibodies	5, 10, 20 min and more	Rab5, Rab7, LAMP1	LAG3 mediated endocytosis of α-syn PFF, which then undergoes receptor-mediated endocytosis	(Mao et al., 2016)
Fibrils	chloroquine	3,15,60 min and longer	Endolysosomal pathway, LAMP1 staining	PFF is transported through the endolysosomal pathway	(Karpowicz et al., 2017)
Fibrils		4 and 24 h		Amyloid fibrils depend on Heparan sulfate for internalization	(Ihse et al., 2017)
Monomer and fibril	Dyngo, Pitstop	24 h	Endosomal maturation, and finally, lysosomes	α-syn monomers use dynamin-mediated endocytosis, colocalize with Rab4, 5, and 7, and trafficking through the endosomal system. α-syn fibrils undertake a different pathway	(Masaracchia et al., 2018)
Monomer, oligomer, and fibril		24 h	Colocalization with endolysosomal markers	Clathrin-mediated endocytosis of α-syn colocalization of synuclein and transferrin	(Hoffmann et al., 2019)
Monomer and fibril	Dynasore, caveolin-1 siRNA,	48 h		Caveolae-dependent uptake of α-syn in dopaminergic neurons	(Kawahata et al., 2021)
Various oligomers (varying sizes)	Pitstop	2 h	Rab5 and LAMP-1	Larger oligomers are more dependent on Clathrin-mediated endocytosis, colocalization with early endosomes and lysosomes	(Shearer et al., 2021)

3.8 Materials and methods

REAGENT or RESOURCE	SOURCE	IDENTIFIER
Antibodies		
LAMP1 (IF)	Cell Signaling	Cat# 9091S
LAMP1 (IP)	Cell Signaling	Cat# 15665
EEA1	BD Biosciences	Cat# 610457
Rab4	Abcam	Cat# ab109009
Rab5 (IF)	Abcam	Cat# ab18211
Rab8	Abcam	Cat# ab188574
Rab9	Abcam	Cat# ab179815
Clathrin heavy chain	Abcam	Cat# ab21679
Rab5 (for WB and IP)	Cell Signaling	Cat# 3547S
GFAP	Invitrogen	Cat# PAS3-16727
MAP2	Abcam	Cat# ab5392
TH	Millipore Sigma	Cat# AB9702

Beta-III Tubulin	Abcam	Cat# ab18207
FOXA2	Abcam	Cat# ab108422
LRRK2	Abcam	Cat# ab133474
LAMP2	Abcam	Cat# ab25631
HSC70	Invitrogen	Cat# PA5-27337
HSP90	Invitrogen	Cat# MA1-10372
GM130	Invitrogen	Cat# PA1-077
CD63	Abcam	Cat# ab1318
HA-Tag	Cell Signaling	Cat# 2367S
Rab7	Abcam	Cat# ab137029
Alpha-synuclein	Invitrogen	Cat# 32-8100
Rac1	Emd Millipore Corp.	Cat# 16319
Phalloidin	Abcam	Cat# ab176756/ ab176759/ ab176752
Alexa Fluor Secondary Antibody	Invitrogen	Multiple: https://www.thermofisher.com/antibody/secondary/query/alexa
Bacterial and virus strains		
LAMP1: pLenti-III-RFP-C	Applied Biological Materials	Cat# LVP719
Chemicals, peptides, and recombinant proteins		
DMEM high-glucose	GE Healthcare	Cat# SH30081.01
Bovine calf serum	GE Healthcare	Cat# SH30072.03
L-glutamate	Wisent	Cat# 609065
Pen/Strep	Wisent	Cat# 450201
DynaMag-2	Invitrogen	Cat# 12321D
anti-HA magnetic beads	Thermo Fisher Scientific	Cat# 88836
Hoechst	Invitrogen	Cat# H3570
DAPI	Invitrogen	Cat# D1306
DRAQ7	Abcam	Cat# ab109202
Latrunculin A	Cayman Chemical	Cat# 10010630
Latrunculin B	Abcam	Cat# ab144920
Ethylisopropylamiloride	Tocris	Cat# 3378
384 well plates	Corning	Cat# 353962
Neomycin	Gibco	LS21810031
Nunc 8-well plate (Permanox)	Lab-Tek	Cat# 177445
Paraformaldehyde	Thermo Fisher Scientific	Cat# A1131322
Triton X-100	Sigma Aldrich	Cat# X100-1L
Phosphate-buffered saline	Wisent	Cat# 311-010-CL
Bovine Serum Albumin	Wisent	Cat# 800-095
Poly-L-Lysine	Sigma Aldrich	Cat# A-005-M

Lysosomal Staining Reagent - Orange - Cytopainter	Abcam	Cat# ab176827
35 mm glass-bottom dish	MatTek	Cat# P35G-1.5-14-C-GRD
Lipofectamine 3000	Invitrogen	Cat# L3000015
Lysotracker Red DND-99	Invitrogen	Cat# L7528
Manumycin A	Cayman Chemical	Cat# 10010497
FluoSpheres	Invitrogen	Cat# F13082
Trypsin	Wisent	Cat# 325-052-EL
Fluorescence Mounting Medium	Dako, Agilent	Cat# S3023
Dextran 10,000 MW	Thermo Fisher Scientific	D1817
Dextran 70,000 MW	Thermo Fisher Scientific	D1818
Dextran 2,000,000 MW	Thermo Fisher Scientific	D7139
Transferrin	Invitrogen	Cat# T13342
Epidermal Growth Factor	Invitrogen	Cat# E13345
Glutaraldehyde 2.5% in Sodium Cacodylate Buffer	Electron Microscopy Sciences	Cat# 1653715
Matrigel	Corning	354277
mTeSR1 medium	STEMCELL Technologies	Cat# 85857
StemPro Accutase	Thermo Fisher Scientific	Cat# A1110501
DMEM/F12	Thermo Fisher Scientific	Cat# A4192001
N2 Supplement	Thermo Fisher Scientific	Cat# 17502001
B27 Supplement	Thermo Fisher Scientific	Cat# 17504044
Brainphys Neuronal medium	STEMCELL Technologies	Cat# 05790
Neurocult SM1 Neuronal Supplement	STEMCELL Technologies	Cat# 05711
N2A Supplement A	STEMCELL Technologies	Cat# 07152
BDNF	Peprotech	Cat# 450-02
laminin	Sigma Aldrich	Cat# L2020
Ascorbic acid	Sigma Aldrich	Cat# A5960
db-cAMP	Carbosynth	Cat# ND07996
Compound E	STEMCELL Technologies	Cat# 73954
Carbon-covered grids	Electron Microscopy Sciences	Cat# FCF400CU50
5 nm gold beads	Cytodiagnostics	Cat# CGN5K-5-2

Trypan Blue Solution, 0.4%	Gibco	Cat# 15250061
Critical commercial assays		
Mycoplasma detection kit	Biotool	Cat# B39038
Cytotune reprogramming kit	Thermo Fisher Scientific	Cat# A34546
Deposited data		
Raw data and analysis	This paper	doi:10.17632/nh3cvm3m3p.1
Experimental models: Cell lines		
HeLa	ATCC	Cat# CRM-CCL-2
U-2 OS	ATCC	HTB-96
U-87	ATCC	HTB-14
U-343	ATCC	Discontinued
RAW 264.7	ATCC	TIB-71
U-251	Sigma Aldrich	09063001
Human Fetal Astrocyte	Cell Applications	882AK-05f
Human Adult Astrocyte	Cell Applications	882AK-05a
AIW002-2	Neuro's C-BIG Biorepository	https://www.mcgill.ca/neuro/files/neuro/aiw002-02-datasheet.pdf
Oligonucleotides		
ON-TARGETplus Human CLTC siRNA	Horizon Dharmacon	L-004001-01-0010
Recombinant DNA		
EBFP2-Lysosomes-20	Michael Davidson, Unpublished	Addgene plasmid# 55246
tdTurboRFP-Lysosomes-20	Michael Davidson, Unpublished	Addgene plasmid# 58061
pLJM1-Tmem192-mRFP-3xHA	(Lim et al., 2019)	Addgene plasmid# 134631
pLJC5-Tmem192-3xHA	(Abu-Remaileh et al., 2017)	Addgene plasmid # 102930
CD63-pEGFP C2	Paul Luzio, Unpublished	Addgene plasmid# 62964
Software and algorithms		
ImageJ	(Schneider et al., 2012)	https://imagej.nih.gov/ij/
LAS X 3.5.5	Leica	https://www.leica-microsystems.com/products/microscope-software/p/leica-las-x-ls/
Prism	Gaphpad	https://www.graphpad.com/scientific-software/prism/

ZEN 3.5	Zeiss	https://www.zeiss.com/microscopy/int/products/microscope-software/zen.html
GMS 3	Gatan	https://www.gatan.com/products/tem-analysis/gatan-microscopy-suite-software

RESOURCE AVAILABILITY

Lead Contact

Further information and requests for resources and reagents should be directed to the Lead Contact, Dr. Peter Scott McPherson (peter.mcpherson@mcgill.ca) and will be fulfilled.

Materials Availability

This study did not generate new unique reagents.

Data and Code Availability

All the raw data, along with statistical calculations used in this paper have been deposited at Mendeley Data. and is publicly available as of the date of publication. DOIs are listed in the key resources table. This paper does not report original code. Any additional information required to reanalyze the data reported in this paper is available from the lead contact upon request.

EXPERIMENTAL MODELS AND SUBJECT DETAILS

Cell lines

HeLa, U2OS, U87, U-343, RAW 264.7 were obtained from American Type Culture Collection (Cat# CRM-CCL-2, HTB-96, HTB-14, discontinued, TIB-71, respectively). U-251 cells were obtained from Sigma (Cat# 09063001). Human fetal and adult astrocytes were obtained from Cell Applications (Cat# 882AK-05f and 882AK-05a, respectively). For studies with iPSCs, we used the line AIW002-2 obtained from the Neuro's C-BIG Biorepository. This line was reprogrammed from peripheral blood mononuclear cells of a healthy donor with the Cytotune reprogramming kit

(Thermo Fisher, Cat# A34546). The process of reprogramming and quality control profiling for this iPSC was outlined in a previous study (Chen et al., 2021). The use of iPSCs in this project is approved by the McGill University Health Centre Research Ethics Board (DURCAN_IPSC / 2019-5374).

All cells were cultured in DMEM high-glucose (GE Healthcare, Cat# SH30081.01) containing 10% bovine calf serum (GE Healthcare, Cat# SH30072.03), 2 mM L-glutamate (Wisent, Cat# 609065, 100 IU penicillin and 100 μg/ml streptomycin (Wisent cat# 450201). Cell lines were routinely checked for mycoplasma contamination using the mycoplasma detection kit (Biotool cat# B39038).

Production, Characterization, and Nanogold labeling of PFF

Production and characterization of recombinant α-syn monomers and PFFs have been described previously (Del Cid Pellitero et al., 2019; Maneca et al., 2019). Both electron microscopy and dynamic light scattering were used for the characterization of α-syn monomers and PFFs (Supplementary Figure 3.1 A-B). Previously characterized PFF, was then conjugated with 5 nm gold beads (Cytodiagnostics, Cat# CGN5K-5-2), immediately before experimental use. Cytodianostic's conjugation protocol was optimized to conjugate gold onto PFF. Following conjugation, some PFF was collected for characterization on carbon-covered grids (Electron Microscopy Sciences, Cat# FCF400CU50) (Supplementary Figure 3.1 C).

IPSC Culturing

AIW002-2 hiPSC cultures were maintained as feeder-free cultures following the protocol described previously (Chen et al., 2021). AIW002-2 hiPSCs were plated onto Matrigel (Corning,

Cat# 354277)-coated plates containing mTeSR1 medium (STEMCELL Technologies, Cat# 85857). The culture medium was changed daily until cells reached ~80% or required confluency (usually 5-7 days after plating). The cells were then passaged, frozen, or differentiated. A previously described protocol was used to generate ventral midbrain dopaminergic neural progenitor cells (Jefri et al., 2020). Dopaminergic neural progenitor cells were dissociated with StemPro Accutase Cell Dissociation Reagent (Thermo Fisher, Cat# A1110501) into single-cell suspensions. 50,000 cells were plated onto coated coverslips in 24-well plates with neural progenitor plating medium (DMEM/F12 supplemented with N2, B27 supplement; Thermo Fisher, Cat# A4192001, 17502001, 17504044). To further differentiate into dopaminergic neurons, neural progenitor medium was switched to dopaminergic neural differentiation medium (Brainphys Neuronal medium, STEMCELL Technologies, Cat# 05790) supplemented with N2A Supplement A (STEMCELL Technologies; Cat# 07152), Neurocult SM1 Neuronal Supplement (STEMCELL Technologies; Cat# 05711), BDNF (20 ng/mL; Peprotech, Cat# 450-02), GDNF (20 ng/mL; Peprotech, Cat# 450-10), Compound E (0.1 μM; STEMCELL Technologies, Cat# 73954), db-cAMP (0.5 mM; Carbosynth, Cat# ND07996), Ascorbic acid (200 μM; Sigma Aldrich, Cat# A5960) and laminin (1 μg/mL, Sigma Aldrich, Cat# L2020).

Plasmids and lentivirus

EBFP2-Lysosomes-20, tdTurboRFP-Lysosomes-20 were gifts from Michael Davidson (Addgene plasmid# 55246 and 58061). pLJM1-Tmem192-mRFP-3xHA was a gift from Roberto Zoncu (Addgene, plasmid# 134631). pLJC5-Tmem192-3xHA was a gift from David Sabatini (Addgene plasmid # 102930). CD63-pEGFP C2 was a gift from Paul Luzio (Addgene, Cat# 62964). LAMP1-RFP lentivirus was obtained from Applied Biological Materials Inc. (Cat# LVP719).

Trypan Blue Exclusion Assay

HeLa (ATCC, Cat# CRM-CCL-2) cells were grown on poly-L-lysine coated 35 mm glass-bottom dishes (MatTek, Cat# P35G-1.5-14-C-GRD) for 48 h to 50% confluency. When ready for imaging, cells were stained with Hoechst (Invitrogen, Cat# H3570) for 30 min and dishes were placed in the pre-heated live imaging chamber of the Zeiss LSM-880 confocal microscope. Imaging was commenced before the addition of PFF tagged with Alexa Fluor 488 (PFF488) at a speed of 1 frame/sec. PFF was added during live imaging.

PFF Live Internalization Assay

U2OS (ATCC, HTB-96) cells were grown on Poly-L-Lysine (Sigma Aldrich, Cat# A-005-M) coated 35 mm glass-bottom dish (MatTek, Cat# P35G-1.5-14-C-GRD) for 72 h to 70% confluency. Before imaging, cells were stained with Lysosomal Cytopainter (Abcam, Cat# ab176827) for 30min. Dishes were placed in the pre-heated live imaging chamber of the Zeiss LSM-880 confocal microscope. Imaging was commenced before the addition of PFF at a speed of 1 frame/sec using the Airy imaging mode for higher resolution (~1.3x resolution of conventional confocal microscopy). PFF488 was added during imaging.

Live MVB Assay

These live experiments were carried out the same way as above. For the hollow lysosome morphology, the “Find Edges” processing was used on ImageJ (NIH, https://imagej.net/software/fiji/).

Lysosomal Staining in Fixed Samples

Lysosomal staining was achieved in one of the following ways: transfection with plasmids stated above with the aid of Lipofectamine 3000 (Thermo Fisher, Invitrogen, Cat# L3000015), fixable Lysotracker (Thermo Fisher, Invitrogen, Cat# L7528) for staining of lysosomes in neurons and neural progenitor cells, or with the use of LAMP1 antibody (Cell Signaling, Cat# 9091S). Transfection was done 24 h prior to experimentation. Staining with Lysotracker was done 30 min before experimentation. LAMP1 antibody staining was done following fixation and permeabilization.

PFF Endocytosis Assays

Cells mounted on coverslips were plated in 24 well plates at 37°C with 200 µl of media in each well. Immediately prior to experimentation, cells were taken out of incubators and placed in the cell culture hood. PFF aliquots were then removed from dry ice, diluted with serum-free media, and added to each well. Cells were then incubated at 37°C for 0, 2, 10, 30, or longer. Cells were then placed on ice and washed with trypsin (Wisent, Cat# 325-052-EL) for 90 sec (to remove extracellular PFF). Following 2 washes with PBS (Wisent, Cat# 311-010-CL), cells were fixed. In experiments where trypsin was not used, cells were washed three times with PBS and fixed. In experiments using iPSC neurons, trypsinization was avoided and only PBS was used to wash cells. Same protocol was followed for samples prepared for EM, except for plating cells on Nunc 8-well dishes (Lab-Tek, Nunc, Thermo Scientific, Cat# 177445) and fixation with Glutaraldehyde and not PFA.

PFF Long-term Endocytosis Assays

Cell plating and culturing was done as described above. Cells were then incubated at 37°C for 24 h. Following 24 h, cells were trypsin washed three times, pelleted, resuspended and re-plated onto fresh coverslips. For iPSC neurons, trypsinization (Wisent, Cat# 325-052-EL) and re-plating was avoided and only the media was changed at 24 h. Cells were then incubated for varying amount time afterwards. Prior to imaging, sample fixation and mounting were conducted as above.

For quantifying the PFF fluorescence over 14 d, the same protocol as above was employed; however, in order to control for cell growth, human adult astrocytes (Cell Applications, Cat# 882AK-05a) at passage 7 were used as these cells have a very slow doubling time. This allowed us to control for growth without needing to inhibit cell replication through treatment with chemicals that could have a negative effect on PFF uptake, fluorescence, or retention.

Macropinocytic Inhibitors

Ethylisopropylamiloride (EIPA; R&D Systems, Tocris, Cat# 3378), Latrunculin A (LatA; Cayman Chemical, Cat# 10010630), and Latrunculin B (LatB, respectively; Abcam, Cat# ab144920, ab144291) were the macropinocytic inhibitors used in this study. Cells normally incubated in media with serum were washed 3 times with serum-free media to remove any remaining serum. Serum-free media was added with a final concentration of 20 μM of EIPA, 0-2 μM of LatA, 5 μM of LatB. Cells were then incubated at 37°C for 30 min before experimentation for EIPA and LatB, and 1 h for LatA. Due to the autofluorescence of EIPA, DRAQ7 (Abcam, Cat# ab109202) was used to stain cell nuclei.

LatA Inhibition in Dopaminergic NPCs

Dopaminergic NPCs were seeded in polyornithine/ laminin coated 384 well plates (Corning, Cat# 353962) at 4000cells/ well. After 24 h Latrunculin A (LatA; Cayman Chemical, Cat# 10010630) was added. After 1 h, Alexa488-PFF was added. After another 24 h incubation period, the wells were washed twice with PBS (Wisent, Cat# 311-010-CL) and the cells fixed with 2% FA/PBS. Cells were counterstained with Hoechst 33342 (Thermo Fisher, Cat# H3570) and imaged on a high content imager (CellInsight CX7, Thermo Fisher Scientific). The amount of intracellular Alexa488-PFF was measured as the total intensity of Alexa488 fluorescent stain in the perinuclear area. Nuclei count and nuclear area (px^2) were also obtained as indicators for cell toxicity. All data was normalized against DMSO (vehicle) only controls. Data represents the mean and standard deviation of 3 independent experiments.

Lysosomal Immunoprecipitation

U2OS cells expressing 3xHA-TMEM192-RFP were incubated with PFF for varying lengths of time, washed with trypsin (Wisent, Cat# 325-052-EL) three times to remove extracellular PFF, and then trypsinized and pelleted. Lysosomes were immunoprecipitated based on the protocol described in Abu-Remaileh et al. (2018). Briefly, cells were washed twice with KPBS and centrifuged at 4°C for 2 minutes at 1000 x g. Pelleted cells were resuspended in lysis buffer (20 mM HEPES pH 7.4, 100 mM NaCl, and protease and phosphatase inhibitor cocktail) and manually homogenized with 25 up and down strokes. Homogenates were centrifuged for 2 min at 4°C at 1000 x g and 10% of the total volume for each IP was reserved for starting material (SM) fractions. Homogenates were incubated with gentle rocking at 4°C for 3 minutes with 100 µL anti-HA magnetic beads (Thermo Fisher, Thermo Scientific, Cat# 88836) pre-washed with KPBS. After collecting the total IP volume for the unbound materials (UM), immunoprecipitates were

washed three times with KPBS using a DynaMag-2 Magnet (Thermo Fisher, Invitrogen, Cat# 12321D) before resuspension in 1X SDS-PAGE sample buffer. Protein aliquots were then analyzed by SDS-PAGE and Immunoblot.

For samples to be processed via confocal microscopy, 20 µL pre-washed anti-HA beads were used in the IP and were resuspended using PFA. The sample was then pelleted and resuspended with PBS (Wisent, Cat# 311-010-CL) and mounted onto slides.

PFF Intercellular (with contact) Transfer Assay

U2OS cells were transfected with CD63-EGFP or LAMP1-tdTurboRFP using Lipofectamine 3000 transfection reagent and incubated for 24 h. Cell media was then changed, and cell selection process was initiated through the addition of Neomycin (Gibco Cat# LS21810031). U2OS cells stably expressing CD63-GFP were exposed to PFF or PBS (vehicle control) for 24 h. CD63-GFP (donor cells) were then trypsin washed three times, pelleted, trypsinized again, pelleted and PBS washed, prior to being co-plated with acceptor cells (PFF naïve cells stably expressing LAMP1-tdTurboRFP). Donor and Acceptor cells were then incubated for 12 or 24 h. Half of the 24 h sample were given Manumycin A (MA; Cayman Chemical, Cat# 10010497) at 1.2 µM while the other half was given DMSO (vehicle control) at the time of plating. Cells were then fixed, mounted, and imaged.

PFF Intercellular (without contact) Transfer Assay

U2OS cells were stably expressing with CD63-EGFP, the cells were exposed to PFF, for 24 h then trypsin washed three times and re-plated prior to the addition of serum-free media. The media was collected following 36 h of incubation at 37°C and given to naïve U2OS cells. Some of

the cells given this media were exposed to EIPA while others were given DMSO as a vehicle control. For fluorescent microscopy samples, the naïve cells were plated on coverslips, while for samples to be examined with EM, naïve cells were plated on Nunc 8-well plates (Lab-Tek, Nunc, Thermo Scientific, Cat# 177445).

Fixation and Antibody Staining Following PFF Uptake

Fixation was done with 2% freshly made paraformaldehyde (PFA; Thermo Fisher Scientific, A1131322) for 10-15 min on ice. In experiments where antibody staining was done, cells were then blocked and permeabilized for 30 min using 0.05% Triton X-100 (Sigma, Cat# X100-1L) in Phosphate-buffered saline (PBS; Wisent, Cat# 311-010-CL) along with 5% BSA (Wisent, Cat# 800-095). Coverslips were then transferred into a wet chamber and incubated with 1:500 dilution of the antibody in 0.01% Triton X-100 and 5% BSA. Cells were incubated with the diluted antibody for 2 h at room temperature. Coverslips were then gently washed 3 times with PBS, and 1:500 dilution of secondary antibody was added in 0.01% Triton X-100 and 5% BSA. Cells were then washed 2 more times with PBS and stained with DAPI (Thermo Fisher, Invitrogen, Cat# D1306) for 10 min at 1 μg/ml concentration. Coverslips were then mounted on a glass slide using Fluorescence Mounting Medium (Dako, Agilent, Cat#S3023). All fixed samples were then imaged using a Leica TCS SP8 confocal microscope. STED samples were imaged using Abberior STED super-resolution nanoscope.

CHC Knockdown

U2OS cells at 60% confluency were transfected with siRNA retrieved from Dharmacon (SMARTpool, ONTARGETplus, see KRT) or control siRNA (Dharmacon; ON-TARGETplus

CONTROL) using Lipofectamine 3000 (Thermo Fisher, Invitrogen, Cat# L3000015). At 24 h following transfection, cells were passaged, with some cells retrieved for imaging experiments and mounted onto coverslips. At 48 h, cells were collected in HEPES lysis buffer (20 mM HEPES, 150 mM sodium chloride, 1% Triton X-100, pH 7.4) accompanied with protease inhibitors. Cells in lysis buffer were then placed at 4°C and gently rocked for 30 min. Lysates were then spun at 238,700 x g for 15 min at 4°C. Lysates were run on 5-16% gradient polyacrylamide gel and transferred onto nitrocellulose membranes. Subsequently, proteins were visualized using Ponceau staining. Blots were then blocked with 5% milk for 1 h. Antibodies were then incubated overnight at 4% in bovine serum albumin/TBS/0.1 Tween 20. The secondary antibody was incubated at 1:2500 dilution in 5% milk/TBS/0.1 Tween 20 for 1 h at room temperature. Concurrently, cells mounted onto coverslips underwent the endocytosis assay with both knockdown and control cells mounted onto the same coverslips.

FluoSpheres and Dextran Uptake Assays

RAW 264.7 cells (ATCC, Cat# TIB-71) were plated onto coverslips treated with Poly-L-Lysine (Sigma, Cat# A-005-M). FluoSpheres (Thermo Fisher, Invitrogen, Cat# F13082), latex beads with 1 μm diameter, and orange fluorescence were incubated with PFF. Cells were then washed with trypsin (Wisent, Cat# 325-052-EL), washed twice with PFF, and fixed. Cells were then counterstained with DAPI prior to mounting using Fluorescence Mounting Medium (Dako, Agilent, Cat#S3023).

U2OS cells were used in the dextran and PFF uptake experiment. U2OS cells were plated and prepared as described above. Three different dextran (10,000 MW, 70,000 MW, 2,000,000 MW; Thermo Fisher, Cat# D1817, D1818, D7139) were added to cells alongside PFF.

Membrane Ruffling Assay

Cellular response to PFF addition was done using human fetal astrocytes (Cell Applications, 882AK-05f). Cells were treated with PFF, and their recruitment of Rac1 (Emd Millipore Corporation, Cat# 16319) to the cell surface and colocalization with F-actin (Phalloidin; Abcam, Cat# A22287) was analyzed. For negative and positive control, Transferrin (Tf; Thermo Fisher, Invitrogen, Cat# T13342) Epidermal growth factor (EGF; Thermo Fisher, Invitrogen, Cat# E13345) were added to cells, respectively. A null condition was also in place, where cells were administered PBS (a vehicle control for PFF).

Exosomal Isolation

For exosomal isolation, a previously published protocol was followed (Chhoy et al., 2021). Following isolation, samples were prepared for immunoblotting and EM. For immunoblotting, a portion of exosomes retrieved from PFF treated cells were treated with trypsin for 5 min. The exosomes were then re-pelleted at 10,000 g's, and the supernatant removed. These trypsinized exosomes were run alongside exosomes collected from PBS and PFF treated cells, to compare PFF content.

TEM

Human astrocytes and U2OS cells were plated onto 8 well chamber slides (Lab-Tek, Nunc, Thermo Scientific, Cat# 177445) and were administered PFF conjugated with gold. Cells were then fixed with glutaraldehyde 2.5% in 0.1M sodium cacodylate buffer (Electron Microscopy, Cat# 1653715), post-fixed with 1% OsO_4 and 1.5% potassium ferrocyanide in sodium cacodylate buffer.

Cells were then *en bloc* stained with 4% uranyl acetate. Post-embedding, some grids were stained with uranyl acetate for enhanced membrane staining. Samples were viewed with a Tecnai Spirit 120 kV electron microscope and captured using a Gatan Ultrascan 4000 camera.

Graphical Abstract

Created with BioRender.com

QUANTIFICATION AND STATISTICAL ANALYSIS

Colocalization Analysis

Colocalization analysis was conducted using JACoP plugin (Bolte & Cordelieres, 2006) in ImageJ (imagej.net). This plugin was used to calculate the Manders' Colocalization Coefficients (MCC) as performed previously. Unlike Pearson's correlation coefficient, MCC provides a direct measure colocalization: the ratio of with which one probe co-occurs with a second probe (Dunn et al., 2011), hence we found it to be the most appropriate measure of colocalization for our study. Due to the sensitivity of MCC to background noise, a 20% threshold was used for all colocalization analysis to minimize the effect of fluorescent noise and bleed-through on our colocalization analysis. M_1 coefficient represents the ratio of the sum of pixel intensities in probe 1 for which probe 2 has an intensity above zero compared to the total intensity of probe 1. M_2 represents the same concept for probe 2. For consistency, M_1 and M_2 were calculated so that M_1 would always represent the ratio to which lysosomes (LAMP1/Lysotracker) colocalize with PFF (i.e., the portion of lysosomes that contain PFF) while M_2 always represents the ratio in which PFF colocalizes with lysosomes (i.e., the portion of PFF that colocalize with lysosomes). In

experiments where different markers or cargo were used alongside PFF, M_2 still represents the degree in which PFF colocalizes to the other probe.

Quantification and Statistics

For all quantifications, including uptake and colocalization, the Leica LAS X and ImageJ (imagej.net) software were used. Readout from ImageJ for signal intensity and colocalization (using the JACoP plugin) was then used to tabulate results. In each experiment, images were selected from a large field imaged at low quality using the Leica SP8 spiral scan. From the large field, regions were selected that contained a minimum of 4 cells. Graphs were then prepared using GraphPad Prism 9 software. For statistical comparisons, two-sample *t*-test and one-way ANOVA were used. When significance was detected under ANOVA, multiple comparisons Tukey's test was conducted to find significant differences across means. All data is shown as mean ± SD, with only a few exceptions. For statistical significance, $p < 0.05$ was used.

3.9 References

Abounit, S., Bousset, L., Loria, F., Zhu, S., de Chaumont, F., Pieri, L., Olivo-Marin, J. C., Melki, R., & Zurzolo, C. (2016). Tunneling nanotubes spread fibrillar alpha-synuclein by intercellular trafficking of lysosomes. *EMBO J*, *35*(19), 2120-2138. https://doi.org/10.15252/embj.201593411

Abu-Remaileh, M., Wyant, G. A., Kim, C., Laqtom, N. N., Abbasi, M., Chan, S. H., Freinkman, E., & Sabatini, D. M. (2017). Lysosomal metabolomics reveals V-ATPase- and mTOR-dependent regulation of amino acid efflux from lysosomes. *Science*, *358*(6364), 807-813. https://doi.org/10.1126/science.aan6298

Alam, P., Bousset, L., Melki, R., & Otzen, D. E. (2019). alpha-synuclein oligomers and fibrils: a spectrum of species, a spectrum of toxicities. *J Neurochem*, *150*(5), 522-534. https://doi.org/10.1111/jnc.14808

Arias, R. L., Sung, M. L., Vasylyev, D., Zhang, M. Y., Albinson, K., Kubek, K., Kagan, N., Beyer, C., Lin, Q., Dwyer, J. M., Zaleska, M. M., Bowlby, M. R., Dunlop, J., & Monaghan, M. (2008). Amiloride is neuroprotective in an MPTP model of Parkinson's disease. *Neurobiol Dis*, *31*(3), 334-341. https://doi.org/10.1016/j.nbd.2008.05.008

Bayati, A., Kumar, R., Francis, V., & McPherson, P. S. (2021). SARS-CoV-2 infects cells following viral entry via clathrin-mediated endocytosis. *J Biol Chem*, 100306. https://doi.org/10.1016/j.jbc.2021.100306

Betemps, D., Verchere, J., Brot, S., Morignat, E., Bousset, L., Gaillard, D., Lakhdar, L., Melki, R., & Baron, T. (2014). Alpha-synuclein spreading in M83 mice brain revealed by detection of pathological alpha-synuclein by enhanced ELISA. *Acta Neuropathol Commun*, *2*, 29. https://doi.org/10.1186/2051-5960-2-29

Bieri, G., Gitler, A. D., & Brahic, M. (2018). Internalization, axonal transport and release of fibrillar forms of alpha-synuclein. *Neurobiol Dis*, *109*(Pt B), 219-225. https://doi.org/10.1016/j.nbd.2017.03.007

Bolte, S., & Cordelieres, F. P. (2006). A guided tour into subcellular colocalization analysis in light microscopy. *J Microsc*, *224*(Pt 3), 213-232. https://doi.org/10.1111/j.1365-2818.2006.01706.x

Bousset, L., Pieri, L., Ruiz-Arlandis, G., Gath, J., Jensen, P. H., Habenstein, B., Madiona, K., Olieric, V., Bockmann, A., Meier, B. H., & Melki, R. (2013). Structural and functional characterization of two alpha-synuclein strains. *Nat Commun*, *4*, 2575. https://doi.org/10.1038/ncomms3575

Braak, H., Tredici, K. D., Rüb, U., de Vos, R. A. I., Jansen Steur, E. N. H., & Braak, E. (2003). Staging of brain pathology related to sporadic Parkinson's disease. *Neurobiology of Aging*, *24*(2), 197-211. https://doi.org/10.1016/s0197-4580(02)00065-9

Bryant, D. M., Kerr, M. C., Hammond, L. A., Joseph, S. R., Mostov, K. E., Teasdale, R. D., & Stow, J. L. (2007). EGF induces macropinocytosis and SNX1-modulated recycling of E-cadherin. *J Cell Sci*, *120*(Pt 10), 1818-1828. https://doi.org/10.1242/jcs.000653

Chen, C. X.-Q., Abdian, N., Maussion, G., Thomas, R. A., Demirova, I., Cai, E., Tabatabaei, M., Beitel, L. K., Karamchandani, J., Fon, E. A., & Durcan, T. M. (2021). Standardized quality control workflow to evaluate the reproducibility and differentiation potential of human iPSCs into neurons. *bioRxiv*, 2021.2001.2013.426620. https://doi.org/10.1101/2021.01.13.426620

Chhoy, P., Brown, C. W., Amante, J. J., & Mercurio, A. M. (2021). Protocol for the separation of extracellular vesicles by ultracentrifugation from in vitro cell culture models. *STAR Protoc*, *2*(1), 100303. https://doi.org/10.1016/j.xpro.2021.100303

Commisso, C., Flinn, R. J., & Bar-Sagi, D. (2014). Determining the macropinocytic index of cells through a quantitative image-based assay. *Nat Protoc*, *9*(1), 182-192. https://doi.org/10.1038/nprot.2014.004

Condon, N. D., Heddleston, J. M., Chew, T. L., Luo, L., McPherson, P. S., Ioannou, M. S., Hodgson, L., Stow, J. L., & Wall, A. A. (2018). Macropinosome formation by tent pole ruffling in macrophages. *J Cell Biol*, *217*(11), 3873-3885. https://doi.org/10.1083/jcb.201804137

Conway, K. A., Harper, J. D., & Lansbury, P. T. (1998). Accelerated in vitro fibril formation by a mutant alpha-synuclein linked to early-onset Parkinson disease. *Nat Med*, *4*(11), 1318-1320. https://doi.org/10.1038/3311

Cox, D., Chang, P., Zhang, Q., Reddy, P. G., Bokoch, G. M., & Greenberg, S. (1997). Requirements for both Rac1 and Cdc42 in membrane ruffling and phagocytosis in leukocytes. *J Exp Med*, *186*(9), 1487-1494. https://doi.org/10.1084/jem.186.9.1487

Danzer, K. M., Haasen, D., Karow, A. R., Moussaud, S., Habeck, M., Giese, A., Kretzschmar, H., Hengerer, B., & Kostka, M. (2007). Different species of alpha-synuclein oligomers induce calcium influx and seeding. *J Neurosci*, *27*(34), 9220-9232. https://doi.org/10.1523/JNEUROSCI.2617-07.2007

Datta, A., Kim, H., Lal, M., McGee, L., Johnson, A., Moustafa, A. A., Jones, J. C., Mondal, D., Ferrer, M., & Abdel-Mageed, A. B. (2017). Manumycin A suppresses exosome biogenesis and secretion via targeted inhibition of Ras/Raf/ERK1/2 signaling and hnRNP H1 in castration-resistant prostate cancer cells. *Cancer Lett*, *408*, 73-81. https://doi.org/10.1016/j.canlet.2017.08.020

Del Cid Pellitero, E., Shlaifer, R., Luo, W., Krahn, A., Nguyen-Renou, E., Manecka, D.-L., Rao, T., Beitel, L., & Durcan, T. M. (2019). Quality Control Characterization of α-Synuclein Preformed Fibrils (PFFs) [Technical Note]. *Zenodo*. https://doi.org/https://doi.org/10.5281/zenodo.3738340

Desplats, P., Lee, H.-J., Bae, E.-J., Patrick, C., Rockenstein, E., Crews, L., Spencer, B., Masliah, E., & Lee, S.-J. (2009). Inclusion formation and neuronal cell death through neuron-to-neuron transmission of α-synuclein. *Proceedings of the National Academy of Sciences*, *106*(31), 13010-13015. https://doi.org/10.1073/pnas.0903691106

Desplats, P., Lee, H. J., Bae, E. J., Patrick, C., Rockenstein, E., Crews, L., Spencer, B., Masliah, E., & Lee, S. J. (2009). Inclusion formation and neuronal cell death through neuron-to-neuron transmission of alpha-synuclein. *Proc Natl Acad Sci U S A*, *106*(31), 13010-13015. https://doi.org/10.1073/pnas.0903691106

Dieriks, B. V., Park, T. I., Fourie, C., Faull, R. L., Dragunow, M., & Curtis, M. A. (2017). alpha-synuclein transfer through tunneling nanotubes occurs in SH-SY5Y cells and primary brain pericytes from Parkinson's disease patients. *Sci Rep*, *7*, 42984. https://doi.org/10.1038/srep42984

Dunn, K. W., Kamocka, M. M., & McDonald, J. H. (2011). A practical guide to evaluating colocalization in biological microscopy. *Am J Physiol Cell Physiol*, *300*(4), C723-742. https://doi.org/10.1152/ajpcell.00462.2010

Emadi, S., Kasturirangan, S., Wang, M. S., Schulz, P., & Sierks, M. R. (2009). Detecting morphologically distinct oligomeric forms of alpha-synuclein. *J Biol Chem*, *284*(17), 11048-11058. https://doi.org/10.1074/jbc.M806559200

Erami, Z., Khalil, B. D., Salloum, G., Yao, Y., LoPiccolo, J., Shymanets, A., Nürnberg, B., Bresnick, A. R., & Backer, J. M. (2017). Rac1-stimulated macropinocytosis enhances Gβγ activation of PI3Kβ. *Biochemical Journal*, *474*(23), 3903-3914.

Fenyi, A., Leclair-Visonneau, L., Clairembault, T., Coron, E., Neunlist, M., Melki, R., Derkinderen, P., & Bousset, L. (2019). Detection of alpha-synuclein aggregates in gastrointestinal biopsies by protein misfolding cyclic amplification. *Neurobiol Dis*, *129*, 38-43. https://doi.org/10.1016/j.nbd.2019.05.002

Fink, A. L. (2006). The Aggregation and Fibrillation of α-Synuclein. *Accounts of Chemical Research*, *39*(9), 628-634. https://doi.org/10.1021/ar050073t

Fortin, D. L., Troyer, M. D., Nakamura, K., Kubo, S., Anthony, M. D., & Edwards, R. H. (2004). Lipid rafts mediate the synaptic localization of alpha-synuclein. *J Neurosci*, *24*(30), 6715-6723. https://doi.org/10.1523/JNEUROSCI.1594-04.2004

Fujiwara, I., Zweifel, M. E., Courtemanche, N., & Pollard, T. D. (2018). Latrunculin A Accelerates Actin Filament Depolymerization in Addition to Sequestering Actin Monomers. *Curr Biol*, *28*(19), 3183-3192 e3182. https://doi.org/10.1016/j.cub.2018.07.082

Furstner, A., De Souza, D., Turet, L., Fenster, M. D., Parra-Rapado, L., Wirtz, C., Mynott, R., & Lehmann, C. W. (2007). Total syntheses of the actin-binding macrolides latrunculin A, B, C, M, S and 16-epi-latrunculin B. *Chemistry*, *13*(1), 115-134. https://doi.org/10.1002/chem.200601135

Galvez, T., Teruel, M. N., Heo, W. D., Jones, J. T., Kim, M. L., Liou, J., Myers, J. W., & Meyer, T. (2007). siRNA screen of the human signaling proteome identifies the PtdIns(3,4,5)P3-mTOR signaling pathway as a primary regulator of transferrin uptake. *Genome Biol*, *8*(7), R142. https://doi.org/10.1186/gb-2007-8-7-r142

Gelpi, E., Navarro-Otano, J., Tolosa, E., Gaig, C., Compta, Y., Rey, M. J., Marti, M. J., Hernandez, I., Valldeoriola, F., Rene, R., & Ribalta, T. (2014). Multiple organ involvement by alpha-synuclein pathology in Lewy body disorders. *Mov Disord*, *29*(8), 1010-1018. https://doi.org/10.1002/mds.25776

Grimmer, S., van Deurs, B., & Sandvig, K. (2002). Membrane ruffling and macropinocytosis in A431 cells require cholesterol. *115*(14), 2953-2962. https://jcs.biologists.org/content/joces/115/14/2953.full.pdf

Grozdanov, V., & Danzer, K. M. (2018). Release and uptake of pathologic alpha-synuclein. *Cell Tissue Res*, *373*(1), 175-182. https://doi.org/10.1007/s00441-017-2775-9

Gu, C., Yaddanapudi, S., Weins, A., Osborn, T., Reiser, J., Pollak, M., Hartwig, J., & Sever, S. (2010). Direct dynamin-actin interactions regulate the actin cytoskeleton. *EMBO J*, *29*(21), 3593-3606. https://doi.org/10.1038/emboj.2010.249

Hansen, C., Angot, E., Bergstrom, A. L., Steiner, J. A., Pieri, L., Paul, G., Outeiro, T. F., Melki, R., Kallunki, P., Fog, K., Li, J. Y., & Brundin, P. (2011). alpha-Synuclein propagates from mouse brain to grafted dopaminergic neurons and seeds aggregation in cultured human cells. *J Clin Invest*, *121*(2), 715-725. https://doi.org/10.1172/JCI43366

Hoffmann, A. C., Minakaki, G., Menges, S., Salvi, R., Savitskiy, S., Kazman, A., Vicente Miranda, H., Mielenz, D., Klucken, J., Winkler, J., & Xiang, W. (2019). Extracellular aggregated alpha synuclein primarily triggers lysosomal dysfunction in neural cells prevented by trehalose. *Sci Rep*, *9*(1), 544. https://doi.org/10.1038/s41598-018-35811-8

Holmes, B. B., DeVos, S. L., Kfoury, N., Li, M., Jacks, R., Yanamandra, K., Ouidja, M. O., Brodsky, F. M., Marasa, J., Bagchi, D. P., Kotzbauer, P. T., Miller, T. M., Papy-Garcia, D., & Diamond, M. I. (2013). Heparan sulfate proteoglycans mediate internalization and propagation of specific proteopathic seeds. *Proc Natl Acad Sci U S A*, *110*(33), E3138-3147. https://doi.org/10.1073/pnas.1301440110

Huotari, J., & Helenius, A. (2011). Endosome maturation. *EMBO J*, *30*(17), 3481-3500. https://doi.org/10.1038/emboj.2011.286

Ihse, E., Yamakado, H., van Wijk, X. M., Lawrence, R., Esko, J. D., & Masliah, E. (2017). Cellular internalization of alpha-synuclein aggregates by cell surface heparan sulfate depends on aggregate conformation and cell type. *Sci Rep*, *7*(1), 9008. https://doi.org/10.1038/s41598-017-08720-5

Jao, C. C., Der-Sarkissian, A., Chen, J., & Langen, R. (2004). Structure of membrane-bound alpha-synuclein studied by site-directed spin labeling. *Proc Natl Acad Sci U S A*, *101*(22), 8331-8336. https://doi.org/10.1073/pnas.0400553101

Jefri, M., Bell, S., Peng, H., Hettige, N., Maussion, G., Soubannier, V., Wu, H., Silveira, H., Theroux, J. F., Moquin, L., Zhang, X., Aouabed, Z., Krishnan, J., O'Leary, L. A., Antonyan, L., Zhang, Y., McCarty, V., Mechawar, N., Gratton, A., . . . Ernst, C. (2020). Stimulation of L-type calcium channels increases tyrosine hydroxylase and dopamine in ventral midbrain cells induced from somatic cells. *Stem Cells Transl Med*, *9*(6), 697-712. https://doi.org/10.1002/sctm.18-0180

Karpowicz, R. J., Jr., Haney, C. M., Mihaila, T. S., Sandler, R. M., Petersson, E. J., & Lee, V. M. (2017). Selective imaging of internalized proteopathic alpha-synuclein seeds in primary neurons reveals mechanistic insight into transmission of synucleinopathies. *J Biol Chem*, *292*(32), 13482-13497. https://doi.org/10.1074/jbc.M117.780296

Kawahata, I., Sekimori, T., Wang, H., Wang, Y., Sasaoka, T., Bousset, L., Melki, R., Mizobata, T., Kawata, Y., & Fukunaga, K. (2021). Dopamine D2 Long Receptors Are Critical for Caveolae-Mediated alpha-Synuclein Uptake in Cultured Dopaminergic Neurons. *Biomedicines*, *9*(1). https://doi.org/10.3390/biomedicines9010049

Kim, M. L., Sorg, I., & Arrieumerlou, C. (2011). Endocytosis-independent function of clathrin heavy chain in the control of basal NF-kappaB activation. *PLoS One*, *6*(2), e17158. https://doi.org/10.1371/journal.pone.0017158

Koivusalo, M., Welch, C., Hayashi, H., Scott, C. C., Kim, M., Alexander, T., Touret, N., Hahn, K. M., & Grinstein, S. (2010). Amiloride inhibits macropinocytosis by lowering submembranous pH and preventing Rac1 and Cdc42 signaling. *J Cell Biol*, *188*(4), 547-563. https://doi.org/10.1083/jcb.200908086

Konno, M., Hasegawa, T., Baba, T., Miura, E., Sugeno, N., Kikuchi, A., Fiesel, F. C., Sasaki, T., Aoki, M., Itoyama, Y., & Takeda, A. (2012). Suppression of dynamin GTPase decreases alpha-synuclein uptake by neuronal and oligodendroglial cells: a potent therapeutic target for synucleinopathy. *Mol Neurodegener*, *7*, 38. https://doi.org/10.1186/1750-1326-7-38

Krueger, E. W., Orth, J. D., Cao, H., & McNiven, M. A. (2003). A dynamin-cortactin-Arp2/3 complex mediates actin reorganization in growth factor-stimulated cells. *Mol Biol Cell*, *14*(3), 1085-1096. https://doi.org/10.1091/mbc.e02-08-0466

Kumar, S. T., Jagannath, S., Francois, C., Vanderstichele, H., Stoops, E., & Lashuel, H. A. (2020). How specific are the conformation-specific alpha-synuclein antibodies? Characterization and validation of 16 alpha-synuclein conformation-specific antibodies using well-characterized preparations of alpha-synuclein monomers, fibrils and oligomers with distinct structures and morphology. *Neurobiol Dis*, *146*, 105086. https://doi.org/10.1016/j.nbd.2020.105086

Lazaro, D. F., Dias, M. C., Carija, A., Navarro, S., Madaleno, C. S., Tenreiro, S., Ventura, S., & Outeiro, T. F. (2016). The effects of the novel A53E alpha-synuclein mutation on its oligomerization and aggregation. *Acta Neuropathol Commun*, *4*(1), 128. https://doi.org/10.1186/s40478-016-0402-8

Lee, H. J., Choi, C., & Lee, S. J. (2002). Membrane-bound alpha-synuclein has a high aggregation propensity and the ability to seed the aggregation of the cytosolic form. *J Biol Chem*, *277*(1), 671-678. https://doi.org/10.1074/jbc.M107045200

Lee, H. J., Suk, J. E., Bae, E. J., Lee, J. H., Paik, S. R., & Lee, S. J. (2008). Assembly-dependent endocytosis and clearance of extracellular alpha-synuclein. *Int J Biochem Cell Biol*, *40*(9), 1835-1849. https://doi.org/10.1016/j.biocel.2008.01.017

Lee, H. J., Suk, J. E., Patrick, C., Bae, E. J., Cho, J. H., Rho, S., Hwang, D., Masliah, E., & Lee, S. J. (2010). Direct transfer of alpha-synuclein from neuron to astroglia causes inflammatory responses in synucleinopathies. *J Biol Chem*, *285*(12), 9262-9272. https://doi.org/10.1074/jbc.M109.081125

Levenson, R., Housman, D., & Cantley, L. (1980). Amiloride Inhibits Murine Erythroleukemia Cell Differentiation: Evidence for a Ca²⁺ Requirement for Commitment. *Proceedings of the National Academy of Sciences of the United States of America*, *77*(10), 5948-5952. http://www.jstor.org/stable/9446

Lewy, F. (1912). *Handbuch der Neurologie*. Julius Springer.

Li, J., Uversky, V. N., & Fink, A. L. (2002). Conformational Behavior of Human α-Synuclein is Modulated by Familial Parkinson's Disease Point Mutations A30P and A53T. *NeuroToxicology*, *23*(4-5), 553-567. https://doi.org/10.1016/s0161-813x(02)00066-9

Li, J. Y., Englund, E., Holton, J. L., Soulet, D., Hagell, P., Lees, A. J., Lashley, T., Quinn, N. P., Rehncrona, S., Bjorklund, A., Widner, H., Revesz, T., Lindvall, O., & Brundin, P. (2008). Lewy bodies in grafted neurons in subjects with Parkinson's disease suggest host-to-graft disease propagation. *Nat Med*, *14*(5), 501-503. https://doi.org/10.1038/nm1746

Li, J. Y., Englund, E., Widner, H., Rehncrona, S., Bjorklund, A., Lindvall, O., & Brundin, P. (2010). Characterization of Lewy body pathology in 12- and 16-year-old intrastriatal mesencephalic grafts surviving in a patient with Parkinson's disease. *Mov Disord*, *25*(8), 1091-1096. https://doi.org/10.1002/mds.23012

Li, L., Wan, T., Wan, M., Liu, B., Cheng, R., & Zhang, R. (2015). The effect of the size of fluorescent dextran on its endocytic pathway. *Cell Biol Int*, *39*(5), 531-539. https://doi.org/10.1002/cbin.10424

Lim, C. Y., Davis, O. B., Shin, H. R., Zhang, J., Berdan, C. A., Jiang, X., Counihan, J. L., Ory, D. S., Nomura, D. K., & Zoncu, R. (2019). ER-lysosome contacts enable cholesterol sensing by mTORC1 and drive aberrant growth signalling in Niemann-Pick type C. *Nat Cell Biol*, *21*(10), 1206-1218. https://doi.org/10.1038/s41556-019-0391-5

Liu, J., Zhou, Y., Wang, Y., Fong, H., Murray, T. M., & Zhang, J. (2007). Identification of proteins involved in microglial endocytosis of alpha-synuclein. *J Proteome Res*, *6*(9), 3614-3627. https://doi.org/10.1021/pr0701512

Luk, K. C., Covell, D. J., Kehm, V. M., Zhang, B., Song, I. Y., Byrne, M. D., Pitkin, R. M., Decker, S. C., Trojanowski, J. Q., & Lee, V. M. (2016). Molecular and Biological Compatibility with Host Alpha-Synuclein Influences Fibril Pathogenicity. *Cell Rep*, *16*(12), 3373-3387. https://doi.org/10.1016/j.celrep.2016.08.053

Luk, K. C., Kehm, V., Carroll, J., Zhang, B., O'Brien, P., Trojanowski, J. Q., & Lee, V. M. (2012). Pathological alpha-synuclein transmission initiates Parkinson-like neurodegeneration in nontransgenic mice. *Science*, *338*(6109), 949-953. https://doi.org/10.1126/science.1227157

Luk, K. C., Song, C., O'Brien, P., Stieber, A., Branch, J. R., Brunden, K. R., Trojanowski, J. Q., & Lee, V. M. (2009). Exogenous alpha-synuclein fibrils seed the formation of Lewy body-like intracellular inclusions in cultured cells. *Proc Natl Acad Sci U S A*, *106*(47), 20051-20056. https://doi.org/10.1073/pnas.0908005106

Madeira, A., Yang, J., Zhang, X., Vikeved, E., Nilsson, A., Andren, P. E., & Svenningsson, P. (2011). Caveolin-1 interacts with alpha-synuclein and mediates toxic actions of cellular alpha-synuclein overexpression. *Neurochem Int*, *59*(2), 280-289. https://doi.org/10.1016/j.neuint.2011.05.017

Maneca, D.-L., Luo, W., Krahn, A., Del Cid Pellitero, E., Shlaifer, I., Beitel, L. K., Rao, T., & Durcan, T. M. (2019). Production of Recombinant α Synuclein Monomers and Preformed Fibrils (PFFs). *Zenodo*. https://doi.org/http://doi.org/10.5281/zenodo.3738335

Manning-Bog, A. B., McCormack, A. L., Li, J., Uversky, V. N., Fink, A. L., & Di Monte, D. A. (2002). The herbicide paraquat causes up-regulation and aggregation of alpha-synuclein in mice: paraquat and alpha-synuclein. *J Biol Chem*, *277*(3), 1641-1644. https://doi.org/10.1074/jbc.C100560200

Mao, X., Ou, M. T., Karuppagounder, S. S., Kam, T. I., Yin, X., Xiong, Y., Ge, P., Umanah, G. E., Brahmachari, S., Shin, J. H., Kang, H. C., Zhang, J., Xu, J., Chen, R., Park, H., Andrabi, S. A., Kang, S. U., Goncalves, R. A., Liang, Y., . . . Dawson, T. M. (2016). Pathological alpha-synuclein transmission initiated by binding lymphocyte-activation gene 3. *Science*, *353*(6307). https://doi.org/10.1126/science.aah3374

Masaracchia, C., Hnida, M., Gerhardt, E., Lopes da Fonseca, T., Villar-Pique, A., Branco, T., Stahlberg, M. A., Dean, C., Fernandez, C. O., Milosevic, I., & Outeiro, T. F. (2018). Membrane binding, internalization, and sorting of alpha-synuclein in the cell. *Acta Neuropathol Commun*, *6*(1), 79. https://doi.org/10.1186/s40478-018-0578-1

Masuda-Suzukake, M., Nonaka, T., Hosokawa, M., Kubo, M., Shimozawa, A., Akiyama, H., & Hasegawa, M. (2014). Pathological alpha-synuclein propagates through neural networks. *Acta Neuropathol Commun*, *2*, 88. https://doi.org/10.1186/s40478-014-0088-8

Masuda-Suzukake, M., Nonaka, T., Hosokawa, M., Oikawa, T., Arai, T., Akiyama, H., Mann, D. M., & Hasegawa, M. (2013). Prion-like spreading of pathological alpha-synuclein in brain. *Brain*, *136*(Pt 4), 1128-1138. https://doi.org/10.1093/brain/awt037

Mayor, S., & Pagano, R. E. (2007). Pathways of clathrin-independent endocytosis. *Nat Rev Mol Cell Biol*, *8*(8), 603-612. https://doi.org/10.1038/nrm2216

Mills, I. G., Jones, A. T., & Clague, M. J. (1998). Involvement of the endosomal autoantigen EEA1 in homotypic fusion of early endosomes. *Current Biology*, *8*(15), 881-884. https://doi.org/10.1016/s0960-9822(07)00351-x

Mine, Y., Shuto, T., Nikawa, H., Kawai, T., Ohara, M., Kawahara, K., Ohta, K., Kukita, T., Terada, Y., & Makihira, S. (2015). Inhibition of RANKL-dependent cellular fusion in pre-osteoclasts by amiloride and a NHE10-specific monoclonal antibody. *Cell Biol Int*, *39*(6), 696-709. https://doi.org/10.1002/cbin.10447

Morton, W. M., Ayscough, K. R., & McLaughlin, P. J. (2000). Latrunculin alters the actin-monomer subunit interface to prevent polymerization. *Nat Cell Biol*, *2*(6), 376-378. https://doi.org/10.1038/35014075

Mougenot, A. L., Nicot, S., Bencsik, A., Morignat, E., Verchere, J., Lakhdar, L., Legastelois, S., & Baron, T. (2012). Prion-like acceleration of a synucleinopathy in a transgenic mouse model. *Neurobiol Aging*, *33*(9), 2225-2228. https://doi.org/10.1016/j.neurobiolaging.2011.06.022

Mulherkar, N., Raaben, M., de la Torre, J. C., Whelan, S. P., & Chandran, K. (2011). The Ebola virus glycoprotein mediates entry via a non-classical dynamin-dependent macropinocytic pathway. *Virology*, *419*(2), 72-83. https://doi.org/10.1016/j.virol.2011.08.009

Nakamura, K., Mori, F., Kon, T., Tanji, K., Miki, Y., Tomiyama, M., Kurotaki, H., Toyoshima, Y., Kakita, A., Takahashi, H., Yamada, M., & Wakabayashi, K. (2015). Filamentous aggregations of phosphorylated alpha-synuclein in Schwann cells (Schwann cell cytoplasmic inclusions) in multiple system atrophy. *Acta Neuropathol Commun*, *3*, 29. https://doi.org/10.1186/s40478-015-0208-0

Nakamura, K., Nemani, V. M., Wallender, E. K., Kaehlcke, K., Ott, M., & Edwards, R. H. (2008). Optical reporters for the conformation of alpha-synuclein reveal a specific interaction with mitochondria. *J Neurosci*, *28*(47), 12305-12317. https://doi.org/10.1523/JNEUROSCI.3088-08.2008

Nakase, I., Kobayashi, N. B., Takatani-Nakase, T., & Yoshida, T. (2015). Active macropinocytosis induction by stimulation of epidermal growth factor receptor and oncogenic Ras expression potentiates cellular uptake efficacy of exosomes. *Sci Rep*, *5*, 10300. https://doi.org/10.1038/srep10300

Oh, P., McIntosh, D. P., & Schnitzer, J. E. (1998). Dynamin at the neck of caveolae mediates their budding to form transport vesicles by GTP-driven fission from the plasma membrane of endothelium. *J Cell Biol*, *141*(1), 101-114. https://doi.org/10.1083/jcb.141.1.101

Oh, S. H., Kim, H. N., Park, H. J., Shin, J. Y., Bae, E. J., Sunwoo, M. K., Lee, S. J., & Lee, P. H. (2016). Mesenchymal Stem Cells Inhibit Transmission of alpha-Synuclein by Modulating Clathrin-Mediated Endocytosis in a Parkinsonian Model. *Cell Rep*, *14*(4), 835-849. https://doi.org/10.1016/j.celrep.2015.12.075

Park, J. Y., Kim, K. S., Lee, S. B., Ryu, J. S., Chung, K. C., Choo, Y. K., Jou, I., Kim, J., & Park, S. M. (2009). On the mechanism of internalization of alpha-synuclein into microglia: roles of ganglioside GM1 and lipid raft. *J Neurochem*, *110*(1), 400-411. https://doi.org/10.1111/j.1471-4159.2009.06150.x

Park, R. J., Shen, H., Liu, L., Liu, X., Ferguson, S. M., & De Camilli, P. (2013). Dynamin triple knockout cells reveal off target effects of commonly used dynamin inhibitors. *J Cell Sci*, *126*(Pt 22), 5305-5312. https://doi.org/10.1242/jcs.138578

Pelkmans, L., Puntener, D., & Helenius, A. (2002). Local actin polymerization and dynamin recruitment in SV40-induced internalization of caveolae. *Science*, *296*(5567), 535-539. https://doi.org/10.1126/science.1069784

Peng, C., Gathagan, R. J., & Lee, V. M. (2018). Distinct alpha-Synuclein strains and implications for heterogeneity among alpha-Synucleinopathies. *Neurobiol Dis*, *109*(Pt B), 209-218. https://doi.org/10.1016/j.nbd.2017.07.018

Pieri, L., Madiona, K., & Melki, R. (2016). Structural and functional properties of prefibrillar alpha-synuclein oligomers. *Sci Rep*, *6*, 24526. https://doi.org/10.1038/srep24526

Preta, G., Cronin, J. G., & Sheldon, I. M. (2015). Dynasore - not just a dynamin inhibitor. *Cell Commun Signal*, *13*, 24. https://doi.org/10.1186/s12964-015-0102-1

Recasens, A., & Dehay, B. (2014). Alpha-synuclein spreading in Parkinson's disease. *Front Neuroanat*, *8*, 159. https://doi.org/10.3389/fnana.2014.00159

Recasens, A., Ulusoy, A., Kahle, P. J., Di Monte, D. A., & Dehay, B. (2018). In vivo models of alpha-synuclein transmission and propagation. *Cell Tissue Res*, *373*(1), 183-193. https://doi.org/10.1007/s00441-017-2730-9

Reyes, J. F., Rey, N. L., Bousset, L., Melki, R., Brundin, P., & Angot, E. (2014). Alpha-synuclein transfers from neurons to oligodendrocytes. *Glia*, *62*(3), 387-398. https://doi.org/10.1002/glia.22611

Rodriguez, L., Marano, M. M., & Tandon, A. (2018). Import and Export of Misfolded alpha-Synuclein. *Front Neurosci*, *12*, 344. https://doi.org/10.3389/fnins.2018.00344

Rutherford, N. J., Moore, B. D., Golde, T. E., & Giasson, B. I. (2014). Divergent effects of the H50Q and G51D SNCA mutations on the aggregation of alpha-synuclein. *J Neurochem*, *131*(6), 859-867. https://doi.org/10.1111/jnc.12806

Samuel, F., Flavin, W. P., Iqbal, S., Pacelli, C., Sri Renganathan, S. D., Trudeau, L. E., Campbell, E. M., Fraser, P. E., & Tandon, A. (2016). Effects of Serine 129 Phosphorylation on alpha-Synuclein Aggregation, Membrane Association, and Internalization. *J Biol Chem*, *291*(9), 4374-4385. https://doi.org/10.1074/jbc.M115.705095

Sandal, M., Valle, F., Tessari, I., Mammi, S., Bergantino, E., Musiani, F., Brucale, M., Bubacco, L., & Samori, B. (2008). Conformational equilibria in monomeric alpha-synuclein at the single-molecule level. *PLoS Biol*, *6*(1), e6. https://doi.org/10.1371/journal.pbio.0060006

Schneider, C. A., Rasband, W. S., & Eliceiri, K. W. (2012). NIH Image to ImageJ: 25 years of image analysis. *Nat Methods*, *9*(7), 671-675. https://doi.org/10.1038/nmeth.2089

Shahmoradian, S. H., Lewis, A. J., Genoud, C., Hench, J., Moors, T. E., Navarro, P. P., Castano-Diez, D., Schweighauser, G., Graff-Meyer, A., Goldie, K. N., Sutterlin, R., Huisman, E., Ingrassia, A., Gier, Y., Rozemuller, A. J. M., Wang, J., Paepe, A., Erny, J., Staempfli, A., . . . Lauer, M. E. (2019). Lewy pathology in Parkinson's disease consists of crowded organelles and lipid membranes. *Nat Neurosci*, *22*(7), 1099-1109. https://doi.org/10.1038/s41593-019-0423-2

Shearer, L. J., Petersen, N. O., & Woodside, M. T. (2021). Internalization of alpha-synuclein oligomers into SH-SY5Y cells. *Biophys J*. https://doi.org/10.1016/j.bpj.2020.12.031

Sigismund, S., Woelk, T., Puri, C., Maspero, E., Tacchetti, C., Transidico, P., Di Fiore, P. P., & Polo, S. (2005). Clathrin-independent endocytosis of ubiquitinated cargos. *Proc Natl Acad Sci U S A*, *102*(8), 2760-2765. https://doi.org/10.1073/pnas.0409817102

Spillantini, M. G., Schmidt, M. L., Lee, V. M.-Y., Trojanowski, J. Q., Jakes, R., & Goedert, M. J. N. (1997). α-Synuclein in Lewy bodies. *388*(6645), 839-840.

Sung, J. Y., Kim, J., Paik, S. R., Park, J. H., Ahn, Y. S., & Chung, K. C. (2001). Induction of neuronal cell death by Rab5A-dependent endocytosis of alpha-synuclein. *J Biol Chem*, *276*(29), 27441-27448. https://doi.org/10.1074/jbc.M101318200

Tanaka, M., Kim, Y. M., Lee, G., Junn, E., Iwatsubo, T., & Mouradian, M. M. (2004). Aggresomes formed by alpha-synuclein and synphilin-1 are cytoprotective. *J Biol Chem*, *279*(6), 4625-4631. https://doi.org/10.1074/jbc.M310994200

Trischler, M., Stoorvogel, W., & Ullrich, O. (1999). Biochemical analysis of distinct Rab5- and Rab11-positive endosomes along the transferrin pathway. *112*(24), 4773-4783. https://jcs.biologists.org/content/joces/112/24/4773.full.pdf

Uemura, N., Uemura, M. T., Luk, K. C., Lee, V. M., & Trojanowski, J. Q. (2020). Cell-to-Cell Transmission of Tau and alpha-Synuclein. *Trends Mol Med*. https://doi.org/10.1016/j.molmed.2020.03.012

Uemura, N., Yagi, H., Uemura, M. T., Hatanaka, Y., Yamakado, H., & Takahashi, R. (2018). Inoculation of alpha-synuclein preformed fibrils into the mouse gastrointestinal tract induces Lewy body-like aggregates in the brainstem via the vagus nerve. *Mol Neurodegener*, *13*(1), 21. https://doi.org/10.1186/s13024-018-0257-5

Underwood, R., Wang, B., Pathak, A., Volpicelli-Daley, L., & Yacoubian, T. A. (2020). Rab27 GTPases regulate alpha-synuclein uptake, cell-to-cell transmission, and toxicity [Preprint]. *bioRxiv*. https://doi.org/10.1101/2020.11.17.387449

Uversky, V. N. (2007). Neuropathology, biochemistry, and biophysics of alpha-synuclein aggregation. *J Neurochem*, *103*(1), 17-37. https://doi.org/10.1111/j.1471-4159.2007.04764.x

Vargas, K. J., Schrod, N., Davis, T., Fernandez-Busnadiego, R., Taguchi, Y. V., Laugks, U., Lucic, V., & Chandra, S. S. (2017). Synucleins Have Multiple Effects on Presynaptic Architecture. *Cell Rep*, *18*(1), 161-173. https://doi.org/10.1016/j.celrep.2016.12.023

Vila-Carriles, W. H., Kovacs, G. G., Jovov, B., Zhou, Z. H., Pahwa, A. K., Colby, G., Esimai, O., Gillespie, G. Y., Mapstone, T. B., Markert, J. M., Fuller, C. M., Bubien, J. K., & Benos, D. J. (2006). Surface expression of ASIC2 inhibits the amiloride-sensitive current and migration of glioma cells. *J Biol Chem*, *281*(28), 19220-19232. https://doi.org/10.1074/jbc.M603100200

Volpicelli-Daley, L. A., Luk, K. C., & Lee, V. M. (2014). Addition of exogenous alpha-synuclein preformed fibrils to primary neuronal cultures to seed recruitment of endogenous alpha-synuclein to Lewy body and Lewy neurite-like aggregates. *Nat Protoc*, *9*(9), 2135-2146. https://doi.org/10.1038/nprot.2014.143

Volpicelli-Daley, L. A., Luk, K. C., Patel, T. P., Tanik, S. A., Riddle, D. M., Stieber, A., Meaney, D. F., Trojanowski, J. Q., & Lee, V. M. (2011). Exogenous alpha-synuclein fibrils induce Lewy body pathology leading to synaptic dysfunction and neuron death. *Neuron*, *72*(1), 57-71. https://doi.org/10.1016/j.neuron.2011.08.033

Wakatsuki, T., Schwab, B., Thompson, N. C., & Elson, E. L. (2001). Effects of cytochalasin D and latrunculin B on mechanical properties of cells. *Journal of Cell Science*, *114*(5), 1025-1036. https://jcs.biologists.org/content/joces/114/5/1025.full.pdf

Westphal, C. H., & Chandra, S. S. (2013). Monomeric synucleins generate membrane curvature. *J Biol Chem*, *288*(3), 1829-1840. https://doi.org/10.1074/jbc.M112.418871

Williams, T. D., & Kay, R. R. (2018). The physiological regulation of macropinocytosis during Dictyostelium growth and development. *131*(6), jcs213736. https://doi.org/10.1242/jcs.213736 %J Journal of Cell Science

Yan, F., Chen, Y., Li, M., Wang, Y., Zhang, W., Chen, X., & Ye, Q. (2018). Gastrointestinal nervous system alpha-synuclein as a potential biomarker of Parkinson disease. *Medicine (Baltimore)*, *97*(28), e11337. https://doi.org/10.1097/MD.0000000000011337

Yoshida, S., Pacitto, R., Inoki, K., & Swanson, J. (2018). Macropinocytosis, mTORC1 and cellular growth control. *Cell Mol Life Sci*, *75*(7), 1227-1239. https://doi.org/10.1007/s00018-017-2710-y

Zeineddine, R., Pundavela, J. F., Corcoran, L., Stewart, E. M., Do-Ha, D., Bax, M., Guillemin, G., Vine, K. L., Hatters, D. M., Ecroyd, H., Dobson, C. M., Turner, B. J., Ooi, L., Wilson, M. R., Cashman, N. R., & Yerbury, J. J. (2015). SOD1 protein aggregates stimulate macropinocytosis in neurons to facilitate their propagation. *Mol Neurodegener*, *10*, 57. https://doi.org/10.1186/s13024-015-0053-4

Zhang, Q., Xu, Y., Lee, J., Jarnik, M., Wu, X., Bonifacino, J. S., Shen, J., & Ye, Y. (2020). A myosin-7B-dependent endocytosis pathway mediates cellular entry of alpha-synuclein fibrils and polycation-bearing cargos. *Proc Natl Acad Sci U S A*, *117*(20), 10865-10875. https://doi.org/10.1073/pnas.1918617117

Zhang, W., Wang, T., Pei, Z., Miller, D. S., Wu, X., Block, M. L., Wilson, B., Zhang, W., Zhou, Y., Hong, J. S., & Zhang, J. (2005). Aggregated alpha-synuclein activates microglia: a process leading to disease progression in Parkinson's disease. *FASEB J*, *19*(6), 533-542. https://doi.org/10.1096/fj.04-2751com

Zwartkruis, F. J., & Burgering, B. M. (2013). Ras and macropinocytosis: trick and treat. *Cell Res*, *23*(8), 982-983. https://doi.org/10.1038/cr.2013.79

Preface to Chapter 4

The momentum in the field towards an immune-centered aspect of neurodegeneration, coupled with the nanogold-labeled PFF internalization assay established in chapter 2 and 3, served as the perfect platform for us to explore the destiny of exogenous PFFs internalized into neurons. In data presented in chapter 3, we found that PFFs maintain a punctate morphology, with most remaining localized to lysosomes, days after internalization. We were not able to observe PFF-related aggregation, and inclusion formation under standard conditions. It was at this point that we decided to further stress cells, with a proinflammatory cytokine, IFN-γ, which drastically altered our results. We found that IFN-γ, works in concert with PFF to create an environment in which DA neurons form LB-like inclusions. We decided to further characterize the formed inclusions and investigate the molecular changes in neurons as they undergo PFF and IFN-γ exposure. This led us to the findings presented in chapter 5.

CHAPTER 4. A DUAL HIT OF ALPHA-SYNUCLEIN INTERNALIZATION AND IMMUNE-CHALLENGE LEADS TO FORMATION AND MAINTENANCE OF LEWY BODY-LIKE INCLUSIONS IN HUMAN DOPAMINERGIC NEURONS

4.1 Abstract

Lewy bodies (LBs), rich in α-synuclein, are a hallmark of Parkinson's disease (PD). Understanding their biogenesis is likely to provide insight into the pathophysiology of PD, yet a cellular model for LB formation remains elusive. The realization that the immune challenge is a trigger for neurodegenerative diseases has been a breakthrough in the understanding of PD. Here, iPSC-derived human dopaminergic (DA) neurons from multiple healthy donors were found to form LB-like inclusions following treatment with α-synuclein preformed fibrils, but only when coupled to an immune challenge (interferon-gamma or interleukin-1 beta) or when co-cultured with activated microglia. Human cortical neurons derived from the same iPSC lines did not form LB-like inclusions. Exposure to interferon-gamma impairs autophagy in a lysosomal-specific manner *in vitro,* similar to the disruption of proteostasis pathways that contribute to PD. We find that lysosomal membrane proteins LAMP1 and LAMP2 and transcription factors regulating lysosomal biogenesis and function are downregulated in DA but not cortical neurons. Finally, due to the excellent sample preservation afforded by cells compared to post-mortem PD brain tissue, we conclude that the LB-like inclusions in DA neurons are membrane-bound, suggesting they are not limited to the cytoplasmic compartment.

4.2 Introduction

Lewy bodies (LBs) are proteinaceous inclusions that are a prevalent pathological marker in Parkinson's disease (PD) (M. Baba et al., 1998; M. G. Spillantini et al., 1997). Their presence in

patients can only be confirmed using post-mortem tissue. LBs are present in most patients diagnosed with idiopathic/sporadic PD (Braak et al., 2003), which comprises almost 80-90% of cases (Rajput et al., 1984). LBs also appear in many of the familial forms of PD. Coupled with the appearance of LBs, dysfunctional neurons also exhibit granular and filamentous deposits, referred to as Lewy neurites (LNs) (Braak et al., 1999). Despite their incidence in PD and other synucleinopathies such as Lewy body dementia (LBD) (Kim et al., 2014; Wakabayashi et al., 2013), and their histological discovery in the early 20th century (Engelhardt & Gomes, 2017), insights into the formation, structure, and function of LBs remain limited. This is primarily due to reliance on post-mortem tissue, in which LB morphology and content may be affected by alterations in tissue pH, oxygen levels, and autolytic activity during the post-mortem interval (Glausier et al., 2019). Using superior approaches to collecting and processing post-mortem tissue, Shahmoradian et al. (2019) demonstrated that LBs are not exclusively filamentous aggregates but are composed of a collection of membrane-bound compartments and organelle fragments. Their data, corroborating other previous studies (L. S. Forno & R. L. Norville, 1976; Gai et al., 2000; James H Soper et al., 2008), has spurred renewed interest in the structural study of LBs, the role that dysfunctional organelles play in the formation of LBs, and the underlying causes leading to the formation of membranous, proteinaceous, and organelle-filled inclusions.

While LBs may be a symptom of cellular dysfunction, they might also play a role in PD pathophysiology, neurotoxicity, or neuroprotection(Wakabayashi et al., 2013). LBs have been hypothesized to be an aggresomal response to the accumulation of aggregated proteins (Frigerio et al., 2011), which is perhaps a symptom of dysfunction in the degradative/autophagic machinery of the cell, a pattern also observed in lysosomal storage diseases (Monaco & Fraldi, 2020). PD bears many similarities with lysosomal storage diseases (Klein & Mazzulli, 2018), and PD has been

linked to impaired autophagy (Durcan & Fon, 2015). Moreover, mutations in mitochondrial proteins PINK1 and parkin result in dysfunctional mitophagy (Sato et al., 2018). It is thus plausible that deficits in autophagy found in PD are responsible for LB formation (Boman et al., 2016).

Consistent with protein degradation defects in LB formation, lysosomal proteins including GBA and TMEM175, are implicated in PD pathophysiology (Navarro-Romero et al., 2020; Sato et al., 2018). LAMP1 and LAMP2 are major lysosomal proteins that maintain lysosome integrity, pH, catabolism, and both function in autophagy (Eskelinen, 2006; Eskelinen et al., 2002). Interestingly, there are reduced levels of both proteins in PD (Boman et al., 2016). Such perturbations to the protein degradation machinery are not only common in PD, but a combination of such disturbances to lysosomal activity may play a crucial role in PD pathophysiology.

There is growing interest in the role of microglia and the immune system in neurodegenerative diseases. A seminal paper by Matheoud et al. (2019) reveals that PINK1$^{-/-}$ mice only exhibit PD-like symptoms when introduced to infections, emphasizing the importance of an immune-related trigger in the manifestation of PD motor symptoms. Further, the authors found cytotoxic T-cells, trained on recognizing mitochondrial antigen-presenting cells, targeted PINK1-knockout dopaminergic neurons in culture. The role of an immune challenge in PD has been highlighted by other studies, focusing on LRRK2 and cytokines (Ahmadi Rastegar et al., 2022; Panagiotakopoulou et al., 2020). In a mouse model of amyotrophic lateral sclerosis, the same line housed at two different facilities had different phenotypic outcomes, with more severe motor symptoms in animals at a facility where they had measurably more exposure to bacterial pathogens (Burberry et al., 2020). Clearly, the immune system and cytokines play a role in neurodegenerative diseases (Kulkarni et al., 2016; Roy & Cao, 2022; Seifert et al., 2014).

Given the link between the immune system and neurodegenerative disease, we hypothesized that a dual hit of a PD-insult followed by an immune challenge led to the formation of LBs. We exposed iPSC-derived dopaminergic (DA) neurons to α-synuclein (α-syn) preformed fibrils (PFFs), which are rapidly internalized and transported to lysosomes (Bayati et al., 2022). After a delay, we presented the neurons with an acute treatment of IFN-gamma (IFN-γ), a compound shown to be released by microglia and immune cells in response to infections (Kawanokuchi et al., 2006; Lv et al., 2020; Wang & Suzuki, 2007; Yang et al., 2022). As Matheoud et al. (2019) demonstrated the targeting of PINK1-knockout DA neurons by T-cells, who are major producers of IFN-γ (Ghanekar et al., 2001; Jorgovanovic et al., 2020; Nicolet et al., 2020; Wang & Suzuki, 2007), we decided that IFN-γ would be a good candidate to represent the involvement of the immune system. Exposure to PFF and IFN-γ results in the formation and long-term maintenance of PFF-positive inclusions absent in neurons treated with either substance alone. Like LBs, the LB-like inclusions formed in DA neurons are organellar, membranous and filamentous as determined by light and electron microscopy. LB-like inclusions also formed when interleukin-1 beta (IL-1β), a more microglia-specific proinflammatory cytokine, was used instead of IFN-γ. Remarkably, the resulting LB-like inclusions were membrane-bound, suggesting that they do not form in the cytoplasm but within an organelle lumen, likely in the endo/lysosomal system, or that they originate in the cytoplasm but are eventually engulfed by membranous organelles such as autophagosomes. These inclusions do not form in other cell types, including cortical neurons. Analysis of protein expression in response to the dual hit treatment reveals DA neuron-specific downregulation of transcription factor EB (TFEB) and nuclear factor erythroid 2-related factor 2 (NRF2), transcription factors involved in lysosomal biogenesis and function, along with the

downregulation of lysosomal membrane proteins LAMP1 and LAMP2. These data provide a unique cellular model for LB formation

4.3 Results

DA neurons form LB-like inclusions following a dual hit of PFF internalization and immune challenge

α-syn PFFs, a potentially toxic form of the protein, are internalized into a variety of cell types by macropinocytosis and are rapidly transported to lysosomes and multivesicular bodies (MVBs) where they remain for several days (Bayati et al., 2022). Given the growing link between immune challenges and neurodegenerative diseases, we sought to examine if an immune challenge could alter the cellular fate of internalized PFFs. IFN-γ, a cytokine released by immune cells and microglia in response to infections (Kawanokuchi et al., 2006), affects autophagy and inhibits lysosomal activity by downregulating lysosomal membrane proteins LAMP1 and LAMP2 (Fang et al., 2021). Our treatment regime, described in Figure 4.1 A and in Extended Data Figure 4.1 A and 4.1 B, involves the addition of sonicated PFFs (Extended Data Figure 4.1 C) and/or IFN-γ to DA neurons derived from human iPSCs, which express IFN-γ receptor 1 and 2 (IFNGR1 and IFNGR2; Extended Data Figure 4.1 D and 4.2 A). Remarkably, we observe the formation of PFF-positive inclusions using both light and electron microscopy analysis but only when the PFF treatment is combined with 0.2 mg/mL of IFN-γ (Figure 4.1 B and C, Extended Data Figure 4.2 B). PFFs pre-labeled with nanogold are seen in dark lysosomes and autolysosomes inside the inclusions, which also contain mitochondria and filamentous materials, all characteristic of LBs (Shahmoradian et al., 2019; J. H. Soper et al., 2008). These LB-like inclusionary bodies are ~5-10 μm, located in the perinuclear region, and in most cases, there is only one of these bodies per neuron. Approximately

10-15% of neurons form LB-like inclusions (Supplementary Figure 4.1). Some neurons also form inclusions within neurites (Figure 4.1 D), similar to Lewy neurites in PD. Formation of LB-like inclusions was achieved in DA neurons generated from three different iPSC cell lines (Extended Data Figure 4.2 C and D; Supplementary Figure 4.2 A-G).

In the treatment regime, we added PFF for 48 h, and then waited 3 days to add IFN-γ. This maximized cell survival compared to when we added PFF and IFN-γ simultaneously. PFF fluorescence and cell counts were quantified over 14 d (Figure 4.1 E and F). Neurons treated with PFFs alone exhibited significantly less PFF fluorescence than those treated with PFFs and IFN-γ, suggesting disruption of lysosomal degradation caused by IFN-γ treatment. A general decrease in cell count was observed with the treatment of PFF and IFN-γ. There was also a significant increase in the number and size of inclusions with increased incubation time (Figure 4.1 G and H).

Lastly, to ascertain whether the formation of LBs using the dual hit treatment regime was IFN-γ specific, we conducted the same experiments but replaced IFN-γ with 50ng/mL of IL-1β. We found that DA neurons treated with PFF and then IL-1β also formed PFF-positive inclusions (Extended Data Figure 4.3 A and B). Using EM, we found that these inclusions are filled with aberrant lysosomes, dysfunctional mitochondria, and are also membrane bound as seen with the IFN-γ treated samples.

Evaluation of the formation of LB-like inclusions

Following LB-like inclusions in cultured neurons allows for observation of the sequence of events leading to their formation and maturation. The inclusions formed in DA neurons (Figure 4.1 C, Extended Data Figure 4.2 C and D, and Supplementary Figure 4.2 A-G) are very similar to

those observed by Shahmoradian et al. (2019) in PD brains in that they both contain a medley of organelles, membranous fragments, filaments, lysosomes, autolysosomes, and mitochondria. To explore how they develop, a timeline of inclusion formation was established over 14 d (Figure 4.2 A and B). At 2 d (described in Extended Data Figure 4.1 B), an accumulation of nanogold PFFs in lysosomes occurs in both PFF-only and the PFF + IFN-γ conditions. In the 6 d samples, where neurons were recently treated with IFN-γ (or vehicle in the PFF-only samples), we see dramatic signs of cellular stress including swollen mitochondria and endoplasmic reticulum, along with dark, aberrant lysosomes. In the 7 d samples, the formation of miniature LB-like inclusions containing aberrant lysosomal structures can be observed. In the 10 d samples, a larger LB-like inclusion has formed, containing not only aberrant lysosomal structures but also mitochondrial fragments and a plethora of filamentous structures.

The most noticeable difference between the PFF-treated neurons and those treated with PFF + IFN-γ is seen at 14 d. The PFF + IFN-γ samples exhibit large inclusions that contain dark lysosomes, MVBs, filaments, and mitochondria. Additional examples can be found in Extended Data Figure 4.2 C-D and Supplementary Figure 4.2 A-G. Almost all inclusions formed by the 14 d PFF + IFN-γ treated DA neurons are membrane-bound. We followed the LB-like inclusions for up to 30 days, revealing highly compact, complex, filamentous/organelle-filled, membrane-enclosed inclusions (Figure 4.3 A-C). Additional examples of inclusions formed in 30 d DA neurons can be found in Supplementary Figure 4.3 A-D.

IFN-γ-treated samples exhibit lysosomal leaking of PFFs

The mechanism by which internalized oligomeric α-syn, which is in the lumen of the endosomal system, leads to seeding and misfolding of endogenous α-syn found in the cytoplasm has been a topic of study for many years (Bieri et al., 2018). More recently, the presence and characterization of lysosomal membrane permeabilization have provided clues as to how this process might occur (Freeman et al., 2013; Jiang et al., 2017). Here, we observe that neurons treated with PFF + IFN-γ show clear signs of PFF leakage from lysosomes at early time points (Extended Data Figure 4.4 A), where ruptured lysosomes have nanogold PFFs within their lumen and immediately outside their lumen. Coinciding with leakage of PFF into the cytosol, IFN-γ-treated samples show many large autolysosome/autophagosome structures containing organelle fragments (Extended Data Figure 4.4 B), indicating impairment in autophagy (Vergarajauregui et al., 2008). In the 14 d PFF + IFN-γ samples, where neurons have formed inclusions, leakage of PFFs into the cytosol, is a common occurrence (*E*xtended Data Figure 4.4 C). Multiple examples of PFFs leaking outside of lytic compartments can be seen in the collection of LB-like inclusions shown in Supplementary Figure 4.2.

Biochemical extraction of inclusions

We extracted the inclusions formed in DA neurons by subcellular fractionation. Their large size allowed for pelleting with low-speed centrifugation after cellular homogenization. DA neurons undergoing the dual hit treatment regime exhibited an accumulation of PFF in the pelleted inclusions compared to the total homogenate (Extended Data Figure 5A), whereas those not receiving IFN-γ treatment had a far less prominent accumulation of PFF. The same trend was present when examining the accumulation of phospho-α-syn. Compared to DA neurons, U2OS, an osteosarcoma cell line, had no noticeable accumulation of PFF or phospho-α-syn in the pellet

fractions in either PFF-only or PFF + IFN-γ treatment (Extended Data Figure 4.5 B). Additionally, we noted that the α-syn signal in DA neurons consists of a double band, a likely indication of α-syn phosphorylation in DA neurons that does not occur in U2OS. This is further confirmed by *our* phospho-*α*-syn blots. Inclusions formed in DA neurons were concentrated and prepared for EM. Detergent-free cell lysis preserved the structure of the inclusions and the resulting samples showed morphologically similar structures to those observed within DA neurons (Extended Data Figure 4.5 C and Supplementary Figure 4.4). The isolated inclusions were filled with lytic compartments (lysosomes and autolysosomes), MVBs, and most importantly, even in their isolated state, still maintained a relatively intact surrounding membrane*,* further suggesting that these inclusions are membrane-enclosed structures.

Activated microglia cause inclusion formation in neighboring DA neurons

Proinflammatory cytokine-producing immune cells infiltrate the central nervous system in multiple sclerosis and other neurodegenerative diseases (Duffy et al., 2014; Lees & Cross, 2007; Molteni & Rossetti, 2017; Rezai-Zadeh et al., 2009; Yang et al., 2020). To assess whether communication between microglia, which produce both IL-1β and IFN-γ (De Simone et al., 1998; Kawanokuchi et al., 2006; Liu & Quan, 2018; Suzuki et al., 2005; Wang & Suzuki, 2007)*,* and neurons leads to formation of LB-like inclusions in DA neurons, we co-cultured a human microglial cell line (HMC3), treated with LPS (10 μg/mL) to induce microglial activation*,* with fully differentiated DA neurons (Figure 4.4 A). Neurons co-cultured with activated microglia formed PFF-positive inclusions. Large-field images of co-cultured microglia and neuronal samples reveal that DA neurons neighboring microglia were most affected by microglial secretions (Extended Data Figure 4.6 A). These neurons have significantly higher PFF fluorescence than the

control (i.e., neurons co-cultured with PBS-treated microglia; Figure 4.4 B). Media from microglia exposed to phosphate-buffered saline (PBS), PFF, LPS, and LPS + PFF were collected and analyzed for the presence of IFN-γ (Figure 4.4 C). Microglia treated with LPS, PFF, and LPS + PFF showed elevated levels of IFN-γ. It is, therefore, clear that IFN-γ are released by microglia and lead to inclusion formation in neurons. Consistent with previous findings, PFF treatment alone elicited a microglial response (Zhang et al., 2005), suggesting a positive feedback loop might be at play.

LB-like inclusions are primarily restricted to DA versus other neuronal types.

Although the substantia nigra is most studied for its degeneration in PD, cortical neurons also degenerate in this disease (Zhang et al., 2018). We generated forebrain cortical neurons from the same lines used to produce DA neurons (Extended Data Figure 4.6 B) and subjected them to the 14 d dual hit treatment regime. Cortical neurons did not form PFF-positive LB-like inclusions up to the 14 d time point (Figure 4.4 D). They did contain aberrant, dark, and large lysosomes (Figure 4.4 E), similar to the lysosomes observed within the LB-like inclusions of DA neurons; however, unlike DA neurons, the cortical neurons were unable to package these structures into LB-like inclusions, i.e., structures that are compact, tightly packed with multiple vesicular and organellar structures, and distinct in morphology. Neurogenin 2 (NGN2)-induced neurons, broad spectrum excitatory neurons also failed to form inclusions (Figure Extended Data 4.6 C and D) but exhibited dark lysosomes filled with PFF throughout the cytoplasm. Quantification of PFF fluorescence in cortical neurons over 14 d (Figure 4.4 F) showed a similar trend to DA neurons (Figure 4.1 E); however, overall cell numbers were markedly decreased in the PFF and IFN-γ-treated samples in cortical neurons (Figure 4.4 G) relative to DA neurons (Figure 4.1 F). Since the

reduction in cortical neurons occurs very quickly, we rule out the possibility that the formation of LB-like inclusions causes the death of the neurons, as the formation process takes some time to occur.

The specificity of inclusion formation in DA neurons was further explored by examining neuroblastoma (SH-SY5Y), glioblastoma (U87), and osteosarcoma (U2OS) cells. When treated with the dual hit regime, none of these cells formed inclusions (Extended Data Figure 4.7 A and B); however, each cell line exhibited signs of lysosomal abnormalities: a loss of LAMP1 and an increase in lysosomal size (Extended Data Figure 4.7 C and D). Thus, treatment of various cell types with PFF and IFN-γ causes lysosomal defects, but the formation of LB-like inclusions is restricted to DA neurons.

The formation of LB-like inclusions is dependent on the endogenous levels of α-syn

α-syn is present in LBs (M. Baba et al., 1998; Conway et al., 1998; Polymeropoulos et al., 1997; M. G. Spillantini et al., 1997). The phosphorylation of α-syn in these aggregates is considered the best marker for α-syn aggregation and LB formation (Luk et al., 2009). To explore whether the inclusions formed in our treatment regime coincide with the presence of phospho-α-syn, DA neurons that underwent the dual hit regime were stained with phospho-α-syn antibody. These neurons formed phospho-α-syn-positive inclusions (Extended Data Figure 4.8 A), and PFFs were localized in inclusions along with phospho-α-syn (Extended Data Figure 4.8 B). To assess the influence of endogenous α-syn levels on LB-like inclusions, we used iPSCs from a patient with an *SNCA* triplication, in which we used a double knockout (KO) to generate wildtype (WT) cells and a quadruple KO to generate an *SNCA* null. These isogenic lines were differentiated into DA neurons and exposed to PFFs and *IFN*-γ. The level of phospho-α-syn fluorescence was influenced

by α-syn expression levels more so than the addition of PFFs (Extended Data Figure 4.8 C, D, and E). We observed a striking increase in phospho-α-syn fluorescence following treatment with IFN-γ. α-syn expression levels also influenced the formation of PFF-positive inclusions with higher levels leading to a progressive increase in the number and size of these structures (Extended Data Figure 4.8 F, G and H). We noted, however, that SNCA triplication could form phospho-α-syn-positive inclusions, but at a much smaller level than when coupled with IFN-γ administration (Extended Data Figure 4.8 I)

We next transduced WT neurons with α-syn-HA adenovirus and treated them with IFN-γ (Extended Data Figure 4.8 J and K). We observed formation of phospho-α-syn-positive inclusions in the absence of PFFs (Extended Data Figure 4.8 L and M). In summary, IFN-γ can also induce the formation of inclusions using endogenously expressed α-syn.

Downregulation of lysosomal proteins and disruption in autophagic flux coincides with the formation of LB-like inclusions

Given the numerous lysosomal defects seen in cells treated with PFF and IFN-γ we sought to examine if this treatment alters proteins regulating lysosomal biogenesis and function. NRF2 and TFEB are transcription factors regulating the expression of lysosomal proteins and function (Abokyi et al., 2020; Dodson et al., 2021; Joshi et al., 2021; Pajares et al., 2018; Park et al., 2019). As LAMP1 and LAMP2, major lysosomal proteins have previously been implicated in PD (Boman et al., 2016), and both TFEB and NRF2 have been suggested to play a role in neurodegenerative diseases (Cortes & La Spada, 2019; Suzen et al., 2022), we sought to examine expression levels in these proteins. While LAMP1 and LAMP2 expression were higher in cortical neurons than DA

neurons at baseline conditions, treatment with PFF and IFN-γ caused a strong reduction in LAMP1 and LAMP2 levels in DA neurons but not in cortical neurons. TFEB and NRF2 followed a similar trend and were downregulated in DA neurons but remained nearly unaffected in cortical neurons (Figure 4.5 A-H). Using CellROX and MitoSOX to look at generalized oxidative stress and superoxide production, respectively, we found that general oxidative stress levels were similar in both DA and cortical neurons (Figure 4.5 I); however, the production of superoxide species was found to be significantly different, as cortical neurons treated with PFF and those treated with PFF + IFN-γ exhibited significantly higher levels of MitoROX fluorescence compared to DA neurons (Figure 4.5 J).

Due to their constant need to mitigate oxidative stress generated through the production and metabolism of dopamine (Meiser et al., 2013; Zhang et al., 2019), DA neurons are probably more adept at dealing with oxidative stresses, partly through the sequestration of damaged organelles. Should oxidative species impair organellar function, specifically mitochondria, the release of cytochrome c can lead to Caspase-dependent cell death (Callizot et al., 2019). Furthermore, protecting the cell from leaky lysosomes, another consequence of oxidative stress (Nagakannan et al., 2020), is also vital for cell survival (Zhu et al., 2020). This is why the sequestration of damaged organelles is protective. Cortical neurons, unable to form LB-like inclusions, leave themselves vulnerable to the consequences of oxidative stress. This is perhaps why DA neurons can survive at much higher rates than cortical neurons when confronted with our treatment regime.

By tracking LC3B staining, a marker for autophagy (Huang et al., 2015), over the 14 d treatment regime, we found that large autophagosomes form, merge, and then eventually result in the large PFF-positive structures we have repeatedly observed (Extended Data Figure 4.9 A and B). These large LC3B-positive structures are only present in PFF + IFN-γ treated samples. The

accumulation and perseverance of these large LC3B structures is indicative of autophagic dysfunction and an inability of the cell to clear the contents within these autophagosomes (Runwal et al., 2019). Furthermore, when we observed lysosomal pH using LysoSensor and LysoTracker as done previously by Guerra et al. (2019), we found that neurons treated with IFN-γ or PFF + IFN-γ all presented with lysosomes at a higher pH compared to the control and PFF-treated samples (Extended Data Figure 4.9 C). This was complemented by our Lysotracker staining, which showed neurons treated with IFN-γ or PFF + IFN-γ as having lower numbers of LysoTracker-positive lysosomes (Extended Data Figure 4.9 D and E).

Lastly, the expression levels of lysosomal proteins were also examined in SH-SY5Y, U87, and U2OS (Extended Data Figure 4.9 F), cells that did not form inclusions. Although NRF2, LAMP1, and LAMP2 levels were decreased in samples treated with PFF + IFN-γ, TFEB was unaffected, indicating that impairment of lysosomal biogenesis is critical for a more detrimental impairment of lysosomal function, which may lead to the formation of inclusions.

Formation of LB-like inclusions is prevented by Perillaldehyde (PAH)

As NRF2 and LAMP2 are highly downregulated in samples treated with both PFF and IFN-γ we searched to use a chemical activator for the lysosomal-inflammasome pathway and found PAH to be a perfect candidate. PAH is an activator of NRF2 and its ability to activate NRF2 and therefore increase lysosomal activity and degradation has been shown repeatedly in previous studies (Fan et al., 2020; Fuyuno et al., 2018; Tang et al., 2023; Zheng et al., 2021). To reduce/counteract the inclusion-forming effects in neurons caused by PFF and IFN-γ, PAH treatment experiments were conducted on neurons treated with PFF + IFN-γ (Figure 4.6 A and B).

A cell survival assay indicated that PAH was cytotoxic at higher concentrations (Figure 4.6 C), therefore the concentration of 10 μM of PAH was used to minimize cell death related to PAH treatment. Samples treated with PAH 1 d following IFN-γ treatment, exhibited significantly less PFF-positive inclusions compared to those not treated with PAH (Figure 4.6 D). The 1 d samples also exhibited significantly smaller inclusions compared to the PAH-untreated condition (Figure 4.6 E).

Lastly, we found that TFEB, LAMP1, LAMP2, and NRF2 protein expression levels were similar to control levels in the 1 d and 4 d PAH conditions (Figure 4.7 A-H). IFN-γ-only conditions exhibited a higher level of α-syn expression than control, as was observed previously (Figure 4.5 A). In addition, an increase in IFN-γ incubation time in previously PFF-treated neurons also resulted in higher levels of α-syn. Taken together, these results demonstrate that the DA neurons undergoing the dual hit treatment regime exhibit lysosomal impairment through the downregulation of LAMP1 and LAMP2, and the transcription factors NRF2 and TFEB, which creates an environment allowing for the formation of large LB-like inclusions. This phenotype can be partially prevented by recovering these lysosomal proteins after 1 d of PAH treatment.

4.4 Discussion

LBs are a hallmark of PD, LBD and other synucleinopathies. Although many studies have reported the ultrastructure of LBs, the reliance on post-mortem tissue has resulted in less-than-ideal analysis and an ongoing dispute regarding their origins. Many studies report that LBs are cytoplasmic structures, filamentous, and lacking a delineating membrane (M. Baba et al., 1998; Colosimo et al., 2003; Philip E Duffy & Virginia M Tennyson, 1965; Lysia S Forno & Roxana L Norville, 1976; Gai et al., 2000; Galloway et al., 1992; Watanabe et al., 1977). However, a recent

study using a shorter post-mortem interval and better processing of post-mortem tissues indicates that LBs contain filaments but also numerous organelles, vesicles, and membrane fragments (Shahmoradian et al., 2019). Despite this, limited information can be understood from post-mortem tissue samples, such as the formative stages involved in assembling LBs, their progression, and the incorporation of organelles and membranes. Here we determine that a dual treatment of a PD insult (fibrils of α-syn) and an immune challenge (IFN-γ or IL-1β) leads to structures with a remarkable similarity to LBs, and this occurs specifically in DA neurons. This has allowed us to study the stages involved in their formation and their morphology. Our findings bring together two separate fields of inquiry into the pathophysiology of PD: (1) the internalization, propagation, seeding, overexpression, and incorporation of α-syn in LBs (Lam et al., 2022); (2) the involvement of the immune system in PD (Matheoud et al., 2019).

IFN-γ is one of many proinflammatory cytokines released by microglia and other immune cells that can serve as an immune challenge. IL-1β used in this paper, tumor necrosis factor, and other cytokines are also released by immune cells (Smith et al., 2012). These cytokines could also contribute to an environment in which DA neurons can form inclusions in PD. In our co-culture experiments, we found that DA neurons readily formed inclusions within 48 h following co-culturing with microglia. Although IFN-γ secretion by microglia was detected and has been reported previously (Fares et al., 2021; Mahul-Mellier et al., 2020), it is likely a combination of microglia-secreted factors driving this effect *in vitro*, including IL-1β. In addition to microglia, we believe that neuronal exposure to IFN-γ may also occur through immune cell secretions, following their infiltration into the brain (Yang et al., 2020), as immune cells are robust producers and secretors of IFN-γ (Lam et al., 2022). In fact, aging microglia have been shown to facilitate

immune system infiltration into the brain (Zhang et al., 2022). Exposure to IFN-γ can induce antigen presentation in neurons (Lam et al., 2022), which may lead neurons to be further vulnerable to the immune system via autoimmune-mediated mechanisms (Frucht et al., 2001), and perhaps more likely to form inclusions as a response to α-syn upregulation and oxidative stress (Kasen et al., 2022; Scudamore & Ciossek, 2018). Overall, our goal is not to implicate any one specific cell type for the secretion of proinflammatory cytokines, or that one specific cytokine is responsible for inclusion formation. We simply present a model in which proinflammatory cytokines IFN-γ and IL-1β administered alongside a PD-insult, result in the formation LB-like inclusions.

Due to their formation in cultured cells, we can examine LB-like inclusions with ultrastructural integrity not currently possible with post-mortem tissue. This has allowed us to make a significant observation regarding the structure of these LB-like inclusions: they are membrane-bound. Whether LBs are membrane-enclosed has significant implications for their origin. If LBs are formed in the cytoplasmic compartment aided by the fibrilization of α-syn, which allows for the tethering and pulling of organelles and membranes together, then α-syn aggregation becomes the central event in inclusion formation and will lead to the formation of LBs given enough time (Fares et al., 2021). If LBs are membrane-bound, they may form within the lumen of the endo/lysosomal system. This would rely on impairments in autophagy and lysosomal function and would be less dependent on α-syn aggregation. Our *in vitro* LB-like inclusions were consistently membrane-bound across all our EM data, even when biochemically isolated. Coupled with our findings regarding the downregulation of lysosomal transcription factors and proteins, our data support the latter hypothesis that LBs are membrane-bound and ultimately form in the lumen

of ever expanding, dysfunctional autophagosomes since the PFF-positive inclusions that form are LC3B-positive and enveloped by a double membrane.

As shown in our model (Extended Data Figure 4.10), α-syn aggregation occurs, for the most part, in the cytosol. This is initiated by cytosolic seeding of aggregation through the leaking of PFFs from lysosomes into the cytosol. Downregulation of LAMP2 results in impaired chaperone-mediated autophagy, resulting in a buildup of monomeric α-syn in the cytosol, contributing to aggregation. While aggregating in the cytosol, phosphorylation of α-syn also takes place. The cell, in an attempt to degrade aggregates, induces autophagy, and takes up aggregated α-syn along with damaged organelles. Contents within autophagosomes are not degraded however due to dysfunctional lysosomal activity, and the lack of lysosomal fusion with autophagosomes, which is caused by the downregulation of LAMP1 and LAMP2. Autophagosomes continue to take up more aggregates from the cytosol but continue building in size as no degradation takes place. These events finally lead to the formation of membrane-bound inclusions.

In our study, PFF and IFN-γ cooperatively enable the downregulation of lysosomal transcriptional factors and lysosomal proteins, most notably LAMP2. Downregulation of LAMP2 inhibits the degradative activity of lysosomes by blocking chaperone-mediated autophagy and autophagosome-lysosomal fusion (Morell et al., 2016). LAMP2A, the isoform responsible for chaperone-mediated autophagy, has been previously studied for its potential role in PD (Morell et al., 2016). The mutant forms of α-syn are responsible for altering the chaperone-mediated autophagy activity of LAMP2A (Martinez-Vicente et al., 2008). LAMP2 downregulation in brain regions has also been associated with increased α-syn aggregation in those regions (Malkus & Ischiropoulos, 2012). Whether PFF and IFN-γ downregulate LAMP2 expression by affecting NRF2 expression, and, therefore, the transcription of LAMP2, or by affecting LAMP2 expression

through other means remains to be studied. Still, the downregulation of NRF2 ensures that the cell cannot increase LAMP2 expression when needed as an inflammasome response (Saha et al., 2021).

It is worth noting that the lack of inclusion formation in cortical neurons in our treatment regime is not an indicator of LB formation in PD. Clearly, cortical neurons form LBs in PD as shown by Braak et al. (2003); however, the mechanism by which these neurons are pushed into forming inclusions is perhaps different and may rely on α-syn overexpression as other models have suggested (Yang et al., 2020). In our model, we find that DA neurons respond to the dual hit treatment regime, as they have evolved mechanisms to mitigate the deleterious effects of oxidative stress response *(Meiser et al., 2013; Zhang et al., 2019)*, which doesn't occur with cortical neurons. Through sequestration of damaged mitochondria and leaky lysosomes into inclusions, LB-like inclusions protect DA neurons from harmful species that can play a role in neuronal apoptosis, including the release of cytochrome c from mitochondria and the release of degradative enzymes from lysosomes (Callizot et al., 2019; Nagakannan et al., 2020). This is perhaps why DA neurons survive at much higher numbers than cortical neurons. We believe that the dual hit treatment may, therefore, not facilitate the appropriate environment for the formation of LB-like inclusions in cortical neurons. Different neuronal subtypes probably require different conditions to induce the formation of LB-like inclusions, which needs to be explored in future research.

α-syn likely plays a large role in formation of inclusions, and our findings do not discount that. In patients with overexpression of α-syn due to locus duplication and triplication, and in models where overexpression of α-syn is used to drive inclusion formation, it is very likely that the tethering of organelles by α-syn fibrils does in fact result in inclusions. Our model aims to only suggest another possible way for the formation of inclusions, that has not been studied previously.

It is very likely that both pathways are at play in PD: the overexpression of α-syn driving inclusion formation, and the intercellular transport of α-syn oligomers coupled with immune system activation. We believe our results, along with more recent work on inclusions formation shown by Mahul-Mellier et al. (2020), Tanudjojo et al. (2021), Iannielli et al. (2022), and Gribaudo et al. (2019), mark the beginning of new era, where the formation of LB-like inclusions can be studied and the mechanisms involved in the formation can be understood.

The consistent formation of LB-like inclusions *in vitro* marks the next step in investigating the molecular underpinnings of LB formation. Our *in vitro* treatment regime can serve as a starting point for future investigators to modify our protocol and explore the different stages of LB formation, changes in protein expression, and the onset of protein sequestration into LB-like inclusions. This treatment regime provides a reproducible and unlimited source of LB-like inclusions. It allows for a level of sample preservation and ultrastructural resolution that is currently impossible to attain with post-mortem tissue. Biochemical isolation of these LB-like inclusions at different time points and assessment of their protein contents over time will provide the field with a wealth of information regarding the molecular changes underlying LB formation. Lastly, adapting our protocol for use with midbrain organoids (Mohamed et al., 2021), brain assembloids (Birey et al., 2017; Miura et al., 2022), and other 3D models can allow for the recreation of PD *in vitro*, mapping the entire sequence of events in neurodegenerative disorders, ushering in the next era of research into neurodegenerative diseases.

4.5 Acknowledgements

We acknowledge the Advanced BioImaging Facility and the Facility for Electron Microscopy Research at McGill University. We thank Dr. Kelly Sears for all his help with the EM.

We thank Dr. Bruce Wright, the head of the Division of Medical Sciences at the University of Victoria. We also thank Drs. Sabatini and Zoncu for the HA-TMEM192 plasmids. AB is supported by Fonds de recherche du Québec doctoral award and a studentship from the Parkinson Society of Canada. This work was supported by financial support from the Canada First Research Excellence Fund, Healthy Brain, Healthy Lives, McGill University, awarded to TMD and PSM. EAF is supported by Foundation Grant from CIHR (FDN-154301) and a Canada Research Chair (Tier 1) in Parkinson disease. TMD is supported by a project grant from CIHR (PJT – 169095). PSM is a Distinguished James McGill Professor and Fellow of the Royal Society of Canada.

4.6 Figures

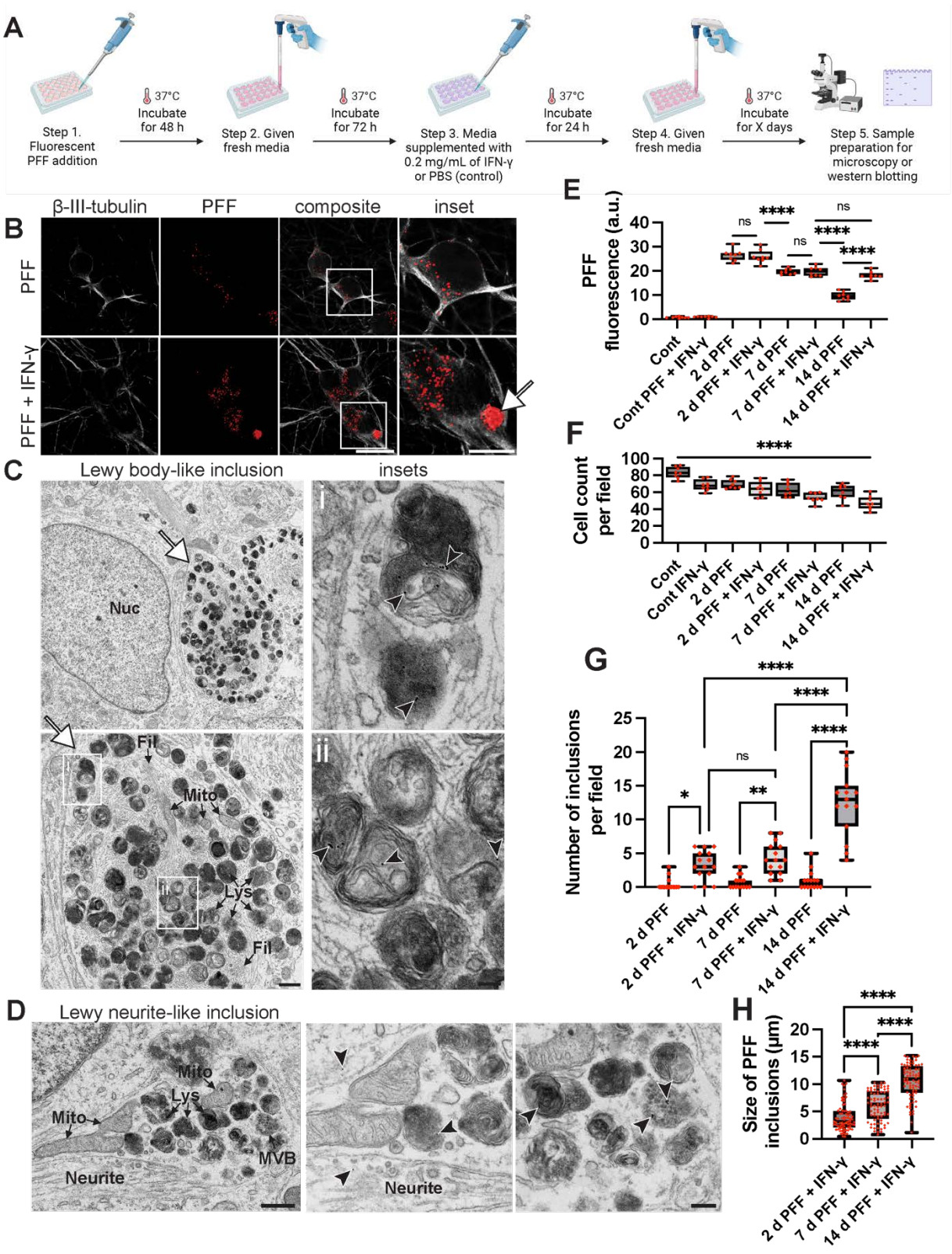
A
Step 1. Fluorescent PFF addition
37°C Incubate for 48 h
Step 2. Given fresh media
37°C Incubate for 72 h
Step 3. Media supplemented with 0.2 mg/mL of IFN-γ or PBS (control)
37°C Incubate for 24 h
Step 4. Given fresh media
37°C Incubate for X days
Step 5. Sample preparation for microscopy or western blotting
B
β-III-tubulin
PFF
composite
inset
PFF
PFF + IFN-γ
C
Lewy body-like inclusion
insets
Nuc
Fil
Mito
Lys
i
ii
D
Lewy neurite-like inclusion
Mito
Lys
MVB
Neurite
E
PFF fluorescence (a.u.)
Cont
Cont PFF + IFN-γ
2 d PFF
2 d PFF + IFN-γ
7 d PFF
7 d PFF + IFN-γ
14 d PFF
14 d PFF + IFN-γ
F
Cell count per field
Cont IFN-γ
G
Number of inclusions per field
H
Size of PFF inclusions (µm)

Figure 4.1

IFN-γ treated DA neurons form PFF-positive inclusions.

(**A**) Graphical representation indicates the steps involved in the dual hit regime. iPSC-derived DA neurons underwent a 14 d dual hit treatment, in which fluorescent PFFs were administered for 48 h, incubated in fresh media for 72 h, followed by the administration of IFN-γ (or PBS for control) for 24 h. Neurons were then incubated for 8 d, in fresh media. (**B**) Samples were fixed, stained with β-III-tubulin antibody, and prepared for confocal microscopy. Confocal images indicate the formation of PFF-positive inclusions in PFF + IFN-γ-treated neurons. These inclusions are not present in neurons only treated with PFF at 14 d. Arrowhead points to the PFF-positive inclusion. Scale bar = 20 μm and 10 μm for inset. (**C**) Following the same protocol as in **A**, but using nanogold-labeled PFF, neurons underwent the dual hit treatment regime, were fixed, and processed for EM. Lys (lysosome), Mito (mitochondria), Nuc (nucleus), Fil (filaments). Arrowhead points to the inclusion spotted in the neuron. Arrows point to nanogold-labeled PFF. Scale bar = 500 nm and 100 nm for insets. (**D**) Neurons undergoing the same treatment described in **A** showed inclusions within neurites. MVB (multivesicular bodies). Scale bar = 500 nm and 200 nm for insets. (**E**) Quantification of PFF fluorescence over 14 d in neurons both treated and not treated with IFN-γ, n = 8 for each condition, and quantification was done on data collected from three independent samples. One-way ANOVA and *post-hoc* Tukey's test were conducted to ascertain the significance between means. (**F**) Cell count was quantified over 14 days, n = 8 for each condition, and quantification was done on three independent samples. The control (Cont) and IFN-only conditions were fixed and counted simultaneously to the 14 d samples; this allows our control conditions to serve as a better control for our main experimental conditions: 14 d PFF and 14 d PFF + IFN. Conditions were analyzed using one-way ANOVA. (**G**) The number of inclusions per 387.5 x

387.5 μm images was counted. PFF puncta of 2 μm and larger were counted as inclusions, n = 15 for each condition, from three independent experiments. One-way ANOVA and *post hoc* Tukey's test were conducted for statistical analysis. (**H**) The size/diameter of inclusions was calculated, n = 75 for each condition, and data was collected from three independent experiments, with ANOVA and *post hoc* Tukey's test for statistical analysis. **** denotes $p < 0.0001$, *** denotes $p < 0.001$, and ** denotes $p < 0.01$. ns = not significant.

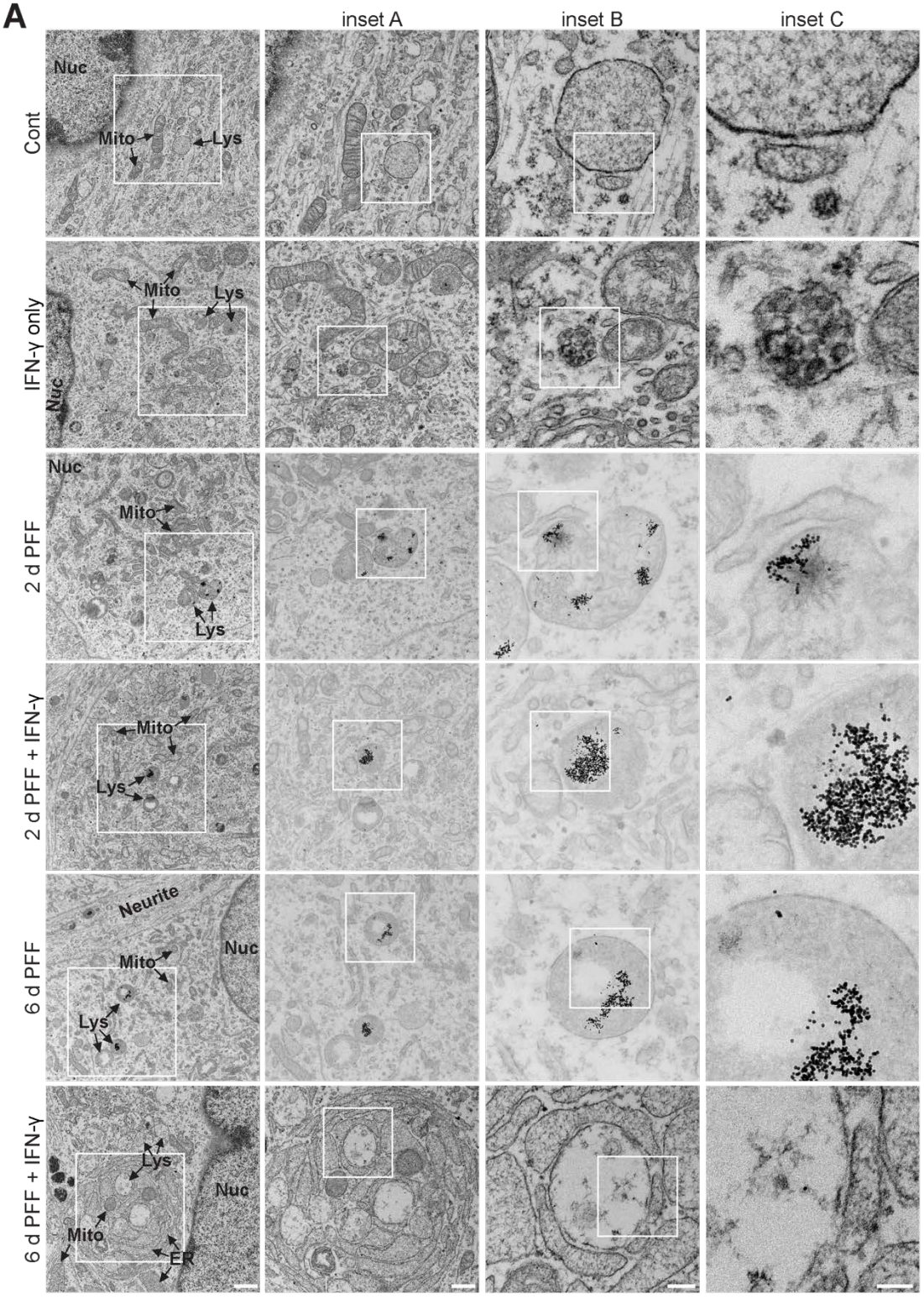
A
inset A
inset B
inset C
Cont
IFN-γ only
2 d PFF
2 d PFF + IFN-γ
6 d PFF
6 d PFF + IFN-γ
Nuc
Mito
Lys
Neurite
ER

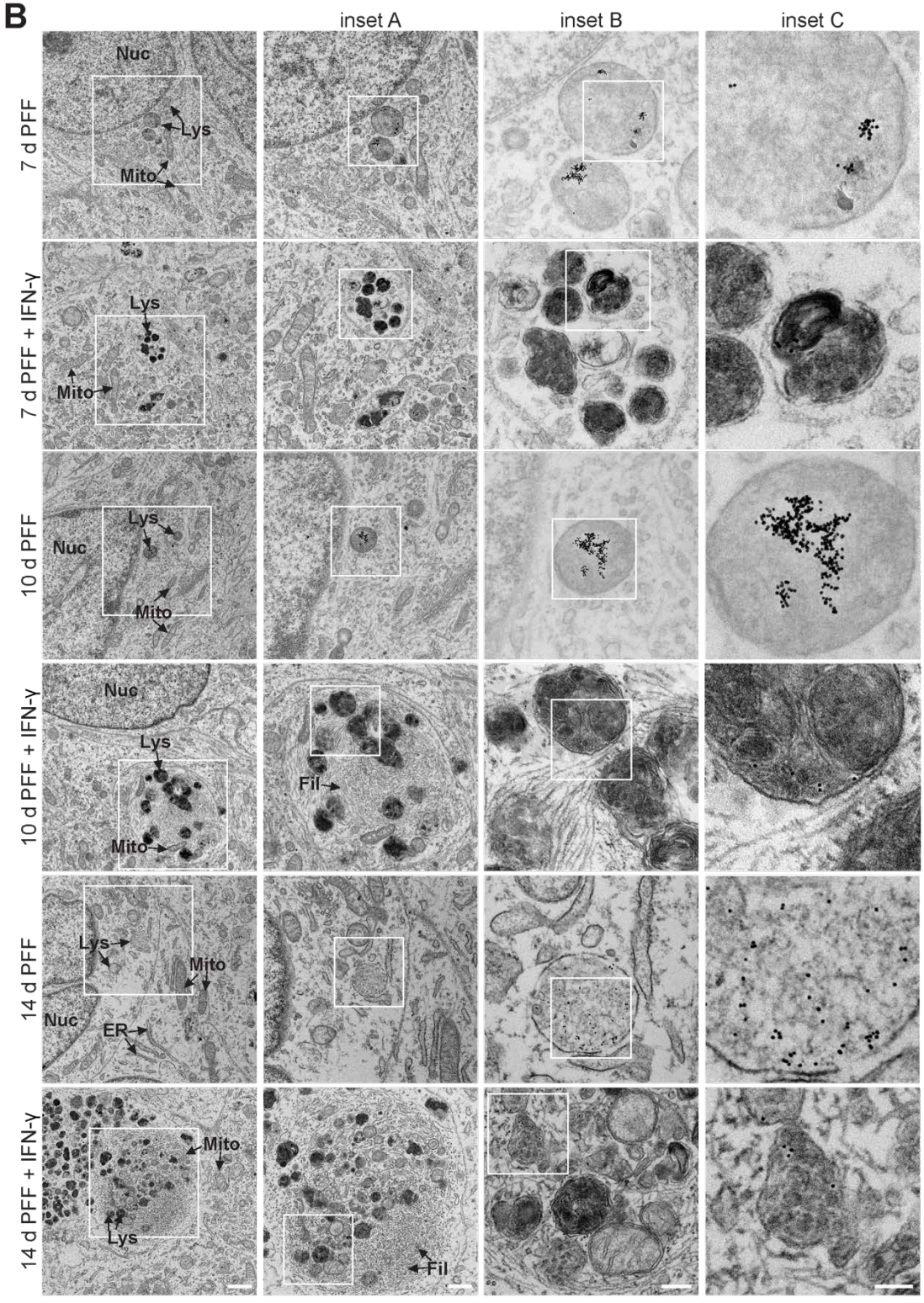
B
inset A
inset B
inset C
7 d PFF
7 d PFF + IFN-γ
10 d PFF
10 d PFF + IFN-γ
14 d PFF
14 d PFF + IFN-γ
Nuc
Lys
Mito
Fil
ER

Figure 4.2

LB-like inclusions form over 14 d.

(**A**) DA neurons' ultrastructure and organelle morphology were analyzed over 14 d, as neurons were put through the dual hit treatment. In the control (Cont) sample, lysosomes are unremarkable and appropriately sized (~1 μm in diameter), and mitochondria show healthy, and the cristae are not as defined as in the control neurons. In the IFN-only condition, mitochondria are more prominent and swollen, and the cristae are not as perfectly defined as in Cont. Neurons in the 2 d PFF condition exhibit lysosomes that have accumulated nanogold-labeled PFFs and lysosomes that have increased in size compared to the control. In the 2 d PFF + IFN-γ sample, mitochondria have irregular cristae, and an accumulation of nanogold-labeled PFF is seen. 6 d PFF neurons show accumulation of nanogold-PFF in their lumen, with enlarged lysosomes compared to control. 6 d PFF + IFN-γ samples show signs of drastic levels of ER stress, swollen mitochondria, and lysosomes with nanogold-PFFs. (**B**) 7 d PFF samples show lower PFF accumulation levels in lysosomes than 2 d PFF neurons. 7 d PFF and IFN-γ treated neurons exhibit miniature LB-like inclusions with aberrant lysosomal structures within them. 10 d PFF samples show very similar morphology to 7 d PFF neurons. 10 d PFF + IFN-γ-treated neurons exhibit larger LB-like structures (compared to the 7 d PFF + IFN-γ samples) with aberrant lytic structures and abnormal mitochondria with irregular cristae. Accumulation of a dense web of cytoskeletal filaments is evident around some of the dense lysosomes. 14 d PFF neurons look very similar to the control, except that they show nanogold-PFF accumulation. Finally, 14 d PFF and IFN-γ samples show large inclusions containing a collection of filaments, granules, lysosomes, MVBs, and mitochondria. Lys (lysosome, autolysosomes), Mito (mitochondria), ER (endoplasmic reticulum),

Nuc (nucleus), and Fil (filaments). Scale bar = 1 μm, 500 nm for inset A, 200 nm for inset B, and 100 nm for inset C.

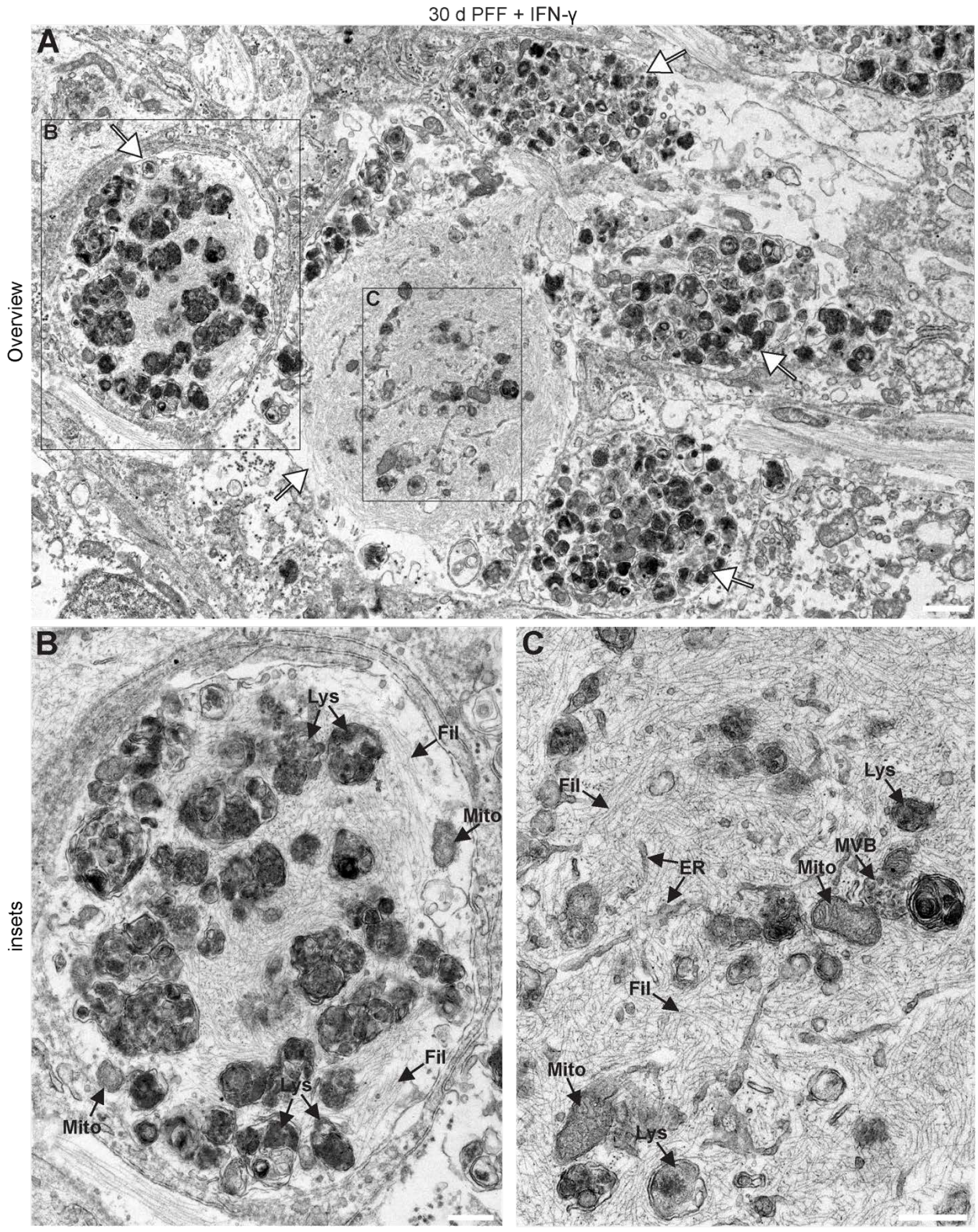
30 d PFF + IFN-γ
Overview
insets
A
B
C
Lys
Fil
Mito
ER
MVB

Figure 4.3

Highly dense, mature inclusions form in DA neurons with increased incubation time.

(**A**) DA neurons underwent the 14 d dual hit treatment regime and were then incubated for an additional 16 d, for a total of 30 d in culture since the beginning of the experiment. Since the end of the 14 d treatment, neurons were given fresh media every 3 d and incubated at 37°C. A large overview shows the presence of five inclusions (arrows) in close proximity. The inclusions appear to be at various stages of development within the neurites, some containing an extensive collection of cytoskeletal filaments (Fil). Magnified views of the enclosed areas are seen in **B** and **C**. Mito (Mitochondria), Lys (lysosome/autolysosome), MVB (multivesicular body). Scale bar = 1 μm and 0.5 μm for insets.

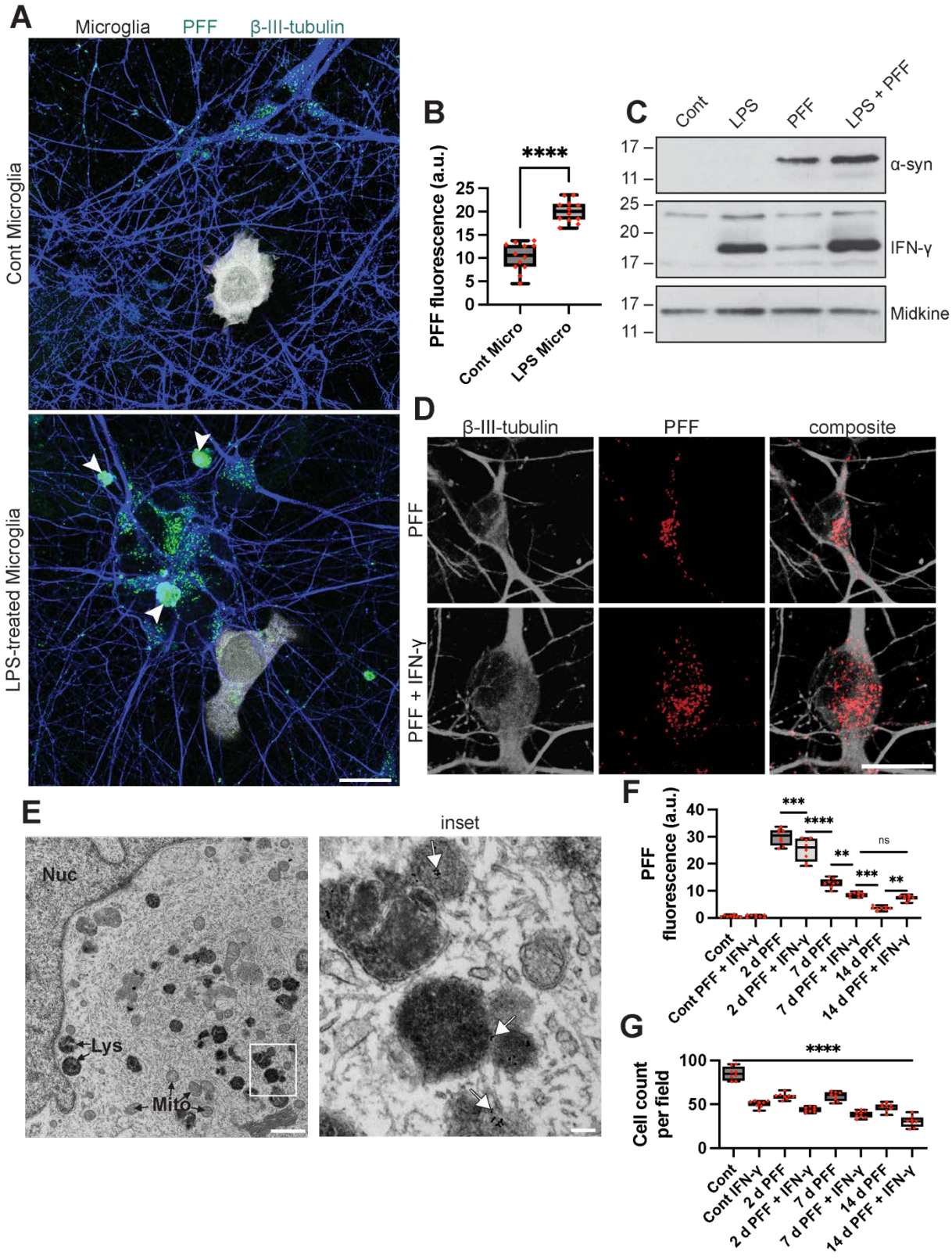
A
Microglia
PFF
β-III-tubulin
Cont Microglia
LPS-treated Microglia
B
PFF fluorescence (a.u.)
****
Cont Micro
LPS Micro
C
Cont
LPS
PFF
LPS + PFF
α-syn
IFN-γ
Midkine
D
β-III-tubulin
PFF
composite
PFF
PFF + IFN-γ
E
inset
Nuc
Lys
Mito
F
PFF fluorescence (a.u.)
Cont
Cont PFF + IFN-γ
2 d PFF
2 d PFF + IFN-γ
7 d PFF
7 d PFF + IFN-γ
14 d PFF
14 d PFF + IFN-γ
ns
G
Cell count per field
Cont
Cont IFN-γ
2 d PFF
2 d PFF + IFN-γ
7 d PFF
7 d PFF + IFN-γ
14 d PFF
14 d PFF + IFN-γ

Figure 4.4

Microglial co-culture led to inclusions in DA neurons while cortical neurons did not form inclusions with IFN-γ treatment

(**A**) DA neurons previously exposed to PFF for 48 h and given fresh media for 72 h were co-cultured with LPS-treated and PBS-treated microglia (previously treated with Cell Tracker Violet dye). Microglia, HMC3 cell line, were co-cultured with neurons for 48 h prior to sample fixation and staining for β-III-tubulin. Neurons co-cultured with PBS-treated (Cont) Microglia exhibited small PFF puncta, while those co-cultured with LPS-treated microglia showed large PFF-positive inclusions. Scale bar = 20 μm. (**B**) PFF fluorescence of DA neurons co-cultured with microglia treated with LPS (or PBS for control: Cont) was quantified where n = 12 for each condition, and data was collected from three independent experiments. (**C**) Microglia were treated with PBS (Cont), LPS, PFF, and PFF + LPS for 24 h. They were then washed with trypsin to remove PFF from the cell surface. They were washed three times with PBS, given serum-free media, and incubated for 48 h. Media were then collected, concentrated, and secreted proteins were analyzed for each condition. Equal amounts of protein from the media were resolved by SDS-PAGE followed by a WB to detect secretory proteins. Microglia treated with LPS, PFF, and LPS + PFF secreted IFN-γ, with the LPS + PFF condition showing the most IFN-γ expression. Microglia treated with PFF also secreted α-syn, with the LPS + PFF treated microglia showing higher levels of α-syn release. Midkine secretion is shown as a loading control. (**D**) iPSC-derived forebrain cortical neurons, derived from iPSCs, underwent the 14 d dual hit treatment, with the control receiving PBS treatment while the IFN-γ condition was exposed to IFN-γ. Scale bar = 20 μm. (**E**) Samples were prepared in the same way described in **D** but given nanogold-labeled PFF and prepared for EM. Dark lysosomes and autolysosomes are scattered across the cytosol and not

packed into inclusions; Lys (lysosomes and autolysosomes) and Mito (mitochondria). White arrows point to nanogold-labeled PFF. Scale bar = 1 μm and 100 nm for inset. (**F** and **G**) 14 d experiments were conducted to explore the effects of PFF and IFN-γ on cortical neurons with PFF fluorescence and cell count being quantified, n = 8 for each condition. Data were statistically analyzed using one-way ANOVA and PFF fluorescence data was further analyzed using *post-hoc* Tukey's test.

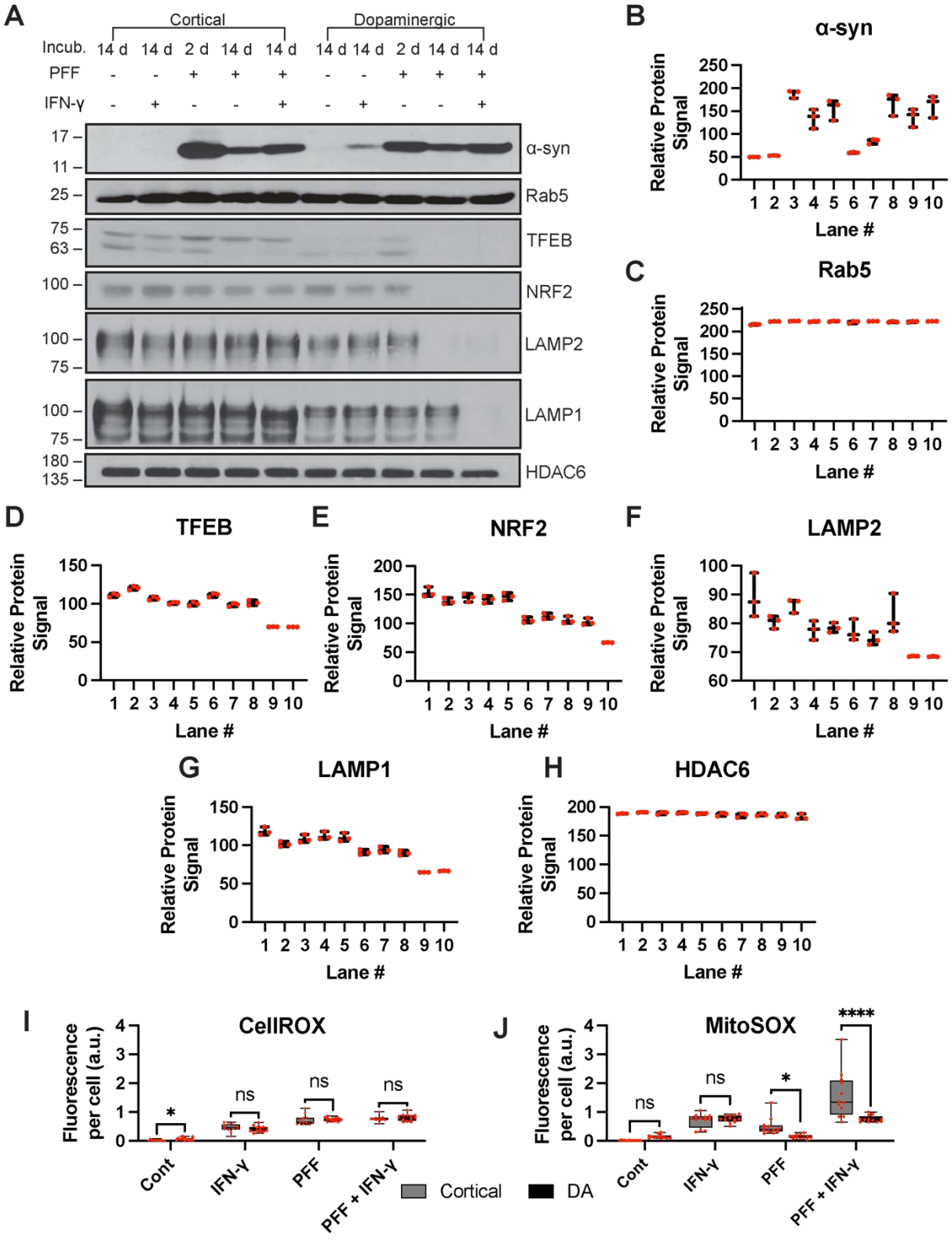
A
Cortical
Dopaminergic
Incub. 14 d 14 d 2 d 14 d 14 d 14 d 14 d 2 d 14 d 14 d
PFF - - + + + - - + + +
IFN-γ - + - - + - + - - +
17
11
25
75
63
100
100
75
100
75
180
135
α-syn
Rab5
TFEB
NRF2
LAMP2
LAMP1
HDAC6
B
α-syn
C
Rab5
D
TFEB
E
NRF2
F
LAMP2
G
LAMP1
H
HDAC6
Relative Protein Signal
Lane #
I
CellROX
J
MitoSOX
Fluorescence per cell (a.u.)
ns
*
****
Cont
IFN-γ
PFF
PFF + IFN-γ
Cortical
DA

Figure 4.5

The dual hit treatment resulted in the downregulation of lysosomal proteins.

(**A**) Protein expression in cortical and DA neurons were measured across five conditions. DA neurons show downregulation in LAMP1, LAMP2, NRF2, and TFEB, to a greater extent than cortical neurons in response to PFF and IFN-γ. At base line, LAMP1 and LAMP2 expression is much higher in cortical than in DA neurons. This is also the case with TFEB. Additionally, treatment with IFN-γ alone resulted in elevated α-syn expression in DA but not cortical neurons. (**B-H**) Protein expression was quantified across three independent Western blot experiments, using ImageJ. The mean gray value for each signal was quantified, subtracted from 255, and then plotted. (**I** and **J**) Cortical and DA neurons were plated onto separate glass-bottomed dishes, given CellROX and MitoSOX, and imaged live at 14 d across four conditions. n = 12 for each condition, collected from three independent experiments. Two-way ANOVA and *post-hoc* Tukey's test were done to compare each condition to the control. **** denotes $p < 0.0001$, ** denotes $p < 0.01$, and ns = not significant.

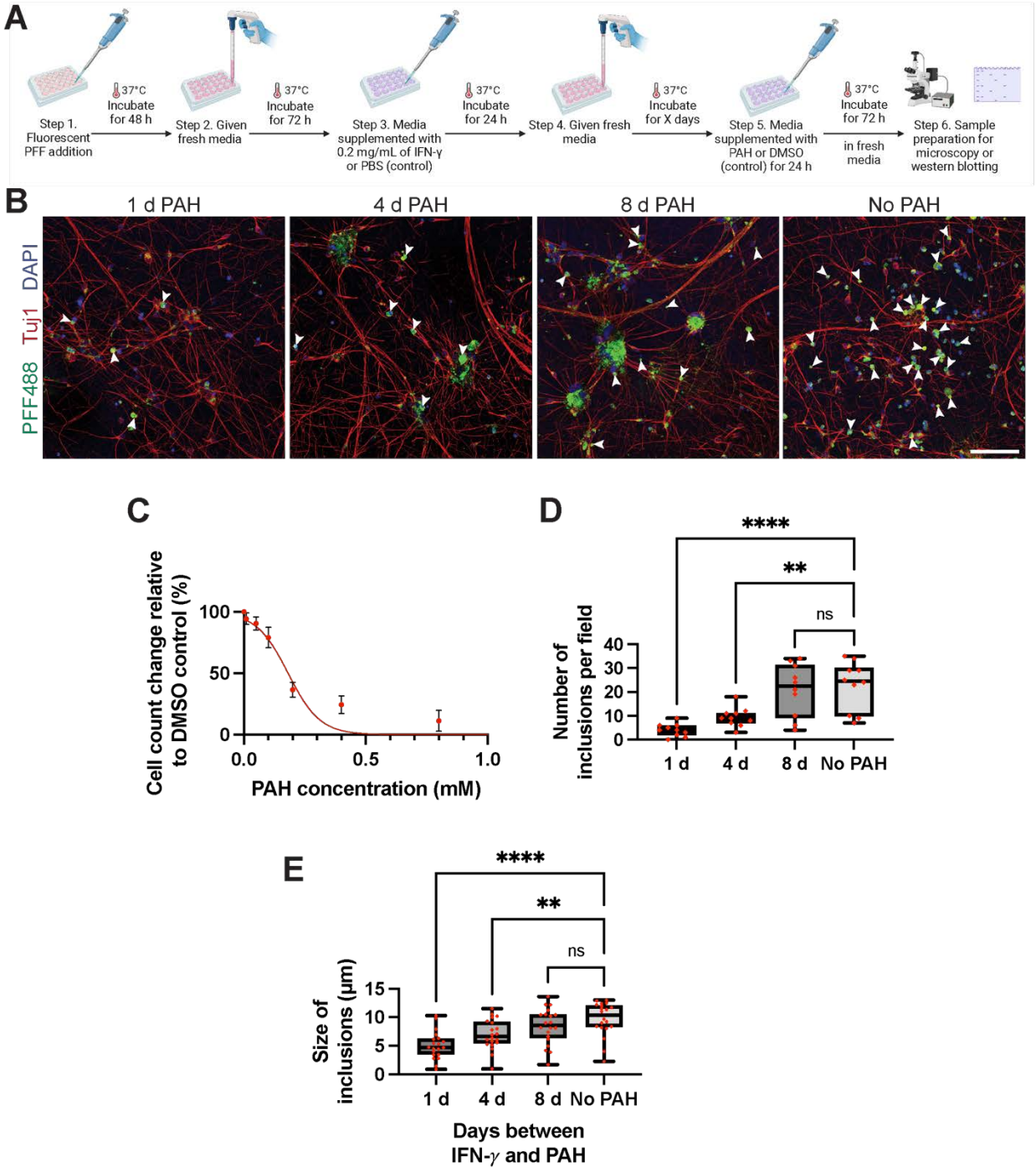
A
Step 1. Fluorescent PFF addition
37°C Incubate for 48 h
Step 2. Given fresh media
37°C Incubate for 72 h
Step 3. Media supplemented with 0.2 mg/mL of IFN-γ or PBS (control)
37°C Incubate for 24 h
Step 4. Given fresh media
37°C Incubate for X days
Step 5. Media supplemented with PAH or DMSO (control) for 24 h
37°C Incubate for 72 h in fresh media
Step 6. Sample preparation for microscopy or western blotting
B
1 d PAH
4 d PAH
8 d PAH
No PAH
PFF488 Tuj1 DAPI
C
Cell count change relative to DMSO control (%)
PAH concentration (mM)
D
Number of inclusions per field
****
**
ns
1 d
4 d
8 d
No PAH
E
Size of inclusions (µm)
Days between IFN-γ and PAH

Figure 4.6

PAH treatment reduces inclusion formation.

(**A**) An overview of the PFF, IFN-γ, and PAH treatment regime. DA neurons were given fluorescently labeled PFF for 48 h and then fresh media for 72 h, followed by treatment with IFN-γ for 24 h. All conditions were then given fresh media. PAH was administered at different time points following IFN-γ administration at a concentration of 10 μM. Some conditions received no PAH treatment (**B**) Neurons treated with PAH, or DMSO as a control, were fixed, stained with Tuj1 and DAPI, and prepared for fluorescence microscopy. Arrowheads point to PFF-positive inclusions. Scale bar = 80 μm. (**C**) PAH concentration was determined through a cell survival experiment, where DA NPCs were differentiated into neurons on 24-well plates. They were then treated with different concentrations of PAH for 24 h, stained with Hoechst, and the fluorescence of each well was calculated using a plate reader, with laser excitation set at 400 nm and emission detectors set to 450 nm. A rapid decline in neuronal survival occurs at concentrations higher than 0.2 mM. n = 6 for each condition. A log (agonist) vs. normalized response function was used to calculate the survival curve. (**D**) The number of inclusions per field (387.5 μm by 387.5 μm) was quantified with inclusions larger than 2.0 μm being incorporated in the calculation, n = 10 for each condition, and data was collected from five independent experiments. (**E**) The size of inclusions in each condition was calculated following thresholding of images to exclude faint and smaller PFF puncta, n = 20 for each condition, and data was collected from five independent experiments. Data in **D** and **E** were analyzed using one-way ANOVA and *post hoc* Tukey's test.

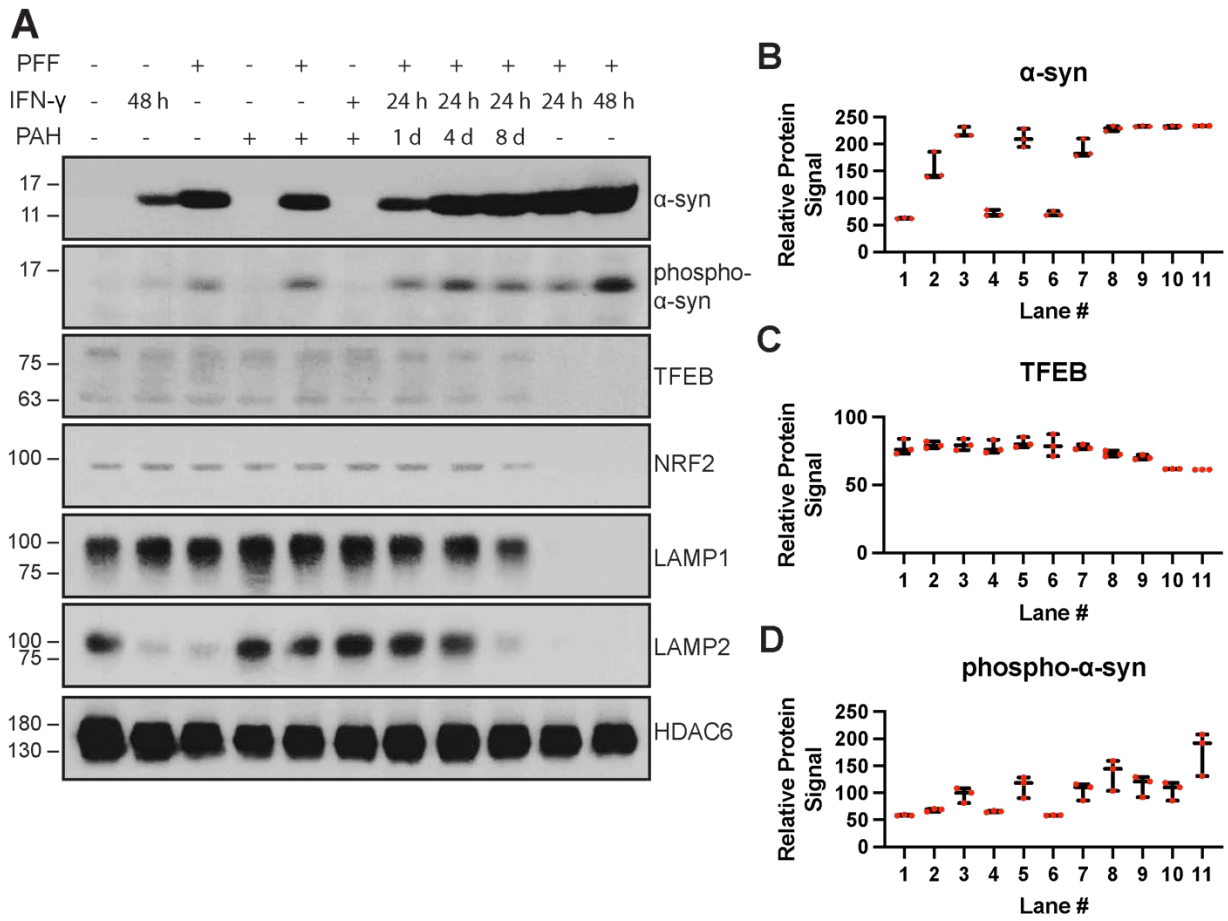
A
PFF - - + - + - + + + + +
IFN-γ - 48 h - - - + 24 h 24 h 24 h 24 h 48 h
PAH - - - + + + 1 d 4 d 8 d - -
17 –
11 –
α-syn
17 –
phospho-α-syn
75 –
63 –
TFEB
100 –
NRF2
100 –
75 –
LAMP1
100 –
75 –
LAMP2
180 –
130 –
HDAC6
B
α-syn
Relative Protein Signal
Lane #
C
TFEB
Relative Protein Signal
Lane #
D
phospho-α-syn
Relative Protein Signal
Lane #

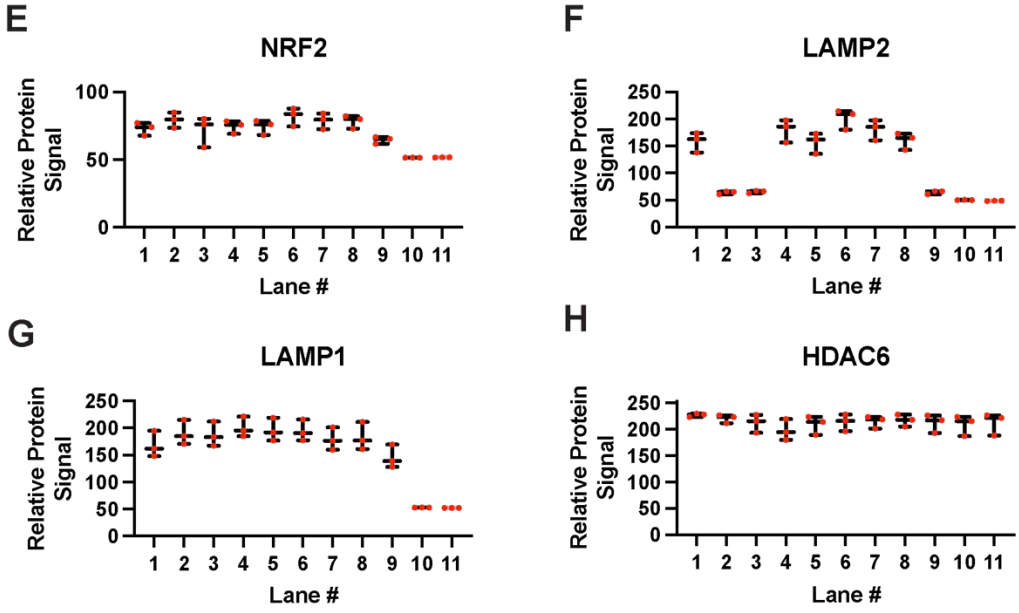
E
NRF2
Relative Protein Signal
Lane #
F
LAMP2
Relative Protein Signal
Lane #
G
LAMP1
Relative Protein Signal
Lane #
H
HDAC6
Relative Protein Signal
Lane #

Figure 4.7

PAH restores lysosomal protein expression.

(**A**) Western blot was conducted to analyze protein expression changes in response to PAH exposure in DA neurons that underwent the treatment described in Figure 4.6 A. (**B**-**H**) Protein expression was quantified across three independent Western blot experiments, using ImageJ. The mean gray value for each signal was quantified, subtracted from 255, and then plotted. An increase in IFN-γ incubation time results in even more α-syn signal coupled with a higher phospho-α-syn signal. A decrease in the time between PAH treatment following IFN-γ results in the upregulation of LAMP1, LAMP2, TFEB, and NRF2.

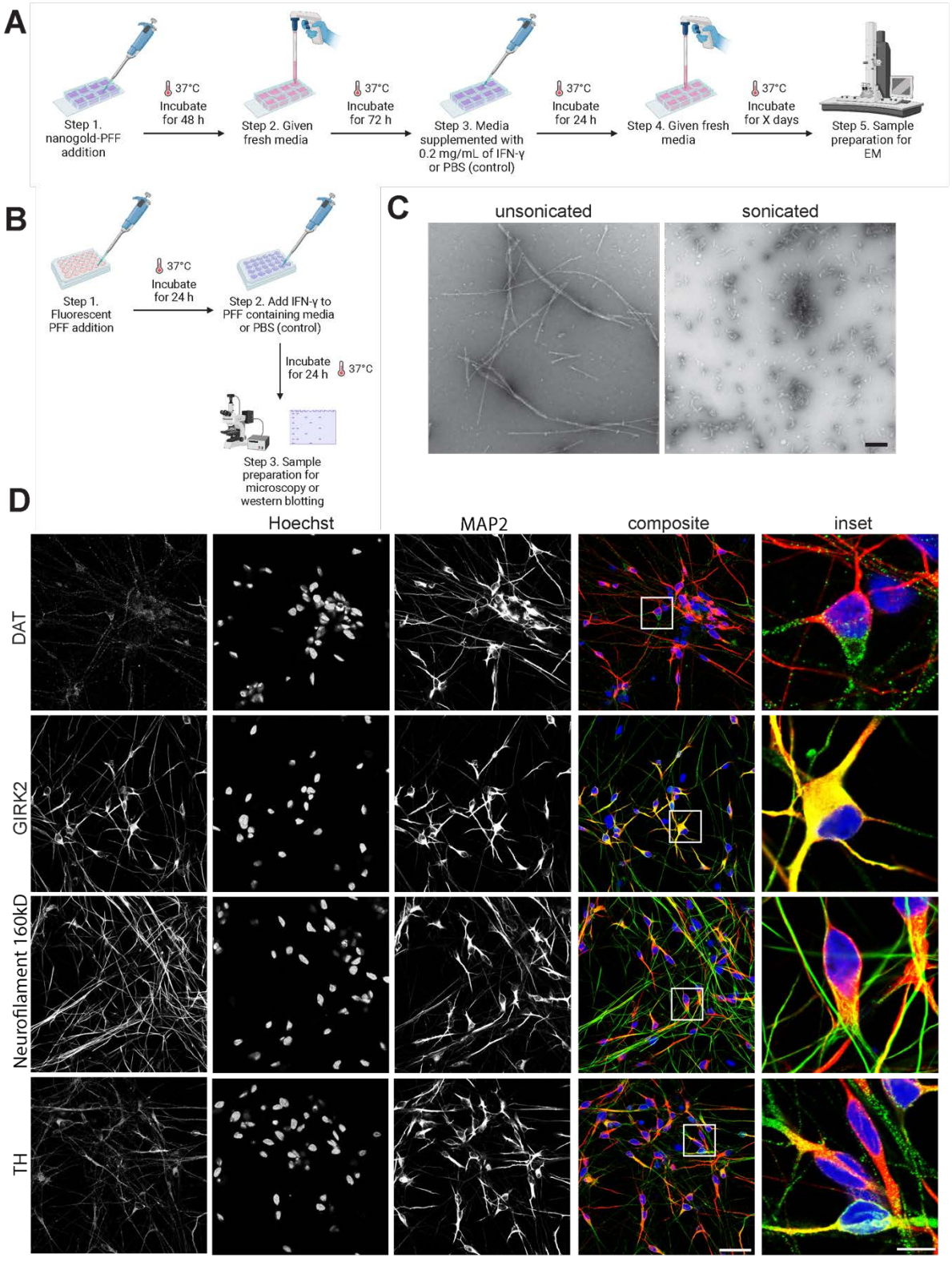
A
Step 1. nanogold-PFF addition
37°C Incubate for 48 h
Step 2. Given fresh media
37°C Incubate for 72 h
Step 3. Media supplemented with 0.2 mg/mL of IFN-γ or PBS (control)
37°C Incubate for 24 h
Step 4. Given fresh media
37°C Incubate for X days
Step 5. Sample preparation for EM
B
Step 1. Fluorescent PFF addition
37°C Incubate for 24 h
Step 2. Add IFN-γ to PFF containing media or PBS (control)
Incubate for 24 h 37°C
Step 3. Sample preparation for microscopy or western blotting
C
unsonicated
sonicated
D
Hoechst
MAP2
composite
inset
DAT
GIRK2
Neurofilament 160kD
TH

Extended Data Figure 4.1

Dual hit treatment, PFF characterization, and neuronal characterization.

(**A**) Graphical representation for the dual hit treatment regime used for DA neurons grown and differentiated in 8 well permanox chambers. (**B**) Graphical representation of the shortened dual hit treatment protocol for the 2 d time point. (**C**) Characterization of unsonicated (full length) and sonicated α-syn fibrils. Scale bar = 200 nm. (**D**) DA neurons that were differentiated and matured were characterized using the following antibodies: Dopamine Transporter (DAT), GIRK2, Neurofilaments (160kD), and Tyrosine Hydroxylase (TH). Neurons were also positive for MAP2. While DAT and TH confirm the dopaminergic identity of the neurons, GIRK2 specifies the regional specificity of these DA neurons to the substantia nigra. MAP2 and Neurofilaments confirm the neuronal maturity of the neurons.

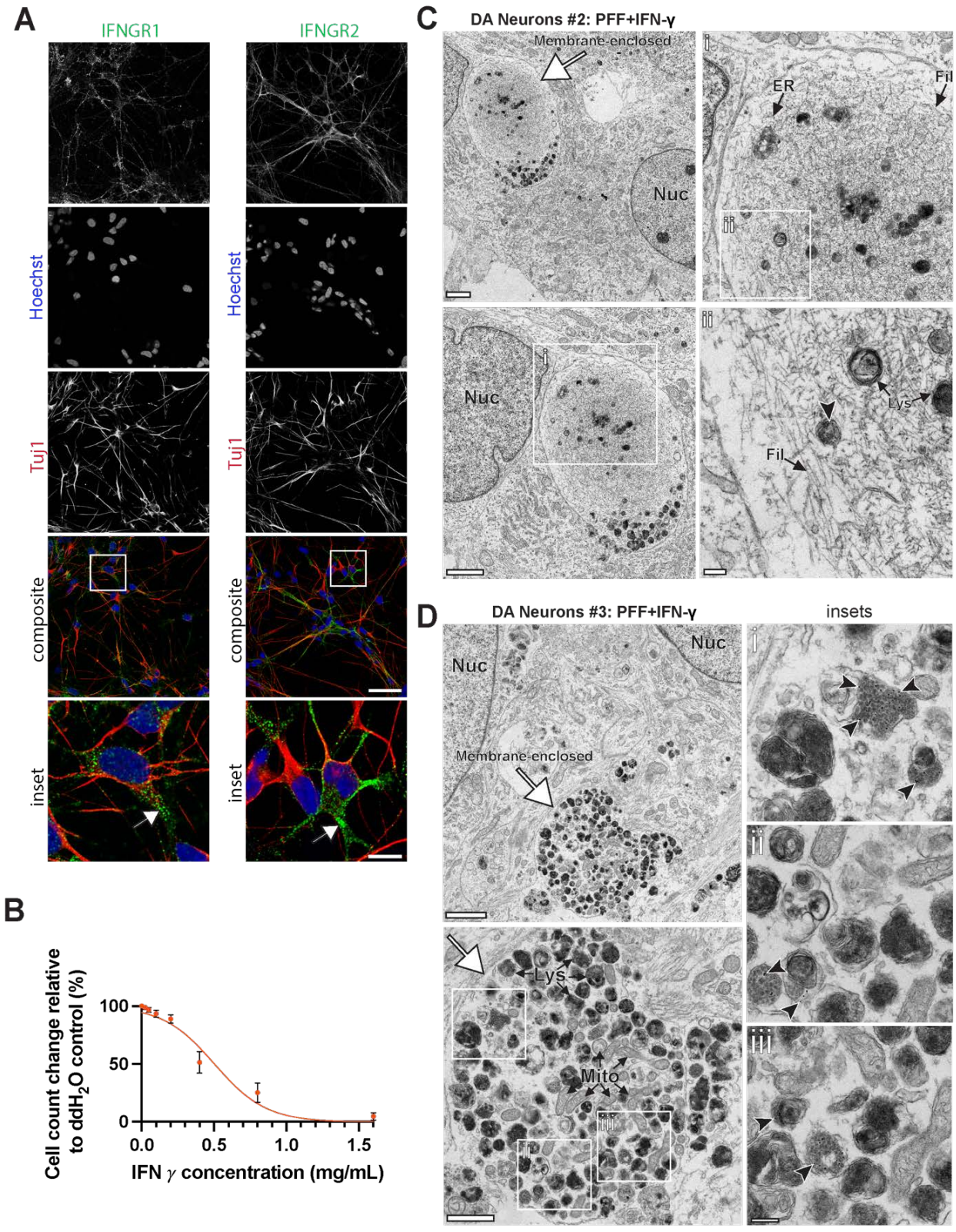
A
IFNGR1
IFNGR2
Hoechst
Tuj1
composite
inset
B
Cell count change relative to ddH2O control (%)
100
50
0
0.0
0.5
1.0
1.5
IFN γ concentration (mg/mL)
C
DA Neurons #2: PFF+IFN-γ
Membrane-enclosed
Nuc
ER
Fil
Lys
D
DA Neurons #3: PFF+IFN-γ
insets
Membrane-enclosed
Lys
Mito

Extended Data Figure 4.2

IFN-γ receptor expression, IFN-γ dose-response curve, and inclusions in DA neurons from other iPSC cell lines.

(**A**) Antibodies against IFN-γ receptors 1 and 2 were used to illustrate the expression of these receptors in DA neurons. Scale bars = 40 μm and 10 μm for insets. (**B**) The dose-response curve for the concentration of IFN-γ used and the corresponding cell count, using Hoechst to stain nuclei. Cells were counted using plate reader (Tecnai). (**C**) Inclusions found within DA neurons generated from the DYR-0100 line (cell line #2). An exceptionally large inclusion that is mostly filled with filamentous materials, with islands of organelles, can be observed. Scale bars = 2 μm, 1μm and 200 nm, respectively from lowest to highest magnification images. (**D**) A mostly lysosomal- and mitochondrial-filled inclusion generated in 3450 iPSC DA neurons (cell line #3). Scale bar = 2 μm for large field, 1 μm for inclusion, and 200 nm for insets. Lysosomes/autolysosomes (Lys), mitochondria (Mito), filaments (Fil), endoplasmic reticulum (ER), white arrows point to the membrane surrounding the inclusions, and dark arrowheads point to a few examples of nanogold-labeled PFF inside lytic vesicles.

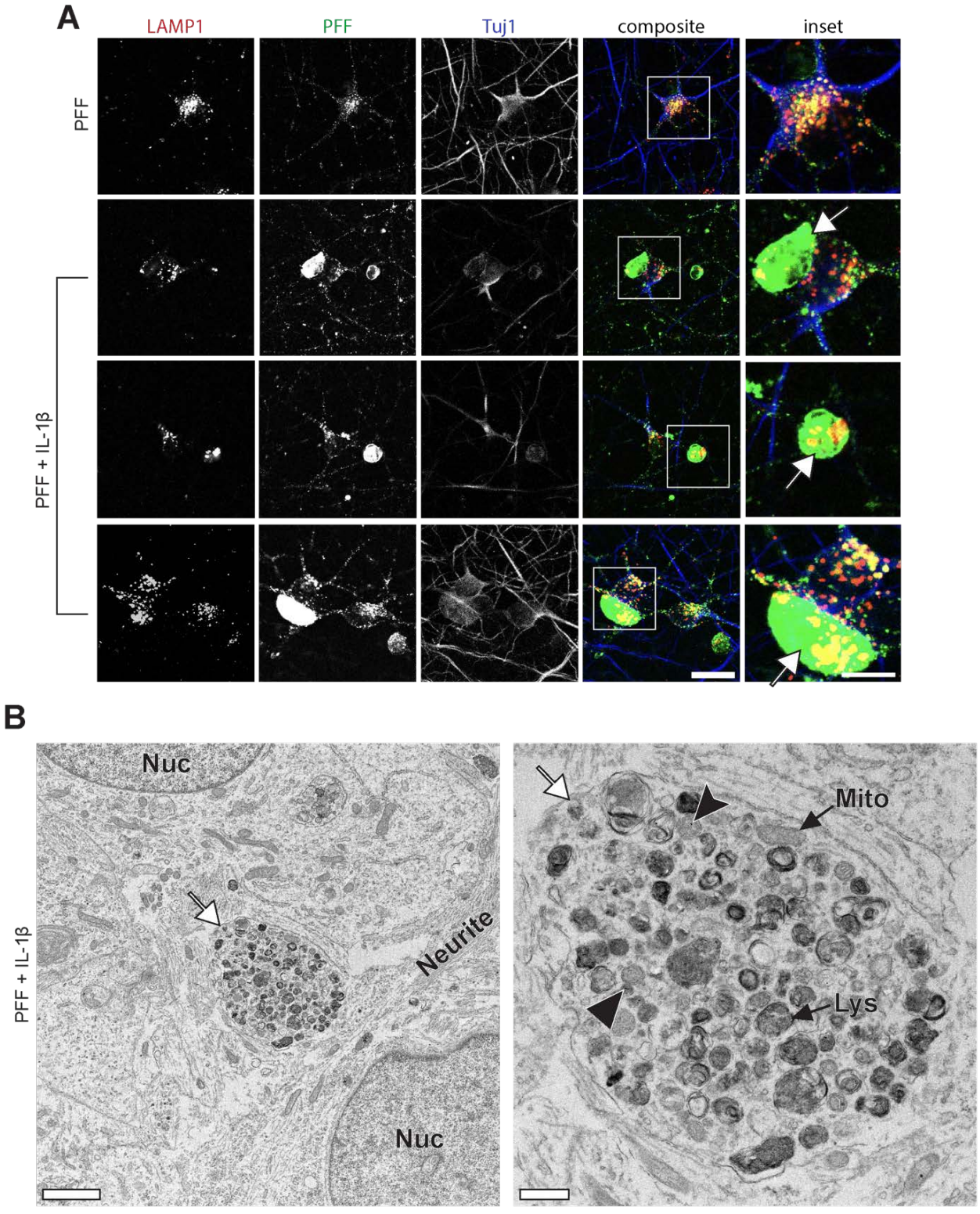
A
LAMP1
PFF
Tuj1
composite
inset
PFF
PFF + IL-1β
B
Nuc
Neurite
Nuc
Mito
Lys
PFF + IL-1β

Extended Data Figure 4.3

IL-1β administration following PFF treatment also leads to the formation of PFF-positive inclusions.

(**A**) DA neurons were treated with PFF for 48 h, followed by 72 h rest following administration of 50 ng/mL of IL-1β for 24 h. The cells were then incubated in fresh media until day 14. Neurons were stained for LAMP1 and Tuj1. IL-1β data treated cells formed PFF-positive inclusions. Scale bar = 20 μm and 10 μm for insets. (**B**) Inclusions formed in neurons following dual hit treatment regime using IL-1β. Lysosomes/autolysosomes (Lys), mitochondria (Mito), white arrows point to the membrane surrounding the inclusions, and dark arrowheads point to a few examples of nanogold-labeled PFF inside lytic vesicles. Scale bar = 2 μm and 0.5 μm for insets.

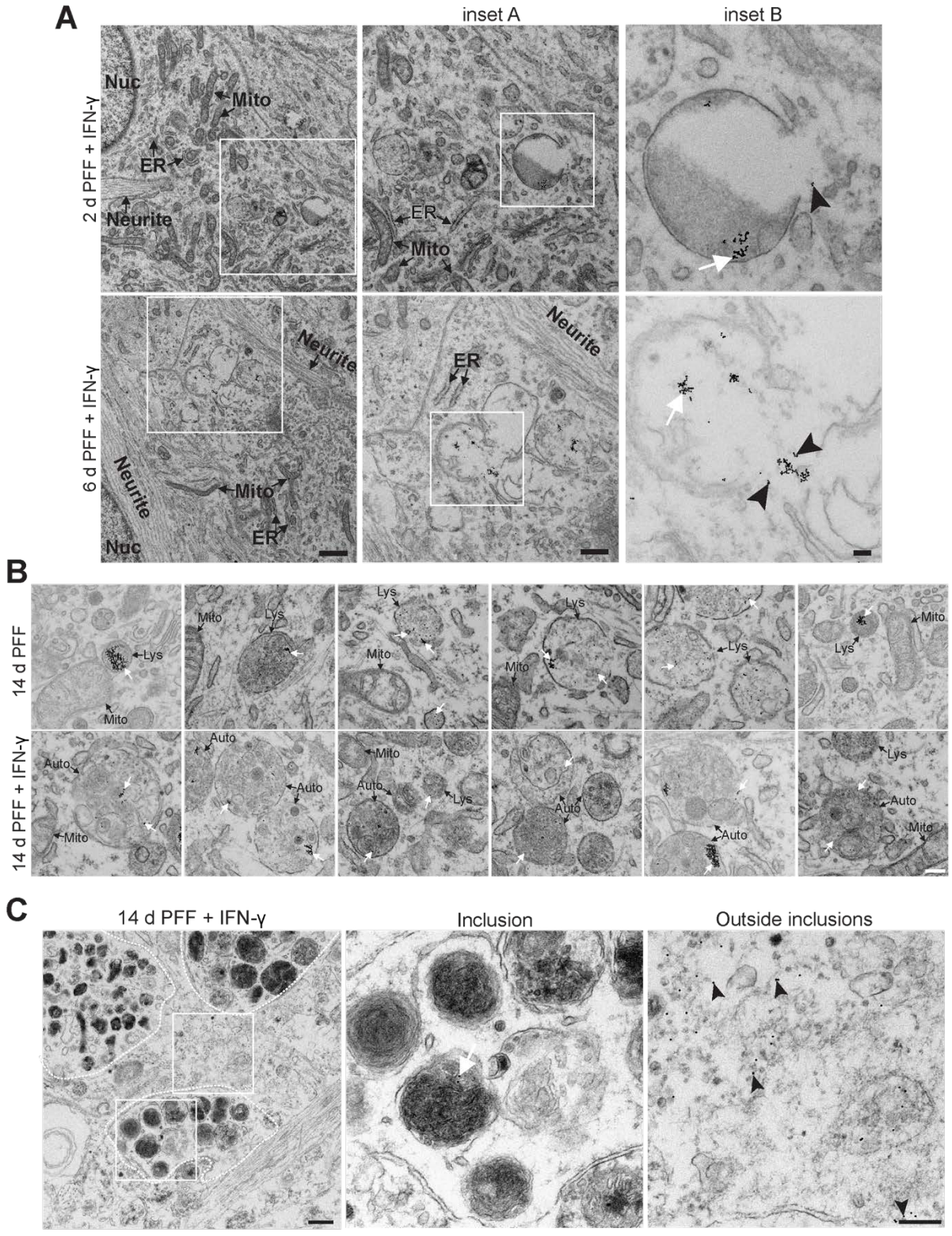
A
inset A
inset B
2 d PFF + IFN-γ
6 d PFF + IFN-γ
Nuc
Mito
ER
Neurite
B
14 d PFF
14 d PFF + IFN-γ
Lys
Mito
Auto
C
14 d PFF + IFN-γ
Inclusion
Outside inclusions

Extended Data Figure 4.4

Lysosomal leakage of PFFs occurs in PFF + IFN-γ treated samples.

(**A**) DA neurons that underwent the dual hit treatment regime and the more rapid 2 d treatment were fixed and processed for EM. PFFs can be seen accumulating in lysosomes, and some can be spotted outside of lysosomes as early as 2 d. More evidence for the leaking of PFFs into the cytosol can be seen with the 6 d samples. White arrows point to nanogold-labeled PFF inside lysosomal/autolysosome compartments, and arrowheads point to nanogold-labeled PFF outside lysosomes and in the cytosol. Few examples of endoplasmic reticulum (ER), mitochondria (Mito), and nuclei (Nuc) have been indicated. Scale bar = 1 μm, and 0.5 μm for inset A, and 100 nm for inset B. (**B**) Lytic compartments showing nanogold-PFF localization differ in the 14 d PFF-treated and the 14 d PFF + IFN-γ-treated samples. In the 14 d PFF-treated samples, very few nanogold-PFFs can be seen inside autolysosomes/autophagosomes, and lysosomes contain most of the internalized pool PFFs. In the 14 d PFF + IFN-γ-treated samples, PFFs are mostly localized in autolysosomes and autophagosomes. An accumulation of autolysosomes and autophagosomes can be seen in the PFF + IFN-γ-treated samples which are not present in the PFF-only samples. White arrows point to nanogold-labeled PFF inside lysosomal/autolysosome compartments. Scale bar = 200 nm. (**C**) In neurons where inclusions have formed, clear evidence of PFF leakage into the cytosol can be seen. Arrowheads point to cytosolic PFF. Scale bar = 500 nm and 200 nm for inset.

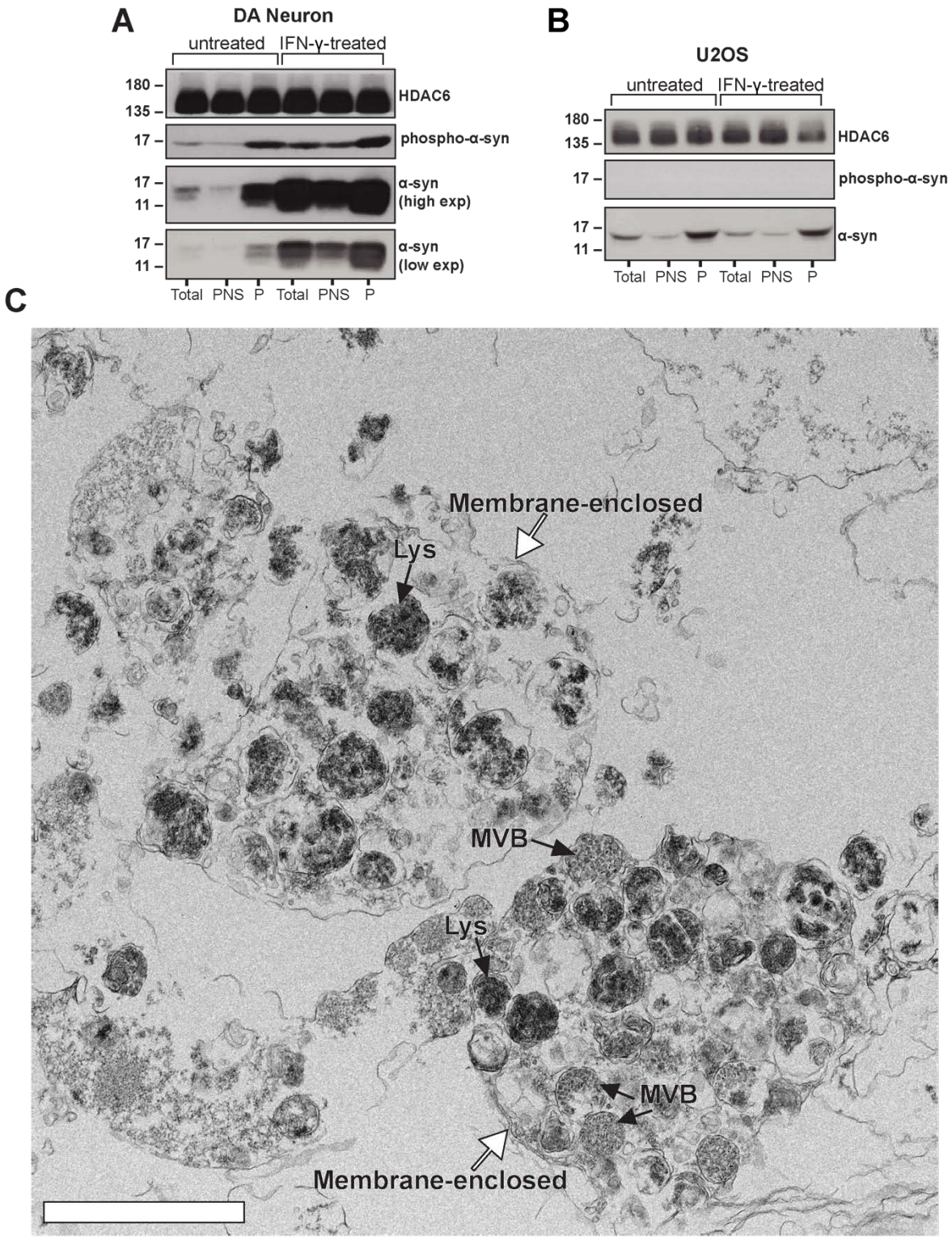
A
DA Neuron
untreated
IFN-γ-treated
180 –
135 –
HDAC6
17 –
phospho-α-syn
17 –
11 –
α-syn
(high exp)
17 –
11 –
α-syn
(low exp)
Total PNS P Total PNS P
B
U2OS
untreated
IFN-γ-treated
180 –
135 –
HDAC6
17 –
phospho-α-syn
17 –
11 –
α-syn
Total PNS P Total PNS P
C
Membrane-enclosed
Lys
MVB
Lys
MVB
Membrane-enclosed

Extended Data Figure 4.5

Isolation of inclusions formed in DA neurons.

(**A** and **B**) α-syn WB in DA neurons and U2OS in different subcellular fractions. In DA neurons, the LB-like inclusions and some enlarged lysosomes were pelleted at low speed after cellular homogenization in a detergent-free buffer. Control DA, where only PFF is added, shows the enrichment of α-syn in large organelles found in the pellet (P) compared to the total homogenate (total) and post-nuclear supernatant (PNS). IFN-γ-treated DA shows a much greater α-syn enrichment in the pellet, where more LB-like inclusions are collected compared to the control. In U2OS, where no LB-like inclusions are formed, no significant enrichment of α -syn was seen in the pellet, and no difference was observed between control and IFN-γ-treated cells. HDAC6 WB is shown as a loading control. Note that the difference in the total α-syn signal in the PFF condition compared to the PFF + IFN-γ-treated samples indicate a much more active degradation system in the PFF-only neurons compared to the PFF + IFN-γ-treated ones. Also note the double band in the α-syn signal, present only in DA and not U2OS cells. This is an indication of phosphorylation. (**C**) Inclusions isolated by subcellular fractionation were fixed, embedded, and sectioned for EM. Inclusions imaged were membrane-enclosed with the same morphology as those found in DA neurons. Lysosomes/autolysosomes (Lys), mitochondria (Mito), multivesicular bodies (MVB), and white arrows point to the membrane surrounding the inclusions. Scale bar = 2 μm.

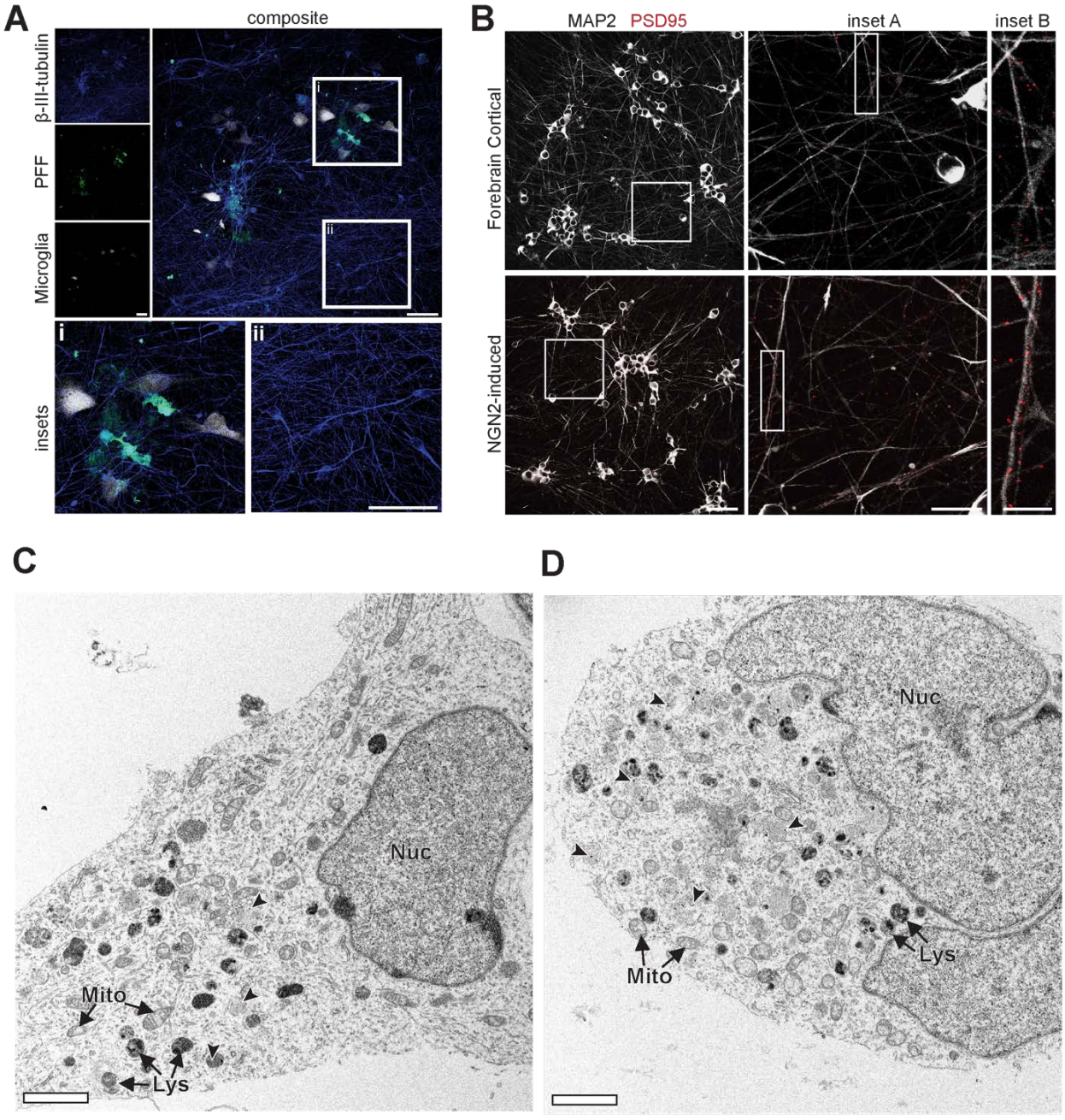
A
composite
β-III-tubulin
PFF
Microglia
insets
i
ii
B
MAP2 PSD95
inset A
inset B
Forebrain Cortical
NGN2-induced
C
Nuc
Mito
Lys
D
Nuc
Mito
Lys

Extended Data Figure 4.6

Microglia-neuron co-culture, characterization of forebrain and NGN2-induced neurons, and NGN2-induced neurons did not form inclusions.

(**A**) Microglia, treated with LPS, were co-cultured with differentiated DA neurons with previous exposure to fluorescently labeled PFFs. Neurons near microglia were seen to form PFF-positive inclusions, as shown in **i**. Neurons not in proximity to microglia did not form inclusions and showed lower PFF fluorescence, as shown in **ii**. Scale bar = 80 μm and 50 μm for insets. (**B**) Cortical and NGN2-induced neurons were characterized using microtubule-associated protein 2 (MAP2) and post-synaptic density 95 (PSD95). Using a broad-spectrum induction process, forebrain cortical neurons derived from iPSC include excitatory and inhibitory neurons. NGN2-induced neurons are exclusively excitatory neurons and hence showed much higher levels of PSD95 fluorescence. Scale bar = 80 μm, 20 μm for inset A, and 5 μm for inset B. (**C** and **D**) EM images showing NGN2-induced excitatory neurons filled with swollen mitochondria and dark lysosomes; however, these compartments are not packaged into inclusions. Lysosomes/autolysosomes (Lys), mitochondria (Mito), and dark arrowheads point to examples of nanogold-labeled PFF inside lytic vesicles. Scale bar = 2 μm.

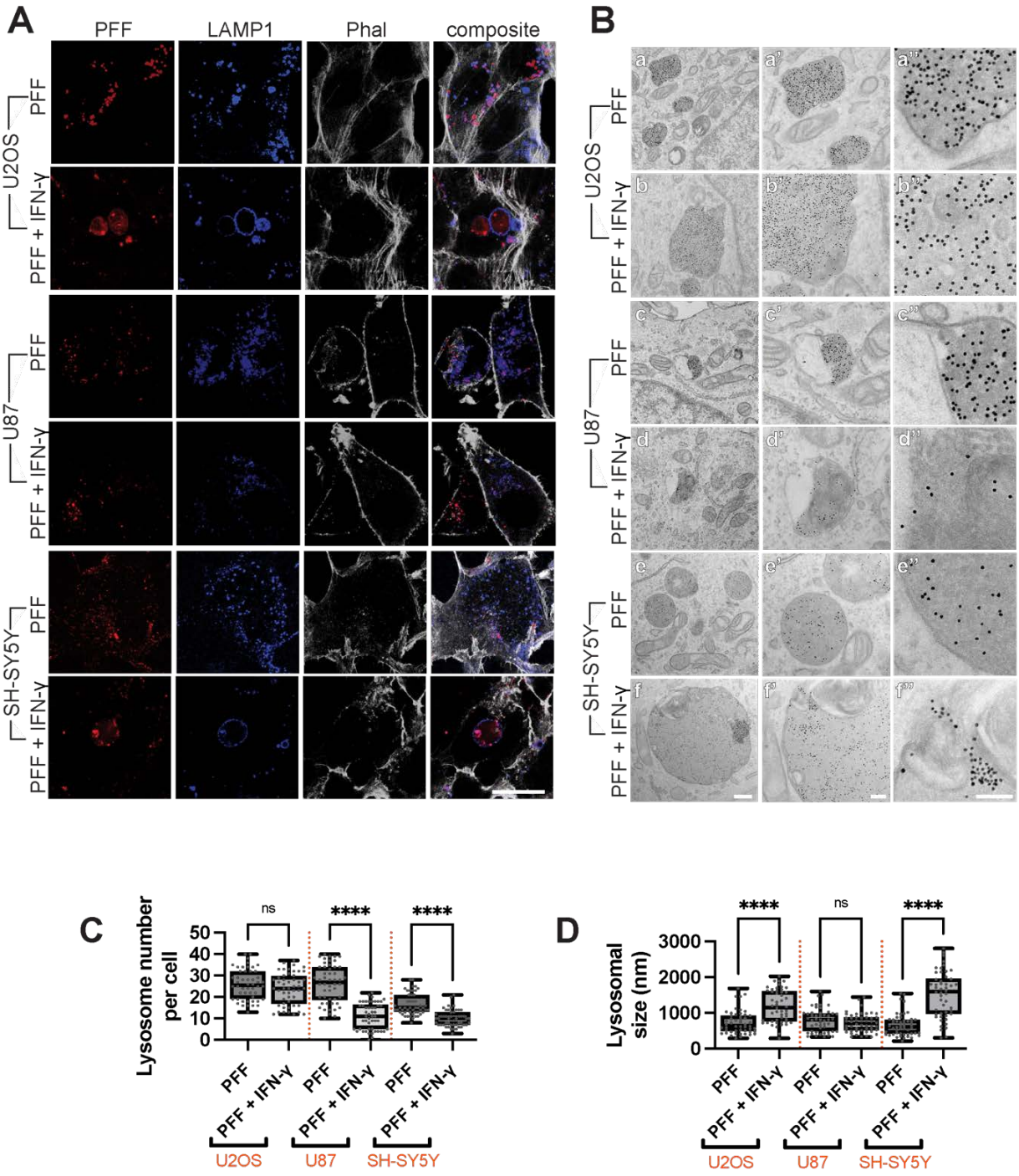
A
PFF
LAMP1
Phal
composite
U2OS
PFF
PFF + IFN-γ
U87
PFF
PFF + IFN-γ
SH-SY5Y
PFF
PFF + IFN-γ
B
U2OS
PFF
PFF + IFN-γ
U87
PFF
PFF + IFN-γ
SH-SY5Y
PFF
PFF + IFN-γ
C
Lysosome number per cell
50
40
30
20
10
0
ns
****
****
PFF
PFF + IFN-γ
PFF
PFF + IFN-γ
PFF
PFF + IFN-γ
U2OS
U87
SH-SY5Y
D
Lysosomal size (nm)
3000
2000
1000
0
****
ns
****
PFF
PFF + IFN-γ
PFF
PFF + IFN-γ
PFF
PFF + IFN-γ
U2OS
U87
SH-SY5Y

Extended Data Figure 4.7

Cell lines do not form LB-like inclusions but show signs of lysosomal dysfunction.

(**A**) U2OS, U87, and SH-SY5Y cells were given PFF and grown on 6-well plates before being passaged onto coverslips at low confluency to be treated with IFN-γ or PBS (control). Cells were then incubated for 8 d prior to fixation. Cells only given PFF showed LAMP1-PFF colocalization. U2OS and SH-SY5Y cells treated with PFF + IFN-γ formed large lysosomal structures, while U87 cells exhibited a loss in LAMP1 staining. Scale bar = 25 μm. (**B**) Cells underwent the 14 d dual hit treatment regime, described in **A**, except that they were given nanogold-labeled PFF and grown on 6-well plates prior to being passaged onto 8-well permanox chambers. They were then treated with IFN-γ or PBS and prepared for EM. U2OS and SH-SY5Y treated with PFF showed an accumulation of nanogold-PFF in electron-dense lysosomes. U2OS and SH-SY5Y cells treated with PFF + IFN-γ showed large lysosomal structures containing high amounts of nanogold-PFF. U87 cells exhibited abnormal lysosomal morphology in both IFN-γ-treated and untreated samples. Scale bar for a-f is 500 nm, for a' to f' is 200 nm, and for a'' to f'' is 100 nm. (**C**) The number of lysosomes (LAMP1-positive puncta) was quantified. U87 and SH-SY5Y showed a significant decrease in lysosomal number, n = 50 for each condition, and data was collected from five independent experiments. (**D**) The lysosomal size was calculated using electron micrographs collected following the dual hit treatment. U2OS and SH-SY5Y showed a significant increase in lysosomal size with IFN-γ treatment, n = 50 for each condition. Data were collected from two independent experiments. Both data collected in **C** and **D** were analyzed using one-way ANOVA with *post-hoc* Tukey's test to compare means.

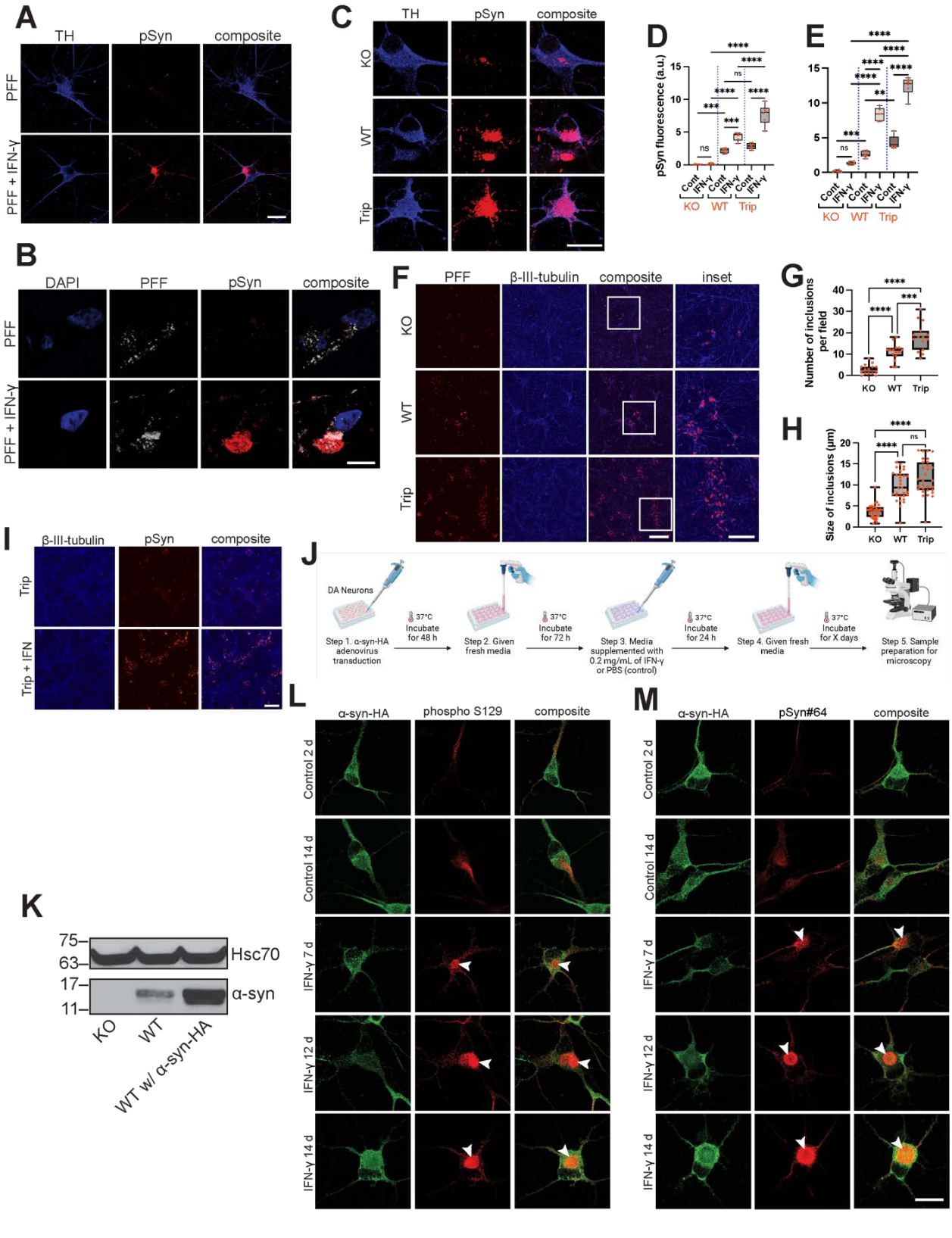
A
TH
pSyn
composite
PFF
PFF + IFN-γ
B
DAPI
PFF
pSyn
composite
C
TH
pSyn
composite
KO
WT
Trip
D
pSyn fluorescence (a.u.)
Cont
IFN-γ
KO
WT
Trip
E
F
PFF
β-III-tubulin
composite
inset
G
Number of inclusions per field
H
Size of inclusions (μm)
I
β-III-tubulin
pSyn
composite
Trip
Trip + IFN
J
DA Neurons
Step 1. α-syn-HA adenovirus transduction
37°C Incubate for 48 h
Step 2. Given fresh media
37°C Incubate for 72 h
Step 3. Media supplemented with 0.2 mg/mL of IFN-γ or PBS (control)
37°C Incubate for 24 h
Step 4. Given fresh media
37°C Incubate for X days
Step 5. Sample preparation for microscopy
K
75
63
17
11
Hsc70
α-syn
KO
WT
WT w/ α-syn-HA
L
α-syn-HA
phospho S129
composite
Control 2 d
Control 14 d
IFN-γ 7 d
IFN-γ 12 d
IFN-γ 14 d
M
α-syn-HA
pSyn#64
composite

Extended Data Figure 4.8

Phospho-α-syn is a marker for inclusions and is dependent on the endogenous pool of α-syn. (**A**) iPSC-derived DA neurons underwent the 14 d dual hit treatment regime, in which unlabeled PFFs were administered to neurons for 48 h, incubated in fresh media for 72 h, followed by the administration of IFN-γ (or PBS for control) for 24 h. Neurons were then incubated for 8 d in fresh media, fixed, and stained with tyrosine hydroxylase antibody (TH, blue) and phospho-α-syn (pSyn) antibody (red). Scale bar = 20 μm and 10 μm for insets. (**B**) Neurons underwent the same experiment as described in **A**, except fluorescent PFFs were used to ascertain localization. Both PFFs and phospho-α-syn localized to inclusions. Scale bar = 10μm. (**C**) DA NPCs derived from patient cells with *SNCA* triplication were knocked out to WT (two copies of *SNCA*) and KO (no *SNCA*). NPCs were then differentiated into neurons, and the dual hit treatment regime was carried out using unlabeled PFF. Scale bar = 20 μm. (**D**) Neurons with different levels of endogenous α-syn expression underwent the dual hit treatment regime without PFF treatment. (**E**) phospho-α-syn fluorescence was calculated in neurons that underwent the dual hit treatment regime with fluorescently labeled PFF, n = 6 for each condition. A threshold was set to exclude small and faint PFF puncta. (**F**) DA neurons with different number of copies of *SNCA* underwent the dual hit assay. Scale bar = 200 μm and 100 μm for insets. (**G**) The number of PFF-positive inclusions per field in experiment **F** were quantified, with only inclusions larger than 2.0 μm included in the calculation, n = 15 for each condition (**H**) Size of PFF-positive inclusions in the experiment described in **F**, were quantified, following thresholding. n = 30 for each condition, collected from three independent experiments. Data in **D**, **E**, **G**, and **H** were collected from three independent experiments, and one-way ANOVA and Tukey's test were used to analyze the data. **** denotes that $p < 0.0001$, *** denotes $p < 0.001$, ** denotes $p < 0.01$, and ns = not significant. (**I**) Phospho-

α-syn staining in SNCA triplication line (in absence of PFF) shows possible inclusions even without IFN-γ; however, number of inclusions is drastically increased with the treatment of IFN-γ for 24 h. Cells were maintained until 14 d and then fixed and stained. (**J**) Protocol used to form phospho-α-syn positive inclusions through α-syn overexpression. (**K**) WT DA neurons were transduced with α-syn-HA adenovirus DA for 48 h, given fresh media for 72 h, and collected for Western blotting. Transduced DA neurons showed higher levels of α-syn expression compared to WT and *SNCA* KO neurons. (**L** and **M**) WT neurons transduced with α-syn-HA adenovirus then underwent the dual hit treatment regime shown in **J**. Neurons were then fixed and stained for phospho-α-syn antibodies. Neurons not treated with IFN-γ did not form inclusions at the earlier time point, immediately following α-syn-HA adenovirus transduction at day 2, nor did they show inclusions at day 14. Neurons treated with IFN-γ begin showing accumulation of phospho-α-syn in the cell body at day 7. This accumulation becomes more apparent and more prominent with an increase in incubation time, leading to large phospho-α-syn positive accumulations (white arrowhead). Scale bar = 20 μm.

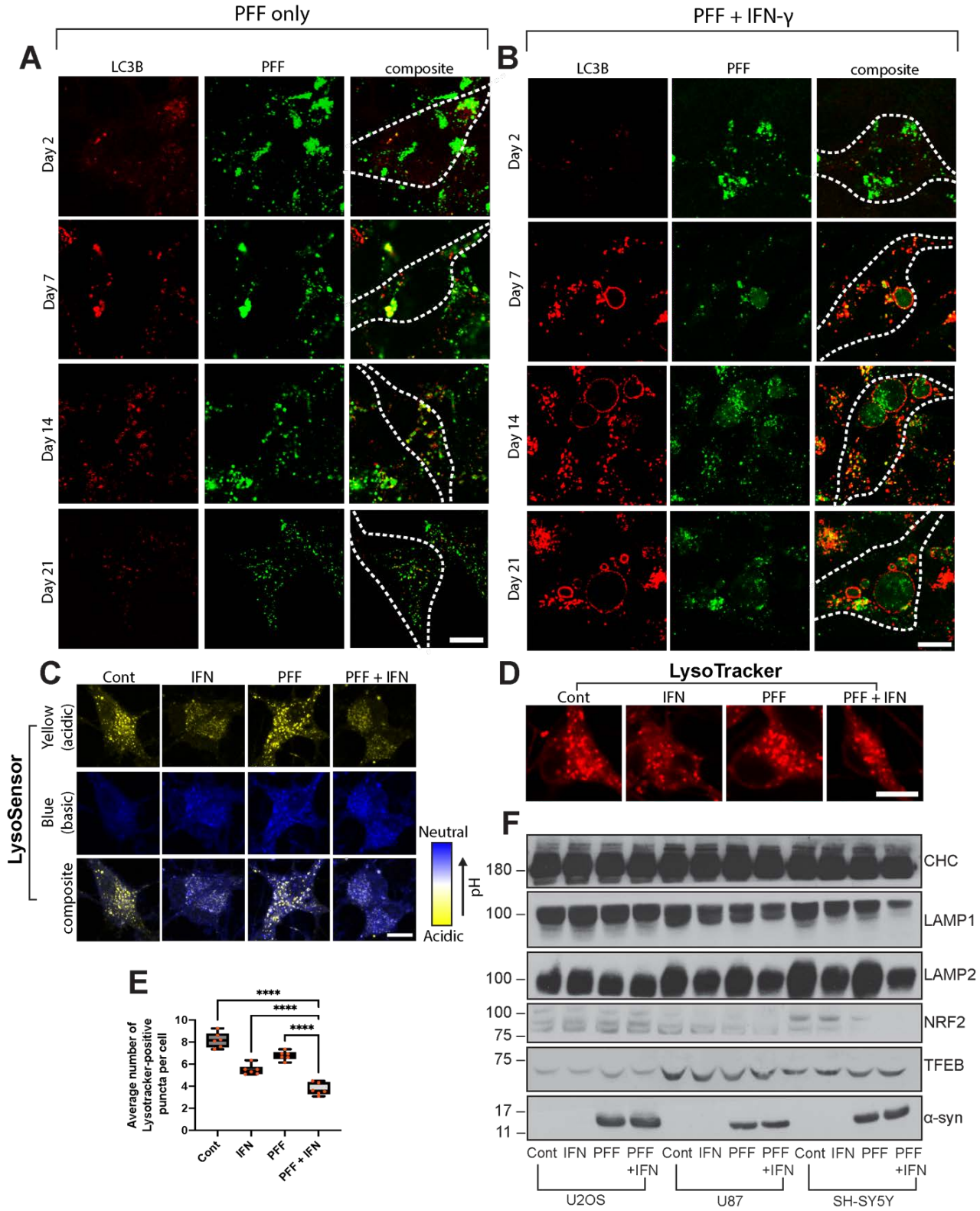
A
PFF only
LC3B
PFF
composite
Day 2
Day 7
Day 14
Day 21
B
PFF + IFN-γ
LC3B
PFF
composite
Day 2
Day 7
Day 14
Day 21
C
Cont
IFN
PFF
PFF + IFN
LysoSensor
Yellow (acidic)
Blue (basic)
composite
Neutral
pH
Acidic
D
LysoTracker
Cont
IFN
PFF
PFF + IFN
E
Average number of Lysotracker-positive puncta per cell
****
****
****
Cont
IFN
PFF
PFF + IFN
F
180
100
100
100
75
75
17
11
CHC
LAMP1
LAMP2
NRF2
TFEB
α-syn
Cont IFN PFF PFF +IFN Cont IFN PFF PFF +IFN Cont IFN PFF PFF +IFN
U2OS
U87
SH-SY5Y

Extended Data Figure 4.9

Inclusions forming in DA neurons are enveloped by LC3B, PFF and IFN-γ impair autophagic flux by altering lysosomal pH, and lysosomal proteins are also affected in cell lines undergoing the dual hit treatment.

(**A** and **B**) Neurons undergoing the 14 d treatment regime, were tracked overtime for their staining of LC3B. At day 2, just following the administration of PFF barely any LC3B staining can be seen. Following 48 h following IFN-γ administration on day 5, the PFF + IFN-γ sample show large LC3B positive structures. LC3B staining is also high in the PFF only samples, but the neurons in this condition do not possess large LC3B structures. While the LC3B staining abates in the PFF only sample following the passage of time, the LC3B staining in the PFF + IFN-γ sample remains high and large LC3B-positive autophagosomes still remain at 21 d. Scale bar = 10 μm. (**C**) Lysosomal acidity was ascertained in DA neurons at day 7 of the dual hit treatment regime using LysoSensor (Thermo Fisher Scientific). The IFN-γ-treated neurons showed much higher lysosomal pH (more blue staining) compared to the PFF-only and the control neurons. Scale bar = 10 μm. (**D**) Lysosomal pH was also tested using LysoTracker (Thermo Fisher Scientific) which fluoresces at a pH of ~ 6. Scale bar = 10 μm. (**E**) LysoTracker-positive punctae were counted using ImageJ (NIH) and divided by the number of cells per field across conditions. Data was collected from three independent experiments, (n=6 for each condition). One-way ANOVA and Tukey's test were used to analyze the data. **** denotes that $p < 0.0001$. (**F**) U2OS, U87, and SH-SY5Y cells were given PFF and grown on 6-well plates at low confluency to be treated with IFN-γ or PBS (control). Cells were then incubated for 8 d prior to collection. Protein expression in cells that underwent the 14 d dual hit treatment regime (with or without IFN-γ treatment), along with control (labeled as Cont,

No IFN-γ + No PFF) and IFN-γ were examined via WB. LAMP1, LAMP2, and NRF2 expression decreased with exposure to PFF and IFN-γ, while TFEB was unaffected.

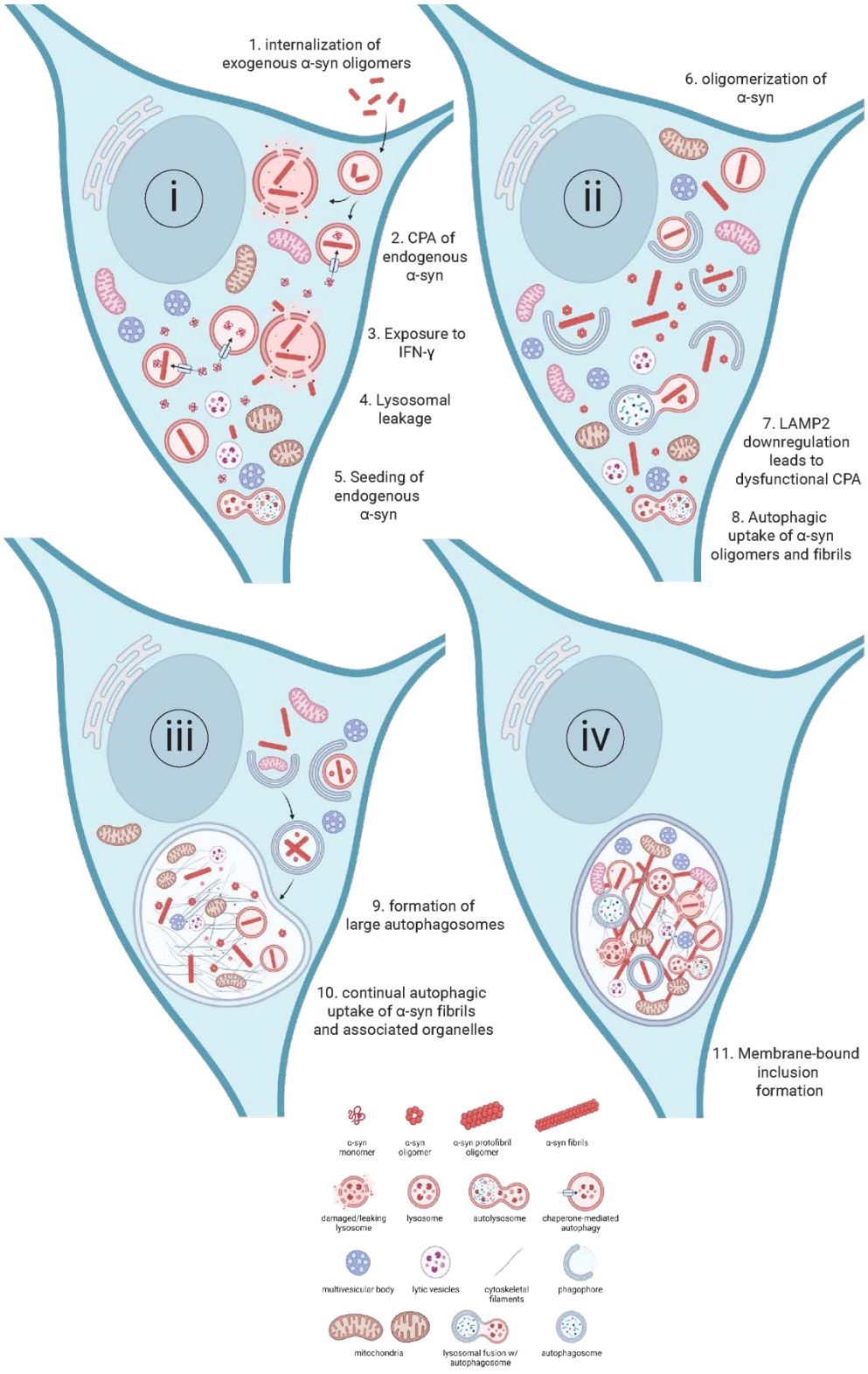
1. internalization of exogenous α-syn oligomers
i
2. CPA of endogenous α-syn
3. Exposure to IFN-γ
4. Lysosomal leakage
5. Seeding of endogenous α-syn
6. oligomerization of α-syn
ii
7. LAMP2 downregulation leads to dysfunctional CPA
8. Autophagic uptake of α-syn oligomers and fibrils
iii
9. formation of large autophagosomes
10. continual autophagic uptake of α-syn fibrils and associated organelles
iv
11. Membrane-bound inclusion formation
α-syn monomer
α-syn oligomer
α-syn protofibril oligomer
α-syn fibrils
damaged/leaking lysosome
lysosome
autolysosome
chaperone-mediated autophagy
multivesicular body
lytic vesicles
cytoskeletal filaments
phagophore
mitochondria
lysosomal fusion w/ autophagosome
autophagosome

Extended Data Figure 4.10

Possible mechanism for the formation of membrane-bound, membranous, organelle filled, LB-like inclusions.

The internalization of oligomeric forms of α-syn, released by neighboring neurons serves as the first insult to lysosomal activity (1). The transport of monomeric α-syn into lysosomes through chaperone-mediated autophagy (CPA) leads to aggregation of α-syn inside lysosomes (2). Further lysosomal stress caused by IFN-γ results in lysosomal leakage (3 and 4). Leaking of oligomeric/misfolded α-syn leads to seeding and oligomerization of endogenous α-syn into aggregates (5 and 6). Downregulation of LAMP2 leads to dysfunctional CPA, leading to a buildup of endogenous α-syn, allowing more α-syn to be available for aggregation (7). To clear aggregates from the cytosol, autophagosomes form and take up α-syn aggregates and damaged organelles (8). Dysfunctional lysosomes are unable to fuse with autophagosomes, and even when fused with autophagosomes, are unable to degrade organelles and aggregates. This leads to the enlargement of autophagosomes (9). α-syn aggregation continues within the lumen of the autophagosomes (10), leading to the formation of membrane-bound LB-like inclusions (11).

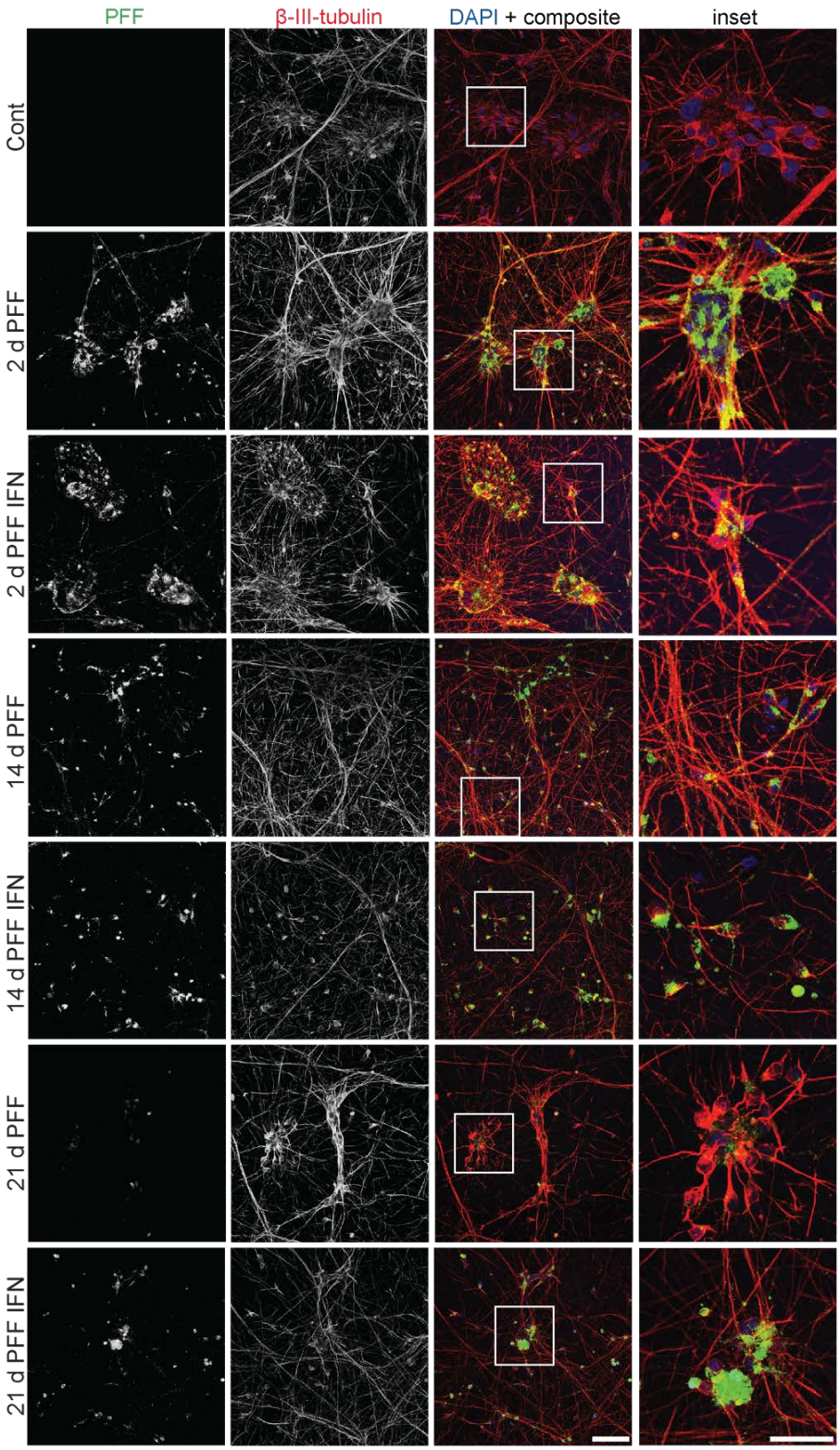
PFF
β-III-tubulin
DAPI + composite
inset
Cont
2 d PFF
2 d PFF IFN
14 d PFF
14 d PFF IFN
21 d PFF
21 d PFF IFN

Supplementary Figure 4.1

Overview of PFF staining over 21 days in DA neurons undergoing the treatment regime.

DA neurons underwent the dual-hit assay with fluorescent PFF as described previously, were stained with β-III-tubulin, and prepared for confocal microscopy. With the passage of time, PFF-only treated samples showed a decline in PFF fluorescence while PFF + IFN-γ treated samples formed inclusions. Scale bar = 80 μm and 40 μm for insets.

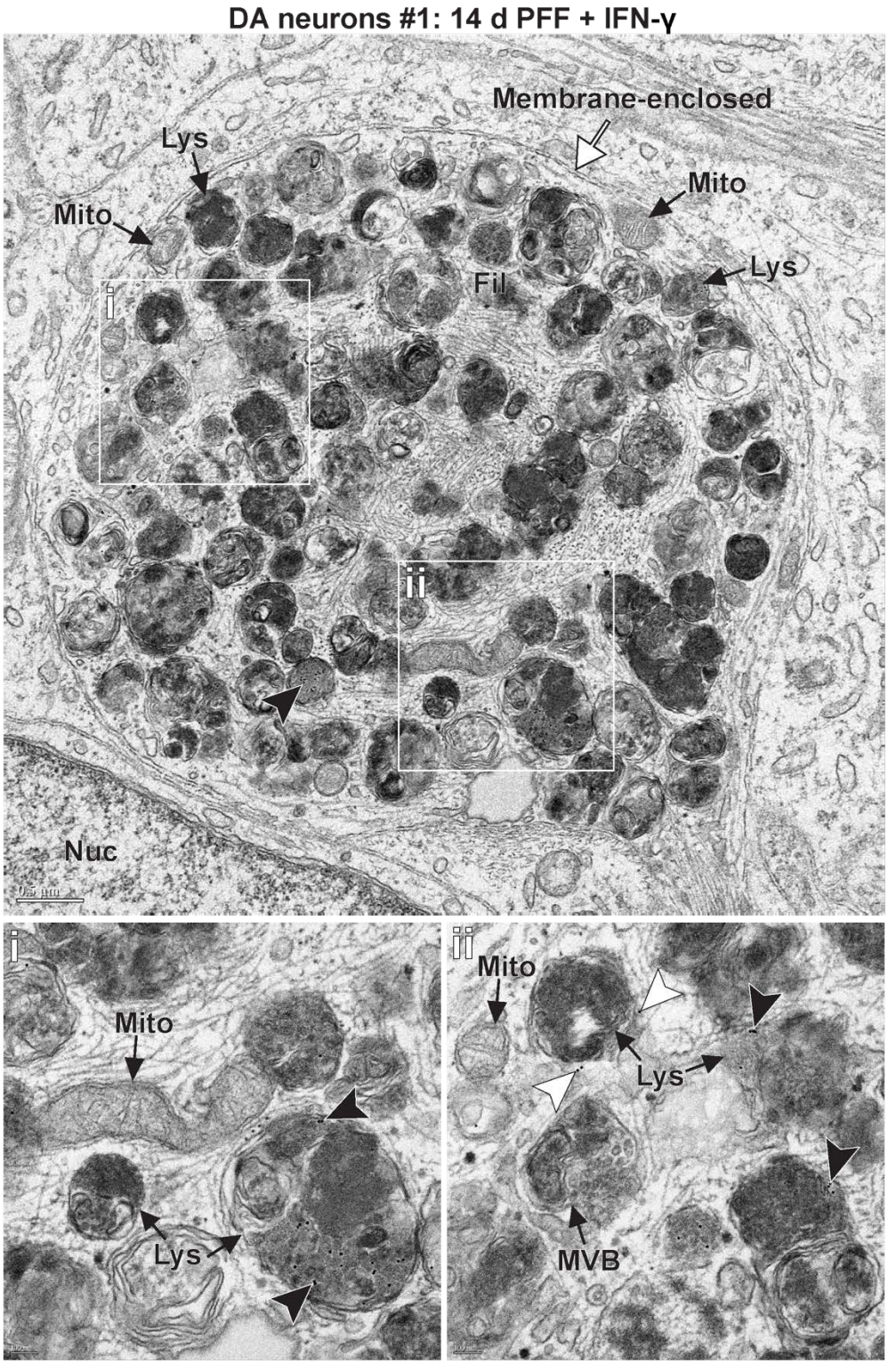
DA neurons #1: 14 d PFF + IFN-γ
Membrane-enclosed
Lys
Mito
Mito
Lys
Fil
i
ii
Nuc
i
Mito
Lys
ii
Mito
Lys
MVB

DA neurons #1 : 14 d PFF + IFN-γ

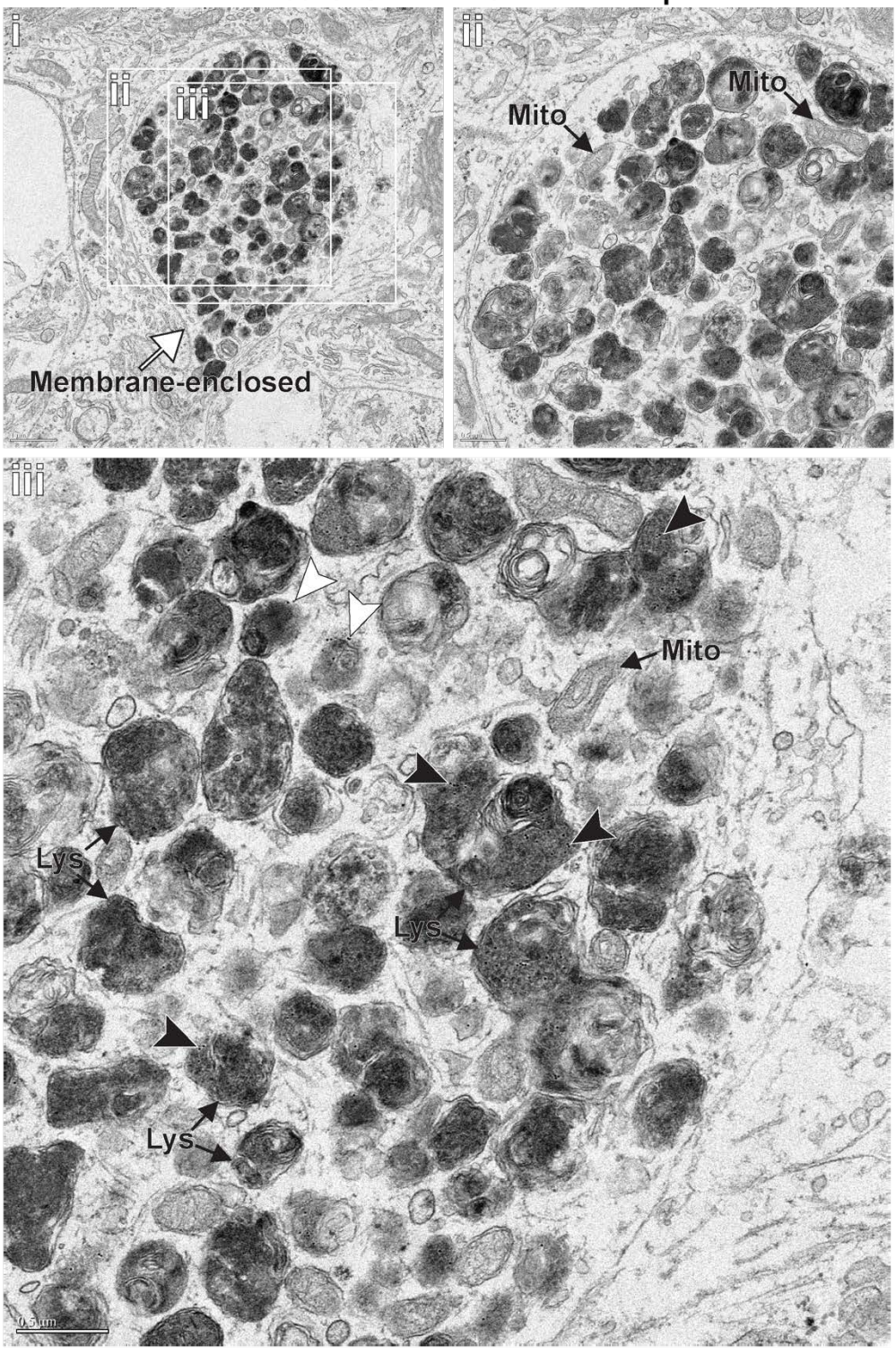

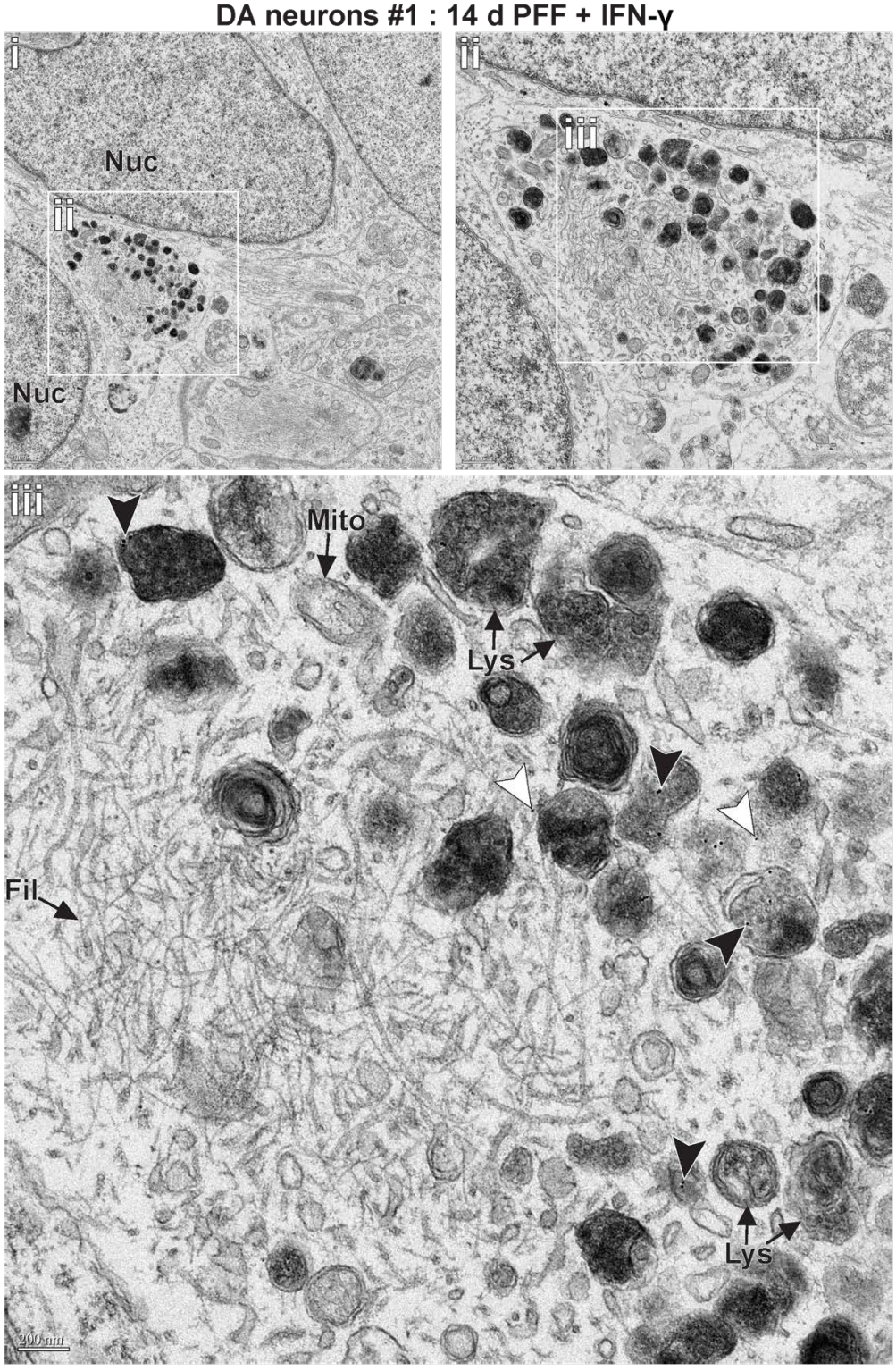
DA neurons #1 : 14 d PFF + IFN-γ
i
Nuc
ii
Nuc
ii
iii
iii
Mito
Lys
Fil
Lys
200 nm

DA neurons #2 : 14 d PFF + IFN-γ

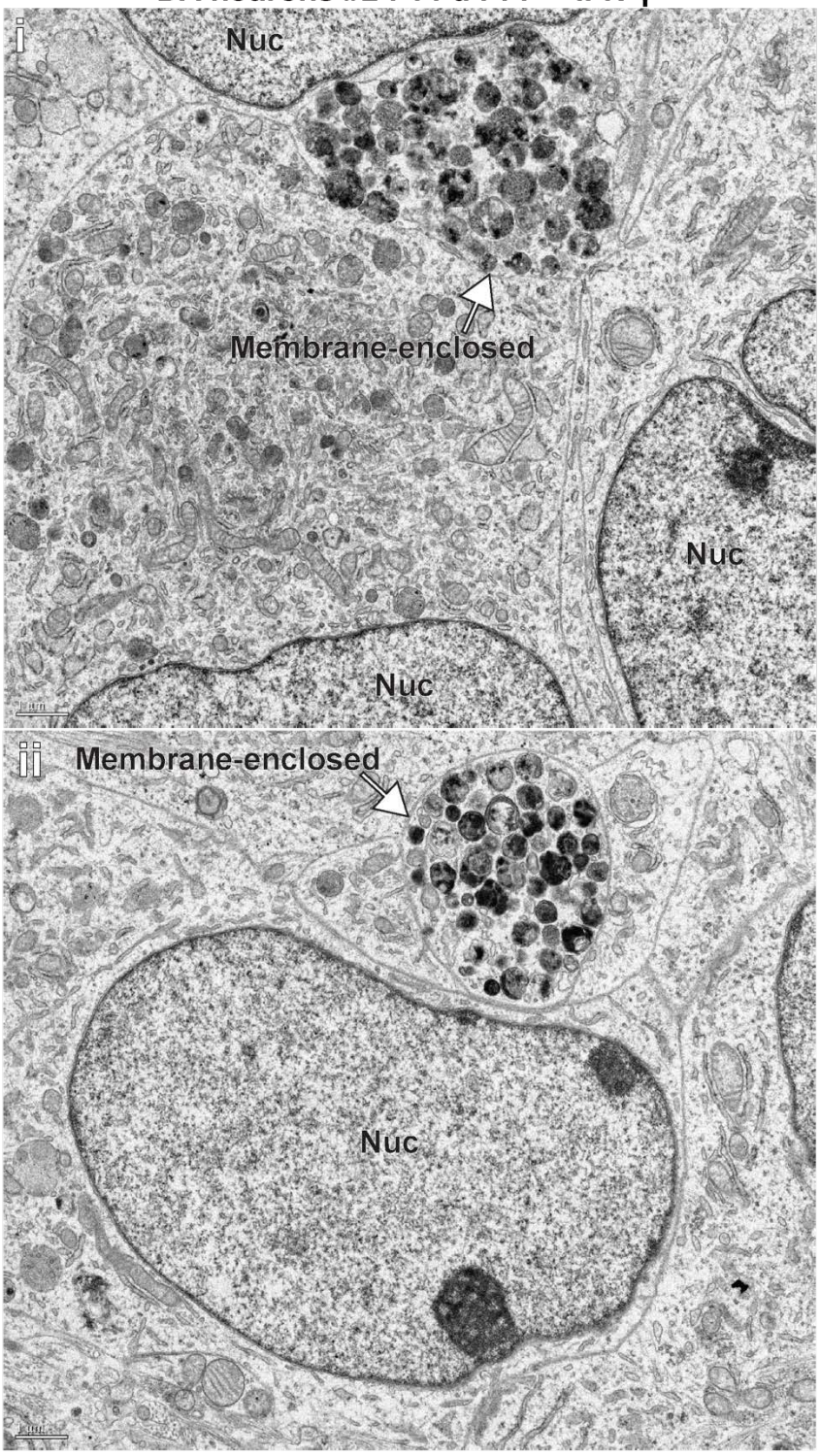

DA neurons #2 : 14 d PFF + IFN-γ

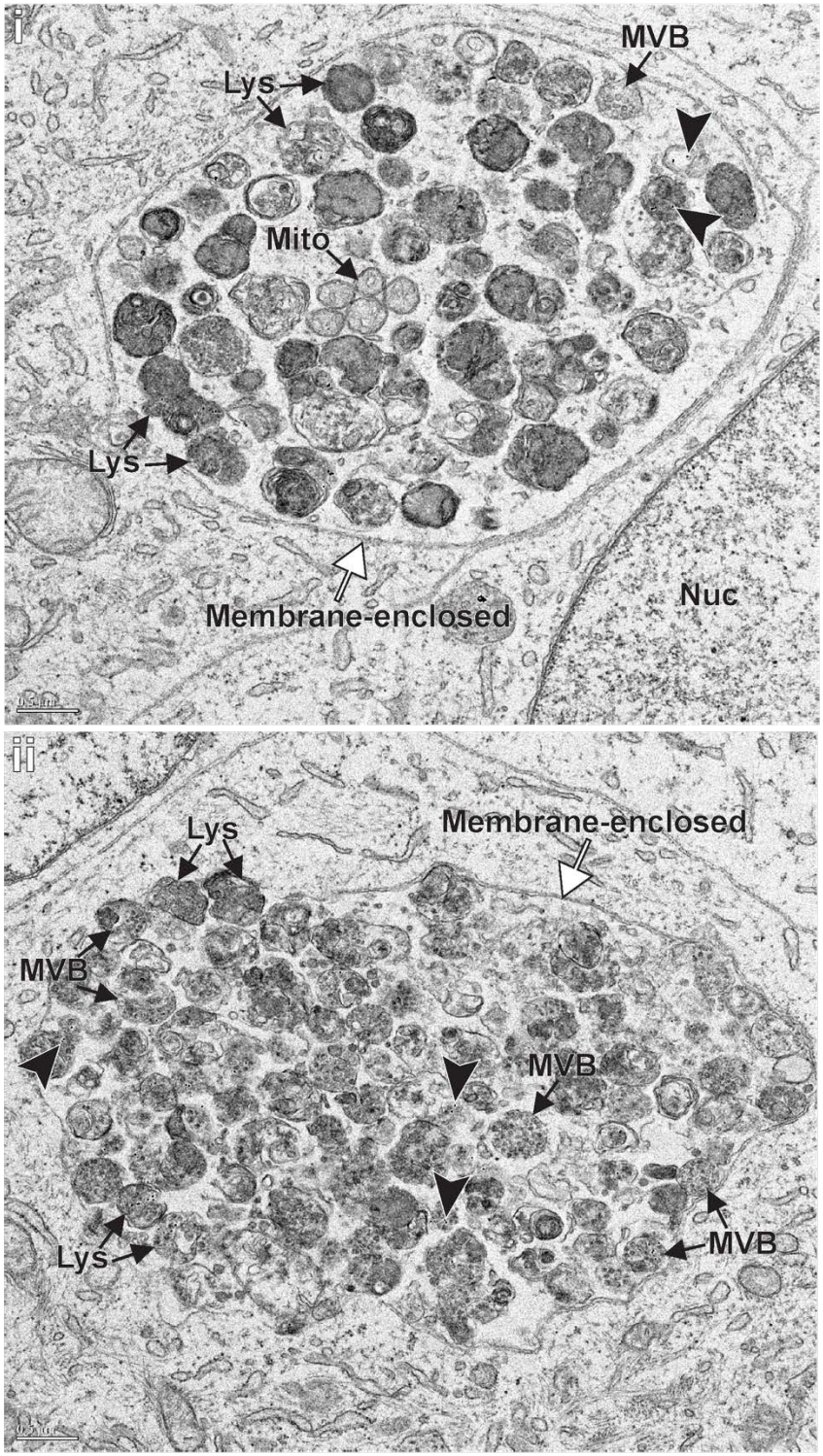

DA neurons #3 : 14 d PFF + IFN-γ

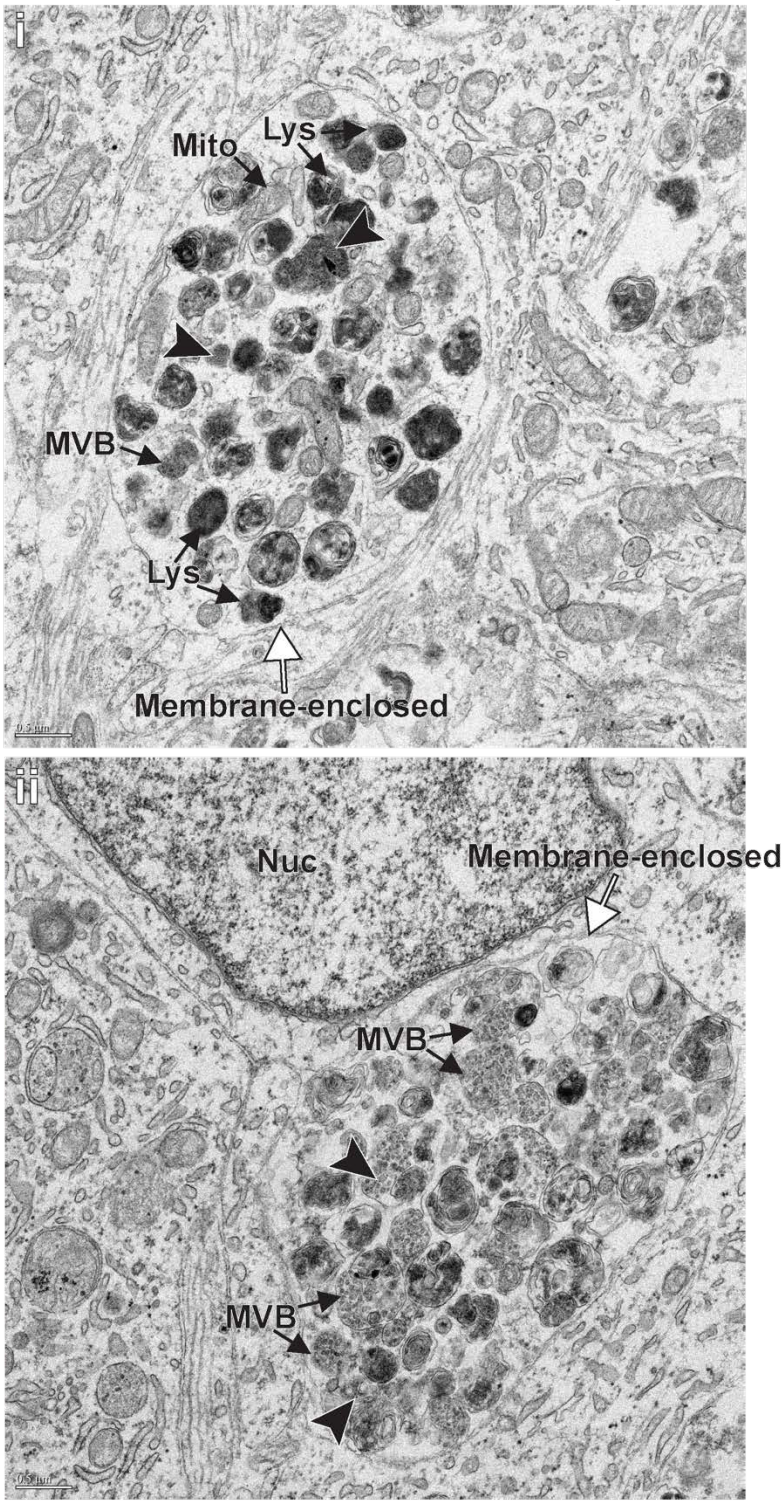

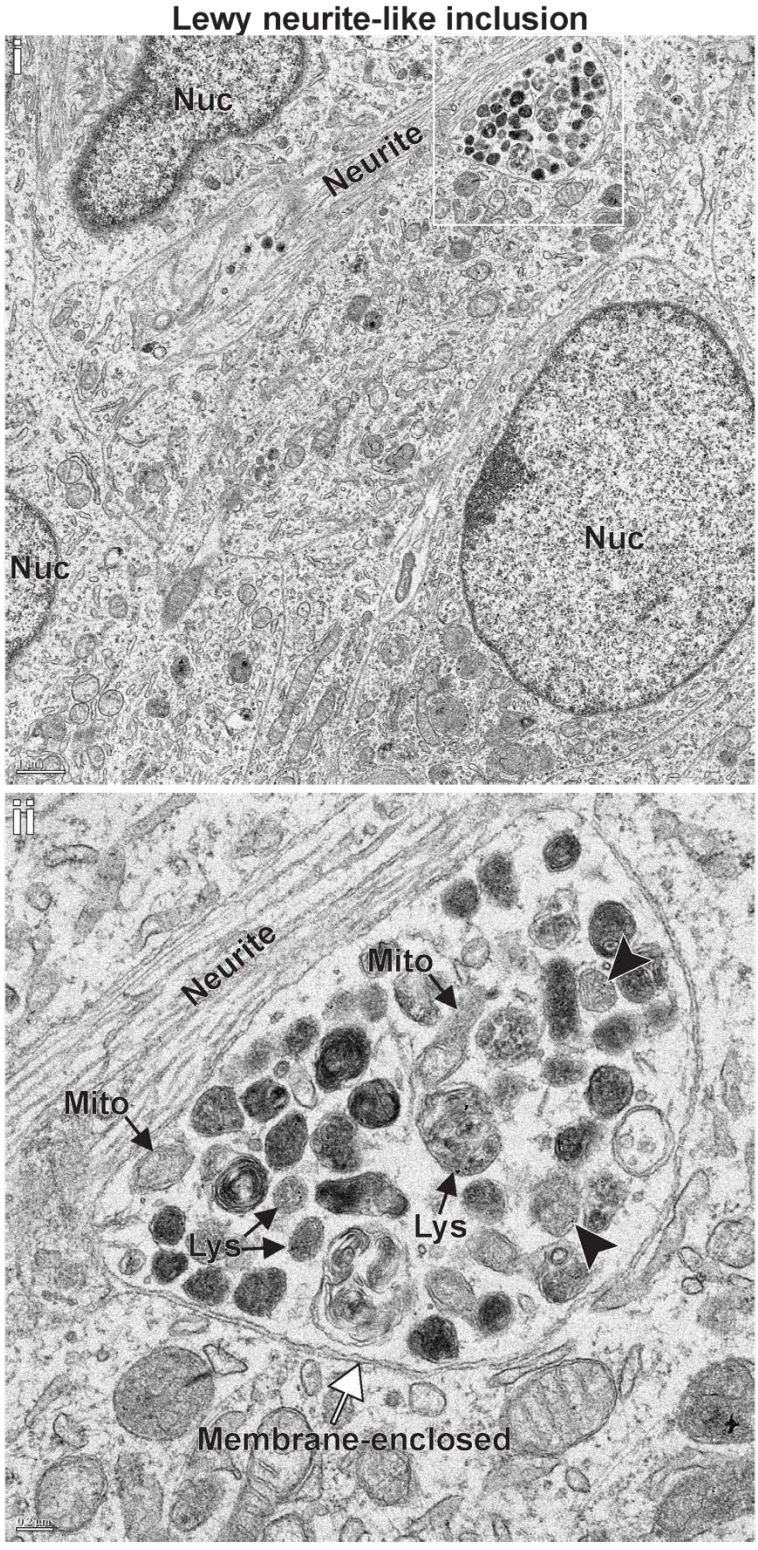
Lewy neurite-like inclusion
i
Nuc
Neurite
Nuc
Nuc
ii
Neurite
Mito
Mito
Lys
Lys
Membrane-enclosed

Supplementary Figure 4.2

Collection of inclusions formed in DA neurons.

(**A**-**C**) Inclusions formed within DA neurons generated from the AIW002-02 iPSC cell line. Inclusion showed in **A** contains a variety of organelles and filamentous (cytoskeletal) materials. Inclusion showed in **B**, consists of a collection of organelles but does not show a lot of filaments. In **C**, we see a mostly filamentous (a variety of filaments with different thickness) inclusion that contains islands of organelles at its edge. (**D** – **E**) shows inclusions, representative of the type of inclusions commonly found in the DYR-0100-derived DA neurons. (**F**) Inclusions formed within DA neurons generated from the 3450 iPSC cell lines. Similar to **E**, the inclusion shown in **i** is filled with lytic compartments (lysosomes and autolysosomes); however, **ii** shows a membrane-enclosed inclusion mostly filled with electron-dense MVBs. (**G**) Lewy neurite-like inclusion formed in DA neurons generated from AIW002-02. Lysosomes/autolysosomes (Lys), mitochondria (Mito), multivesicular bodies (MVB), filaments (Fil), white arrows point to the membrane surrounding the inclusions, white arrowheads point to nanogold-labeled PFFs found outside of lytic compartments, and dark arrowheads point to a few examples of nanogold-labeled PFF inside lytic vesicles.

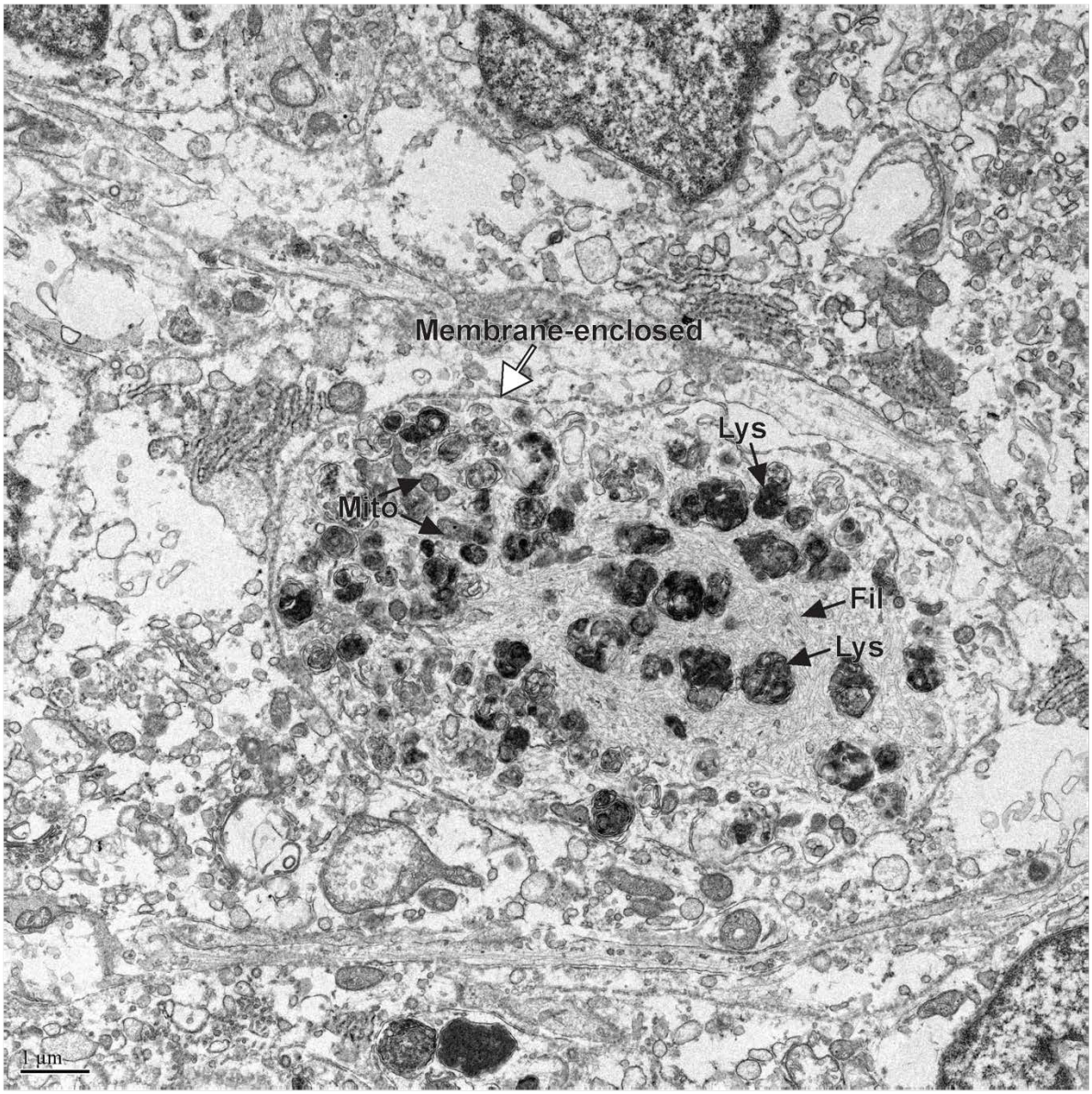
Membrane-enclosed
Lys
Mito
Fil
Lys
1 μm

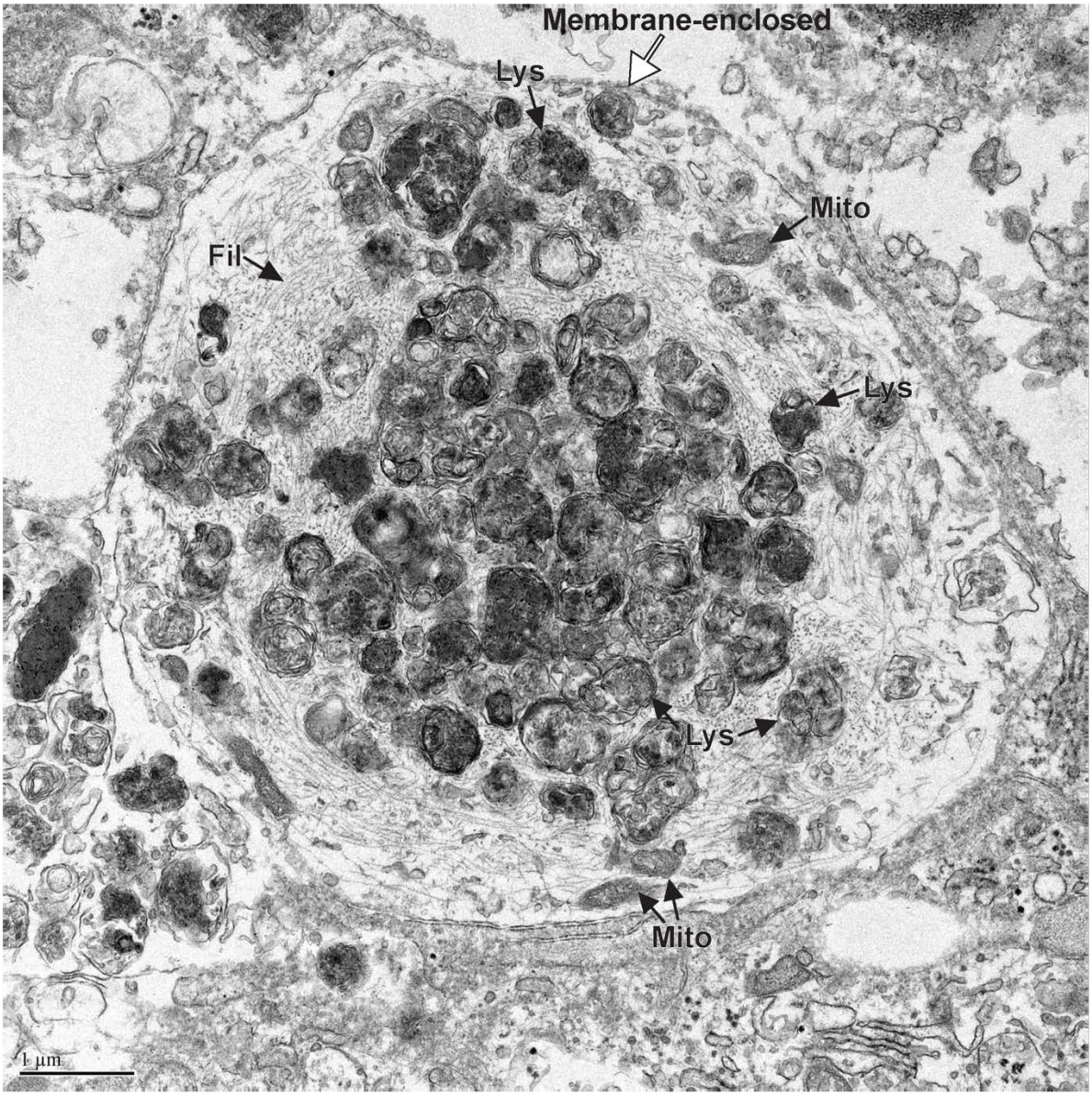
Membrane-enclosed
Lys
Mito
Fil
Lys
Lys
Mito
1 µm

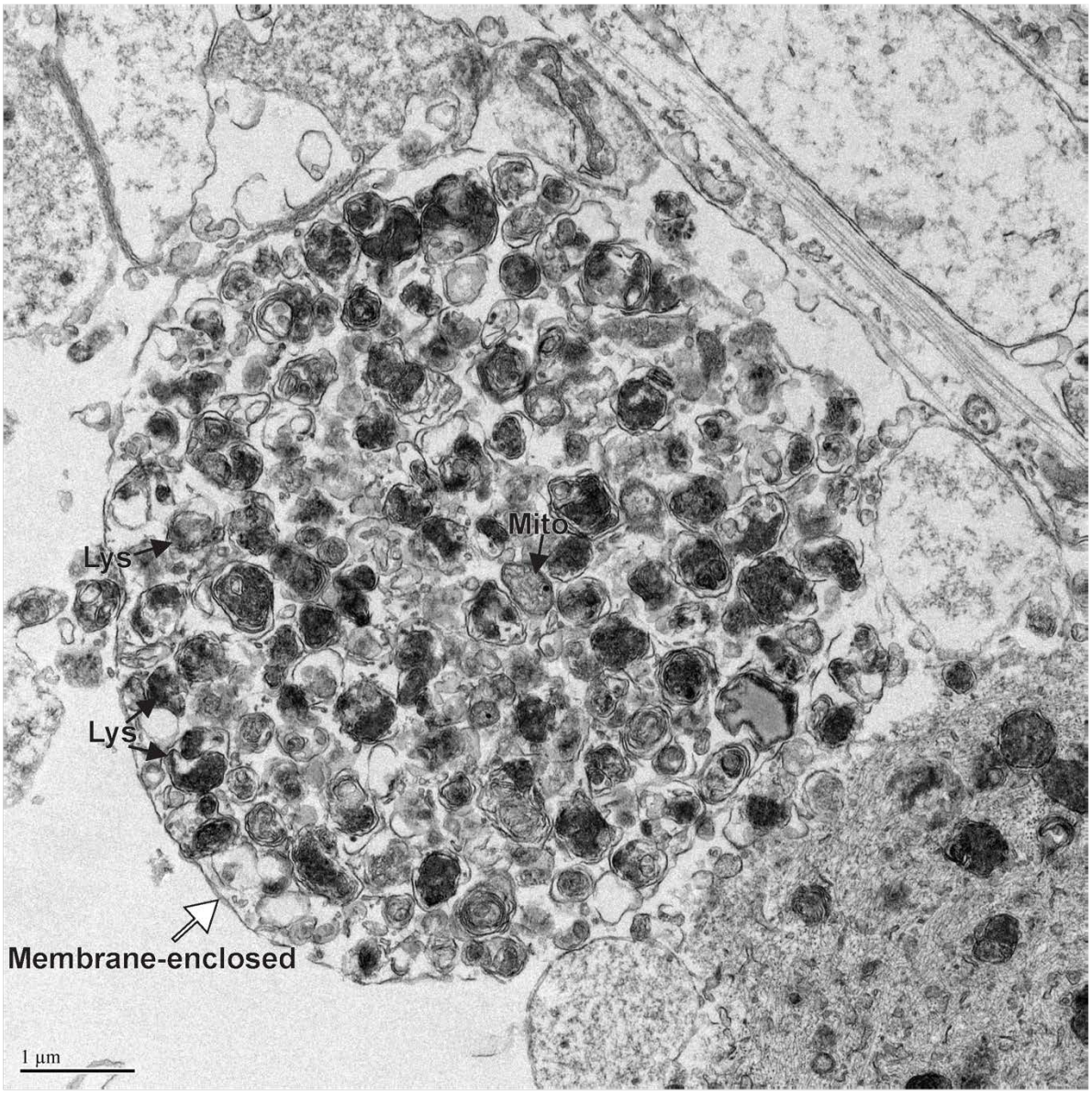
Mito
Lys
Lys
Membrane-enclosed
1 µm

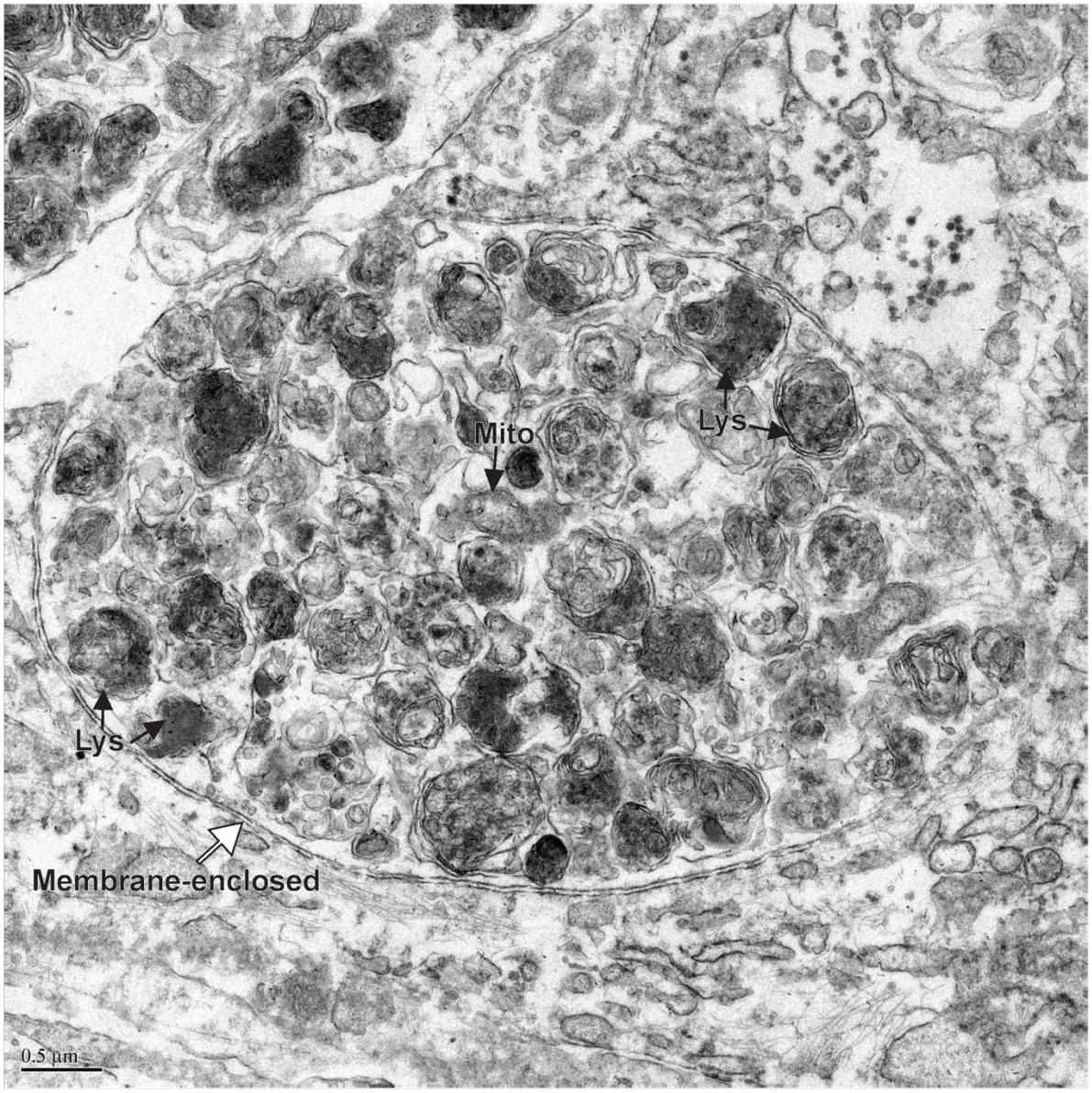
Mito
Lys
Lys
Membrane-enclosed
0.5 µm

Supplementary Figure 4.3

Collection of inclusions formed in DA neurons after 30 d of incubation.

(**A**-**D**) Inclusions formed in DA neurons generated from the 3450 iPSC line. Neurons underwent the 14 d treatment regime, with PFF + IFN-γ treatment, and were then allowed to incubate an additional 16 d, for a total of 30 d in culture since the beginning of the treatment regime. The resulting inclusions are very tightly packed and compressed. Some inclusions contain a highly dense array of filaments (cytoskeletal), as seen in **A** and **B**. In contrast**,** others contain large amounts of seemingly dysfunctional organelles, as seen in **C** and **D**. Lysosomes/autolysosomes (Lys), mitochondria (Mito), multivesicular bodies (MVB), filaments (Fil), white arrows point to the membrane surrounding the inclusions.

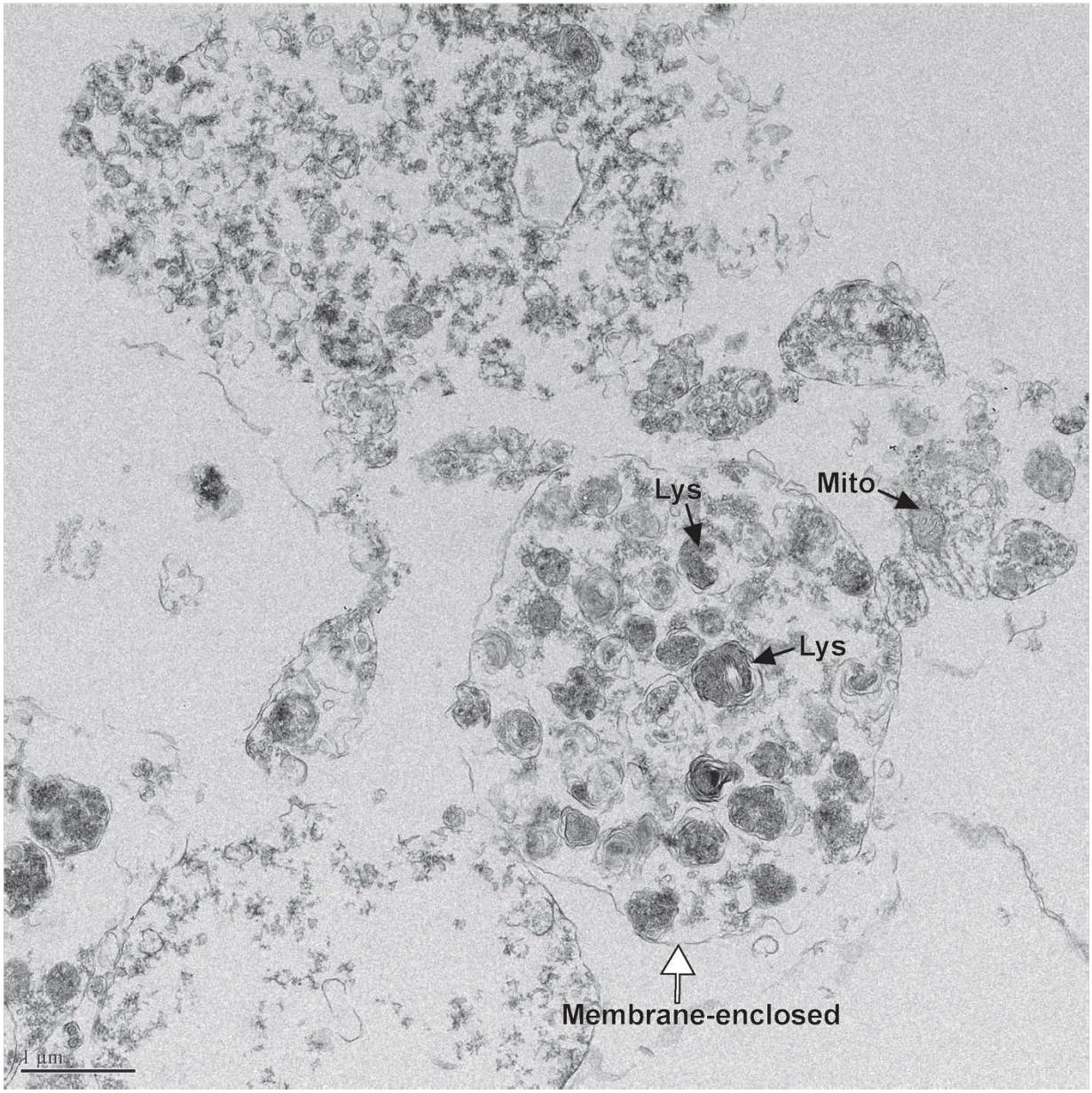
Lys
Mito
Lys
Membrane-enclosed
1 µm

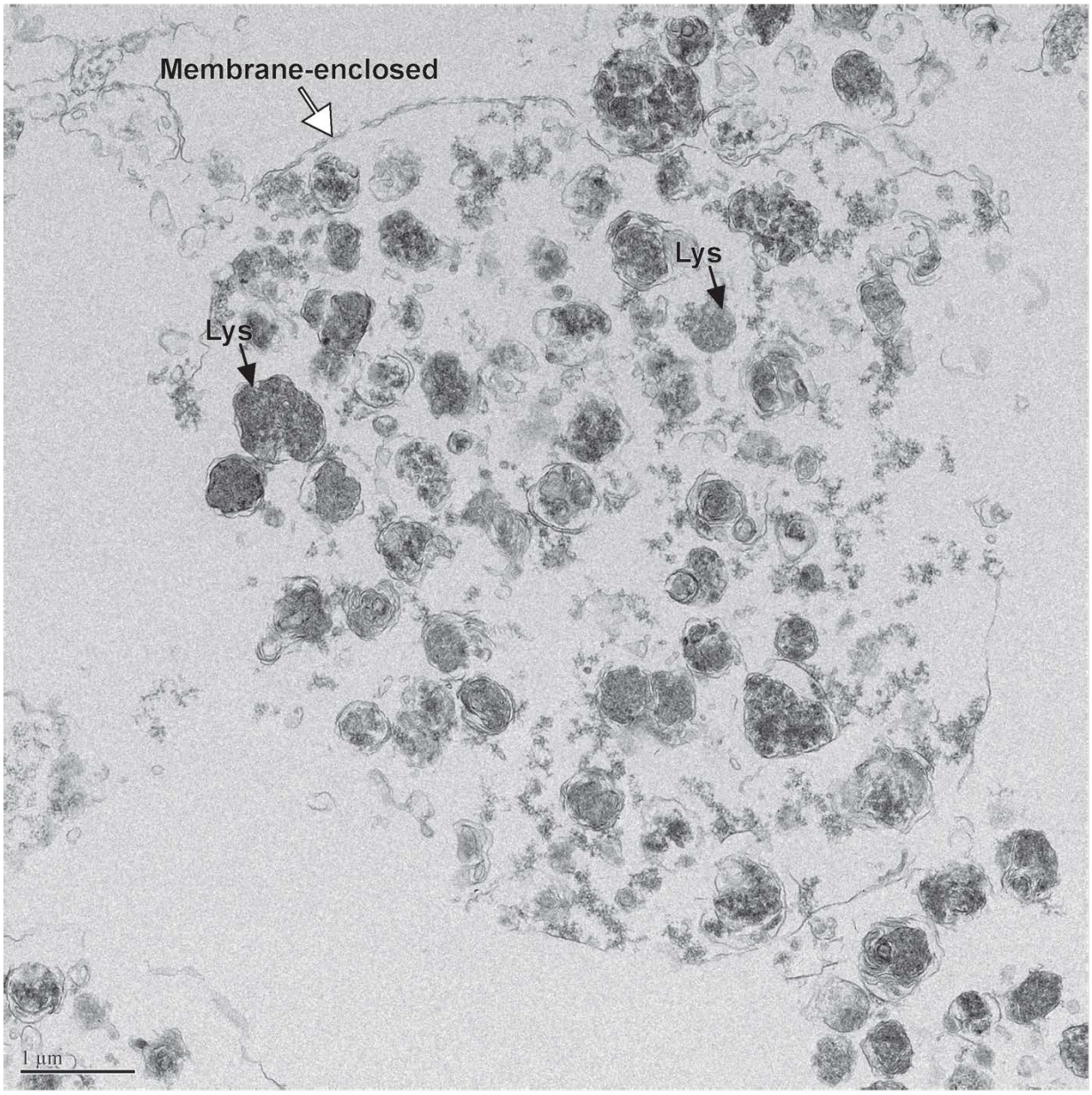
Membrane-enclosed
Lys
Lys
1 µm

Supplementary Figure 4.4

Isolated inclusions formed in DA neurons.

(**A** and **B**) Inclusions isolated by subcellular fractionation were fixed, embedded, and sectioned for EM. Inclusions imaged were membrane-enclosed with the same morphology as those found in DA neurons. Lysosomes/autolysosomes (Lys), mitochondria (Mito), multivesicular bodies (MVB), and white arrows point to the membrane surrounding the inclusions.

4.8 Materials and methods

Reagents/Resources/Equipment Table

RESOURCE	MANUFACTURER	CAT# OR URL
Antibodies		
LAMP1 (D2D11) XP Rabbit Antibody	Cell Signaling Technology	Cat# 9091, RRID:AB_2687579
Tyrosine Hydroxylase antibody	Abcam	Cat# ab76442, RRID:AB_1524535
LAMP2 antibody [H4B4] - Lysosome Marker	Abcam	Cat# ab25631, RRID:AB_47070
HDAC6 (D2E5) Rabbit monoclonal Antibody	Cell Signaling Technology	Cat# 7558, RRID:AB_10891804
Anti-NRF2 (D1Z9C) XP Rabbit monoclonal Antibody	Cell Signaling Technology	Cat# 12721, RRID:AB_2715528
Clathrin heavy chain antibody	Abcam	Cat# ab21679, RRID:AB_2083165
alpha Synuclein antibody [syn211]	Abcam	Cat# ab75305, RRID:AB_1309948
TMEM106B (E7H7Z) Rabbit mAb	Cell Signaling Technology	Cat# 93334, RRID:AB_2924267
Rab5 Antibody	Cell Signaling Technology	Cat# 2143, RRID:AB_823625
alpha Synuclein (phospho S129) antibody	Abcam	Cat# ab59264, RRID:AB_2270761
Anti-Phosphorylated α-Synuclein, Monoclonal Antibody (pSyn#64)	Wako, FUJIFILM	Cat# 015-25191, RRID:AB_2537218
Beta-III-Tubulin antibody	Abcam	Cat# ab41489, RRID:AB_727049

MAP2 Antibody	Novus	Cat# NBP1-48604, RRID:AB_10011223
Anti-PSD95 antibody [7E3-1B8]	Abcam	Cat# ab18258, RRID:AB_444362
Anti-HA tag antibody - ChIP Grade (ab9110)	Abcam	Cat# ab9110, RRID:AB_307019
Anti-HA tag antibody [HA.C5] (ab18181)	Abcam	Cat# ab137838, RRID:AB_2810986
IFN-γ (D3H2) XP Rabbit mAb #8455	Cell Signaling Technology	Cat# 8455, RRID:AB_2797644
IFN-γ (3F1E3) Mouse mAb #3159	Cell Signaling Technology	Cat# 3159, RRID: N/A
Midkine antibody	Thermo Fisher Scientific	Cat# MA5-32538, RRID: AB_2809815
Alexa Fluor Plus 405 Phalloidin	Thermo Fisher Scientific	Cat# A30104, RRID: N/A
TFEB (D2O7D) Rabbit mAB	Cell Signaling Technology	Cat# 37785, RRID:AB_2799119
Recombinant Anti-TFEB antibody [EPR22941-6]	Abcam	Cat# ab267351, RRID: N/A
Human TFEB Antibody	R&D Systems	Cat# MAB9170 RRID: N/A
TFEB Antibody	Cell Signaling Technology	Cat# 4240, RRID:AB_11220225
Hsc70/Hsp73 monoclonal antibody	Enzo Life Sciences	Cat# ADI-SPA-815-488-E, RRID: AB_2039277
Goat anti-Chicken IgY Secondary Antibody, Alexa Fluor 647	Thermo Fisher Scientific	Cat# A-21449, RRID:AB_2535866
Goat anti-Mouse IgG Highly Cross-Adsorbed Secondary Antibody, Alexa Fluor 647	Thermo Fisher Scientific	Cat# A-21236, RRID:AB_2535805
Goat anti-Mouse IgG Highly Cross-Adsorbed Secondary Antibody, Alexa Fluor Plus 488	Thermo Fisher Scientific	Cat# A32723, RRID:AB_2633275
Goat anti-Rabbit IgG Highly Cross-Adsorbed Secondary Antibody, Alexa Fluor 568	Thermo Fisher Scientific	Cat# A-11036, RRID:AB_10563566
Goat anti-Chicken IgY Cross-Adsorbed Secondary Antibody, Alexa Fluor Plus 405	Thermo Fisher Scientific	Cat# A48260, RRID:AB_2890271
Bacterial and virus strains		
(α-syn) *SNCA*-HA Adenovirus (Human)	Applied Biological Materials Inc.	Cat# 445410520200
Chemicals, peptides, and recombinant proteins		
Advanced DMEM/F-12	Gibco, Thermo Fisher Scientific	Cat# 12634028
Eagle's Minimum Essential Medium (EMEM)	ATCC	Cat# 30-2003
Human IFN-gamma Recombinant Protein	Gibco, Thermo Fisher Scientific	Cat# PHC4033
DMEM high-glucose	Gibco, Thermo Fisher Scientific	Cat# 11965092
Bovine calf serum	GE Healthcare	Cat# SH30072.03

L-Glutamate	Wisent	Cat# 609065
Pen/Strep	Wisent	Cat# 450201
DynaMag-2	Invitrogen	Cat# 12321D
Anti-HA magnetic beads	Thermo Fisher Scientific	Cat# 88836
Hoechst	Invitrogen	Cat# H3570
DAPI	Invitrogen	Cat# D1306
DRAQ7	Abcam	Cat# ab109202
Paraformaldehyde	Thermo Fisher Scientific	Cat# A1131322
Triton X-100	Sigma Aldrich	Cat# X100-1L
Phosphate-buffered saline	Wisent	Cat# 311-010-CL
Bovine Serum Albumin	Wisent	Cat# 800-095
Poly-L-Lysine	Sigma Aldrich	Cat# A-005-M
Trypsin	Wisent	Cat# 325-052-EL
Fluorescence Mounting Medium	Dako, Agilent	Cat# S3023
Glutaraldehyde 2.5% in Sodium Cacodylate Buffer	Electron Microscopy Sciences	Cat# 1653715
Matrigel	Corning	354277
mTeSR1 medium	STEMCELL Technologies	Cat# 85857
StemPro Accutase	Thermo Fisher Scientific	Cat# A1110501
DMEM/F12	Thermo Fisher Scientific	Cat# A4192001
N2 Supplement	Thermo Fisher Scientific	Cat# 17502001
B27 Supplement	Thermo Fisher Scientific	Cat# 17504044
Brainphys Neuronal medium	STEMCELL Technologies	Cat# 05790
Neurocult SM1 Neuronal Supplement	STEMCELL Technologies	Cat# 05711
N2A Supplement A	STEMCELL Technologies	Cat# 07152
STEMdiff™ Midbrain Neuron Maturation Kit	STEMCELL Technologies	Cat# 100-0041
STEMdiff™ Midbrain Neuron Differentiation Kit	STEMCELL Technologies	Cat# 100-0038
STEMdiff™ Neural Progenitor Medium	STEMCELL Technologies	Cat# 05835
Purmorphamine	STEMCELL Technologies	Cat# 72204
GlutaMAX™ Supplement	Gibco, Thermo Fisher Scientific	Cat# 35050061
BDNF	Sigma Aldrich	Cat# SRP3014
Laminin	Sigma Aldrich	Cat# L2020
Ascorbic acid	Sigma Aldrich	Cat# A5960
db-cAMP	Sigma Aldrich	Cat# D0260
Compound E	STEMCELL Technologies	Cat# 73954
Carbon-covered grids	Electron Microscopy Sciences	Cat# FCF400CU50
Poly-L-Ornithine Solution (0.01%)	Millipore Sigma	Cat# A-004-C
GDNF	Peprotech	Cat# 450-10
CNTF	Peprotech	Cat# 450-13
Antibiotic-Antimycotic	Gibco, Thermo Fisher Scientific	Cat# 15240062

MitoSOX	Invitrogen, Thermo Fisher Scientific	Cat# M36008
CellROX	Invitrogen, Thermo Fisher Scientific	Cat# C10444
Trypsin Neutralizer Solution	Gibco, Thermo Fisher Scientific	Cat# R002100
CellTracker Violet BMQC dye	Invitrogen, Thermo Fisher Scientific	Cat# C10094
CellTracker Deep Red Dye	Invitrogen, Thermo Fisher Scientific	Cat# C34565
10nm NHS-Activated Gold Nanoparticle Conjugation Kit	Cytodiagnostics	Cat# CGN5K-10-2
2% Uranyl Acetate	Electron Microscopy Sciences	Cat# 22400-2
Critical commercial assays		
Mycoplasma detection kit	Biotool	Cat# B39038
Cytotune reprogramming kit	Thermo Fisher Scientific	Cat# A34546
Pierce™ Chromogenic Endotoxin Quant Kit	Thermo Fisher Scientific	Cat# A39552
Pierce™ BCA Protein Assay Kit	Thermo Fisher Scientific	Cat# 23225
Deposited data		
Raw and analyzed data	Mendeley Data	doi: 10.17632/kp3774p92d.1
Experimental models: Cell lines		
U-2 OS	ATCC	Cat# HTB-96
U-87 MG	ATCC	Cat# HTB-14
SH-SY5Y	ATCC	Cat# CRL-2266
HMC3	ATCC	Cat# CRL-3304
AIW002-2	MNI C-BIG Biorepository	(Castellanos-Montiel et al., 2023; Chen et al., 2021)
3450	MNI C-BIG Biorepository	(Castellanos-Montiel et al., 2023; Chen et al., 2021)
Patient Synuclein Triplication	Dr. Tilo Kunath/University of Edinburgh.	(Mohamed et al., 2021)
ATCC-DYR0100	ATCC	Cat# ACS-1011
Bacterial strain		
BL21(DE3) Competent *E. coli* cells	New England Biolabs	Cat # C2527H
Recombinant DNA/Vector		
GST-α-synuclein plasmid, human	Maneca, et al. (Maneca et al., 2019)	N/A
GST-HRV 3C plasmid	Maneca, et al. (Maneca et al., 2019)	N/A
pGEX6P1	University of Dundee MRC Protein Phosphorylation and Ubiquitination Unit	Cat# DU30005
Software and algorithms		
ImageJ	(Schneider et al., 2012)	https://imagej.nih.gov/ij/

LAS X 3.5.5	Leica	https://www.leica-microsystems.com/products/microscope-software/p/leica-las-x-ls/
Prism	Gaphpad	https://www.graphpad.com/scientific-software/prism/
ZEN 3.5	Zeiss	https://www.zeiss.com/microscopy/int/products/microscope-software/zen.html
GMS 3	Gatan	https://www.gatan.com/products/tem-analysis/gatan-microscopy-suite-software
Materials & Equipments		
35 mm glass-bottom dish	MatTek	Cat# P35G-1.5-14-C-GRD
Nunc 8-well plate (Permanox)	Lab-Tek	Cat# 177445
200 mesh copper carbon grids	SPI Supplies	Cat# 3520C-FA
0.22 μm PVDF syringe filter	Millipore	Cat# SLGV033RS
100 mesh hex grids	EMS Diasum	Cat# HD100H-Cu
mPrep/ g capsules, storage box, 16 label sets (16/bx)	Microscopy Innovations, EMS	Cat# 85010-04
ThermoMixer C	Eppendorf (purchased from VWR)	Cat# CA11028-280
GSTrap 4B column	Cytiva	Cat# 28401748
Glutathione Sepharose® 4B resin	Cytiva	Cat# 17075601
Tecnai 12 BioTwin 120 kV transmission electron microscope (TEM)	FEI	N/A
Tecnai G2 Spirit Twin 120 kV Cryo-TEM	FEI	N/A
Zetasizer Nano S	Malvern Panalytical	https://www.malvernpanalytical.com/en/support/product-support/zetasizer-range/zetasizer-nano-range/zetasizer-nano-s
Bioruptor® Plus sonication device with metallic soundproof box	Diagenode	Cat# B01020001

Cell Lines

U2OS, U87, SH-SY5Y, and HMC3 were obtained from American Type Culture Collection (HTB-96, HTB-14, CRL-2266, CRL-3304, respectively). For studies with iPSCs, we used the lines AIW002-2 and 3450 obtained from the Neuro's C-BIG Biorepository, and ATCC-DYR0100 obtained from ATCC (ACS-1011). AIW002-2 was reprogrammed from peripheral blood mononuclear cells of a healthy donor with the Cytotune reprogramming kit (Thermo Fisher Scientific, A34546). 3450 was also generated from peripheral blood mononuclear cells, but episomal reprogramming was used as described by Wen et al. (2016). The process of reprogramming and quality control profiling for these iPSCs was outlined in a previous study (Chen et al., 2021). The use of iPSCs in this project is approved by the McGill University Health Centre Research Ethics Board (DURCAN_IPSC / 2019-5374). The *SNCA* lines (originally named AST23, AST23-2KO, AST23-4KO) were provided and generated by Dr. Tilo Kunath from The University of Edinburgh.

Cell lines were routinely checked for mycoplasma contamination using the mycoplasma detection kit (Biotool, B39038).

Production, Characterization, and Nano-Gold Labeling of PFFs

Production, characterization, and conjugation with nanogold beads of recombinant α-syn monomers and PFF were previously described (Del Cid Pellitero et al., 2019; Maneca et al., 2019).

Purification of α-syn was described previously by Feller et al. (2023). In brief, the pGEX-6P-1 plasmid (University of Dundee MRC Protein Phosphorylation and Ubiquitination Unit, DU30005) cloned with full-length human wild-type α-syn was transformed to BL-21(DE3) *E.coli.*

(New England Biolabs, C2527H) and over-expressed as GST-tagged α-syn in the presence of inducer IPTG. The protein was isolated by affinity binding to Glutathione Sepharose® 4B resin (GE Healthcare, 17075601). GST tag was then cleaved off with GST-HRV 3C protease, and α-syn was purified by passing through a GSTrap 4B column (GE Healthcare, 28401748). The purified α-syn was evaluated to be of homogeneity on SDS-PAGE, adjusted to a final concentration of 5 mg/mL with PBS (pH 7.4), and filter-sterilized througth a 0.22-μm PVDF syringe filter (MilliporeSigma, SLGV033RS). The endotoxin level was less than 0.05 EU per mg of α-syn as assayed with a chromogenic endotoxin quant kit by following the manufacturer's instruction (Thermo Fisher Scientific, A39552). Finally, α-syn was aliquoted and stored at -80ºC.

PFF was prepared by shaking 0.5-mL of purified α-syn held in a 1.5-mL microtube on a ThermoMixer (VWR, CA11028-280) at 37ºC and 1000 rpm for 5 days. Then PFF was sonicated at least 40 cycles of 30-sec on/30-sec off using a Bioruptor® Pico sonication unit (Diogenode, B01020001). Samples (~20 μL) were reserved for PFF quality control by thioflavin T assay, dynamic light scattering (using Zetasizer Nano S, Malvern, DLS assay) and TEM imaging as described (Feller et al., 2023).

PFFs were characterized using a negative staining protocol (Del Cid Pellitero et al., 2019). PFFs were added to 200 mesh copper carbon grids (SPI Supplies, 3520C-FA), fixed with 4% PFA (Thermo Fisher Scientific, A1131322) for 1 min and stained with 2% uranyl acetate (Electron Microscopy Sciences, FCF400CU50) for 1 min. PFFs were visualized using a transmission electron microscope (FEI Tecnai 12 Bio Twin 120kV TEM) coupled to an AMT XR80C CCD Camera and analyzed with Fiji-ImageJ1.5 and GraphPad Prism 9 software.

Characterized PFF were conjugated with 10 nm gold beads (CytoDiagnostics, CGN5K-10-2), immediately before experimental use, as described by A. Bayati et al. (2023).

Differentiation and Culture of AIW002-02 and 3450 DA Neurons

A previously reported differentiation protocol was used to generate DA neurons from two different iPSC cell lines: AIW002-02 (MNI, C-BIG) and 3450 (MNI, C-BIG) (Jefri et al., 2020). hiPSCs were plated onto Matrigel (Corning, 354277)-coated plates in mTeSR1 medium (STEMCELL Technologies, 85857). The culture medium was changed daily until the cells reached ~80% confluency. The cells were then passaged, frozen, or differentiated. A previously described protocol was used to generate ventral midbrain dopaminergic neural progenitor cells (Jefri et al., 2020). Dopaminergic neural progenitor cells were dissociated with StemPro Accutase Cell Dissociation Reagent (Thermo Fisher Scientific, A1110501) into single-cell suspensions. Plating on coverslips was done using neural progenitor plating medium (DMEM/F12 supplemented with N2, B27 supplement from Thermo Fisher Scientific, A4192001, 17502001 and 17504044, respectively). To further differentiate into dopaminergic neurons, neural progenitor medium was switched to dopaminergic neural differentiation medium (Brainphys Neuronal medium from STEMCELL Technologies, 05790) supplemented with N2A Supplement A (STEMCELL Technologies, 07152), Neurocult SM1 Neuronal Supplement (STEMCELL Technologies, 05711), BDNF at 20 ng/mL (MilliporeSigma, SRP3014), GDNF at 20 ng/mL (Peprotech, 450-10), Compound E at 0.1 μM (STEMCELL Technologies, 73954), db-cAMP at 0.5 mM (MilliporeSigma, D0260), Ascorbic acid at 200 μM (MilliporeSigma A5960) and laminin at 1 μg/mL (MilliporeSigma, L2020).

Differentiation and Culture of DYR0100 DA NPCs

The monolayer method was used for the differentiation of DYR0100 iPSCs into DA NPCs as described by Chen *et al*. (Chen, 2019). Frozen DYR0100 NPCs were thawed and allowed to recover for one week prior to seeding for downstream assays.

Generation and Differentiation of NGN2-induced Neurons

AIW002-02 iPSCs expressing doxycycline-inducible *NGN2* were generated as described previously (Sheta et al., 2022). Briefly, the parental AIW002-02 iPSC line was split with ReLesR (STEMCELL Technologies, 100-0484) and seeded at a density of 135,000 cells per well in a 6-well plate in mTesR1 media plus Y27632 one day prior to simultaneous transduction with separate lentiviruses encoding Ngn2 and rtTA. The media was changed to mTesR1 only 1 h prior to transduction at a dilution factor of 1/100 for each virus. This resulted in a MOI of one. The transduction was carried out in mTesR1 media plus 4ug/ml of polybrene over a period of 24 h prior to puromycin selection at 1ug/ml for a total of 48 h. Throughout the transduction, selection and iPSC expansion steps, the media was changed daily. The AIW002-02 Ngn2 rtTA line was tested for pluripotency by immunofluorescence for Nanog, Tra-1-80, Oct3/4 and SSEA (positive for all markers, data not shown) and for mycoplasma (negative, data not shown). Subsequently, AIW002-02 iPSCs were differentiated into Ngn2 neurons based on a protocol adapted from Zhang *et al.*(Zhang et al., 2013) and Meijer *et al.*(Meijer et al., 2019) and characterized by immunofluorescence for neuronal markers (MAP2 and PSD95) at the differentiation endpoint.

iPSC Culturing of Forebrain Cortical Neurons

AIW002-02 iPSCs were differentiated into forebrain cortical neurons according to a protocol based on EB formation combined with dual SMAD inhibition (STEMCELL, 08581) (Chen et al., 2021). In summary, AIW002-02 iPSCs were dissociated into single cells and allowed to form EBs on low-attachment plates for one week in DMEM/F12 media supplemented with N2, B27, 10 μM SB431542, and 2 μM DMH1. This was followed by neural rosette formation onto polyornithine- and laminin-coated (MilliporeSigma, A-004-C and L2020, respectively) plates in the same media, which were selected semi-manually after 7 days. The rosettes were dissociated with Gentle Cell Dissociation Reagent for 5 min at room temperature (RT) and cultured on polyornithine- and laminin-coated plates in DMEM/F12 media supplemented with N2 and B27 to generate NPCs. The NPCs were passaged every 5-7 days until day 25. Final differentiation, was carried out in Neurobasal media supplemented with N2, B27, 1 μg/mL laminin, 500 μM db-cAMP, 20 ng/mL BDNF, 20 ng/mL GDNF, 200 μM ascorbic acid, 100 nM Compound E, and 1 ng/mL TGF-β.

SNCA Triplication, Double KO, and Quadruple KO iPSCs

SNCA lines (originally named AST23, AST23-2KO, AST23-4KO) were generated and provided by Dr. Tilo Kunath from The University of Edinburgh according to methodology described previously (Chen et al., 2019; Mohamed et al., 2021). The AST23 line carries a triplication of the *SNCA* gene, while the AST23-2KO line has been corrected by CRISPR/Cas9-

mediated deletion of 2 copies of the *SNCA* gene to create the isogenic control for the former. The AST23-4KO line is a complete *SNCA* knockout.

PFF + IFN-γ treatment Regime

The 14 d PFF and IFN-γ treatment was described for confocal and Western blot analysis in Figure 4.1 A. For EM, the regime was described in Extended Data Figure 4.1 A. The earlier 2 d time point, used in Western blots and quantifications, was described in Extended Data Figure 4.1 B. Briefly, differentiated dopaminergic neurons, grown on 15 mm coverslips, were administered PFFs at 1 μg/mL. The cells were incubated for 48 h with PFF, in Brainphys Neuronal media (STEMCELL Technologies, 05790), and then given fresh Brainphys media and incubated for 72 h. Neurons were then given media supplemented with 0.2 μg/mL of IFN-γ (Thermo Fisher Scientific, PHC4033) or PBS control. Cells were incubated for 24 h, and then given fresh media. 6 d neurons were collected at this point. 7 d neurons were collected 24 h after fresh media was given to cells. 10 d neurons were collected 72 h following the collection of 7 d neurons, and so on. 14 d neurons were collected 8 d following fresh media being given to neurons.

For 2 d neurons, PFF was administered for 24 h, followed by the addition of IFN-γ (or PBS for control) to the PFF containing media for 24 h. A graphical representation of the 2 d treatment is shown in Extended Data Figure 4.1 B.

The staggered nature of the PFF and IFN-γ treatment was to enable neurons to survive and form inclusions. In earlier iterations of this protocol, PFF and IFN-γ were treated simultaneously. This led to massive (over 70%) neuronal cell death, and left very few cells for imaging and analysis, and very few inclusions to study. By increasing PFF exposure to 48 h, we were able to increase PFF fluorescence in samples at 14 d and ensure nanogold-PFF could be easily found in

EM samples. Incubation in fresh media allowed for neuronal recovery and greatly enhanced neuronal survival. IFN-γ treatment was then limited to 24 h to enhance survival while allowing for the formation of PFF-positive inclusions to occur as early as 7 d into our treatment. Overall, our treatment aimed to increase cell survival while creating the environment necessary for the formation of inclusions in DA neurons. All fixed samples were imaged on an SP8 microscope (Leica).

The same protocol was used for the administration of IL-1β (Thermo Fisher Scientific, RIL1BI), where IL-1β was administered at 50 ng/mL instead of IFN-γ. This concentration was used previously by Tong et al. (2008).

Maintenance of iPSC-derived Neurons

We note here, that if stressed, iPSC-derived neurons can present with structures that are ultrastructurally somewhat similar to the inclusions we have observed. These structures can even appear in control cells, if care is not taken to: 1) Incubate iPSCs at the back of the incubator (most stable temperature), 2) Avoid the use of cold media when changing cell media (temperature shock related stress), 3) ensure cells are never dry while changing media, and 4) avoid contamination. All of these factors can lead to cellular stress and cell death, which when viewed under an electron microscope, may lead to cells with dark lysosomes and disorganized cytoskeletal elements, which can be mistaken for Lewy bodies. Fortunately, these apoptotic features in cells lack major compaction and organization when compared to LB-like inclusions, which make them easy to differentiate from bona fide inclusions. Apoptotic cells (or remnants of cells) also lack PFF-gold staining and mitochondrial incorporation.

The utmost importance is to check the quality of the cells and the level of neuronal stress in cultured iPSCs in the control conditions before starting these experiments. If cells are regularly present with pyknotic nuclei, contain dark lysosomes, or unclear mitochondrial cristae in control conditions, measures should be taken to improve cell culturing techniques to ensure the most minimal amount of cellular stress. This will lead to less confusion as to what structures are inclusions and what structures are not when looking at their cellular ultrastructure.

Reactive Oxygen Species Experiment

In order to quantify the amount of reactive oxygen species (ROS) that were forming as a result of our 14 d treatment, DA neurons and forebrain cortical neurons were plated on live imaging chambers and underwent our 14 d treatment in the presence or absence of IFN-γ, along with an IFN-γ only condition and a control condition where no PFF or IFN-γ was administered (PBS was used instead). Cells were then stained with CellROX and MitoSOX (Thermo Fisher Scientific, C10444 and M36008, respectively) for 1 h prior to live imaging. MitoSOX and CellROX fluorescence was then quantified for both cortical and DA neurons, across two independent experiments. Images were captured on an LSM 880 microscope (Zeiss).

EM Processing

Neurons and cell lines were plated in 8 well chamber slides (Lab-Tek, Nunc, Thermo Fisher Scientific, 177445) and were put through the dual hit treatment. After treatment, the media was removed and cells were fixed with 2.5% glutaraldehyde in 0.1 M sodium cacodylate buffer (Electron Microscopy Sciences, 1653715) supplemented with 2 mM calcium chloride, washed in

buffer, and then post-fixed with 1% osmium tetroxide and 1.5% potassium ferrocyanide in sodium cacodylate buffer. Cells were then *en bloc* stained with 4% uranyl acetate (Electron Microscopy Sciences, 22400-2) and dehydrated in ascending ethanol concentration to 100% and infiltrated with a 50:50 mixture of 100% ethanol and Spurr's resin, followed by pure Spurr's resin overnight. After a fresh addition of resin, samples were polymerized overnight at 70°C in an oven. Ultrathin sections were cut on a Leica Ultracut E using a 45° diamond knife and collected on 100 mesh copper hex grids (Electron Microscopy Sciences, HD100H-Cu). Some sections were stained with uranyl acetate for 5 min for enhanced membrane staining. Grids were examined with a FEI Tecnai Spirit 120 kV transmission electron microscope and images captured using a Gatan Ultrascan 4000 camera.

Plasmids and Lentivirus

α-synuclein-HA-tagged adenovirus was obtained from Applied Biological Materials Inc. (LVP719). Protocols provided by the manufacturer were followed for transduction.

Fixation and Antibody Staining

Cells were fixed with 4% paraformaldehyde (PFA; Thermo Fisher Scientific, A1131322) for 10 min at 4°C, washed with PBS and then permeabilized for 30 min with 0.05% Triton X-100 (MilliporeSigma, X100-1L) in PBS (Wisent, 311-010-CL) along with 5% bovine serum albumin (BSA, Wisent, 800-095). Coverslips were then transferred into a wet chamber and incubated for 2 h at RT with a 1:500-1:1000 dilution of the primary antibody diluted in PBS containing 0.01% Triton X-100 and 5% BSA (dilutions varied depending on the antibody). Coverslips were then

gently washed twice with PBS, and a 1:1000 dilution of secondary antibody diluted in the same buffer was added and incubated for 2 h. Cells were then washed with PBS and, in some situations, stained with 1 µg/ml Hoechst 33342 (Fisher Scientific, H3570) diluted in PBS for 10 min at RT. Coverslips were mounted on a glass slide with Fluorescence Mounting Medium (Dako, Agilent, S3023). Samples were then imaged using a Leica TCS SP8 confocal microscope.

LB-like Inclusion Extraction (Western Blot and EM)

Neurons undergoing the dual hit treatment regime were collected at day 7 and 10 for the extraction of inclusions. This was done since previous attempts at extraction of inclusions from 14 d samples resulted in very little isolated material, perhaps due to cellular stress and cell death common with that time point. In brief, cells were washed three times in PBS 1x, pH 7.4 and scraped off in a hypotonic lysis buffer (20 mM HEPES, 1 mM EDTA, pH 7.4) supplemented with protease and phosphatase inhibitor cocktail mix. Cells were kept on ice for 30 min then passed 8 times through a 27G needle until homogenized. Homogenates were kept on ice for 30 min and then 10% of the homogenate was transferred into a fresh tube (total homogenate sample), and the remainder was centrifuged at 720 x *g* for 10 min at 4°C using a tabletop centrifuge. The post-nuclear supernatant (PNS sample) was transferred into a fresh tube and the pellet (P sample) containing large LB-like inclusions and nuclei was suspended in lysis buffer. For Western blot, all samples were sonicated for 10 sec at 40% amplitude and lysates were prepared in Laemmli sample buffer (1x) followed by SDS-PAGE. For EM, the pellet was kept at -80°C until processed.

Western blot protocol

Cells were washed three times in PBS (pH 7.4) and then scraped off in RIPA buffer: 50 mM TRIS-HCl pH 7.4, 150 mM NaCl, 1mM EDTA, 0.5% sodium deoxycholate, 0.1% SDS (pH 7.4). RIPA lysis buffer was supplemented with a protease and phosphatase inhibitor cocktail mix. Lysates were sonicated for 10 sec at 40% amplitude, kept on a nutating rocker for 30 min at 4°C and centrifuged at 21,000 x *g* for 15 min at 4°C using a tabletop centrifuge. Supernatants were collected in a new tube and protein concentrations were measured using a BCA protein assay kit (Thermo Fisher Scientific, 23225).

Equal amounts of protein from each condition tested were prepared in Laemmli sample buffer prior to SDS-PAGE. Samples were resolved on large gels with the appropriate gradient of polyacrylamide. Proteins were transferred to nitrocellulose membrane and labelled appropriately. For Western blot, membranes were blocked in 5% milk in TBST (20 mM TRIS, 150 mM NaCl, 0.1% Tween20, pH 7.4). Primary antibodies were diluted in 5% BSA in TBST and membranes incubated overnight at 4°C with constant rocking. Membranes were washed three times (10 min each) in TBST and then incubated in the corresponding secondary antibody for 1 h at RT. Membranes were then washed three times in TBST with constant rocking. For signal exposure, membranes were incubated with the Pierce ECL Western Blotting Substrate (Thermo Fisher Scientific, 32106) for 1 min and developed on autoradiography film in a dark room.

All Western blots were done three times prior to being incorporated into the manuscript. For Figures 5 and 7, Western blots were quantified across three experiments using the mean gray value measurement function in ImageJ (NIH). Outputs were then subtracted by 255 (pixel range) in order to invert the expression levels so that higher expression would correspond to a higher number.

IFN-γ and PAH Treatment in DA Neurons and Cell Survival

DA NPCs were thawed and cultured on 24 well plates, pre-treated with PO and laminin. NPCs were then matured into neurons using the Midbrain Neuronal Maturation Kit (STEMCELL Technologies, 100-0041) for 14 d. Following differentiation, neurons were treated with varying concentrations of IFN-γ or PAH for 24 h. Cells were then stained with Hoechst 33342 for 20 min at RT, washed with PBS and nuclear fluorescence quantified using Infinite 200 Pro Tecan plate reader. Six measurements for each concentration of PAH were conducted and used in the quantification. Quantification was done by setting the control condition's nuclear fluorescence to 100% and dividing all subsequent cell counts by the control, resulting in the percentage of cell count compared to control.

PAH Treatment in DA Neurons for Western Blot Experiment

DA NPCs were thawed and cultured in 6-well plates in STEMdiff™ Neural Progenitor Medium (STEMCELL Technologies, 05835). The cells were then differentiated into neurons using Midbrain Neuron Maturation Kit (STEMCELL Technologies, 100-0041) for 14 d. Following differentiation, 6 wells were established as various controls: (1) null condition with PBS and DMSO treatment, (2) IFN-γ only condition in which neurons were treated with IFN-γ for 48 h and then incubated in fresh Brainphys Neuronal media (STEMCELL, 05790) and maintained for 14 d, (3) PFF only condition in which neurons were only treated with PFF for 48 h and then incubated in fresh media and maintained for 14 d, (4) PAH only condition in which cells were treated with 10 μM PAH for 24 h, given fresh media and maintained for 14 d, (5) PFF and PAH condition in which neurons were incubated with PFF for 48 h given fresh media for 72 h, and then treated with PAH

for 24 h, (6) IFN-γ and PAH condition, in which neurons were treated with PBS (control for PFF) for 48 h, given fresh media, incubated with IFN-γ for 24 h, given fresh media for 24 h, and then given 0.025 mM of PAH for 24 h, then given fresh media and maintained until 14 d. 5 wells were then designated as experimental conditions: (7) cells were given PFF for 48 h, fresh media for 72 h, IFN-γ for 24 h, 24 h of fresh media, 24 h of media supplemented with 0.025 mM PAH, following by 72 h of incubation with fresh media before cell collection, (8) same as condition 7, except that 96 h elapsed between IFN-γ treatment and PAH treatment, (9) same as condition 7 except that 8 d elapsed between IFN-γ and PAH treatment. (10) same as condition 7 except that no PAH treatment was done and samples were maintained until 14 d, (11) same as condition 10, except that IFN-γ treatment was done for 48 h, followed by incubation in fresh media until 14 d. All cells were fixed 72 h after the addition of PAH.

Endogenous α-syn Expression in KO and WT SNCA DA Neurons

KO and WT *SNCA* DA NPCs from Mohamed et al. (2021) were differentiated into neurons as described above. Neurons were then treated for 48h with α-syn-HA adenovirus (Applied Biological Materials, 445410520200) at concentration of 2 x 10^5 IFU/PFU (infectious unit)/ml. Neurons were then collected, lysed, and processed for Western blotting.

For imaging experiments, neurons grown on coverslips, then underwent the protocol described above and in Extended Data Figure 4.8 J, in which they are given 72 h of rest in fresh media, followed by administration of IFN-γ for 24 h, followed by administration of fresh media. Neurons were then fixed at various timepoints, stained with HA and phospho-α-syn antibodies.

A 2 d shortened treatment was also conducted to serve as controls for the longer timepoint experiments (Extended Data Figure 4.1 B).

Microglia Media Analysis

HMC3 cells were grown on 150 mm plates using EMEM (ATCC, 30-2003) supplemented with 10% bovine calf serum (GE Healthcare, SH30072.03) and Pen/Strep (Wisent, 450201). Once cells reached 80% confluency, cells were given PBS, LPS, PFF, and LPS + PFF. LPS (Thermo Fisher Scientific, 00-4976-93) was administered at 10 µg/mL concentration, while PFF was administered at 1 µg/mL concentration. Cells were incubated for 24 h in the treatment media then trypsin washed three times to remove PFF on the cell surface. Cells were passaged onto new plates and incubated in complete media for 24 h. Cells were washed four times with PBS 1x and incubated in serum-free media (EMEM + Pen/Strep) for 48 h. Media from each condition were collected, centrifuged for 10 min at 500 x *g* to eliminate any cells or large contaminants, then for 10 min at 4000 x *g* to eliminate any small contaminants. Media were concentrated by centrifuging at 4000 x *g* for 30min using Amicon Ultra-15 Centrifugal Filter Units with a membrane NMWL of 10kDa (MilliporeSigma, UFC901024). Concentrations of protein in the media were quantified and equal amounts of protein from each condition were resolved by SDS-PAGE followed by the corresponding Western blot to detect each protein.

LysoTracker and LysoSensor Experiment

To assess the lysosomal pH and health of neurons undergoing the 14 d dual hit treatment regime, LysoTracker (Thermo Fisher Scientific, L7528) and LysoSensor (Thermo Fisher

Scientific, L7545) were used. LysoTracker was added to cells 15 min prior to imaging, while LysoSensor was added 5 min prior to imaging. Neurons were plated on 35 mm glass bottomed dishes (MatTek, Cat# P35G-1.5-14-C-GRD). Cells were imaged using LSM 880 (Zeiss), equipped with a live imaging chamber.

LysoTracker lysosomal count was done by taking thresholded images (50% threshold) and loading them into ImageJ (NIH) and using the "3D Object Counter" function. The software then outputted the number of lysosomes in each image. Cell count was done by taking the Cell tracker (Thermo Fisher Scientific, C10094) channel and loading it into ImageJ and using the "Find Maxima" function to count the number of cells. The number of lysosomes was then divided by the number of cells to attain the "Number of Lysosomes per Cell" quantity. This was averaged across three independent experiments, with 3 images from each experiment being taken.

Co-culture experiments

HMC3 cells were grown in EMEM media supplemented with 10% of bovine calf serum and 1x of Gibco Antibiotic and Antimycotic (Thermo Fisher Scientific, 15240062). Glioblastoma, U87 cell line were grown in DMEM media (Gibco, Thermo Fisher Scientific, 11965092) supplemented with 10% of bovine calf serum, 2 mM of L-Glutamine (Wisent, 609065), and 100 IU Penicillin 100 µg/ml Streptomycin. Cells were grown and expanded on 150 mm plates and were passaged onto 6-well plates prior to the beginning of the experiment. HMC3 (microglia) were treated with LPS at 10 µg/mL concentration or given PBS of equal volume (for control). Cells were also given 5 µL of CellTracker Violet dye (Thermo Fisher Scientific, C10094). 24 h following LPS treatment, cells were trypsinized, washed and pelleted three times, and added to

coverslips containing differentiated DA neurons previously exposed to PFFs (5.0 x 10^4 cells per coverslip). Microglia were incubated with DA neurons, in Neurobasal media for 48 h prior to fixation. Samples were then stained with β-III tubulin and prepared for microscopy.

Cell Line Panel Experiments

U87 and U2OS cells were grown in 500 mL DMEM media, supplemented with 10% bovine calf serum, 2 mM of L-Glutamine, and 100 IU Penicillin 100 µg/ml Streptomycin. SH-SY5Y cells were grown in 500 mL of Advanced DMEM (Gibco, Thermo Fisher Scientific, 12634028) supplemented with 10% bovine calf serum, 2 mM of L-Glutamine, and Antibiotic-Antimycotic at 1x. Cells were grown and expanded on 150 mm plates and were passaged onto 6-well plates. Cells were treated with PFF for 48 h, trypsin washed on ice for 30 s, trypsinized, plated onto new 6-well plates and incubated for 48 h. Cells were then plated at low confluency onto poly-L-lysine (MilliporeSigma, A-004-M) treated coverslips and incubated in fresh media for another 24 h. Cells were then treated with IFN-γ (or PBS for the PFF-only condition), for 24 h. Cells were then given fresh media, and incubated for 8 days. The cells in the PFF-only condition had to be passaged once more 96 h later, due to overconfluency. Cells were then fixed, stained with LAMP1 (Cell Signaling Technology, 9091S) and Phalloidin (Thermo Fisher Scientific, A30104) and prepared for imaging.

Graphical Abstract and Graphical Representation of treatment regimes

Graphical abstract, graphical representation of treatments, and models were created using Biorender.com.

Cell and Inclusion Count

An automated approach was taken for the cell and inclusion counts as described by Labno . Cells and inclusions were counted by loading single-channel images into ImageJ (NIH) and performing the "analyze particles" function, following thresholding of images. The same threshold was used for all the conditions within each experiment (thresholds were different for different experiments). For cell count, the nuclear staining channel was used, and for inclusions the PFF channel was used. For inclusions, particles smaller than 2.0 μm in diameter were not included in our count.

Inclusion Size

Using the "analyze particles" function in ImageJ, thresholded single channel images were loaded into ImageJ and particles of high circularity and 0-infinity in size were selected. The "show" and "outline" options were also chosen. From the outlines produced by ImageJ, the diameters of the inclusions were then measured manually. For the images in which inclusion size was measured, a high threshold was set to exclude most lysosomal-PFF but include smaller puncta with high intensity levels. This was done so that a measure of the more intensely fluorescent puncta was incorporated in our size calculation. Although some puncta measured were under 2.0 μm in diameter, which is below our inclusion definition set above, we believe that this provides a better representation of where most PFFs are located, and what sort of structures they are localized to. In samples where PFFs are less aggregated, the brightest puncta were smaller, whereas in 14 d samples, more of the brightest PFF puncta will be localized to inclusions and therefore the PFF

puncta will be of larger size. In short, we wanted to measure the size of the PFF puncta with the highest fluorescence intensities.

Lysosomal Count, Lysosomal Size, Fluorescence Intensity

To count the number of lysosomes per cell, results shown in Extended Data Figure 4.7, the MorphoLibJ plugin (Legland et al., 2016) was used, using fluorescent microscopy data. Single plane, single cell, single channel images previously thresholded were then loaded into ImageJ, and the number of puncta was calculated according to the methods outlined by Peters et al. (Peters et al., 2021). Lysosomal size was calculated using electron micrographs, and the lysosomes were measured manually using GMS 3.0 (Gatan). Fluorescence intensity was calculated using LAS X (Leica) software, where channel intensities are quantified using the "Quantification" function.

Quantification Analysis

Measurements, including cell/inclusion count, inclusion size and puncta number, were all inputted into Graphpad Prism 9.0. Quantification data was statistically analyzed, using Student's t-test when only two conditions were being compared, one-way ANOVA for multiple conditions (along with post hoc Tukey's test), and two-way ANOVA when comparing multiple independent variables and multiple dependent variables (multiple comparisons was done within each column across different rows). All raw data and statistical analyses (not multiple comparisons analyses) have been deposited into Mendeley data online repository.

Antibodies

Anti-LAMP1 (D2D11) Antibody was from Cell Signaling Technology Cat. number 9091, RRID: AB_2687579. Anti-Tyrosine Hydroxylase antibody was from Abcam Cat. number ab76442, RRID:AB_1524535. Anti-Tyrosine Hydroxylase antibody [EP1532Y] - Neuronal Marker was from Abcam Cat. number ab137869, RRID:AB_2801410. Anti-LAMP2 antibody [H4B4] – Lysosome Marker was from Abcam Cat. number ab25631, RRID:AB_47070. Anti-HDAC6 (D2E5) Rabbit monoclonal Antibody was from Cell Signaling Technology Cat. number 7558, RRID:AB_10891804. Anti-NRF2 (D1Z9C) was from Cell Signaling Technology Cat. number 12721, RRID:AB_2715528. Anti-alpha Synuclein antibody [syn211] was from Abcam Cat. number ab75305, RRID:AB_1309948. Anti-Rab5 Antibody was from Cell Signaling Technology Cat. number 2143, RRID:AB_823625. Anti-alpha Synuclein (phospho S129) antibody was from Abcam Cat. number ab59264, RRID:AB_2270761. Anti-Phosphorylated α-Synuclein (pSyn#64) was from Wako, FUJIFILM Cat. number 015-25191, RRID:AB_2537218. Anti-Beta-III-Tubulin (Tuj1) antibody was from Abcam Cat. number ab41489, RRID:AB_727049. Anti-MAP2 Antibody was from Novus Biologicals Cat. number NBP1-48604, RRID:AB_10011223. Anti-PSD95 antibody [7E3-1B8] was from Abcam Cat. number ab18258, RRID:AB_444362. Anti-HA tag antibody - ChIP Grade (ab9110) was from Abcam Cat. number ab9110, RRID:AB_307019. Anti-HA tag antibody [HA.C5] (ab18181) was from Abcam Cat. number ab137838, RRID:AB_2810986. Anti-IFN-γ (D3H2) was from Cell Signaling Technology Cat. number 8455, RRID:AB_2797644. Anti-GIRK2 antibody was from Abcam Cat. number ab65096, RRID:AB_1139732. Anti-Dopamine Transporter antibody [EPR19695] was from Abcam Cat. number ab184451, RRID:AB_2890225. Anti-160 kDa Neurofilament Medium antibody

[EPR23510-76] was from Abcam Cat. number ab254348, RRID: N/A. Recombinant Anti-IFNGR1 antibody [EPR7866] was from Abcam Cat. number ab134070, RRID: N/A. Anti-IFN gamma Receptor beta/AF-1 antibody (IFNGR2) was from Abcam Cat. number ab77246, RRID:AB_1951968. Anti-LC3B (D11) was from Cell Signaling Technology Cat. number 3868S, RRID:AB_2137707. Anti-Midkine antibody was from Thermo Fisher Scientific Cat. number MA5-32538, RRID: AB_2809815. Anti-TFEB (D2O7D) was from Cell Signaling Technology Cat. number 37785, RRID:AB_2799119. Anti-Recombinant Anti-TFEB antibody [EPR22941-6] was from Abcam Cat. number ab267351, RRID: N/A. Anti-Human TFEB Antibody was from Bio-Techne Cat. number MAB9170, RRID: N/A. Hsc70/Hsp73 monoclonal antibody was from Enzo Life Sciences Cat. number ADI-SPA-815-488-E, RRID:AB_2039277. Alexa Fluor Plus 405 Phalloidin was from Thermo Fisher Scientific Cat. number A30104, RRID: N/A. Alexa Fluor 647 Goat anti-Chicken IgY Secondary Antibody was from Thermo Fisher Scientific Cat. number A-21449, RRID:AB_2535866. Alexa Fluor 647 Goat anti-Mouse IgG Highly Cross-Adsorbed Secondary Antibody was from Thermo Fisher Scientific Cat. number A-21236, RRID:AB_2535805. Alexa Fluor Plus 488 Goat anti-Mouse IgG Highly Cross-Adsorbed Secondary Antibody was from Thermo Fisher Scientific Cat. number A32723, RRID:AB_2633275. Alexa Fluor 568 Goat anti-Rabbit IgG Highly Cross-Adsorbed Secondary Antibody Thermo Fisher Scientific Cat. number A-11036, RRID:AB_10563566. Alexa Fluor Plus 405 Goat anti-Chicken IgY Cross-Adsorbed Secondary Antibody was from Thermo Fisher Scientific Cat. number A48260, RRID:AB_2890271.

Software and algorithms

- ImageJ: https://imagej.nih.gov/ij/
- LAS X 3.5.5 by Leica: https://www.leica-microsystems.com/products/microscope-software/p/leica-las-x-ls/
- Prism by Gaphpad: https://www.graphpad.com/scientific-software/prism/
- ZEN 3.5 by Zeiss: https://www.zeiss.com/microscopy/int/products/microscope-software/zen.html
- GMS 3 by Gatan: https://www.gatan.com/products/tem-analysis/gatan-microscopy-suite-software

Resource Availability

Lead Contact

Further information and requests for resources and reagents should be directed to the Lead Contact, Dr. Peter Scott McPherson (peter.mcpherson@mcgill.ca) and will be fulfilled. Further information regarding experimental protocols and procedures should be directed to Armin Bayati (armin.bayati@mail.mcgill.ca).

Materials Availability

This study did not generate new unique reagents.

Data and Code Availability

- All the raw data, along with statistical calculations used in this paper have been deposited at Mendeley Data: Bayati, Armin; McPherson, Peter (2023), "Formation and maintenance of Lewy body-like inclusions in human dopaminergic neurons", Mendeley Data, V1, doi: 10.17632/kp3774p92d.1. This is publicly available as of the date of submission. DOIs are listed in the key resources table.
- This paper does not report original code.

- Any additional information required to reanalyze the data reported in this paper is available from the lead contact upon request.

4.9 References

Abokyi, S., Shan, S. W., To, C. H., Chan, H. H., & Tse, D. Y. (2020). Autophagy Upregulation by the TFEB Inducer Trehalose Protects against Oxidative Damage and Cell Death Associated with NRF2 Inhibition in Human RPE Cells. *Oxid Med Cell Longev*, *2020*, 5296341. https://doi.org/10.1155/2020/5296341

Ahmadi Rastegar, D., Hughes, L. P., Perera, G., Keshiya, S., Zhong, S., Gao, J., Halliday, G. M., Schule, B., & Dzamko, N. (2022). Effect of LRRK2 protein and activity on stimulated cytokines in human monocytes and macrophages. *NPJ Parkinsons Dis*, *8*(1), 34. https://doi.org/10.1038/s41531-022-00297-9

Baba, M., Nakajo, S., Tu, P. H., Tomita, T., Nakaya, K., Lee, V. M., Trojanowski, J. Q., & Iwatsubo, T. (1998). Aggregation of alpha-synuclein in Lewy bodies of sporadic Parkinson's disease and dementia with Lewy bodies. *The American Journal of Pathology*, *152*(4), 879-884. https://pubmed.ncbi.nlm.nih.gov/9546347
https://www.ncbi.nlm.nih.gov/pmc/articles/PMC1858234/

Bayati, A., Banks, E., Han, C., Luo, W., Reintsch, W. E., Zorca, C. E., Shlaifer, I., Del Cid Pellitero, E., Vanderperre, B., McBride, H. M., Fon, E. A., Durcan, T. M., & McPherson, P. S. (2022). Rapid macropinocytic transfer of alpha-synuclein to lysosomes. *Cell Rep*, *40*(3), 111102. https://doi.org/10.1016/j.celrep.2022.111102

Bieri, G., Gitler, A. D., & Brahic, M. (2018). Internalization, axonal transport and release of fibrillar forms of alpha-synuclein. *Neurobiol Dis*, *109*(Pt B), 219-225. https://doi.org/10.1016/j.nbd.2017.03.007

Birey, F., Andersen, J., Makinson, C. D., Islam, S., Wei, W., Huber, N., Fan, H. C., Metzler, K. R. C., Panagiotakos, G., Thom, N., O'Rourke, N. A., Steinmetz, L. M., Bernstein, J. A., Hallmayer, J., Huguenard, J. R., & Pasca, S. P. (2017). Assembly of functionally integrated human forebrain spheroids. *Nature*, *545*(7652), 54-59. https://doi.org/10.1038/nature22330

Boman, A., Svensson, S., Boxer, A., Rojas, J. C., Seeley, W. W., Karydas, A., Miller, B., Kagedal, K., & Svenningsson, P. (2016). Distinct Lysosomal Network Protein Profiles in Parkinsonian Syndrome Cerebrospinal Fluid. *J Parkinsons Dis*, *6*(2), 307-315. https://doi.org/10.3233/JPD-150759

Braak, H., Sandmann-Keil, D., Gai, W., & Braak, E. (1999). Extensive axonal Lewy neurites in Parkinson's disease: a novel pathological feature revealed by alpha-synuclein immunocytochemistry. *Neurosci Lett*, *265*(1), 67-69. https://doi.org/10.1016/s0304-3940(99)00208-6

Braak, H., Tredici, K. D., Rüb, U., de Vos, R. A. I., Jansen Steur, E. N. H., & Braak, E. (2003). Staging of brain pathology related to sporadic Parkinson's disease. *Neurobiology of Aging*, *24*(2), 197-211. https://doi.org/10.1016/s0197-4580(02)00065-9

Burberry, A., Wells, M. F., Limone, F., Couto, A., Smith, K. S., Keaney, J., Gillet, G., van Gastel, N., Wang, J. Y., Pietilainen, O., Qian, M., Eggan, P., Cantrell, C., Mok, J., Kadiu, I.,

Scadden, D. T., & Eggan, K. (2020). C9orf72 suppresses systemic and neural inflammation induced by gut bacteria. *Nature*, *582*(7810), 89-94. https://doi.org/10.1038/s41586-020-2288-7

Callizot, N., Combes, M., Henriques, A., & Poindron, P. (2019). Necrosis, apoptosis, necroptosis, three modes of action of dopaminergic neuron neurotoxins. *PLoS One*, *14*(4), e0215277. https://doi.org/10.1371/journal.pone.0215277

Colosimo, C., Hughes, A., Kilford, L., & Lees, A. (2003). Lewy body cortical involvement may not always predict dementia in Parkinson's disease. *Journal of Neurology, Neurosurgery & Psychiatry*, *74*(7), 852-856.

Conway, K. A., Harper, J. D., & Lansbury, P. T. (1998). Accelerated in vitro fibril formation by a mutant alpha-synuclein linked to early-onset Parkinson disease. *Nat Med*, *4*(11), 1318-1320. https://doi.org/10.1038/3311

Cortes, C. J., & La Spada, A. R. (2019). TFEB dysregulation as a driver of autophagy dysfunction in neurodegenerative disease: Molecular mechanisms, cellular processes, and emerging therapeutic opportunities. *Neurobiol Dis*, *122*, 83-93. https://doi.org/10.1016/j.nbd.2018.05.012

De Simone, R., Levi, G., & Aloisi, F. (1998). Interferon gamma gene expression in rat central nervous system glial cells. *Cytokine*, *10*(6), 418-422. https://doi.org/10.1006/cyto.1997.0314

Dodson, M., Anandhan, A., Zhang, D. D., & Madhavan, L. (2021). An NRF2 Perspective on Stem Cells and Ageing. *Front Aging*, *2*, 690686. https://doi.org/10.3389/fragi.2021.690686

Duffy, P. E., & Tennyson, V. M. (1965). Phase and electron microscopic observations of Lewy bodies and melanin granules in the substantia nigra and locus caeruleus in Parkinson's disease. *Journal of Neuropathology & Experimental Neurology*, *24*(3), 398-414.

Duffy, S. S., Lees, J. G., & Moalem-Taylor, G. (2014). The contribution of immune and glial cell types in experimental autoimmune encephalomyelitis and multiple sclerosis. *Mult Scler Int*, *2014*, 285245. https://doi.org/10.1155/2014/285245

Durcan, T. M., & Fon, E. A. (2015). The three 'P's of mitophagy: PARKIN, PINK1, and post-translational modifications. *Genes Dev*, *29*(10), 989-999. https://doi.org/10.1101/gad.262758.115

Engelhardt, E., & Gomes, M. D. M. (2017). Lewy and his inclusion bodies: Discovery and rejection. *Dement Neuropsychol*, *11*(2), 198-201. https://doi.org/10.1590/1980-57642016dn11-020012

Eskelinen, E. L. (2006). Roles of LAMP-1 and LAMP-2 in lysosome biogenesis and autophagy. *Mol Aspects Med*, *27*(5-6), 495-502. https://doi.org/10.1016/j.mam.2006.08.005

Eskelinen, E. L., Illert, A. L., Tanaka, Y., Schwarzmann, G., Blanz, J., Von Figura, K., & Saftig, P. (2002). Role of LAMP-2 in lysosome biogenesis and autophagy. *Mol Biol Cell*, *13*(9), 3355-3368. https://doi.org/10.1091/mbc.e02-02-0114

Fan, Y., Li, C., Peng, X., Jiang, N., Hu, L., Gu, L., Zhu, G., Zhao, G., & Lin, J. (2020). Perillaldehyde Ameliorates Aspergillus fumigatus Keratitis by Activating the Nrf2/HO-1 Signaling Pathway and Inhibiting Dectin-1-Mediated Inflammation. *Invest Ophthalmol Vis Sci*, *61*(6), 51. https://doi.org/10.1167/iovs.61.6.51

Fang, C., Weng, T., Hu, S., Yuan, Z., Xiong, H., Huang, B., Cai, Y., Li, L., & Fu, X. (2021). IFN-gamma-induced ER stress impairs autophagy and triggers apoptosis in lung cancer cells. *Oncoimmunology*, *10*(1), 1962591. https://doi.org/10.1080/2162402X.2021.1962591

Fares, M. B., Jagannath, S., & Lashuel, H. A. (2021). Reverse engineering Lewy bodies: how far have we come and how far can we go? *Nat Rev Neurosci*, *22*(2), 111-131. https://doi.org/10.1038/s41583-020-00416-6

Forno, L. S., & Norville, R. L. (1976). Ultrastructure of Lewy bodies in the stellate ganglion. *Acta neuropathologica*, *34*, 183-197.

Forno, L. S., & Norville, R. L. (1976). Ultrastructure of Lewy bodies in the stellate ganglion. *Acta Neuropathol*, *34*(3), 183-197. https://doi.org/10.1007/BF00688674

Freeman, D., Cedillos, R., Choyke, S., Lukic, Z., McGuire, K., Marvin, S., Burrage, A. M., Sudholt, S., Rana, A., O'Connor, C., Wiethoff, C. M., & Campbell, E. M. (2013). Alpha-synuclein induces lysosomal rupture and cathepsin dependent reactive oxygen species following endocytosis. *PLoS One*, *8*(4), e62143. https://doi.org/10.1371/journal.pone.0062143

Frigerio, R., Fujishiro, H., Ahn, T. B., Josephs, K. A., Maraganore, D. M., DelleDonne, A., Parisi, J. E., Klos, K. J., Boeve, B. F., Dickson, D. W., & Ahlskog, J. E. (2011). Incidental Lewy body disease: do some cases represent a preclinical stage of dementia with Lewy bodies? *Neurobiol Aging*, *32*(5), 857-863. https://doi.org/10.1016/j.neurobiolaging.2009.05.019

Frucht, D. M., Fukao, T., Bogdan, C., Schindler, H., O'Shea, J. J., & Koyasu, S. (2001). IFN-gamma production by antigen-presenting cells: mechanisms emerge. *Trends Immunol*, *22*(10), 556-560. https://doi.org/10.1016/s1471-4906(01)02005-1

Fuyuno, Y., Uchi, H., Yasumatsu, M., Morino-Koga, S., Tanaka, Y., Mitoma, C., & Furue, M. (2018). Perillaldehyde Inhibits AHR Signaling and Activates NRF2 Antioxidant Pathway in Human Keratinocytes. *Oxid Med Cell Longev*, *2018*, 9524657. https://doi.org/10.1155/2018/9524657

Gai, W., Yuan, H., Li, X., Power, J., Blumbergs, P., & Jensen, P. (2000). In situ and in vitro study of colocalization and segregation of α-synuclein, ubiquitin, and lipids in Lewy bodies. *Experimental neurology*, *166*(2), 324-333.

Galloway, P., Mulvihill, P., & Perry, G. (1992). Filaments of Lewy bodies contain insoluble cytoskeletal elements. *The American Journal of Pathology*, *140*(4), 809.

Ghanekar, S. A., Nomura, L. E., Suni, M. A., Picker, L. J., Maecker, H. T., & Maino, V. C. (2001). Gamma interferon expression in CD8(+) T cells is a marker for circulating cytotoxic T lymphocytes that recognize an HLA A2-restricted epitope of human cytomegalovirus phosphoprotein pp65. *Clin Diagn Lab Immunol*, *8*(3), 628-631. https://doi.org/10.1128/CDLI.8.3.628-631.2001

Glausier, J. R., Konanur, A., & Lewis, D. A. (2019). Factors Affecting Ultrastructural Quality in the Prefrontal Cortex of the Postmortem Human Brain. *J Histochem Cytochem*, *67*(3), 185-202. https://doi.org/10.1369/0022155418819481

Gribaudo, S., Tixador, P., Bousset, L., Fenyi, A., Lino, P., Melki, R., Peyrin, J. M., & Perrier, A. L. (2019). Propagation of alpha-Synuclein Strains within Human Reconstructed Neuronal Network. *Stem Cell Reports*, *12*(2), 230-244. https://doi.org/10.1016/j.stemcr.2018.12.007

Guerra, F., Girolimetti, G., Beli, R., Mitruccio, M., Pacelli, C., Ferretta, A., Gasparre, G., Cocco, T., & Bucci, C. (2019). Synergistic Effect of Mitochondrial and Lysosomal Dysfunction in Parkinson's Disease. *Cells*, *8*(5). https://doi.org/10.3390/cells8050452

Huang, J., Pan, W., Ou, D., Dai, W., Lin, Y., Chen, Y., & Chen, X. (2015). LC3B, a Protein That Serves as an Autophagic Marker, Modulates Angiotensin II-induced Myocardial

Hypertrophy. *J Cardiovasc Pharmacol*, *66*(6), 576-583. https://doi.org/10.1097/fjc.0000000000000306

Iannielli, A., Luoni, M., Giannelli, S. G., Ferese, R., Ordazzo, G., Fossati, M., Raimondi, A., Opazo, F., Corti, O., Prehn, J. H. M., Gambardella, S., Melki, R., & Broccoli, V. (2022). Modeling native and seeded Synuclein aggregation and related cellular dysfunctions in dopaminergic neurons derived by a new set of isogenic iPSC lines with SNCA multiplications. *Cell Death Dis*, *13*(10), 881. https://doi.org/10.1038/s41419-022-05330-6

Jiang, P., Gan, M., Yen, S. H., McLean, P. J., & Dickson, D. W. (2017). Impaired endo-lysosomal membrane integrity accelerates the seeding progression of alpha-synuclein aggregates. *Sci Rep*, *7*(1), 7690. https://doi.org/10.1038/s41598-017-08149-w

Jorgovanovic, D., Song, M., Wang, L., & Zhang, Y. (2020). Roles of IFN-gamma in tumor progression and regression: a review. *Biomark Res*, *8*, 49. https://doi.org/10.1186/s40364-020-00228-x

Joshi, C. S., Mora, A., Felder, P. A., & Mysorekar, I. U. (2021). NRF2 promotes urothelial cell response to bacterial infection by regulating reactive oxygen species and RAB27B expression. *Cell Rep*, *37*(3), 109856. https://doi.org/10.1016/j.celrep.2021.109856

Kasen, A., Houck, C., Burmeister, A. R., Sha, Q., Brundin, L., & Brundin, P. (2022). Upregulation of alpha-synuclein following immune activation: Possible trigger of Parkinson's disease. *Neurobiol Dis*, *166*, 105654. https://doi.org/10.1016/j.nbd.2022.105654

Kawanokuchi, J., Mizuno, T., Takeuchi, H., Kato, H., Wang, J., Mitsuma, N., & Suzumura, A. (2006). Production of interferon-gamma by microglia. *Mult Scler*, *12*(5), 558-564. https://doi.org/10.1177/1352458506070763

Kim, W. S., Kagedal, K., & Halliday, G. M. (2014). Alpha-synuclein biology in Lewy body diseases. *Alzheimers Res Ther*, *6*(5), 73. https://doi.org/10.1186/s13195-014-0073-2

Klein, A. D., & Mazzulli, J. R. (2018). Is Parkinson's disease a lysosomal disorder? *Brain*, *141*(8), 2255-2262. https://doi.org/10.1093/brain/awy147

Kulkarni, A., Ganesan, P., & O'Donnell, L. A. (2016). Interferon Gamma: Influence on Neural Stem Cell Function in Neurodegenerative and Neuroinflammatory Disease. *Clin Med Insights Pathol*, *9*(Suppl 1), 9-19. https://doi.org/10.4137/CPath.S40497

Lam, I., Ndayisaba, A., Lewis, A. J., Fu, Y., Sagredo, G. T., Zaccagnini, L., Sandoe, J., Sanz, R. L., Vahdatshoar, A., Martin, T. D., Morshed, N., Ichihashi, T., Tripathi, A., Ramalingam, N., Oettgen-Suazo, C., Bartels, T., Schäbinger, M., Hallacli, E., Jiang, X., . . . Khurana, V. (2022). Rapid iPSC inclusionopathy models shed light on formation, consequence and molecular subtype of α-synuclein inclusions. In: BioRxiv.

Lees, J. R., & Cross, A. H. (2007). A little stress is good: IFN-gamma, demyelination, and multiple sclerosis. *J Clin Invest*, *117*(2), 297-299. https://doi.org/10.1172/JCI31254

Liu, X., & Quan, N. (2018). Microglia and CNS Interleukin-1: Beyond Immunological Concepts. *Front Neurol*, *9*, 8. https://doi.org/10.3389/fneur.2018.00008

Luk, K. C., Song, C., O'Brien, P., Stieber, A., Branch, J. R., Brunden, K. R., Trojanowski, J. Q., & Lee, V. M. (2009). Exogenous alpha-synuclein fibrils seed the formation of Lewy body-like intracellular inclusions in cultured cells. *Proc Natl Acad Sci U S A*, *106*(47), 20051-20056. https://doi.org/10.1073/pnas.0908005106

Lv, D., Liu, Y., Guo, F., Wu, A., Mo, Y., Wang, S., & Chu, J. (2020). Combining interferon-gamma release assays with lymphocyte enumeration for diagnosis of Mycobacterium tuberculosis

infection. *J Int Med Res*, *48*(6), 300060520925660. https://doi.org/10.1177/0300060520925660

Mahul-Mellier, A. L., Burtscher, J., Maharjan, N., Weerens, L., Croisier, M., Kuttler, F., Leleu, M., Knott, G. W., & Lashuel, H. A. (2020). The process of Lewy body formation, rather than simply alpha-synuclein fibrillization, is one of the major drivers of neurodegeneration. *Proc Natl Acad Sci U S A*, *117*(9), 4971-4982. https://doi.org/10.1073/pnas.1913904117

Malkus, K. A., & Ischiropoulos, H. (2012). Regional deficiencies in chaperone-mediated autophagy underlie alpha-synuclein aggregation and neurodegeneration. *Neurobiol Dis*, *46*(3), 732-744. https://doi.org/10.1016/j.nbd.2012.03.017

Martinez-Vicente, M., Talloczy, Z., Kaushik, S., Massey, A. C., Mazzulli, J., Mosharov, E. V., Hodara, R., Fredenburg, R., Wu, D. C., Follenzi, A., Dauer, W., Przedborski, S., Ischiropoulos, H., Lansbury, P. T., Sulzer, D., & Cuervo, A. M. (2008). Dopamine-modified alpha-synuclein blocks chaperone-mediated autophagy. *J Clin Invest*, *118*(2), 777-788. https://doi.org/10.1172/JCI32806

Matheoud, D., Cannon, T., Voisin, A., Penttinen, A. M., Ramet, L., Fahmy, A. M., Ducrot, C., Laplante, A., Bourque, M. J., Zhu, L., Cayrol, R., Le Campion, A., McBride, H. M., Gruenheid, S., Trudeau, L. E., & Desjardins, M. (2019). Intestinal infection triggers Parkinson's disease-like symptoms in Pink1(-/-) mice. *Nature*, *571*(7766), 565-569. https://doi.org/10.1038/s41586-019-1405-y

Meiser, J., Weindl, D., & Hiller, K. (2013). Complexity of dopamine metabolism. *Cell Commun Signal*, *11*(1), 34. https://doi.org/10.1186/1478-811X-11-34

Miura, Y., Li, M. Y., Revah, O., Yoon, S. J., Narazaki, G., & Pasca, S. P. (2022). Engineering brain assembloids to interrogate human neural circuits. *Nat Protoc*, *17*(1), 15-35. https://doi.org/10.1038/s41596-021-00632-z

Mohamed, N. V., Sirois, J., Ramamurthy, J., Mathur, M., Lepine, P., Deneault, E., Maussion, G., Nicouleau, M., Chen, C. X., Abdian, N., Soubannier, V., Cai, E., Nami, H., Thomas, R. A., Wen, D., Tabatabaei, M., Beitel, L. K., Singh Dolt, K., Karamchandani, J., . . . Durcan, T. M. (2021). Midbrain organoids with an SNCA gene triplication model key features of synucleinopathy. *Brain Commun*, *3*(4), fcab223. https://doi.org/10.1093/braincomms/fcab223

Molteni, M., & Rossetti, C. (2017). Neurodegenerative diseases: The immunological perspective. *J Neuroimmunol*, *313*, 109-115. https://doi.org/10.1016/j.jneuroim.2017.11.002

Monaco, A., & Fraldi, A. (2020). Protein Aggregation and Dysfunction of Autophagy-Lysosomal Pathway: A Vicious Cycle in Lysosomal Storage Diseases. *Front Mol Neurosci*, *13*, 37. https://doi.org/10.3389/fnmol.2020.00037

Morell, C., Bort, A., Vara-Ciruelos, D., Ramos-Torres, A., Altamirano-Dimas, M., Diaz-Laviada, I., & Rodriguez-Henche, N. (2016). Up-Regulated Expression of LAMP2 and Autophagy Activity during Neuroendocrine Differentiation of Prostate Cancer LNCaP Cells. *PLoS One*, *11*(9), e0162977. https://doi.org/10.1371/journal.pone.0162977

Nagakannan, P., Tabeshmehr, P., & Eftekharpour, E. (2020). Oxidative damage of lysosomes in regulated cell death systems: Pathophysiology and pharmacologic interventions. *Free Radic Biol Med*, *157*, 94-127. https://doi.org/10.1016/j.freeradbiomed.2020.04.001

Navarro-Romero, A., Montpeyo, M., & Martinez-Vicente, M. (2020). The Emerging Role of the Lysosome in Parkinson's Disease. *Cells*, *9*(11). https://doi.org/10.3390/cells9112399

Nicolet, B. P., Guislain, A., van Alphen, F. P. J., Gomez-Eerland, R., Schumacher, T. N. M., van den Biggelaar, M., & Wolkers, M. C. (2020). CD29 identifies IFN-gamma-producing human CD8(+) T cells with an increased cytotoxic potential. *Proc Natl Acad Sci U S A*, *117*(12), 6686-6696. https://doi.org/10.1073/pnas.1913940117

Pajares, M., Rojo, A. I., Arias, E., Diaz-Carretero, A., Cuervo, A. M., & Cuadrado, A. (2018). Transcription factor NFE2L2/NRF2 modulates chaperone-mediated autophagy through the regulation of LAMP2A. *Autophagy*, *14*(8), 1310-1322. https://doi.org/10.1080/15548627.2018.1474992

Panagiotakopoulou, V., Ivanyuk, D., De Cicco, S., Haq, W., Arsic, A., Yu, C., Messelodi, D., Oldrati, M., Schondorf, D. C., Perez, M. J., Cassatella, R. P., Jakobi, M., Schneiderhan-Marra, N., Gasser, T., Nikic-Spiegel, I., & Deleidi, M. (2020). Interferon-gamma signaling synergizes with LRRK2 in neurons and microglia derived from human induced pluripotent stem cells. *Nat Commun*, *11*(1), 5163. https://doi.org/10.1038/s41467-020-18755-4

Park, J. Y., Kim, S., Sohn, H. Y., Koh, Y. H., & Jo, C. (2019). TFEB activates Nrf2 by repressing its E3 ubiquitin ligase DCAF11 and promoting phosphorylation of p62. *Sci Rep*, *9*(1), 14354. https://doi.org/10.1038/s41598-019-50877-8

Polymeropoulos, M. H., Lavedan, C., Leroy, E., Ide, S. E., Dehejia, A., Dutra, A., Pike, B., Root, H., Rubenstein, J., Boyer, R., Stenroos, E. S., Chandrasekharappa, S., Athanassiadou, A., Papapetropoulos, T., Johnson, W. G., Lazzarini, A. M., Duvoisin, R. C., Di Iorio, G., Golbe, L. I., & Nussbaum, R. L. (1997). Mutation in the alpha-synuclein gene identified in families with Parkinson's disease. *Science*, *276*(5321), 2045-2047. https://doi.org/10.1126/science.276.5321.2045

Rajput, A. H., Offord, K. P., Beard, C. M., & Kurland, L. T. (1984). Epidemiology of parkinsonism: incidence, classification, and mortality. *Ann Neurol*, *16*(3), 278-282. https://doi.org/10.1002/ana.410160303

Rezai-Zadeh, K., Gate, D., & Town, T. (2009). CNS infiltration of peripheral immune cells: D-Day for neurodegenerative disease? *J Neuroimmune Pharmacol*, *4*(4), 462-475. https://doi.org/10.1007/s11481-009-9166-2

Roy, E., & Cao, W. (2022). Glial interference: impact of type I interferon in neurodegenerative diseases. *Mol Neurodegener*, *17*(1), 78. https://doi.org/10.1186/s13024-022-00583-3

Runwal, G., Stamatakou, E., Siddiqi, F. H., Puri, C., Zhu, Y., & Rubinsztein, D. C. (2019). LC3-positive structures are prominent in autophagy-deficient cells. *Sci Rep*, *9*(1), 10147. https://doi.org/10.1038/s41598-019-46657-z

Saha, S., Buttari, B., Profumo, E., Tucci, P., & Saso, L. (2021). A Perspective on Nrf2 Signaling Pathway for Neuroinflammation: A Potential Therapeutic Target in Alzheimer's and Parkinson's Diseases. *Front Cell Neurosci*, *15*, 787258. https://doi.org/10.3389/fncel.2021.787258

Sato, S., Uchihara, T., Fukuda, T., Noda, S., Kondo, H., Saiki, S., Komatsu, M., Uchiyama, Y., Tanaka, K., & Hattori, N. (2018). Loss of autophagy in dopaminergic neurons causes Lewy pathology and motor dysfunction in aged mice. *Sci Rep*, *8*(1), 2813. https://doi.org/10.1038/s41598-018-21325-w

Scudamore, O., & Ciossek, T. (2018). Increased Oxidative Stress Exacerbates alpha-Synuclein Aggregation In Vivo. *J Neuropathol Exp Neurol*, *77*(6), 443-453. https://doi.org/10.1093/jnen/nly024

Seifert, H. A., Collier, L. A., Chapman, C. B., Benkovic, S. A., Willing, A. E., & Pennypacker, K. R. (2014). Pro-inflammatory interferon gamma signaling is directly associated with stroke induced neurodegeneration. *J Neuroimmune Pharmacol*, *9*(5), 679-689. https://doi.org/10.1007/s11481-014-9560-2

Shahmoradian, S. H., Lewis, A. J., Genoud, C., Hench, J., Moors, T. E., Navarro, P. P., Castano-Diez, D., Schweighauser, G., Graff-Meyer, A., Goldie, K. N., Sutterlin, R., Huisman, E., Ingrassia, A., Gier, Y., Rozemuller, A. J. M., Wang, J., Paepe, A., Erny, J., Staempfli, A., . . . Lauer, M. E. (2019). Lewy pathology in Parkinson's disease consists of crowded organelles and lipid membranes. *Nat Neurosci*, *22*(7), 1099-1109. https://doi.org/10.1038/s41593-019-0423-2

Smith, J. A., Das, A., Ray, S. K., & Banik, N. L. (2012). Role of pro-inflammatory cytokines released from microglia in neurodegenerative diseases. *Brain Res Bull*, *87*(1), 10-20. https://doi.org/10.1016/j.brainresbull.2011.10.004

Soper, J. H., Roy, S., Stieber, A., Lee, E., Wilson, R. B., Trojanowski, J. Q., Burd, C. G., & Lee, V. M. (2008). Alpha-synuclein-induced aggregation of cytoplasmic vesicles in Saccharomyces cerevisiae. *Mol Biol Cell*, *19*(3), 1093-1103. https://doi.org/10.1091/mbc.e07-08-0827

Soper, J. H., Roy, S., Stieber, A., Lee, E., Wilson, R. B., Trojanowski, J. Q., Burd, C. G., & Lee, V. M.-Y. (2008). α-Synuclein–induced Aggregation of Cytoplasmic Vesicles in Saccharomyces cerevisiae. *Molecular biology of the cell*, *19*(3), 1093-1103.

Spillantini, M. G., Schmidt, M. L., Lee, V. M., Trojanowski, J. Q., Jakes, R., & Goedert, M. (1997). Alpha-synuclein in Lewy bodies. *Nature*, *388*(6645), 839-840. https://doi.org/https://doi.org/10.1038/42166

Suzen, S., Tucci, P., Profumo, E., Buttari, B., & Saso, L. (2022). A Pivotal Role of Nrf2 in Neurodegenerative Disorders: A New Way for Therapeutic Strategies. *Pharmaceuticals (Basel)*, *15*(6). https://doi.org/10.3390/ph15060692

Suzuki, Y., Claflin, J., Wang, X., Lengi, A., & Kikuchi, T. (2005). Microglia and macrophages as innate producers of interferon-gamma in the brain following infection with Toxoplasma gondii. *Int J Parasitol*, *35*(1), 83-90. https://doi.org/10.1016/j.ijpara.2004.10.020

Tang, L. F., Ma, X., Xie, L. W., Zhou, H., Yu, J., Wang, Z. X., & Li, M. (2023). Perillaldehyde Mitigates Ionizing Radiation-Induced Intestinal Injury by Inhibiting Ferroptosis via the Nrf2 Signaling Pathway. *Mol Nutr Food Res*, e2300232. https://doi.org/10.1002/mnfr.202300232

Tanudjojo, B., Shaikh, S. S., Fenyi, A., Bousset, L., Agarwal, D., Marsh, J., Zois, C., Heman-Ackah, S., Fischer, R., Sims, D., Melki, R., & Tofaris, G. K. (2021). Phenotypic manifestation of alpha-synuclein strains derived from Parkinson's disease and multiple system atrophy in human dopaminergic neurons. *Nat Commun*, *12*(1), 3817. https://doi.org/10.1038/s41467-021-23682-z

Vergarajauregui, S., Connelly, P. S., Daniels, M. P., & Puertollano, R. (2008). Autophagic dysfunction in mucolipidosis type IV patients. *Hum Mol Genet*, *17*(17), 2723-2737. https://doi.org/10.1093/hmg/ddn174

Wakabayashi, K., Tanji, K., Odagiri, S., Miki, Y., Mori, F., & Takahashi, H. (2013). The Lewy body in Parkinson's disease and related neurodegenerative disorders. *Mol Neurobiol*, *47*(2), 495-508. https://doi.org/10.1007/s12035-012-8280-y

Wang, X., & Suzuki, Y. (2007). Microglia produce IFN-gamma independently from T cells during acute toxoplasmosis in the brain. *J Interferon Cytokine Res*, *27*(7), 599-605. https://doi.org/10.1089/jir.2006.0157

Watanabe, I., Vachal, E., & Tomita, T. (1977). Dense core vesicles around the Lewy body in incidental Parkinson's disease: an electron microscopic study. *Acta neuropathologica*, *39*(2), 173-175.

Yang, Q., Wang, G., & Zhang, F. (2020). Role of Peripheral Immune Cells-Mediated Inflammation on the Process of Neurodegenerative Diseases. *Front Immunol*, *11*, 582825. https://doi.org/10.3389/fimmu.2020.582825

Yang, Y., Wang, H. J., Hu, W. L., Bai, G. N., & Hua, C. Z. (2022). Diagnostic Value of Interferon-Gamma Release Assays for Tuberculosis in the Immunocompromised Population. *Diagnostics (Basel)*, *12*(2). https://doi.org/10.3390/diagnostics12020453

Zhang, L., Wang, M., Sterling, N. W., Lee, E. Y., Eslinger, P. J., Wagner, D., Du, G., Lewis, M. M., Truong, Y., Bowman, F. D., & Huang, X. (2018). Cortical Thinning and Cognitive Impairment in Parkinson's Disease without Dementia. *IEEE/ACM Trans Comput Biol Bioinform*, *15*(2), 570-580. https://doi.org/10.1109/TCBB.2015.2465951

Zhang, S., Wang, R., & Wang, G. (2019). Impact of Dopamine Oxidation on Dopaminergic Neurodegeneration. *ACS Chem Neurosci*, *10*(2), 945-953. https://doi.org/10.1021/acschemneuro.8b00454

Zhang, W., Wang, T., Pei, Z., Miller, D. S., Wu, X., Block, M. L., Wilson, B., Zhang, W., Zhou, Y., Hong, J. S., & Zhang, J. (2005). Aggregated alpha-synuclein activates microglia: a process leading to disease progression in Parkinson's disease. *FASEB J*, *19*(6), 533-542. https://doi.org/10.1096/fj.04-2751com

Zhang, X., Wang, R., Chen, H., Jin, C., Jin, Z., Lu, J., Xu, L., Lu, Y., Zhang, J., & Shi, L. (2022). Aged microglia promote peripheral T cell infiltration by reprogramming the microenvironment of neurogenic niches. *Immun Ageing*, *19*(1), 34. https://doi.org/10.1186/s12979-022-00289-6

Zheng, W., Liu, B., & Shi, E. (2021). Perillaldehyde Alleviates Spinal Cord Ischemia-Reperfusion Injury Via Activating the Nrf2 Pathway. *J Surg Res*, *268*, 308-317. https://doi.org/10.1016/j.jss.2021.06.055

Zhu, S. Y., Yao, R. Q., Li, Y. X., Zhao, P. Y., Ren, C., Du, X. H., & Yao, Y. M. (2020). Lysosomal quality control of cell fate: a novel therapeutic target for human diseases. *Cell Death Dis*, *11*(9), 817. https://doi.org/10.1038/s41419-020-03032-5

CHAPTER 5. DISCUSSION, GENERAL CONCLUSIONS

5.1 The dual nature of α-syn

Since the presence of α-syn was confirmed in LBs (M. G. Spillantini et al., 1997), scientists have tried to understand this protein's characteristics. They have done so through many biochemical studies to understand its affinity towards organelles, membranes, proteins, and its localization in different regions of the cell (Bertoncini et al., 2005; Fredenburg et al., 2007; Heise et al., 2005; H.-J. Lee et al., 2008). At every point, α-syn has remained elusive. While it may have a multimeric form in the cell (Bartels et al., 2011; Dettmer et al., 2017), it is also present in the cell in an intrinsically disordered monomeric form (Ludtmann et al., 2016; Westphal & Chandra, 2013). While it is mostly localized to the synapse in neurons (Vargas et al., 2021; Vargas et al., 2014; Vargas et al., 2017), α-syn's functions seem to go beyond simply the modulating synaptic vesicle release and aiding in their organization in the presynaptic region (Lautenschlager et al., 2017; Vargas et al., 2017). As some have shown, this protein also acts as a stabilizing agent for RNA throughout the cell, and also plays a role in the cellular stress response (Chung et al., 2017; Hallacli et al., 2022). At the same time, *SNCA* knockout mice seem to function normally with regular cognitive and motor functions (Cabin et al., 2002).

As a biological phenomenon, α-syn is the perfect question to be lost in, as a scientist pursuing a career in biomedical research. From a disease/treatment perspective, α-syn could not be a more elusive and indecisive protein. Even its pathological form is puzzling, as different oligomeric sizes of α-syn have a different propensity for aggregation and seeding (A. L. Fink, 2006; Pieri et al., 2016). In addition, α-syn WT oligomers and fibrils act differently than those generated from mutant forms of α-syn (Conway et al., 1998; Conway, Harper, et al., 2000;

Conway, Lee, et al., 2000; Narhi et al., 1999; Stefanis et al., 2001). There are also different strains of α-syn fibrils (Peelaerts et al., 2015; Peng et al., 2018). Also, while the oligomeric form of the protein has a higher affinity for membranes than its endogenous form, its non-oligomeric form still acts as a tether between membranous synaptic vesicles (Vargas et al., 2017).

This elusive nature of α-syn, similar to how matter acts as both a wave and a particle, is not limited to its biochemical characteristics. This elusiveness is also present in the diseases that involve α-syn, otherwise known as synucleinopathies. Current research on the mechanistic aspect of PD falls into one of two main categories: mitochondrial versus α-syn. The mitochondrial approach to the study of the mechanistic underpinnings of PD, suggests that the ultimate dysfunction of mitochondria and impairment of cellular respiration cause all matters that give rise to PD (Surmeier & Sulzer, 2013). This theory is often supported by evidence found in two familial forms of PD: PINK1 and Parkin (Dawson & Dawson, 2010; Valente et al., 2004). These two forms of familial PD are highly penetrant and do not involve Lewy bodies, protein aggregation, and α-syn spread. The other side of PD research focuses exclusively on the aggregation of α-syn (Minami Baba et al., 1998; Beyer, 2006; Anthony L. Fink, 2006; Vilar et al., 2008), whether through the propagation of the exogenous form of α-syn or through using mutations or locus multiplication models of *SNCA*.

Having studied both sides, it was interesting to see how deep the chasm between these two factions of PD research is. Research falling on either side does its best not to acknowledge the other side. Luckily, an emerging and ever-expanding faction exists in PD research: the focus on the lysosomal side of PD (Dehay et al., 2010). The lysosomal side involves studies looking at lysosomal dysfunction caused by mutations in GBA, TMEM175, LRRK2, and others (Alcalay et

al., 2015; Gan-Or et al., 2018; Krohn et al., 2020; Sosero et al., 2021; Ysselstein et al., 2019). While it is easy to imagine that this faction will also become very isolated, as the research on α-syn aggregation and mitochondrial dysfunction have become, the lysosomal side is by its very nature multidisciplinary, due to the role that lysosomes play in autophagy (Gan-Or et al., 2015). Defects in autophagy can bring together all the different sides of PD research under one umbrella.

5.2 PD is a result of dysfunction in autophagy

Looking at PD as a disease of autophagy-lysosomal pathway (ALP), brings together all the separate factions of research into the pathophysiology of PD. For instance, although mitochondrial defects and mitochondrial health play a large part in PD, PINK1 and Parkin mutations specifically alter mitophagy (Durcan & Fon, 2015). This results in poor quality control and an inability to degrade dysfunctional mitochondrial fragments. If the α-syn approach to the disease is taken, whether done through *SNCA* multiplication models, α-syn mutants such as A53T or E46K, or through the use of exogenous α-syn, α-syn accumulation all eventually lead to a failure in cellular lysosomal degradation and autophagy. The overexpression model allows endogenous α-syn more opportunities to aggregate (Lee & Lee, 2002). The aggregated structures then cling to different organelles and impair parts of the cell (Mahul-Mellier et al., 2020). Failure to clear these cytoplasmic aggregates through a functioning autophagic machinery leads to inclusion formation (Malkus & Ischiropoulos, 2012; Manecka et al., 2017; Monaco & Fraldi, 2020). If mutant forms of α-syn are present in the cell, they have a higher propensity to aggregate and associate with membranes (Imberdis et al., 2019; Narhi et al., 1999). They will, just like WT α-syn, aggregate and disrupt organelle function and trafficking (J. H. Soper et al., 2008). Failure to clear these

aggregates through chaperone-mediated autophagy or macroautophagy allows these aggregates to prosper, eventually incorporating more and more proteins and organelles into their orbit (Dehay et al., 2010; Lee et al., 2013; Malkus & Ischiropoulos, 2012; Nash et al., 2017; Xilouri et al., 2016). Finally, if the exogenous form of α-syn is used to model PD propagation, the accumulation of oligomeric forms of α-syn in the cell will lead to dysfunctional lysosomes that are unable to degrade their contents and, therefore cannot fuse with autophagosomes (Dehay et al., 2010; P. Desplats et al., 2009; Kovacs et al., 2014; Lee et al., 2013; Shachar et al., 2011). Even if lysosomes filled with exogenous α-syn were able to fuse with autophagosomes, their degradative activity would be largely impaired (Bayati et al., 2022), leading to the cell's inability to clear harmful and aggregated proteins. All these different pathways, lead to and from autophagy.

Focusing on the lysosomal aspect of PD will lead to a more holistic understanding of the mechanisms at play and will not have the blind spots that more traditional avenues of research into PD's mechanisms have. Looking at PD through the lens of ALP, one can explain almost all the different mutations that can contribute to PD. For instance, LRRK2, physiologically plays a role in protein degradation through regulating ALP. LRRK2 mutations, one of the most common causes of familial PD, lead cells down a road of ALP-related dysfunction, eventually leading to impaired autophagy (Senkevich & Gan-Or, 2020). Mutations in GBA, also very common in familial PD, lead to abnormal lysosomal activity, which lead downstream to impairments in autophagy (Navarro-Romero et al., 2022). Even rare forms of familial PD, stemming from mutations in VPS35, ultimately lead to autophagy impairments caused by the retromer complex's dysfunctional assembly (Cui et al., 2018).

5.3 Lewy bodies are impaired, enlarged, and failed autophagosomes

Our approach to studying the formation of LBs and understanding the cellular dysfunction in PD was to observe how exogenous α-syn fibrils can access the cytosol. Our research reached its first setback as we were unable to develop an assay that allowed us to visualize the escape of PFFs from lysosomes following their initial internalization and rapid transport to lysosomes. Although a decrease in colocalization between LAMP1 and PFFs was observed over time, we failed to see the formation of large PFF-positive aggregates (Bayati et al., 2022). We then hypothesized that another factor may be needed, a trigger of some sort, that leads to further impairment of lysosomes and allows PFFs to robustly gain access to the cytoplasm (i.e., lysosomal membrane permeabilization). We were inspired by case studies conducted during the COVID-19 pandemic in which individuals afflicted with moderate to severe forms of COVID-19, following infection by SARS-CoV-2, developed parkinsonian movement disorders soon after their recovery (Cohen et al., 2020; Faber et al., 2020; Mendez-Guerrero et al., 2020). Mostly, we were inspired by findings by Matheoud et al. (2019), how found that PINK1 knockout mice only exhibit Parkinsonian movement dysfunction following the immune system activation by administration of a gastrointestinal bacteria through oral gavage. This, coupled with research on the deleterious effects of proinflammatory cytokines on lysosomal proteins (Fang et al., 2021), led us to use IFN-γ, as an immune stressor, which turned out to be the missing piece to our puzzle.

The formation of the double membrane-bound LB-like inclusions in our *in vitro* model has led us to believe that at least a subset of LBs may have been membrane-bound at an earlier stage of their formation and maturation. Considering the cellular deterioration that occurs following the formation of LBs, such as apoptosis (P. Desplats et al., 2009), coupled with the poor quality of post-mortem tissue (Lewis et al., 2019; Sele et al., 2019), it is not at all impossible to believe that

the organellar-medley-filled LBs presented to us by Shahmoradian et al. (2019), were at some point an ever-expanding autophagosome. If this were to be true, it would have serious implications for our understanding of LBs. First, it would be clear that LBs were formed as a part of an active process by the cell, similar to the aggresomal response (Johnston et al., 1998), in which cells detect and target the clearance of abnormal organelles and aggregated proteins. This turns the current perception of LBs upside down, as currently, the popular belief suggests that α-syn fibrilization drives the process of inclusion formation (Fares et al., 2021; Lashuel, 2020), indicating that LBs occur passively, without the involvement of the cell: through its fibrillization, α-syn incorporates more and more proteins and organelles, leading to an inclusion that renders a significant portion of the cell useless. If the cellular aggresomal approach is to be adopted, then α-syn fibrillization cannot be the main driving force behind the formation of inclusions, as cellular pathways exist for sequestering and packaging aggregated proteins and harmful materials (Johnston et al., 1998). From the aggresomal perspective, α-syn is simply the passenger and not the driver behind LBs.

Secondly, if LBs are autophagosomes that were not able to degrade their contents, then they are neuroprotective and not the cause of cellular dysfunction, as are aggresomes (Tanaka et al., 2004). Even without the cell being able to clear the contents contained within LBs, packaging all of these organelles and proteins into a membrane-bound inclusion protects the cell from further damage, since damaged mitochondria could release cytochrome c and lysosomes undergoing LMP can release harmful hydrolases into the cell. It could be possible that neurons naturally form precursors to LBs that never get large enough, since a functioning lysosome fuses with the newly formed autophagosomes and degrades its contents. This way of thinking makes the formation of LBs a regular part of cellular processes that went awry.

Lastly, if LBs result from an autophagosome that was not cleared and kept on expanding, then the trickle-down effect of the immune stress in PD must be the impairment of lysosomal activity, which leads to impaired autophagy. Of course, it should be noted that proinflammatory cytokine signaling has been shown to have many deleterious effects on cells and implicated in neurodegeneration (Fang et al., 2021; Hobson & Sulzer, 2022; Kulkarni et al., 2016; Lees & Cross, 2007; Seifert et al., 2014), but this thinking suggests, that at least in the case of PD, the most important downstream effects of immune activation results in lysosomal dysfunction and impairment of the ALP. In our most recent work, we show clearly that a LAMP2 knockdown, coupled with PFF administration, results in the formation of LB-like inclusions ((Armin Bayati et al., 2023).

5.4 α-syn is a bystander in PD pathophysiology

It might be interesting to consider α-syn as a bystander in PD. If α-syn was simply an indicator of cellular stress, as posited by recent research (Hallacli et al., 2022), then its accumulation and increased expression can happen transiently following neuronal stress, which has been shown previously (Sala et al., 2013). With its increased expression, there is an ever-increasing chance for it to aggregate due to its NAC/hydrophobic region (Bisaglia et al., 2006). This results in the formation of aggregates that then lead to the trapping and incorporation of proteins and organelles. Aggregates can alter the shape and function of the LAMP2 pore (Cuervo et al., 2004), which is responsible for transporting materials from the cytoplasm to the lysosomes in CPA. Impairment in CPA leads to more accumulation of proteins in the cytoplasm (Manecka et al., 2017; Sala et al., 2016), and the altered LAMP structures lead to an inability for lysosomes to

fuse with autophagosomes (Huynh et al., 2007). All roads once again lead to a failure in autophagy.

This hypothesis also explains why mutations in α-syn or locus multiplication of *SNCA* result in the formation of LBs. If the *SNCA* mutations increase the aggregative ability of α-syn (Conway et al., 1998; Narhi et al., 1999), then the formation of aggregates leads to the downstream dysfunctions stated above. If more α-syn is present, then α-syn is not only more likely to aggregate (Lee & Lee, 2002), but it is also present in high numbers without the presence of cellular stress: the indicator for cellular stress is present in large amounts without the need for a source of stress. As oxidative stress and the presence of α-syn go hand-in-hand (Luk, 2019; Scudamore & Ciossek, 2018), this becomes a dangerous slippery slope for the cellular health.

Admittedly, when mutations and locus multiplications of the *SNCA* locus are present, α-syn acts as the trigger to the downstream impairment in autophagy. In cases where an increase in α-syn expression has occurred due to exposure to toxins or increased cellular stress (Pinto-Costa et al., 2023; Pukass & Richter-Landsberg, 2014; Puspita et al., 2017; Sala et al., 2013), α-syn accumulation and all the downstream dysfunctions are a by-product of the real trigger, which is cellular stress. It, therefore, makes perfect sense why DA neurons would be the most susceptible to this process: their regular function of anabolism and catabolism of dopamine is a highly oxidative process (Meiser et al., 2013). These neurons endure higher levels of cellular stress compared to other neurons, making them very sensitive to further cellular stress. If any additional source of stress were to present itself, these neurons would be pushed into an environment that would foster the increased expression of α-syn and dysfunctional organelle activity resulting in LB formation.

5.5 Proinflammatory cytokines: the trigger for neurodegeneration

Why does Parkinson's disease mainly affect older adults? Why is the prodromal stage of PD such a long process? What is going wrong in the cell in the prodromal period to cause prodromal symptoms but not result in Parkinson's disease symptoms? Clearly, α-syn aggregates are present years before the onset of the motor symptoms of PD (Stokholm et al., 2016; Wood, 2016). If so, are α-syn aggregates truly pathogenic in that their accumulation results in cellular apoptosis? These are all questions that have been asked in one form or another in more recent years. We believe these questions could all be answered when neuroimmunology is considered, and when the scope of PD is expanded to include more than just neurons.

Astrocytes, which support neurons through the release of trophic factors, also aid neurons with neurotransmission, reduce the metabolite burden, and inflammation (Ricci et al., 2009), may not be as effective as a support system when dealing with an accumulation of α-syn, as it results in an inflammatory response within astrocytes (C. Wang et al., 2021). Astrocytes' neuronal support is further inhibited by the release of proinflammatory cytokines by activated microglia, due to the presence of aggregated α-syn (Kam et al., 2020). Aging microglia can also facilitate the immune system infiltration of the brain, as observed in mice (Zhang et al., 2022), resulting in the presence of even more proinflammatory cytokine-releasing cells within the central nervous system. Essentially, the presence of aggregated α-syn can result in a chain reaction, leading to increasing neuronal stress since astrocytes' supportive activity is heavily compromised. This situation is only exacerbated with aging astrocytes, where their supportive function is even further limited (Palmer & Ousman, 2018).

As indicated above, multiple factors can affect the "perfect storm" of factors that lead to stressed neurons with dysfunctional ALP, but there is a common factor: aging. Aging microglia are

more likely to produce proinflammatory cytokines (Norden & Godbout, 2013). Aging microglia also facilitate the infiltration of T-cells into the brain, perhaps as an effort to restore the lost immune surveillance in the brain. However, like microglia, the aging immune cells are also more likely to release proinflammatory cytokines in response to mild and moderate infections resulting in a cytokine storm (Costagliola et al., 2021; Nidadavolu & Walston, 2021; Tizazu et al., 2022).

All of the above, explains how aging becomes a risk factor for poor neuronal health, and results in an environment where neurodegeneration can occur. Neurons will be more likely to produce high levels of reactive oxygen species and will be unable to rid the cell of harmful materials. In addition, organellar biogenesis may be altered, and dysfunctional organelles cannot be degraded. This will push cells into forming inclusions, to protect healthy parts of the cells from degeneration. We believe it is the combination of a PD-specific insult (e.g., genetic mutation, α-syn upregulation and aggregation) along with an external factor such as toxin exposure, immune system activation, or increased secretion of proinflammatory cytokines, that result in an environment ripe for the onset and occurrence of PD. However, the ease in which this "perfect storm" occurs, and the chances that this dual hit occurs at the same time, is increased with aging, resulting in much higher incidence of PD and other synucleinopathies, to occur later in life.

5.6 General conclusions

Our goal was to understand how α-syn is internalized and how it then seeds the formation of endogenous α-syn and lead to the formation of inclusions. This thesis answered both of those questions using multiple cell types. Our overarching finding, stemming from our data presented in chapter 4, is that the acute immune challenge and the release of proinflammatory cytokines in the brain, may be the triggering event that bridges the gap between prodromal PD and the onset of PD

motor symptoms. The involvement of the immune system and proinflammatory cytokines provide an explanation for the propensity of older populations, susceptible to cytokine storms in response to infections, to develop PD. In short, research into the role of the immune system and microglia may hold the key to our understanding of the pathophysiology of neurodegenerative diseases. Using the conjugation protocol established in chapter 2, the internalization assay described in chapter 3, and the dual hit treatment regime provided in chapter 4, future researchers can explore more findings relating to LB formation, the molecular pathophysiology of PD, and the triggering events that give rise to neurodegeneration.

5.7 References

Alcalay, R. N., Levy, O. A., Waters, C. C., Fahn, S., Ford, B., Kuo, S. H., Mazzoni, P., Pauciulo, M. W., Nichols, W. C., Gan-Or, Z., Rouleau, G. A., Chung, W. K., Wolf, P., Oliva, P., Keutzer, J., Marder, K., & Zhang, X. (2015). Glucocerebrosidase activity in Parkinson's disease with and without GBA mutations. *Brain*, *138*(Pt 9), 2648-2658. https://doi.org/10.1093/brain/awv179

Baba, M., Nakajo, S., Tu, P.-H., Tomita, T., Nakaya, K., Lee, V., Trojanowski, J. Q., & Iwatsubo, T. (1998). Aggregation of alpha-synuclein in Lewy bodies of sporadic Parkinson's disease and dementia with Lewy bodies. *The American Journal of Pathology*, *152*(4), 879.

Bartels, T., Choi, J. G., & Selkoe, D. J. (2011). alpha-Synuclein occurs physiologically as a helically folded tetramer that resists aggregation. *Nature*, *477*(7362), 107-110. https://doi.org/10.1038/nature10324

Bayati, A., Ayoubi, R., Zorca, C. E., Aguila, A., Han, C., Banks, E., Nguyen-Renou, E., Luo, W., Shlaifer, I., Cid-Pellitero, E. D., Yaqubi, M., Fon, E. A., Stratton, J. A., Durcan, T. M., Nahirney, P., & McPherson, P. S. (2023). *A dual hit of α-synuclein internalization and immune challenge leads to formation and maintenance of Lewy body-like inclusions in human dopaminergic neurons* (542776).

Bayati, A., Banks, E., Han, C., Luo, W., Reintsch, W. E., Zorca, C. E., Shlaifer, I., Del Cid Pellitero, E., Vanderperre, B., McBride, H. M., Fon, E. A., Durcan, T. M., & McPherson, P. S. (2022). Rapid macropinocytic transfer of alpha-synuclein to lysosomes. *Cell Rep*, *40*(3), 111102. https://doi.org/10.1016/j.celrep.2022.111102

Bertoncini, C. W., Fernandez, C. O., Griesinger, C., Jovin, T. M., & Zweckstetter, M. (2005). Familial mutants of alpha-synuclein with increased neurotoxicity have a destabilized conformation. *J Biol Chem*, *280*(35), 30649-30652. https://doi.org/10.1074/jbc.C500288200

Beyer, K. (2006). Alpha-synuclein structure, posttranslational modification and alternative splicing as aggregation enhancers. *Acta Neuropathol*, *112*(3), 237-251. https://doi.org/10.1007/s00401-006-0104-6

Bisaglia, M., Trolio, A., Bellanda, M., Bergantino, E., Bubacco, L., & Mammi, S. (2006). Structure and topology of the non-amyloid-beta component fragment of human alpha-synuclein bound to micelles: implications for the aggregation process. *Protein Sci*, *15*(6), 1408-1416. https://doi.org/10.1110/ps.052048706

Cabin, D. E., Shimazu, K., Murphy, D., Cole, N. B., Gottschalk, W., McIlwain, K. L., Orrison, B., Chen, A., Ellis, C. E., Paylor, R., Lu, B., & Nussbaum, R. L. (2002). Synaptic vesicle depletion correlates with attenuated synaptic responses to prolonged repetitive stimulation in mice lacking alpha-synuclein. *J Neurosci*, *22*(20), 8797-8807. https://doi.org/10.1523/JNEUROSCI.22-20-08797.2002

Chung, C. Y., Khurana, V., Yi, S., Sahni, N., Loh, K. H., Auluck, P. K., Baru, V., Udeshi, N. D., Freyzon, Y., Carr, S. A., Hill, D. E., Vidal, M., Ting, A. Y., & Lindquist, S. (2017). In Situ Peroxidase Labeling and Mass-Spectrometry Connects Alpha-Synuclein Directly to Endocytic Trafficking and mRNA Metabolism in Neurons. *Cell Syst*, *4*(2), 242-250 e244. https://doi.org/10.1016/j.cels.2017.01.002

Cohen, M. E., Eichel, R., Steiner-Birmanns, B., Janah, A., Ioshpa, M., Bar-Shalom, R., Paul, J. J., Gaber, H., Skrahina, V., Bornstein, N. M., & Yahalom, G. (2020). A case of probable Parkinson's disease after SARS-CoV-2 infection. *The Lancet Neurology*, *19*(10), 804-805. https://doi.org/10.1016/s1474-4422(20)30305-7

Conway, K. A., Harper, J. D., & Lansbury, P. T. (1998). Accelerated in vitro fibril formation by a mutant alpha-synuclein linked to early-onset Parkinson disease. *Nat Med*, *4*(11), 1318-1320. https://doi.org/10.1038/3311

Conway, K. A., Harper, J. D., & Lansbury, P. T., Jr. (2000). Fibrils formed in vitro from alpha-synuclein and two mutant forms linked to Parkinson's disease are typical amyloid. *Biochemistry*, *39*(10), 2552-2563. https://doi.org/10.1021/bi991447r

Conway, K. A., Lee, S. J., Rochet, J. C., Ding, T. T., Williamson, R. E., & Lansbury, P. T., Jr. (2000). Acceleration of oligomerization, not fibrillization, is a shared property of both alpha-synuclein mutations linked to early-onset Parkinson's disease: implications for pathogenesis and therapy. *Proc Natl Acad Sci U S A*, *97*(2), 571-576. https://doi.org/10.1073/pnas.97.2.571

Costagliola, G., Spada, E., & Consolini, R. (2021). Age-related differences in the immune response could contribute to determine the spectrum of severity of COVID-19. *Immun Inflamm Dis*, *9*(2), 331-339. https://doi.org/10.1002/iid3.404

Cuervo, A. M., Stefanis, L., Fredenburg, R., Lansbury, P. T., & Sulzer, D. (2004). Impaired degradation of mutant alpha-synuclein by chaperone-mediated autophagy. *Science*, *305*(5688), 1292-1295. https://doi.org/10.1126/science.1101738

Cui, Y., Yang, Z., & Teasdale, R. D. (2018). The functional roles of retromer in Parkinson's disease. *FEBS Lett*, *592*(7), 1096-1112. https://doi.org/10.1002/1873-3468.12931

Dawson, T. M., & Dawson, V. L. (2010). The role of parkin in familial and sporadic Parkinson's disease. *Mov Disord*, *25 Suppl 1*(0 1), S32-39. https://doi.org/10.1002/mds.22798

Dehay, B., Bove, J., Rodriguez-Muela, N., Perier, C., Recasens, A., Boya, P., & Vila, M. (2010). Pathogenic lysosomal depletion in Parkinson's disease. *J Neurosci*, *30*(37), 12535-12544. https://doi.org/10.1523/JNEUROSCI.1920-10.2010

Desplats, P., Lee, H. J., Bae, E. J., Patrick, C., Rockenstein, E., Crews, L., Spencer, B., Masliah, E., & Lee, S. J. (2009). Inclusion formation and neuronal cell death through neuron-to-neuron transmission of alpha-synuclein. *Proc Natl Acad Sci U S A*, *106*(31), 13010-13015. https://doi.org/10.1073/pnas.0903691106

Dettmer, U., Ramalingam, N., von Saucken, V. E., Kim, T. E., Newman, A. J., Terry-Kantor, E., Nuber, S., Ericsson, M., Fanning, S., Bartels, T., Lindquist, S., Levy, O. A., & Selkoe, D. (2017). Loss of native alpha-synuclein multimerization by strategically mutating its amphipathic helix causes abnormal vesicle interactions in neuronal cells. *Hum Mol Genet*, *26*(18), 3466-3481. https://doi.org/10.1093/hmg/ddx227

Durcan, T. M., & Fon, E. A. (2015). The three 'P's of mitophagy: PARKIN, PINK1, and post-translational modifications. *Genes Dev*, *29*(10), 989-999. https://doi.org/10.1101/gad.262758.115

Faber, I., Brandao, P. R. P., Menegatti, F., de Carvalho Bispo, D. D., Maluf, F. B., & Cardoso, F. (2020). Coronavirus Disease 2019 and Parkinsonism: A Non-post-encephalitic Case. *Mov Disord*, *35*(10), 1721-1722. https://doi.org/10.1002/mds.28277

Fang, C., Weng, T., Hu, S., Yuan, Z., Xiong, H., Huang, B., Cai, Y., Li, L., & Fu, X. (2021). IFN-gamma-induced ER stress impairs autophagy and triggers apoptosis in lung cancer cells. *Oncoimmunology*, *10*(1), 1962591. https://doi.org/10.1080/2162402X.2021.1962591

Fares, M. B., Jagannath, S., & Lashuel, H. A. (2021). Reverse engineering Lewy bodies: how far have we come and how far can we go? *Nat Rev Neurosci*, *22*(2), 111-131. https://doi.org/10.1038/s41583-020-00416-6

Fink, A. L. (2006). The aggregation and fibrillation of alpha-synuclein. *Acc Chem Res*, *39*(9), 628-634. https://doi.org/10.1021/ar050073t

Fink, A. L. (2006). The Aggregation and Fibrillation of α-Synuclein. *Accounts of Chemical Research*, *39*(9), 628-634. https://doi.org/10.1021/ar050073t

Fredenburg, R. A., Rospigliosi, C., Meray, R. K., Kessler, J. C., Lashuel, H. A., Eliezer, D., & Lansbury, P. T., Jr. (2007). The impact of the E46K mutation on the properties of alpha-synuclein in its monomeric and oligomeric states. *Biochemistry*, *46*(24), 7107-7118. https://doi.org/10.1021/bi7000246

Gan-Or, Z., Dion, P. A., & Rouleau, G. A. (2015). Genetic perspective on the role of the autophagy-lysosome pathway in Parkinson disease. *Autophagy*, *11*(9), 1443-1457. https://doi.org/10.1080/15548627.2015.1067364

Gan-Or, Z., Liong, C., & Alcalay, R. N. (2018). GBA-Associated Parkinson's Disease and Other Synucleinopathies. *Curr Neurol Neurosci Rep*, *18*(8), 44. https://doi.org/10.1007/s11910-018-0860-4

Hallacli, E., Kayatekin, C., Nazeen, S., Wang, X. H., Sheinkopf, Z., Sathyakumar, S., Sarkar, S., Jiang, X., Dong, X., Di Maio, R., Wang, W., Keeney, M. T., Felsky, D., Sandoe, J., Vahdatshoar, A., Udeshi, N. D., Mani, D. R., Carr, S. A., Lindquist, S., . . . Khurana, V. (2022). The Parkinson's disease protein alpha-synuclein is a modulator of processing bodies and mRNA stability. *Cell*, *185*(12), 2035-2056 e2033. https://doi.org/10.1016/j.cell.2022.05.008

Heise, H., Hoyer, W., Becker, S., Andronesi, O. C., Riedel, D., & Baldus, M. (2005). Molecular-level secondary structure, polymorphism, and dynamics of full-length alpha-synuclein fibrils studied by solid-state NMR. *Proc Natl Acad Sci U S A*, *102*(44), 15871-15876. https://doi.org/10.1073/pnas.0506109102

Hobson, B. D., & Sulzer, D. (2022). Neuronal Presentation of Antigen and Its Possible Role in Parkinson's Disease. *J Parkinsons Dis*, *12*(s1), S137-S147. https://doi.org/10.3233/JPD-223153

Huynh, K. K., Eskelinen, E. L., Scott, C. C., Malevanets, A., Saftig, P., & Grinstein, S. (2007). LAMP proteins are required for fusion of lysosomes with phagosomes. *EMBO J*, *26*(2), 313-324. https://doi.org/10.1038/sj.emboj.7601511

Imberdis, T., Negri, J., Ramalingam, N., Terry-Kantor, E., Ho, G. P. H., Fanning, S., Stirtz, G., Kim, T. E., Levy, O. A., Young-Pearse, T. L., Selkoe, D., & Dettmer, U. (2019). Cell models of lipid-rich alpha-synuclein aggregation validate known modifiers of alpha-synuclein biology and identify stearoyl-CoA desaturase. *Proc Natl Acad Sci U S A*, *116*(41), 20760-20769. https://doi.org/10.1073/pnas.1903216116

Johnston, J. A., Ward, C. L., & Kopito, R. R. (1998). Aggresomes: a cellular response to misfolded proteins. *J Cell Biol*, *143*(7), 1883-1898. https://doi.org/10.1083/jcb.143.7.1883

Kam, T. I., Hinkle, J. T., Dawson, T. M., & Dawson, V. L. (2020). Microglia and astrocyte dysfunction in parkinson's disease. *Neurobiol Dis*, *144*, 105028. https://doi.org/10.1016/j.nbd.2020.105028

Kovacs, G. G., Breydo, L., Green, R., Kis, V., Puska, G., Lorincz, P., Perju-Dumbrava, L., Giera, R., Pirker, W., Lutz, M., Lachmann, I., Budka, H., Uversky, V. N., Molnar, K., & Laszlo, L. (2014). Intracellular processing of disease-associated alpha-synuclein in the human brain suggests prion-like cell-to-cell spread. *Neurobiol Dis*, *69*, 76-92. https://doi.org/10.1016/j.nbd.2014.05.020

Krohn, L., Ozturk, T. N., Vanderperre, B., Ouled Amar Bencheikh, B., Ruskey, J. A., Laurent, S. B., Spiegelman, D., Postuma, R. B., Arnulf, I., Hu, M. T. M., Dauvilliers, Y., Hogl, B., Stefani, A., Monaca, C. C., Plazzi, G., Antelmi, E., Ferini-Strambi, L., Heidbreder, A., Rudakou, U., . . . Gan-Or, Z. (2020). Genetic, Structural, and Functional Evidence Link TMEM175 to Synucleinopathies. *Ann Neurol*, *87*(1), 139-153. https://doi.org/10.1002/ana.25629

Kulkarni, A., Ganesan, P., & O'Donnell, L. A. (2016). Interferon Gamma: Influence on Neural Stem Cell Function in Neurodegenerative and Neuroinflammatory Disease. *Clin Med Insights Pathol*, *9*(Suppl 1), 9-19. https://doi.org/10.4137/CPath.S40497

Lashuel, H. A. (2020). Do Lewy bodies contain alpha-synuclein fibrils? and Does it matter? A brief history and critical analysis of recent reports. *Neurobiol Dis*, *141*, 104876. https://doi.org/10.1016/j.nbd.2020.104876

Lautenschlager, J., Kaminski, C. F., & Kaminski Schierle, G. S. (2017). alpha-Synuclein - Regulator of Exocytosis, Endocytosis, or Both? *Trends Cell Biol*, *27*(7), 468-479. https://doi.org/10.1016/j.tcb.2017.02.002

Lee, H.-J., Suk, J.-E., Bae, E.-J., & Lee, S.-J. (2008). Clearance and deposition of extracellular α-synuclein aggregates in microglia. *Biochemical and Biophysical Research Communications*, *372*(3), 423-428. https://doi.org/https://doi.org/10.1016/j.bbrc.2008.05.045

Lee, H. J., Cho, E. D., Lee, K. W., Kim, J. H., Cho, S. G., & Lee, S. J. (2013). Autophagic failure promotes the exocytosis and intercellular transfer of alpha-synuclein. *Exp Mol Med*, *45*, e22. https://doi.org/10.1038/emm.2013.45

Lee, H. J., & Lee, S. J. (2002). Characterization of cytoplasmic alpha-synuclein aggregates. *J Biol Chem*, *277*(50), 48976-48983. https://doi.org/10.1074/jbc.M208192200

Lees, J. R., & Cross, A. H. (2007). A little stress is good: IFN-gamma, demyelination, and multiple sclerosis. *J Clin Invest*, *117*(2), 297-299. https://doi.org/10.1172/JCI31254

Lewis, A. J., Genoud, C., Pont, M., van de Berg, W. D., Frank, S., Stahlberg, H., Shahmoradian, S. H., & Al-Amoudi, A. (2019). Imaging of post-mortem human brain tissue using electron and X-ray microscopy. *Curr Opin Struct Biol*, *58*, 138-148. https://doi.org/10.1016/j.sbi.2019.06.003

Ludtmann, M. H., Angelova, P. R., Ninkina, N. N., Gandhi, S., Buchman, V. L., & Abramov, A. Y. (2016). Monomeric Alpha-Synuclein Exerts a Physiological Role on Brain ATP Synthase. *J Neurosci*, *36*(41), 10510-10521. https://doi.org/10.1523/JNEUROSCI.1659-16.2016

Luk, K. C. (2019). Oxidative stress and alpha-synuclein conspire in vulnerable neurons to promote Parkinson's disease progression. *J Clin Invest*, *129*(9), 3530-3531. https://doi.org/10.1172/JCI130351

Mahul-Mellier, A. L., Burtscher, J., Maharjan, N., Weerens, L., Croisier, M., Kuttler, F., Leleu, M., Knott, G. W., & Lashuel, H. A. (2020). The process of Lewy body formation, rather than simply alpha-synuclein fibrillization, is one of the major drivers of neurodegeneration. *Proc Natl Acad Sci U S A*, *117*(9), 4971-4982. https://doi.org/10.1073/pnas.1913904117

Malkus, K. A., & Ischiropoulos, H. (2012). Regional deficiencies in chaperone-mediated autophagy underlie alpha-synuclein aggregation and neurodegeneration. *Neurobiol Dis*, *46*(3), 732-744. https://doi.org/10.1016/j.nbd.2012.03.017

Manecka, D. L., Vanderperre, B., Fon, E. A., & Durcan, T. M. (2017). The Neuroprotective Role of Protein Quality Control in Halting the Development of Alpha-Synuclein Pathology. *Front Mol Neurosci*, *10*, 311. https://doi.org/10.3389/fnmol.2017.00311

Meiser, J., Weindl, D., & Hiller, K. (2013). Complexity of dopamine metabolism. *Cell Commun Signal*, *11*(1), 34. https://doi.org/10.1186/1478-811X-11-34

Mendez-Guerrero, A., Laespada-Garcia, M. I., Gomez-Grande, A., Ruiz-Ortiz, M., Blanco-Palmero, V. A., Azcarate-Diaz, F. J., Rabano-Suarez, P., Alvarez-Torres, E., de Fuenmayor-Fernandez de la Hoz, C. P., Vega Perez, D., Rodriguez-Montalban, R., Perez-Rivilla, A., Sayas Catalan, J., Ramos-Gonzalez, A., & Gonzalez de la Aleja, J. (2020). Acute hypokinetic-rigid syndrome following SARS-CoV-2 infection. *Neurology*, *95*(15), e2109-e2118. https://doi.org/10.1212/WNL.0000000000010282

Monaco, A., & Fraldi, A. (2020). Protein Aggregation and Dysfunction of Autophagy-Lysosomal Pathway: A Vicious Cycle in Lysosomal Storage Diseases. *Front Mol Neurosci*, *13*, 37. https://doi.org/10.3389/fnmol.2020.00037

Narhi, L., Wood, S. J., Steavenson, S., Jiang, Y., Wu, G. M., Anafi, D., Kaufman, S. A., Martin, F., Sitney, K., Denis, P., Louis, J. C., Wypych, J., Biere, A. L., & Citron, M. (1999). Both familial Parkinson's disease mutations accelerate alpha-synuclein aggregation. *J Biol Chem*, *274*(14), 9843-9846. https://doi.org/10.1074/jbc.274.14.9843

Nash, Y., Schmukler, E., Trudler, D., Pinkas-Kramarski, R., & Frenkel, D. (2017). DJ-1 deficiency impairs autophagy and reduces alpha-synuclein phagocytosis by microglia. *J Neurochem*, *143*(5), 584-594. https://doi.org/10.1111/jnc.14222

Navarro-Romero, A., Fernandez-Gonzalez, I., Riera, J., Montpeyo, M., Albert-Bayo, M., Lopez-Royo, T., Castillo-Sanchez, P., Carnicer-Caceres, C., Arranz-Amo, J. A., Castillo-Ribelles, L., Pradas, E., Casas, J., Vila, M., & Martinez-Vicente, M. (2022). Lysosomal lipid alterations caused by glucocerebrosidase deficiency promote lysosomal dysfunction,

chaperone-mediated-autophagy deficiency, and alpha-synuclein pathology. *NPJ Parkinsons Dis*, *8*(1), 126. https://doi.org/10.1038/s41531-022-00397-6

Nidadavolu, L. S., & Walston, J. D. (2021). Underlying Vulnerabilities to the Cytokine Storm and Adverse COVID-19 Outcomes in the Aging Immune System. *J Gerontol A Biol Sci Med Sci*, *76*(3), e13-e18. https://doi.org/10.1093/gerona/glaa209

Norden, D. M., & Godbout, J. P. (2013). Review: microglia of the aged brain: primed to be activated and resistant to regulation. *Neuropathol Appl Neurobiol*, *39*(1), 19-34. https://doi.org/10.1111/j.1365-2990.2012.01306.x

Palmer, A. L., & Ousman, S. S. (2018). Astrocytes and Aging. *Front Aging Neurosci*, *10*, 337. https://doi.org/10.3389/fnagi.2018.00337

Peelaerts, W., Bousset, L., Van der Perren, A., Moskalyuk, A., Pulizzi, R., Giugliano, M., Van den Haute, C., Melki, R., & Baekelandt, V. (2015). alpha-Synuclein strains cause distinct synucleinopathies after local and systemic administration. *Nature*, *522*(7556), 340-344. https://doi.org/10.1038/nature14547

Peng, C., Gathagan, R. J., & Lee, V. M. (2018). Distinct alpha-Synuclein strains and implications for heterogeneity among alpha-Synucleinopathies. *Neurobiol Dis*, *109*(Pt B), 209-218. https://doi.org/10.1016/j.nbd.2017.07.018

Pieri, L., Madiona, K., & Melki, R. (2016). Structural and functional properties of prefibrillar alpha-synuclein oligomers. *Sci Rep*, *6*, 24526. https://doi.org/10.1038/srep24526

Pinto-Costa, R., Harbachova, E., La Vitola, P., & Di Monte, D. A. (2023). Overexpression-Induced alpha-Synuclein Brain Spreading. *Neurotherapeutics*, *20*(1), 83-96. https://doi.org/10.1007/s13311-022-01332-6

Pukass, K., & Richter-Landsberg, C. (2014). Oxidative stress promotes uptake, accumulation, and oligomerization of extracellular alpha-synuclein in oligodendrocytes. *J Mol Neurosci*, *52*(3), 339-352. https://doi.org/10.1007/s12031-013-0154-x

Puspita, L., Chung, S. Y., & Shim, J. W. (2017). Oxidative stress and cellular pathologies in Parkinson's disease. *Mol Brain*, *10*(1), 53. https://doi.org/10.1186/s13041-017-0340-9

Ricci, G., Volpi, L., Pasquali, L., Petrozzi, L., & Siciliano, G. (2009). Astrocyte-neuron interactions in neurological disorders. *J Biol Phys*, *35*(4), 317-336. https://doi.org/10.1007/s10867-009-9157-9

Sala, G., Arosio, A., Stefanoni, G., Melchionda, L., Riva, C., Marinig, D., Brighina, L., & Ferrarese, C. (2013). Rotenone upregulates alpha-synuclein and myocyte enhancer factor 2D independently from lysosomal degradation inhibition. *Biomed Res Int*, *2013*, 846725. https://doi.org/10.1155/2013/846725

Sala, G., Marinig, D., Arosio, A., & Ferrarese, C. (2016). Role of Chaperone-Mediated Autophagy Dysfunctions in the Pathogenesis of Parkinson's Disease. *Front Mol Neurosci*, *9*, 157. https://doi.org/10.3389/fnmol.2016.00157

Scudamore, O., & Ciossek, T. (2018). Increased Oxidative Stress Exacerbates alpha-Synuclein Aggregation In Vivo. *J Neuropathol Exp Neurol*, *77*(6), 443-453. https://doi.org/10.1093/jnen/nly024

Seifert, H. A., Collier, L. A., Chapman, C. B., Benkovic, S. A., Willing, A. E., & Pennypacker, K. R. (2014). Pro-inflammatory interferon gamma signaling is directly associated with stroke induced neurodegeneration. *J Neuroimmune Pharmacol*, *9*(5), 679-689. https://doi.org/10.1007/s11481-014-9560-2

Sele, M., Wernitznig, S., Lipovsek, S., Radulovic, S., Haybaeck, J., Birkl-Toeglhofer, A. M., Wodlej, C., Kleinegger, F., Sygulla, S., Leoni, M., Ropele, S., & Leitinger, G. (2019). Optimization of ultrastructural preservation of human brain for transmission electron microscopy after long post-mortem intervals. *Acta Neuropathol Commun*, *7*(1), 144. https://doi.org/10.1186/s40478-019-0794-3

Senkevich, K., & Gan-Or, Z. (2020). Autophagy lysosomal pathway dysfunction in Parkinson's disease; evidence from human genetics. *Parkinsonism Relat Disord*, *73*, 60-71. https://doi.org/10.1016/j.parkreldis.2019.11.015

Shachar, T., Lo Bianco, C., Recchia, A., Wiessner, C., Raas-Rothschild, A., & Futerman, A. H. (2011). Lysosomal storage disorders and Parkinson's disease: Gaucher disease and beyond. *Mov Disord*, *26*(9), 1593-1604. https://doi.org/10.1002/mds.23774

Shahmoradian, S. H., Lewis, A. J., Genoud, C., Hench, J., Moors, T. E., Navarro, P. P., Castano-Diez, D., Schweighauser, G., Graff-Meyer, A., Goldie, K. N., Sutterlin, R., Huisman, E., Ingrassia, A., Gier, Y., Rozemuller, A. J. M., Wang, J., Paepe, A., Erny, J., Staempfli, A., . . . Lauer, M. E. (2019). Lewy pathology in Parkinson's disease consists of crowded organelles and lipid membranes. *Nat Neurosci*, *22*(7), 1099-1109. https://doi.org/10.1038/s41593-019-0423-2

Soper, J. H., Roy, S., Stieber, A., Lee, E., Wilson, R. B., Trojanowski, J. Q., Burd, C. G., & Lee, V. M. (2008). Alpha-synuclein-induced aggregation of cytoplasmic vesicles in Saccharomyces cerevisiae. *Mol Biol Cell*, *19*(3), 1093-1103. https://doi.org/10.1091/mbc.e07-08-0827

Sosero, Y. L., Yu, E., Krohn, L., Rudakou, U., Mufti, K., Ruskey, J. A., Asayesh, F., Laurent, S. B., Spiegelman, D., Fahn, S., Waters, C., Sardi, S. P., Bandres-Ciga, S., Alcalay, R. N., Gan-Or, Z., & Senkevich, K. (2021). LRRK2 p.M1646T is associated with glucocerebrosidase activity and with Parkinson's disease. *Neurobiology of Aging*. https://doi.org/10.1016/j.neurobiolaging.2021.02.018

Spillantini, M. G., Schmidt, M. L., Lee, V. M., Trojanowski, J. Q., Jakes, R., & Goedert, M. (1997). Alpha-synuclein in Lewy bodies. *Nature*, *388*(6645), 839-840. https://doi.org/https://doi.org/10.1038/42166

Stefanis, L., Larsen, K. E., Rideout, H. J., Sulzer, D., & Greene, L. A. (2001). Expression of A53T mutant but not wild-type alpha-synuclein in PC12 cells induces alterations of the ubiquitin-dependent degradation system, loss of dopamine release, and autophagic cell death. *J Neurosci*, *21*(24), 9549-9560. https://doi.org/10.1523/JNEUROSCI.21-24-09549.2001

Stokholm, M. G., Danielsen, E. H., Hamilton-Dutoit, S. J., & Borghammer, P. (2016). Pathological alpha-synuclein in gastrointestinal tissues from prodromal Parkinson disease patients. *Ann Neurol*, *79*(6), 940-949. https://doi.org/10.1002/ana.24648

Surmeier, D. J., & Sulzer, D. (2013). The pathology roadmap in Parkinson disease. *Prion*, *7*(1), 85-91. https://doi.org/10.4161/pri.23582

Tanaka, M., Kim, Y. M., Lee, G., Junn, E., Iwatsubo, T., & Mouradian, M. M. (2004). Aggresomes formed by alpha-synuclein and synphilin-1 are cytoprotective. *J Biol Chem*, *279*(6), 4625-4631. https://doi.org/10.1074/jbc.M310994200

Tizazu, A. M., Mengist, H. M., & Demeke, G. (2022). Aging, inflammaging and immunosenescence as risk factors of severe COVID-19. *Immun Ageing*, *19*(1), 53. https://doi.org/10.1186/s12979-022-00309-5

Valente, E. M., Abou-Sleiman, P. M., Caputo, V., Muqit, M. M., Harvey, K., Gispert, S., Ali, Z., Del Turco, D., Bentivoglio, A. R., Healy, D. G., Albanese, A., Nussbaum, R., Gonzalez-

Maldonado, R., Deller, T., Salvi, S., Cortelli, P., Gilks, W. P., Latchman, D. S., Harvey, R. J., . . . Wood, N. W. (2004). Hereditary early-onset Parkinson's disease caused by mutations in PINK1. *Science*, *304*(5674), 1158-1160. https://doi.org/10.1126/science.1096284

Vargas, K. J., Colosi, P. L., Girardi, E., Park, J.-M., & Chandra, S. S. (2021). *α-Synuclein facilitates clathrin assembly in synaptic vesicle endocytosis*.

Vargas, K. J., Makani, S., Davis, T., Westphal, C. H., Castillo, P. E., & Chandra, S. S. (2014). Synucleins regulate the kinetics of synaptic vesicle endocytosis. *J Neurosci*, *34*(28), 9364-9376. https://doi.org/10.1523/JNEUROSCI.4787-13.2014

Vargas, K. J., Schrod, N., Davis, T., Fernandez-Busnadiego, R., Taguchi, Y. V., Laugks, U., Lucic, V., & Chandra, S. S. (2017). Synucleins Have Multiple Effects on Presynaptic Architecture. *Cell Rep*, *18*(1), 161-173. https://doi.org/10.1016/j.celrep.2016.12.023

Vilar, M., Chou, H. T., Luhrs, T., Maji, S. K., Riek-Loher, D., Verel, R., Manning, G., Stahlberg, H., & Riek, R. (2008). The fold of alpha-synuclein fibrils. *Proc Natl Acad Sci U S A*, *105*(25), 8637-8642. https://doi.org/10.1073/pnas.0712179105

Wang, C., Yang, T., Liang, M., Xie, J., & Song, N. (2021). Astrocyte dysfunction in Parkinson's disease: from the perspectives of transmitted alpha-synuclein and genetic modulation. *Transl Neurodegener*, *10*(1), 39. https://doi.org/10.1186/s40035-021-00265-y

Westphal, C. H., & Chandra, S. S. (2013). Monomeric synucleins generate membrane curvature. *J Biol Chem*, *288*(3), 1829-1840. https://doi.org/10.1074/jbc.M112.418871

Wood, H. (2016). Parkinson disease: Peripheral alpha-synuclein deposits - prodromal markers for Parkinson disease? *Nat Rev Neurol*, *12*(5), 249. https://doi.org/10.1038/nrneurol.2016.54

Xilouri, M., Brekk, O. R., & Stefanis, L. (2016). Autophagy and Alpha-Synuclein: Relevance to Parkinson's Disease and Related Synucleopathies. *Mov Disord*, *31*(2), 178-192. https://doi.org/10.1002/mds.26477

Ysselstein, D., Nguyen, M., Young, T. J., Severino, A., Schwake, M., Merchant, K., & Krainc, D. (2019). LRRK2 kinase activity regulates lysosomal glucocerebrosidase in neurons derived from Parkinson's disease patients. *Nat Commun*, *10*(1), 5570. https://doi.org/10.1038/s41467-019-13413-w

Zhang, X., Wang, R., Chen, H., Jin, C., Jin, Z., Lu, J., Xu, L., Lu, Y., Zhang, J., & Shi, L. (2022). Aged microglia promote peripheral T cell infiltration by reprogramming the microenvironment of neurogenic niches. *Immun Ageing*, *19*(1), 34. https://doi.org/10.1186/s12979-022-00289-6